Reducing the Risk of Peri-Prosthetic Femoral Fracture: Prosthesis, Patient or Procedure?

Brad Miles

March 2012

Supervisors

Professor Andrew Ruys
Director of Biomedical Engineering,
School of Aerospace, Mechanical and Mechatronic Engineering, Faculty of Engineering and Information Technologies,
The University of Sydney

Associate Professor Richard Appleyard
Director of the Surgical Skills Centre
Australian School of Advanced Medicine,
Macquarie University

Associate Professor Mark Gillies
Honorary Fellow,
Australian School of Advanced Medicine,
Macquarie University

Associate Professor William L Walter
Clinical Discipline Leader,
School of Medicine,
University of Notre Dame

Table of Contents

Contents

Supervisors *2*

Table of Contents *3*

Table of Figures *7*

Chapter 1 ..... *18*

Introduction *18*

1.1 Background **19**

1.2 Preface **22**

Chapter 2 ..... *25*

Literature Review *25*

2.1 The natural hip **26**

2.1.1 Bone biology 26

2.1.2 The anatomy and physiology of the hip joint 27

2.1.3 Failure of the natural hip joint 36

2.2 Replacement of the hip joint **40**

2.2.1 History of hip replacement surgery 40

2.2.2 Total hip replacement today 42

2.3 Failure of hip replacements **48**

2.3.1 Total hip replacements 48

2.4 Peri-prosthetic femoral fracture **58**

2.4.1 Intra-operative peri-prosthetic femoral fracture 61

2.4.2 Post-operative peri-prosthetic femoral fracture 68

2.4.3 Surgical technique – cementless ABG II [175] and [176] 86

2.5 Computer assisted orthopaedic surgery **95**

2.5.1 Tracking in a Navigation System 96

2.5.2 Components of a computer assisted orthopaedic surgery System 100
2.5.3 Robotic Surgery 109
2.5.4 Total hip replacement- using the Stryker Navigation System 110

2.6 Hip resurfacing 116

2.6.1 History 117
2.6.2 Concepts for hip resurfacing 121
2.6.3 Failure of hip resurfacing 125
2.6.4 Implant positioning and femoral neck fracture 129
2.6.5 Implant positioning with computer assisted surgery 145

2.7 Hip joint loading 149

2.8 Developing subject-specific finite element models of the femur 153

2.8.1 Finite element analysis in biomechanics 153

2.9 Literature review summary and direction 168

2.9.1 Summary 168
2.9.2 Direction 170

Chapter 3 173

A Plasma-Sprayed Titanium Proximal Coating Reduces the Risk of Peri-Prosthetic Femoral Fracture in Cementless Hip Arthroplasty 173

3.1 Introduction 174

3.2 Methods 175

3.2.1 Femoral specimens 175
3.2.2 Strain gauge location 180
3.2.3 Prostheses 181
3.2.4 Biomechanical testing 183
3.2.5 Statistical analysis 188
3.2.6 Data analysis 188

3.3 Results 190

3.3.1 ABG II-plasma versus ABG II-standard 190
The ABG II-plasma, in all of the paired bones tested, showed a significantly higher load to failure, when compared to ABG II-standard. 199

ABG II- Plasma demonstrated higher load tolerance [32% (12% to 102%)] when compared to ABG II-standard ($p<0.05$) (Table 6). 199

3.3.2 ABG II-NMS versus ABG II-standard 201

3.4 Discussion 201

Chapter 4 205

Subject-specific Finite Element Modeling of Peri-prosthetic Femoral Fracture using Element Deactivation to Simulate Bone Failure 205

4.1 Introduction 206

4.2 Methods 208

4.2.1 Experimental testing 208

4.2.2 Generation of a subject-specific finite element model 209

4.2.3 Finite element model development 209

4.3 Results 237

4.3.1 Crack propagation/failure mechanism 237

4.3.2 Failure load 242

4.4 Discussion 244

Chapter 5 249

Subject-specific Finite Element Model with an Optical Tracking System in Total Hip Replacement Surgery 249

5.1 Introduction 250

5.2 Methods 252

5.2.1 Experimental measurement of hammer velocity 252

5.2.2 Construction of a subject-specific finite element analysis model 260

5.2.3 Generation of an finite element mesh 260

5.2.4 Simulation of intra-operative loading scenario 262

5.2.5 Material property assignment 263

5.2.6 Application of adequate boundary conditions 266

5.2.7 Modeling approach 266

5.2.8 Virtual strain gauge locations 266

5.3 Results **268**
5.3.1 Outputs measured 268
5.3.2 Displacement and energy measurements 268
5.3.3 Strain measurements 270
5.3.4 Force measurements 272
5.4 Discussion **275**
Chapter 6 ..... ***280***
Subject-specific Implant Positioning for Femoral Head Resurfacing Using Goal Driven Objective Optimization Techniques and Finite Element Analysis ***280***
6.1 Introduction **281**
6.2 Methods **284**
6.2.1 Goal driven optimisation 291
6.3 Results **291**
6.4 Discussion **294**
Chapter 7 ..... ***296***
Conclusions ***296***
7.1 Concluding Points: **297**
7.1.1 Chapter 3: A Plasma-Sprayed Titanium Proximal Coating Reduces the Risk of Peri-Prosthetic Femoral Fracture in Cementless Hip Arthroplasty 297
7.1.2 Chapter 4: Subject-specific Finite Element Modeling of Peri-prosthetic Femoral Fracture using Element Deactivation to Simulate Bone Failure 299
7.1.3 Chapter 5: Subject-specific finite element model with an optical tracking system in total hip replacement surgery 301
7.1.4 Chapter 6: Patient specific implant positioning for femoral head resurfacing using goal driven objective optimization techniques and Finite Element Analysis 303
7.2 Thesis Summary **304**
References ***307***

Table of Figures

Figure 1 Anatomy of the hip joint 28

Figure 2 Anatomy of the hip bone [42] 29

Figure 3 Anatomy of the femur [1] 30

Figure 4 The upper extremity (proximal extremity) of the right femur viewed from behind and above [3] 31

Figure 5 Lower extremity of right femur viewed from below [3] 33

Figure 6 Ligaments of the pelvis viewed from behind [2] 34

Figure 7 Anterior and posterior view of the main muscles of the lower limb [2] 35

Figure 8 Fractured neck of femur [44] 37

Figure 9 Fractured neck of femur [45] 38

Figure 10 An arthritic hip vs a normal hip [46] 39

Figure 11 Diagnosis of hip OA: Loss of joint space visible on X-ray [47] 39

Figure 12 Total hip joint prosthesis[60] 43

Figure 13 Bilateral cemented total hip replacement [62] 44

Figure 14 Some cementless (press-fit) stems from (Stryker's website) 45

Figure 15 Porous coating only (left) vs HA coating only (implant samples used for testing in chapter 3) 46

Figure 16 Peri-patite HA compared to a plasma sprayed HA on porous coating [65] 47

Figure 17 Peri-Apatite in a canine 1mm gap model from [67, 68] 47

Figure 18 Polyethylene induced osteolytic lesions around femoral stem [72] 49

Figure 19 Periarticular granulomatous inflammation in response to ultrahigh molecular weight polyethylene (UHMWPE) wear debris (From Long 2008) 50

Figure 20 Osteolysis due to alumina ceramic wear [75] 51

Figure 22 MRI image showing a larger pseudotumor resulting from metal sensitivity [84] 53

Figure 23 Radiograph showing results of long-term remodeling [85] 54

Figure 24 Cumulative percent revision by fixation 57

Figure 25 Vancouver classification [111] 60

Figure 26 (a) Intraopearative peri-prosthetic Femoral Fracture in metaphyseal region . 61

Figure 27 Insertion of femoral stem press fit against bone [120] 62

Figure 29 Intraoperative periprosthetic fractures of the femur - Vancouver classification [126] 65

Figure 31 Intraoperative B1 fracture with strut and cerclage wires. [126] 66

Figure 32 Intraoperative acetabular fracture treated with buttress plate. [126] 66

Figure 33 Postoperative peri-prosthetic fractures - Vancouver classification [126] 70

Figure 34 Displaced type A-G fracture. 71

Figure 35 Type A-G fracture treated with trochanteric clamp. 71

Figure 36 Displaced type B1 fracture. 72

Figure 37 Type B1 fracture treated with revision to long-stem prosthesis. 72

Figure 38 Displaced type B2 fracture. 73

Figure 39 Type B2 fracture treated with revision to long-stem prosthesis..... 73

Figure 40 Type B3 fracture revised to distal fit Wagner style stem..... 74

Figure 41 Type C fracture treated with ORIF plate and strut with cerclage wires..... 74

Figure 42 peri-prosthetic femoral fracture after total hip replacement Early vs Later fractures..... 78

Figure 43 ABG I vs ABG II [170]..... 80

Figure 44 ABGII femoral component (Stryker internal presentation)..... 81

Figure 45 From the Australian Joint Registry 2010 report: yearly cumulative percent revision of primary total conventional hip replacement with cementless fixation..... 82

Figure 46 Left-Femoral X ray template Right- Patient positioned in lateral decubitus position on the operating table (ABG Surg tech, 2004)..... 87

Figure 47 Left- Initial incision Right- Deeper incision revealing 1-Trochanter, 2- sciatic nerve 3- short external rotators [176]..... 88

Figure 48 Femur exposed (Left) Femoral canal opened up by the box chisel (Right)..... 90

Figure 49 Femoral stem insertion..... 93

Figure 51 Instrument being tracked by an optical tracking system during a total hip replacement (Picture taken whilst observing surgery)..... 97

Figure 52 Optical Tracking analogous to a Global Positioning System. (Stryker internal presentation)..... 98

Figure 53 Instruments being tracked by a Navigation system (Stryker internal presentation)..... 99

Figure 54 Tracking concept from [182]..... 100

Figure 55 CT image used for Navigation of Pelvic Anatomy (courtesy of Stryker South Pacific) 101

Figure 56 MRI Image used for Cranial Navigation 102

Figure 57 Point to Point registration of image to virtual object (images courtesy of Stryker South Pacific) 104

Figure 58 Acquisition of a point cloud for surface matching (Image courtesy of Stryker Navigation internal presentation) 105

Figure 59 Surface based registration of the head[187] 106

Figure 60 Intraoperative 3D image from a flouroscopy being utilized with a Navigation Solution (From Siemens Website) 107

Figure 62 Imageless representations of Anatomy (Stryker Navigation internal presentation) 109

Figure 63 Trackers affixed to the patient's pelvis 111

Figure 64 Attachment of the femoral tracker to the femur 113

Figure 65 Femoral landmarks are digitized to define the femoral limb axes 113

Figure 66 Acetabular surfaces are digitized 114

Figure 67 Positions of instruments and implants can be characterized with reference to the acetabular anatomy 115

Figure 68 Positions of instruments and implants can be characterized with reference to the femoral anatomy 116

Figure 69 Distance to dislocation is greater when the femoral head size is larger (Stryker internal presentation) 121

Figure 70 A typical resurfacing hip design: A thin walled cup and thin walled hollow femoral head. (Stryker internal presentation) 122

Figure 71 Wear rates of Ultra High Molecular Weight Polyethylene cups indicated with 1.8-fold wear increase over the 22 to 32 mm range of total hip replacement ball sizes. [215] 123

Figure 72 Traditional implant vs. large diameter metal-on-metal femoral head: Greater ROM [226] (but also possibly greater torque on the junction [225]) 126

Figure 74 Anteroposterior radiograph showing the ideal position of the femoral component of the hip resurfacing arthroplasty [233] 132

Figure 75 The effect of neutral versus valgus stem placement (mean ± standard deviation) differed according to the bone mineral density bone mineral density. 134

Figure 77 The template, when placed on the anteroposterior radiograph at 140°, allows visualization of the entry point (red dotted line) of the pin with respect to the location of the ligamentum teres (blue dotted line). 140

Figure 78 Cylindrical reaming 141

Figure 80 The navigated drill guide is inserted into the femoral neck and shaft. On the navigator screen the planned axis is shown (yellow). 147

Figure 81 The implanted position of the femoral component is verified with the navigation tool. Differences between planning and implanted position are shown on the navigator screen 148

Figure 82 Variation in hip joint loading during walking 149

Figure 83 ISO 7206 loading (taken from ISO-7206 part 4 standard document) 152

Figure 84 A series of voxels in a stack with a single voxel highlighted [286] 156

Figure 85 Voxel based meshing used by Keyak et al [287] 156

Figure 86 finite element Meshes of the proximal femur created using geometry based modeling workflow. The bottom left shows both tetrahedron and hexahedron mesh options. [295] 158

Figure 87 Bessho et al. allocates cancellous bone and cortical bone regions to the finite element mesh [306] 161

Figure 88 Simpleware Software Products 163

Figure 89-Representative X-ray of cadaveric femora (top) axial slice of cadaveric femur (bottom) 176

Figure 90 Calculation of cortical index 177

Figure 91 Preparation of cadaveric femurs removal of soft tissue 178

Figure 92 Representative strain gauge attachment to femur 179

Figure 93 Representative potted femur loaded into testing jig in ISO-7206-4 2010 loading orientation 180

Figure 94 Planned locations of strain gauges (top) actual locations (bottom) 181

Figure 95 Experimental stems; ABGII Plasma (far left) ABGII NMS (middle left) ABGII Standard (right) 182

Figure 96 ABGII medial scales visible in region marked "DEPOT H.A" 183

Figure 97 Impaction of stem into femur 184

Figure 98 Implant loaded under compression in the MTS testing system 184

Figure 99 Implant femur loaded to failure 185

Figure 100 Sequence of testing -The grey boxes indicate the steps where the strain was measured 186

Figure 101 Typical testing sequence 187

Figure 102 Example strain versus time plot during impaction stage of the testing 188

Figure 103 Example strain versus time plot for the cyclic loading part of the testing .. 189

Figure 104 Example strain versus force plot. Note that most channels demonstrate a near elastic behavior with only a minimal hysteresis loop 190

Figure 105 Implant heights after impaction measured with MTS machine 191

Figure 106 Hoop strain sensitivity 194

Figure 107 Axial strain sensitivity 196

Figure 108 Hoop residual strain 197

Figure 109 Axial residual strain 198

Figure 110 Failure load vs cortical index 200

Figure 111 Mechanical testing setup implanted stem 209

Figure 112 Relationship between Simpleware modules and workflow 211

Figure 113 Import DICOM file into Scan IP 213

Figure 115 Crop region of interest 215

Figure 116 Floodfill segmentation 215

Figure 117 Apply cavity fill 216

Figure 118 FloodFill tool panel and segmented marrow 217

Figure 119 Apply a morphological close on marrow 218

Figure 120 Femur mask after Boolean subtraction of the marrow 218

Figure 121 Difference after application of recursive Gaussian filter 219

Figure 122 Femoral neck osteotomy with CAD primitive 220

Figure 123 CAD model of ABG II stem, ... 220

Figure 124 Anterior, lateral and 3D views of the model in ScanCAD 221

Figure 125 Inadequate mesh boundary between implant and bone using Simpleware mesh control tools. 222

Figure 126 Inadequate mesh boundary between implant and bone using Simpleware mesh control tools 223

Figure 127 Inadequate mesh boundary between implant and bone using Simpleware mesh controls 224

Figure 128 High strain area resulting from mesh inconsistency a the implant bone boundary 225

Figure 129 Meshing implant in ABAQUS CAE gives consistent mesh boundary at the interface 226

Figure 130 Ten node tetrahedron element used in the mesh of a femur model. [306] .. 227

Figure 131 New approach (right) provided more constant initial contact between the bone and the implant than previous approach (left) 228

Figure 132 Higher friction zone on the implant labeled "DEPOT H.A" 229

Figure 133 Friction Zone (Red) Frictionless Zone (Green) 230

Figure 134 Fixed distal boundary conditions and load orientation (left) set to resemble ISO 7206-4 (right) 231

Figure 135 ISO 7206-4 compliant loading scenarios 232

Figure 136 Typical force vs time plots for failure characterization 233

Figure 137 Different material property assignments used 234

Figure 138 Simpleware Scan FE material property assignment for applying heterogeneous material properties to the bone model 235

Figure 139 Elastic modulus vs density for triphasic bone model 236

Figure 140 Typical failure of bone during experimental testing 238

Figure 141 Force vs time plot for failed bone 239

Figure 143 High strain area in models that would not converge with element deletion- these models converged when element deletion was not used. 241

Figure 144 Typical failure mode physical test specimen (left) biphasic (middle) 242

Figure 146 Comparison of force vs. time (also displacement) plots 243

Figure 148-Stryker Navigation System- commercially available optical tracking system 252

Figure 150 Stryker Hip Navigation Smart Instruments being utilized in a total hip replacement 254

Figure 151 Types of data that can be recorded 256

Figure 152 digitizing a movement 257

Figure 153 Stryker Navigation tracker rigidly attached to the mallet 258

Figure 154 Setup used to record hammer velocity 259

Figure 155 Simulation of loading scenario 262

Figure 156 Typical impaction of stem into femur (From ABG II surgical Technique) .. 263

Figure 157 Material property assignment 264

Figure 158 Virtual strain gauge locations 267

Figure 159 Strain versus time at the quasi-static preload step in (A) friction coefficient = 0.1 271

Figure 160 Strain versus time at the impact loading step in (A) friction coefficient = 0.1 (B) friction coefficient = 0.4 272

Figure 161 Force measured at the hammer impact interface in (A) friction coefficient = 0.1 (B) friction coefficient = 0.4 273

Figure 163 Force measured at the top of the implant in (A) friction coefficient = 0.1 (B) friction coefficient = 0.4 273

Figure 164 Resultant force at the base of the femur (distal restraint) in (A) friction coefficient = 0.1 and (B) friction coefficient = 0.4 274

Figure 165 Proposed flow of Information for clinical implementation 277

Figure 166 peri-prosthetic femoral neck fracture after femoral head resurfacing 282

Figure 167 Proximal geometry of femur from CT scan 284

Figure 168 Proximal geometry of femur segmented from CT scan 285

Figure 168 Proximal femoral mesh created in Simpleware is transferred into the ANSYS Design Modeler software for preprocessing 286

Figure 169 Identify; i) centre of femoral head; ii) centre of femoral neck 287

Figure 170 Femoral component position is defined by a guide wire passing through the head and neck over which a cylindrical reamer is passed 288

Figure 171 Changing the floating point in the superior inferior direction changes the varus valgus position of the femoral implant 289

Figure 172 Changing the anterior/posterior position of the floating point changes the version of the femoral implant 289

Figure 173 Deterministic finite element model 290

Figure 174 Typical strain contour plot- maximum principal strain location 292

Figure 175 Design of Experiments response curve 293

Figure 176 The optimized position and contour plot from the goal driven optimization 294

Chapter 1

Introduction

1.1 Background

Australia, like much of the world, faces significant economic and social challenges associated with its ageing population. A major threat to the health and well-being of the aged is the onset of degenerative joint diseases, particularly osteoarthritis. Osteoarthritis reduces a person's ability to remain active, and makes them vulnerable to diseases such as obesity and heart failure. An Access Economics report published in 2005 indicates that arthritis affects some 17% of the entire Australian population and over 50% of those aged over 70 years [4]. In the United States, Osteoarthritis is the leading cause of chronic disability, affecting nearly 27 million people [5]. Notably, with the over-60 population predicted to double over the next 20 years, the incidence of Osteoarthritis is set to grow exponentially [6, 7].

As a result of the high incidence of Osteoarthritis, total hip arthroplasty is one of the most common operations performed today, and procedure numbers are steadily increasing. In 2010, the Australian Joint Registry reported that the number of hip replacement procedures had increased by 26.3% since 2003, amounting to 33,943 procedures recorded in the 2010 report. In the USA, there are an estimated 230,000 hip replacement procedures per year, with this number predicted to increase to 572,000 by 2030 [8-10]. The majority of hip replacements are conventional total hip arthroplasty; however, femoral head resurfacing has been used as an alternative to total hip arthroplasty for younger and more active patients.

Unfortunately, not all hip replacement procedures are successful. The overall Australian revision rate for all total hip arthroplasty is estimated at 20–24%[11]. Implant related bone fracture is a major contributor to this revision rate. peri-prosthetic femoral fracture early after total hip arthroplasty is the second most common reason for total hip arthroplasty revision[12], and the incidence of femoral neck fracture after femoral head resurfacing has been reported to be as high as 5%[13, 14]. The revision options for

a failed total hip arthroplasty are difficult and are often restricted due to the lack of remaining bone stock. Furthermore, the clinical results obtained from patients receiving a revision for peri-prosthetic femoral fracture are extremely poor, with reoperation rates being high [15].

Many factors have been identified, which increase the likelihood of a patient having a peri-prosthetic femoral fracture in both total hip arthroplasty and femoral head resurfacing. This thesis focuses on three major types of factors; the prosthesis, the patient and the procedure. The type of prosthesis is a factor that affects the risk of fracture in total hip arthroplasty.[16] With different femoral stem designs intentionally transferring load the femur in different ways, this is not surprising. Higher rates of peri-prosthetic femoral fracture have been attributed to patient specific factors such as age and sex, with older and female patients having an increased risk of fracture [16]. These are anthropometric indicators of the patient's likely bone quality or strength. Osteoporosis, which weakens bone, is a problem of the elderly and is more severe in women, thus it is no surprise that these groups have higher rates of fracture. There are also procedure related factors that are known to increase the risk of peri-prosthetic femoral fracture, including operative technique and implant positioning [16]. For example, it is well known that the position of the implant in a femoral head resurfacing with reference to the patient's femoral neck is related to the risk of peri-prosthetic femoral fracture. Valgus positioning of the neck is widely reported to reduce the risk of fracture [17]. It would seem that efforts to reduce the incidence of peri-prosthetic femoral fracture would need to take into account prosthesis design, patient specific factors, and procedure specific factors.

Arguably, the best way to take into account all of these factors would be to create patient-specific models that can predict bone fracture. Much progress has been made to this end with subject-specific finite element analysis created from computed tomography data of bone, proving to be an effective technique for bone fracture

prediction when correct modeling techniques are used [18]. This technology is in its infancy and has not been reported to be applied to the problem of fracture around implants. Much work is needed to make this a viable clinical tool to reduce the risk of peri-prosthetic femoral fracture.

When looking at procedure specific factors associated with increased risk of peri-prosthetic femoral fracture, an emerging trend that may prove to be useful is that towards computer assisted orthopaedic surgery. This technology is changing surgical procedures for implanting total hip arthroplasty and femoral head resurfacing. Computer assisted orthopaedic surgery applications provide the surgeon with precise information about the position of the surgical instruments and the ability to control the positioning of the actual implants in relation to the patient's anatomy [19-21]. This gives the surgeon the ability to place the components with far more precision than has been possible in the past. However, what is surprising is that the actual 'correct position' for the components is not often well understood or adequately quantified [19].

As such, even when using precise computer assisted orthopaedic surgery tools to place the components, surgeons rely on generalized 'rules of thumb' that do not consider patient specific variables. That is to say that all patients receive the same generalized placement of components regardless of differing patient specific factors. Therefore, although computer assisted orthopaedic surgery tools enable surgeons to place the components more precisely, they do not help surgeons decide whether their surgical goal is actually the best goal for that patient.

Considering patient specific finite element analysis and computer assisted orthopaedic surgery as complimentary tools to reduce the risk of peri-prosthetic femoral fracture is one of the main themes of this thesis.

1.2 Preface

This thesis seeks to reduce the risk of peri-prosthetic femoral fracture for total hip replacement and femoral head resurfacing patients by considering; implant design, patient specific factors, and procedure-specific factors. Where possible these factors are considered in a combined sense. Towards this pursuit, attention is given to the application of subject specific finite element analysis and computer assisted orthopaedic surgery.

This work begins with a detailed literature review. This literature review clearly demonstrates that there are three major considerations needed to reduce the risk of peri-prosthetic femoral fracture. That being;

1) Prosthesis design factors,
2) A consideration of subject specific factors and,
3) A consideration of the procedure specific factors- or factors that describe how the surgeon undertakes the actual procedure.

When considering implant design and its impact on peri-prosthetic femoral fracture, little work has been done by previous researchers to understand the effect of incremental design changes on peri-prosthetic femoral fracture. A specific issue that has received no attention is that of the roughness of a femoral stems proximal coating and its effect on peri-prosthetic femoral fracture. Should the proximal femoral coating of a press fit femoral stem be roughened or smooth to reduce the risk of peri-prosthetic femoral fracture? To answer this question mechanical testing with matched pairs of cadaveric femoral specimens was undertaken. This work demonstrates that a roughened coating is superior, and recommends that a currently available implant design (the ABGII from Stryker) be modified. The manufacturer presented with this information has undertaken a worldwide redesign of the stem.

Building on this work, a new patient-specific finite element analysis modeling technique, which considers the design of the implant together with patient-specific bone parameters, is developed. The modeling technique models bone failure by simulating a crack in the bone in the bone tissue. This is achieved by setting a strain based failure threshold at the element level of the finite element mesh. When an element feels a strain that is at the threshold level, the element is considered to have failed. Then the element is removed from the mesh and cannot exert any mechanical influence on its surrounding elements. This approach has the potential to pre-operatively characterize a specific patient's risk of early peri-prosthetic femoral fracture when a specific implant design is chosen.

However, a significant limitation of this approach is that it does not account for many of the surgical variabilities that also contribute to a patient's risk of peri-prosthetic femoral fracture. Utilizing a computer assisted orthopaedic surgery system in a novel way, this project looks to input into the patient-specific finite element analysis models, surgery-specific loading conditions. This technique could be used to reduce the risk of peri-prosthetic femoral fracture by regulating a surgeon's behavior (avoiding overloading) in the operating room whilst also considering that specific patients' bone strength in that specific scenario. The unique combination of all these technologies as a system in the operating theatre could almost eliminate the risk of peri-prosthetic femoral fracture in conventional total hip arthroplasty.

Looking in a different direction, efforts to reduce the risk of peri-prosthetic femoral fracture around a femoral head resurfacing should also consider both procedure-specific and patient-specific factors. Much work has been done by other authors characterizing procedure-specific and patient-specific factors in isolation from each other, with consensus converging on two different focal points. Firstly, that effort should be made by the surgeon to orientate the femoral component into relative valgus and secondly, that patient selection (or patient screening) should be utilized to eliminate

patients with a poor bone strength capacity. To address these issues a patient-specific modeling technique is used to consider both of these focal points together. (And not in isolation) The modeling technique determines at an individual patient level a specific femoral position that would minimize that patient's risk of peri-prosthetic femoral fracture. This is achieved by coupling a subject specific finite element modeling technique with Design of Experiments approach. The Design of Experiments intelligently and efficiently samples a large range of possible femoral component positions without the need to run simulations of every possible position. Then utilizing a goal driven optimization methodology it is possible to isolate an optimum patient-specific femoral component alignment that reduces the strain in the femoral neck.

Although not investigated in this work the subject specific finite element model and optimization would ideally be coupled with computer assisted orthopaedic surgery. That is to say that the subject specific optimization of the implant position could then most easily be delivered in that patient using computer assisted orthopaedic surgery techniques during the surgery. The addition of patient specific analysis does introduce additional complexity; however, as was recently discussed during the plenary session at the 2012 International society for Technology in Arthroplasty in Sydney there is significant capability for cost reduction. This is because the implant companies can reduce inventory costs by knowing in advance that what approximate size of implant is needed and therefore not having to send every implant size to the operation. It was suggested that this is already reducing costs in the public health system.

Chapter 2

Literature Review

2.1 The natural hip

2.1.1 Bone biology

Bone is a composite structure, consisting of an extracellular organic matrix, inorganic mineral crystals, cells, lipids, and water [22-25]. The extracellular organic matrix is mainly composed of type I collagen, together with other types of collagen and some non-collagenous proteins [26], and is mainly responsible for compression strength and stiffness of the bone. Mineral crystals, analogous in composition to hydroxyapatite [27], and containing impurities such as carbonate, magnesium, citrate, and other trace elements determined by diet, provides the corresponding tension properties [28, 29]. Mineralized extracellular matrix is produced, nurtured, and remodeled by cells, which respond to mechanical and other signals to determine the properties (morphology and function) of the bone. Composition of bone is influenced by many factors, varying with sex, age, location, health, and disease [30]

At a macroscopic level, bone is non-homogenous, porous and anisotropic, with the majority of bone having either very low (cortical or compact bone) or very high (trabecular or cancellous bone) porosity. Trabecular bone, with 50-95% porosity, is usually found in cuboidal bones, flat bones, and at the end of long bones[31], whilst cortical bone, with 5-10% porosity, is found in the shafts of long bones and surrounding trabecular bones [32] to form a sandwich-type structure, which provides optimal structural properties [33]. Both cortical and trabecular bone are formed by two types of tissue; woven and lamellar bone. Woven bone, which forms quickly but with poorly organized arrangement of collagen fibers and mineral crystals, is found during the healing process after fracture, and in the skeletal embryo. Over time, normally by the age of four or five, woven bone is replaced by the slow forming, highly organized and stronger, lamellar bone.

Bones have the capacity to grow, change shape, self-repair and continuously renew; processes mediated by mechanical, hormonal, and physiological factors. Although growth and shape modification is generally restricted to childhood, and self-repair to the period following fracture, the internal remodeling of bone is a continual process that is tightly controlled by a fine balance between bone degradation and bone formation. Bone remodeling is co-ordinated by four cell types: osteoclasts, osteoblasts, bone lining cells, and osteocytes, which act together to create basic multicellular units (BMUs). BMUs (basic multicellular units) replace old bone with new bone in a well-defined sequence of activation, destruction, and formation. Osteoclasts orchestrate the process of bone destruction by removing bone tissue through digestion of the mineralized matrix and by breaking up organic bone, a process known as bone resorption. Osteoblasts are mononucleate cells that are responsible for the formation of bone by production and mineralization of the extracellular matrix. Bone lining cells are inactive osteoblasts, which remain on the surface when bone formation stops and can be reactivated in response to chemical and /or mechanical stimuli [34]. Osteocytes are former osteoblasts that become trapped in the bone matrix and remain isolated in the lacunae [32]. Osteocytes form a cannalicular network which is how they are in a opposition to sense and respond to strain. Unlike osteoblasts, osteocytes do not generate osteoid and mineralized matrix, instead they act in a paracrine manner on active osteoblasts. There is some evidence that osteocytes respond to mechanical stimuli [35-38], whilst it can also be conceived that damage to the bone matrix may affect osteocytes and lead to alterations in bone remodeling.

2.1.2 The anatomy and physiology of the hip joint

The hip joint, located where the thigh bone (femur) meets the pelvic bone, is one of the largest joints in the body, and allows the leg a wide range of movement. It is a "ball and socket" joint: the upper end (head) of the femur forming the ball and the cavity in the pelvic bone (acetabulum) forming the socket. (Figure 1) The ball is normally held in the

socket by very powerful ligaments that form a complete sleeve around the joint (the joint capsule). The hip joint is a synovial joint, lined with a layer of synovium, which provides a lubricant to limit friction and reduce wear of the natural components. The spherical head of the femur and the socket are covered with a layer of smooth hyaline cartilage, a fairly soft, white substance about 1/8 inches (approx 3.2mm) thick, which cushions the joint, and allows the bones to move on each other with very little friction.

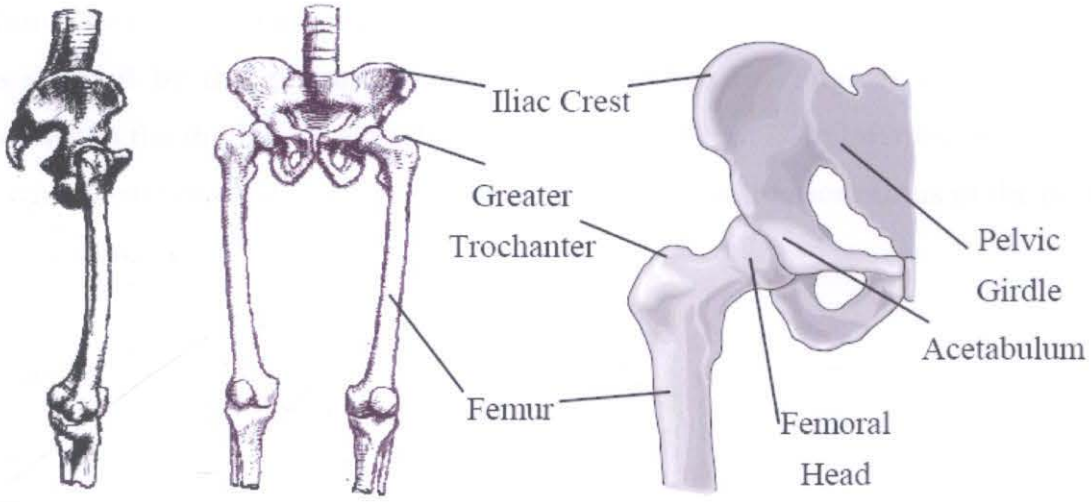

Figure 1 Anatomy of the hip joint

2.1.2.1 Bones of the hip

As shown in Figure 1, the hip bone is a large, irregularly shaped bone formed by three bones: the ilium, pubis and ischium [39-41]. Before puberty, these bones are separated by cartilage, however, in adults they are indistinguishably fused at the acetabulum. The acetabulum is a cup-shaped pocket in the hip bone, on its lateral aspect for articulation with the head of the femur. A fibrocartilaginous rim, called the labrum acetabulare, which provides additional stability to the joint, deepens the acetabulum considerably.

The ilium is a fan shaped bone, which forms the superior two-thirds of the hip bone and the superior two-fifths of the acetabulum. The ilium is composed of two parts, the ala (wing), which resembles the spread of a fan, and the body, which resembles the handle. The superior margin of the ilium is called the iliac crest. The ischium, which forms the posterior-inferior third of the hip bone and the posterior two-fifths of the acetabulum, is roughly L-shaped and passes inferiorly from the acetabulum to join anteriorly to the pubis. The ischium is composed of two parts: a body, and a ramus. The body, the superior thick portion of the ischium, is fused with the ilium and the pubis at the acetabulum. The inferior end has a large, blunt prominence called the ischial tuberosity, which is covered by the gluteus maximus muscle when the thigh is extended, but uncovered when the thigh is flexed. The ramus of the ischium is an inferior, thinner bar of bone, which extends medially from the body and joins the inferior ramus of the pubis to form the ischiopubic ramus.

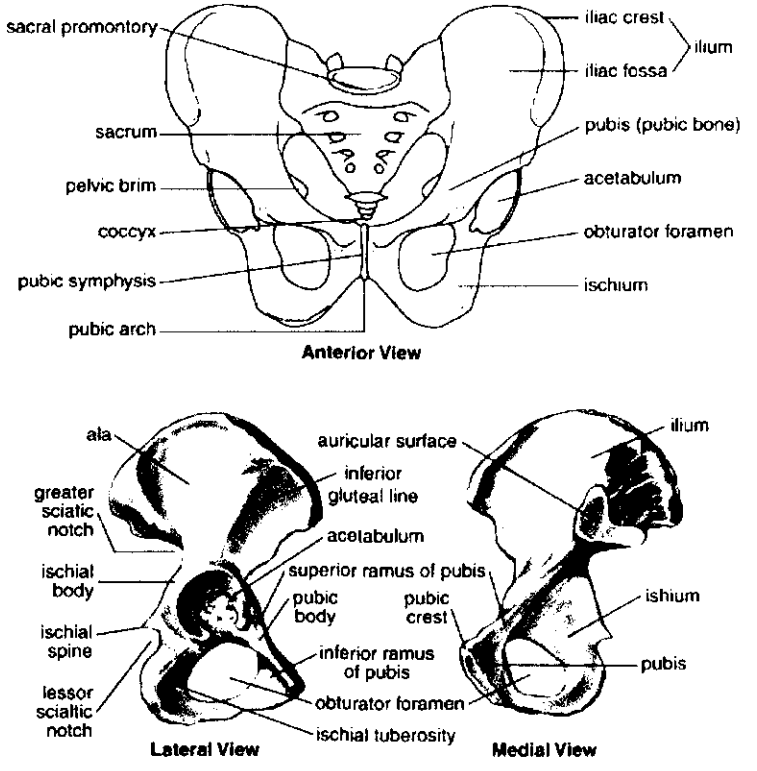

Figure 2 Anatomy of the hip bone [42]

The pubis, an L-shaped bone, which forms the inferoanterior part of the hip bone and the anteromedial one-fifth of the acetabulum, consists of three parts: a body and two rami. The flattened body of the pubis lies medially and joins the body of the opposite pubis at a fibrocartilaginous joint, the pubic symphysis. The superior ramus passes superolaterally to the acetabulum where it fuses with the ilium and ischium whilst the inferior ramus passes posteriorly, inferiorly, and laterally to join the ramus of the ischium and form half of the pubic arch.

The femur (Figure 3) is the longest and strongest bone in the human skeleton, and is almost perfectly cylindrical [39]. In the erect posture, it is not vertical, but inclines gradually downward and medial in order to bring the knee-joint near to the line of gravity of the body.

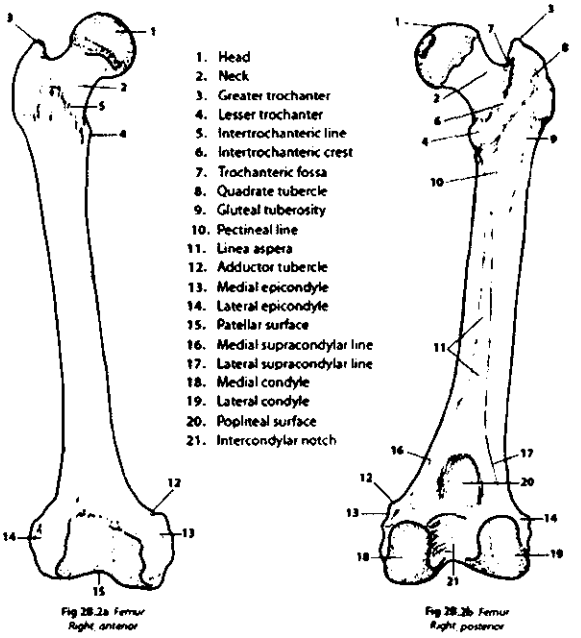

Figure 3 Anatomy of the femur [1]

Like other long bones, it is divisible into a body (shaft) and two extremities. The upper extremity of the femur (proximal extremity) consists of a head, neck, and greater and

lesser trochanters. The lower extremity (distal extremity) is broadened by medial and lateral condyles, where it articulates with the tibia and patella to form the knee joint.

The head of the femur (Figure 4), which is globular and forms about two-thirds of a sphere, is directed medially, superiorly, and slightly anteriorly to fit into the acetabulum of the hip bone. Its surface is smooth and coated with cartilage, except for the fovea capitis femoris, situated slightly inferior and posterior to the centre of the head, which is the site of attachment to the ligamentum teres.

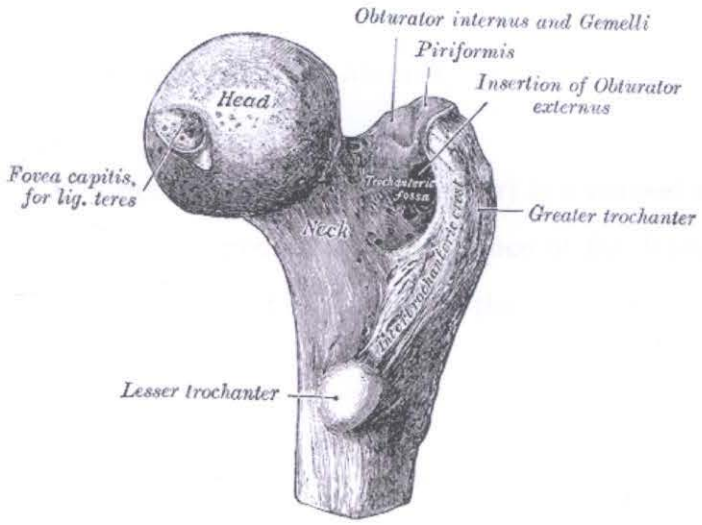

Figure 4 The upper extremity (proximal extremity) of the right femur viewed from behind and above [3]

The head of the femur is connected to the body by the neck (collum femoris), a flattened pyramidal process of bone, which runs obliquely in an inferolateral direction to meet the body of the femur. The angle of the neck is widest in infancy, and lessens during growth, so that at puberty it forms a gentle curve from the axis of the body of the bone.

In adulthood, the neck forms an angle of about 125° with the body and is projected 12° to 14° forward. The neck is limited laterally by the greater trochanter, and is narrowest in diameter in the middle. The surface of the neck is separated from the body of the femur by the intertrochanteric line, produced by attachment of the iliofemoral ligament, which runs inferomedially from the greater trochanter and passes inferior to the lesser trochanter. A prominent ridge, the intertrochanteris crest, unites the two trochanters posteriorly. The anterior surface of the neck is perforated by numerous vascular foramina.

The greater trochanter (trochanter major; great trochanter) is a large, irregular, quadrilateral eminence, situated at the junction of the neck with the upper part of the body [39]. It provides an attachment for several of the gluteal muscles. The greater trochanter lies laterally, and in adults does so about 1 cm lower than the head.

The lesser trochanter (trochanter minor; small trochanter) is a conical eminence, which varies in size and projects from the posteromedial surface of the femur at the inferior end of the intertrochanteric crest [39]. It is located in the angle between the neck and body of the femur.

The body or shaft (corpus femoris) of the femur is almost cylindrical in form, slightly bowed anteriorly, so as to be convex in front and concave behind, and narrowest at its midpoint [39-41]. A prominent longitudinal ridge, the linea aspera, strengthens the middle of the posterior surface. The linea aspera has medial and lateral lips, which diverge inferiorly to form medial and lateral supracondylar lines, and a narrow rough intermediate line. The lateral ridge, termed the gluteal tuberosity, is very rough, and runs almost vertically upward to the base of the greater trochanter and provides attachment to part of the gluteus maximus. The intermediate ridge, or pectineal line, continues to the base of the lesser trochanter and provides attachment to the pectineus. The medial ridge is lost in the intertrochanteric line.

The lower extremity (distal extremity) is larger than the upper and somewhat cuboid in form, with the transverse diameter greater than the antero-posterior diameter (Figure 5). Two large, oblong eminences, known as the condyles, project posteriorly, and are separated by a deep U-shaped intercondylar notch. The lateral condyle is the more prominent of the two and is broader both in its antero-posterior and transverse diameters. Whilst the medial condyle is the longer, and when the femur is held with its body perpendicular, it projects to a lower level. The opposed surfaces of the medial and lateral condyles are small, rough, and concave. In front, the condyles are only slightly prominent, and are separated from one another by a smooth shallow articular depression called the patellar surface. Behind, they project considerably, and the interval between them forms a deep notch, the intercondyloid fossa, limited above by a ridge, called intercondyloid line, and below by the central part of the posterior margin of the patellar surface. Superior to each condyle is a prominent epicondyle to which the tibial and fibular collateral ligaments of the knee joint are attached.

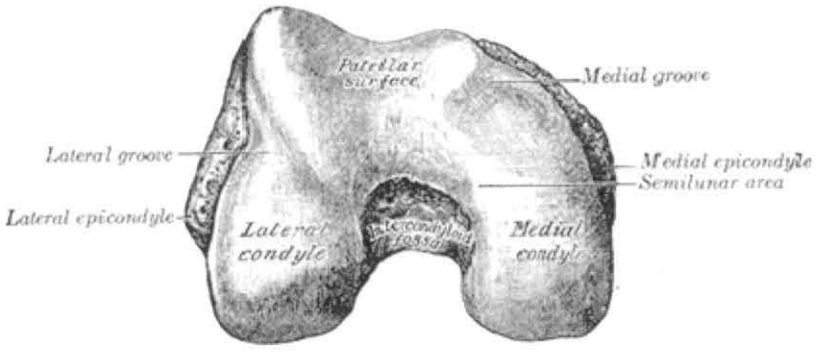

Figure 5 Lower extremity of right femur viewed from below [3]

2.1.2.2 Ligaments of the hip joint

The periarticular ligaments are essential for the stability of the joint. See Figure 6. The capsule, or capsular ligament, a form of cylindrical sleeve that surrounds the joint to

retain the cartilaginous layers and synovial fluid, encloses the femoral head. It is attached to the iliac bone at one end and the upper end of the femoral shaft at the other. It is composed of four distinct sets of fibers that give the joint stability in all articulating directions.

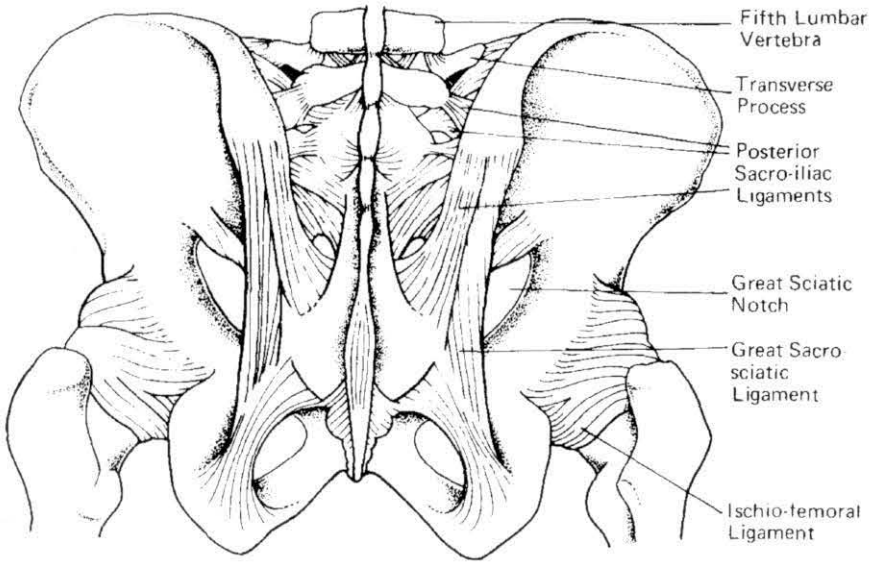

Figure 6 Ligaments of the pelvis viewed from behind [2]

Three main ligaments surround the capsule of the hip both anteriorly and posteriorly [41, 42]..

2.1.2.3 Muscles surrounding the hip joint

The hip joint is encompassed by a number of muscles that enable movement in a variety of directions [41, 42]. Combinations of musculature actions give additional twisting and rotational movements. Figure 7 shows both the anterior and posterior views of the main muscles in the leg. Extension of the hip is primarily caused by the gluteus maximus, the coarsest and strongest muscle in the body. It has an approximate contraction length of 150 mm, and is relaxed when the centre of gravity of the body falls behind the hip joint,

when the iliofemoral ligament is in tension. Its action in straightening the bent thigh is assisted by the hamstring muscles (biceps femoris, semitendinosus, and semiembranosus), whose efficiency is dependent upon the angle of flexion.

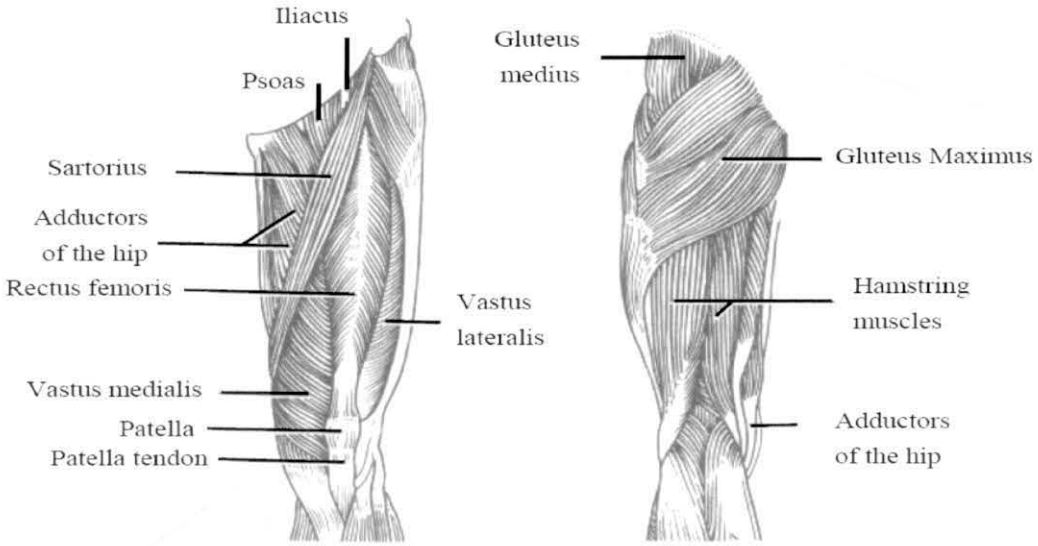

Figure 7 Anterior and posterior view of the main muscles of the lower limb [2]

The groups of muscle which lie anterior to the frontal plane though the hips' centre cause flexion. They consist of the psoas, iliacus, sartorius, rectus femoris, pectineus, adductor longus, and gracilis. Some of the forces created are not necessarily in complete flexion, causing some secondary twisting or rotation, although the primary components produce lifting of the thigh. The main muscle that causes abduction is the gluteus medius, which inserts into the lateral surface of the greater trochanter, and connects to the iliac crest. It has a direction of action almost perpendicular to its lever arm, and is hence highly efficient. It is helped by the action of the gluteus minimus and the tensor fasciae latae. Although numerous muscles are able to pull the leg towards the body centre line, adduction is primarily caused by the action of the adductor magnus, which attaches to the inferior surface of the pubis. All of the normal ranges of hip motions are

obtained through forces applied by one or more of the muscles that surround the hip. Many of these muscles remain redundant during certain actions of the hip, and combinations of muscles are used throughout the gait cycle.

2.1.2.4 Blood supply to the hip

Blood supply to the hip is provided by the medial and lateral circumflex femoral arteries, both usually branches of the deep artery of the thigh (profunda femoris) [42]. In addition, there is a small contribution from an artery in the ligament of the head of the femur, which is a branch of the posterior division of the obturator artery. This supply becomes important to avoid avascular necrosis of the head of the femur, should the blood supply from the medial and lateral circumflex arteries be disrupted (e.g. through fracture of the neck of the femur along their course). The hip has two anatomically important anastomoses: the cruciate and the trochanteric anastomoses, the latter of which provides most of the blood to the head of the femur [43]. These anastomoses exist between the femoral artery or profunda femoris and the gluteal vessels.

2.1.3 Failure of the natural hip joint

The human hip joint is susceptible to failure for a wide variety of reasons. The majority of problems, however, are associated with two main groups of disorders. The first is trauma of the joint, while the second is arthritis.

2.1.3.1 Trauma, osteopenia and osteoporosis

Generally, trauma results in a femoral neck fracture. This is most frequent in the elderly, whose bones are subject to mechanical decline. This decline is mostly the result of degenerative diseases, such as osteopenia and osteoporosis. Osteopenia is the thinning of bone mass and is considered a serious risk factor for the development of osteoporosis.

Osteopenia is commonly seen in people over the age of 50 that have lower than average bone density but do not have osteoporosis. The diagnostic difference between osteopenia and osteoporosis is the measure of bone mineral density. Osteoporosis is characterized by a loss of bone mass caused by a deficiency in calcium, vitamin D, magnesium, and other vitamins and minerals. [4] According to the US National Osteoporosis Foundation, osteoporosis affects 10 million Americans, mostly women. Thirty-four million more Americans are estimated to have osteopenia, putting them at risk for osteoporosis and therefore at higher risk of femoral neck fracture. Total reconstruction of the joint provides one of the most common solutions for a neck fracture patient.

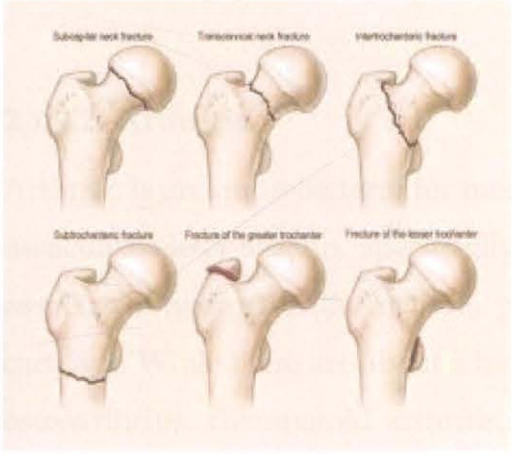

Figure 8 Fractured neck of femur [44]

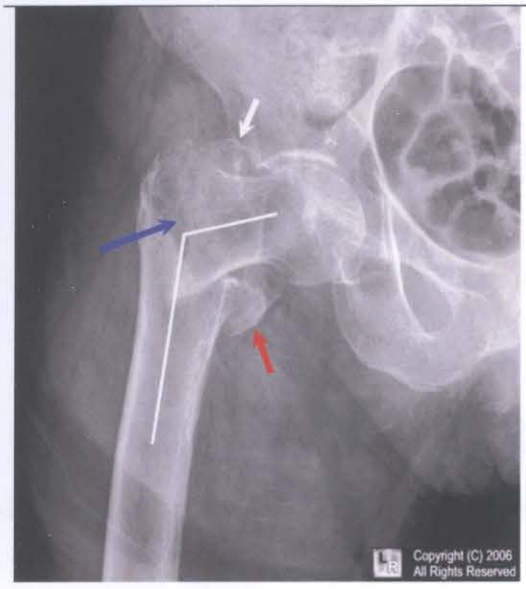

Figure 9 Fractured neck of femur [45]

2.1.3.2 Arthritis

Arthritis is an umbrella term for more than a hundred medical conditions that affect the musculoskeletal system, specifically joints where two or more bones meet. Problems associated with arthritis include, pain, stiffness, inflammation, and damage to joint cartilage. While there are about a hundred forms of arthritis, the three most significant - osteoarthritis, rheumatoid arthritis, and gout - account for more than 95 per cent of cases in Australia [4]

The great majority of total hip replacement candidates have osteoarthritis. As described in the introduction this has a significant impact on modern society. Osteoarthritis is the most common type of hip arthritis. Also called wear-and-tear arthritis or degenerative joint disease, osteoarthritis is characterized by progressive wearing away of the cartilage of the joint. As the protective cartilage is worn away by hip arthritis, bare bone is exposed within the joint. See Figure 10. The condition is most commonly diagnosed on an X-ray with loss of joint space being the telling sign. See Figure 11.

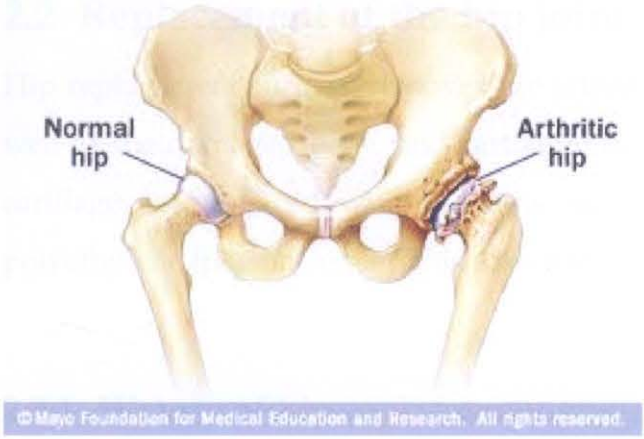

Figure 10 An arthritic hip vs a normal hip [46]

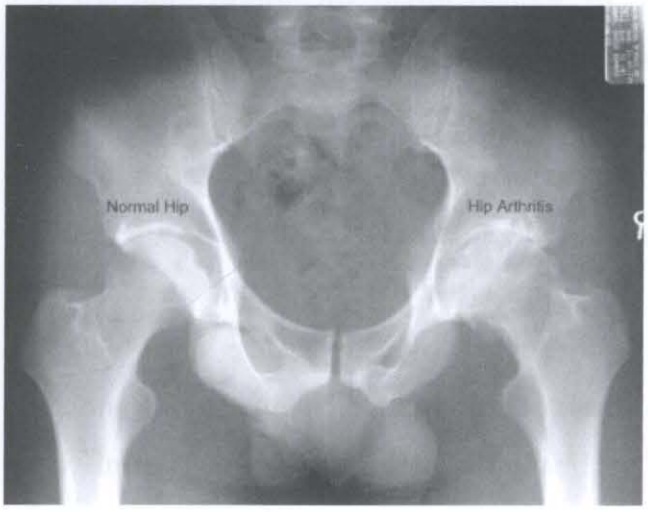

Figure 11 Diagnosis of hip OA: Loss of joint space visible on X-ray [47]

It is thought that general wear and tear, and joint overloading cause osteoarthritis. Generally, the disease occurs later in life. Surgical intervention can often diminish these problems, but ultimately replacement of the joint is currently the best solution. [4]

2.2 Replacement of the hip joint

Hip replacement surgery removes the arthritic ball of the upper femur (thigh bone) as well as the damaged bone, and cartilage from the hip socket. The damaged bone, and cartilage are replaced with implants made from materials including metal alloys, polyethylene (plastic), or ceramic material.

2.2.1 History of hip replacement surgery

For well over a century surgeons have been searching for strategies to treat arthritis. Due to the progression, destruction, and deterioration of joints, it was clear that surgery was the only option for many people, in order to relieve the pain associated with arthritis and to keep their joints mobile. Initial attempts to treat arthritic hips included arthrodesis (fusion), osteotomy, nerve division, and joint debridements. The goal of these early debridements was to remove arthritic spurs, calcium deposits, and irregular cartilage in an attempt to smooth the surfaces of the joint. Materials that could be utilized to resurface or even replace the hip were investigated, including muscle, fat, chromatized pig bladder, gold, magnesium, and zinc. However, all met with failure; surgeons and scientists were unable to find a material that was biocompatible with the body, and yet strong enough to withstand the tremendous forces placed on the hip joint.

The earliest recorded attempts at hip replacement, by Gluck in Germany in 1891, used ivory to replace the femoral head. In 1925, Smith-Petersen, a Norwegian-born American physician and orthopaedic surgeon, developed the concept of 'mould arthroplasty' when he produced a piece of glass in the shape of a hollow hemisphere, which could fit over the ball in the hip joint and therefore provide a smooth surface for movement [48]. Although incompatible with the stress of walking, the concept of "mould arthroplasty" was born and new materials, most notably corrosion-resistant stainless steel, were investigated and developed. Perhaps the most important early breakthrough in the search for new materials was the manufacture of a cobalt-chromium alloy called

Vitallium in 1936, which was both very strong and resistant to corrosion [49]. It was immediately applied to orthopaedics and has continued to be employed in various prostheses since. However, although a great success, the inadequacy of the resurfacing technique resulted in unpredictable pain relief and limited hip movement for many patients. Thus, the technique was limited in the types of deformity to which it could be applied.

In 1939, hemiarthroplasty was introduced. This procedure involved replacing the entire ball of the hip with a metal stem that was placed into the marrow cavity of the femur, and connected to a metal ball which fitted into the hip socket, [50]. Hemiarthroplasty could be used to treat both hip fractures and certain arthritis cases; however, it only addressed the problem of the arthritic femoral head (the ball), and did not prevent continued deterioration of the diseased acetabulum (hip socket). Although very popular in the 1950's, results of hemi-arthroplasties remained unpredictable, and with no truly effective method of securing the component to the bone, many patients developed pain due to loosening of the implant.

The continual search for improved materials saw the introduction of acrylic material to replace arthritic hip surfaces in 1938 [49]. However, although providing a smooth surface, the acrylic had a tendency to loosen. This problem was overcome by a Dr. Edwarc J. Haboush who utilized a fast setting dental acrylic to glue the prosthesis to the bone.

Arguably, the key figure in the history of total joint replacement was Sir John Charnley, an innovative English surgeon who aggressively pursued effective methods of replacing both the femoral head and acetabulum of the hip [50]. In 1958, he addressed the eroded arthritic socket by replacing it with a Teflon implant with the aim of providing a smooth joint surface to articulate with the metal ball component. Although unsuccessful, later trials with polyethylene realised this goal. The polyethylene socket,

as well as the femoral implant to the bone, was secured to the bone using polymethylmethacrylate (bone cement) and "total hip replacement" was born.

By 1961, Charnley was performing the surgery regularly and with good results. He further improved the techniques and component designs. Thousands of people were successfully relieved of their hip pain and the long term results became very predictable. In recent years, there has been considerable effort and research to try to further improve the methods of fixation. Occasionally, it has been found that cement fixation breaks down over time. A living type of bond would theoretically be longer lasting and possibly stronger. To this end, implants with textured surfaces, which allow bone to grow into them, were developed. These were used experimentally in animals before being used extensively in humans [51, 52]. Following on from this early success various cementless implants, used in total hip replacement today, have shown excellent long-term success rates [53-57]. Advantages of cementless implants include decreased operating time [58] and lower complication rate, but they could be considered to be more technically demanding when compared to cemented implants. [59]

2.2.2 Total hip replacement today

Total hip joint replacement is an orthopaedic success story, enabling hundreds of thousands of people to live fuller, more active lives.

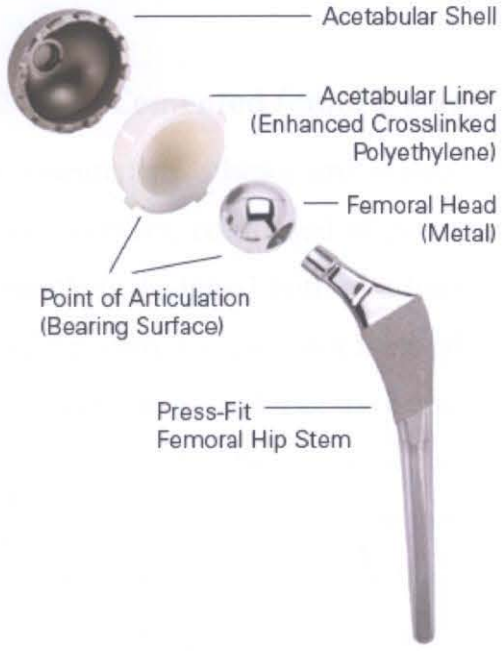

Figure 12 Total hip joint prosthesis typical components [60]

Using metal alloys, high-grade plastics, and polymeric materials, orthopaedic surgeons can replace a painful, dysfunctional joint with a highly functional, long-lasting prosthesis. The hip joint is called a ball-and-socket joint, because the spherical head of the thighbone (femur) moves inside the cup-shaped hollow socket (acetabulum) of the pelvis. To duplicate this action, a total hip replacement implant has three parts: (i) the stem (or femoral component), which fits into the femur, (ii) the prosthetic femoral head (ball), which replaces the spherical head of the femur, and (iii) the acetabular cup, which replaces the worn out hip socket (Figure 12). Each part comes in various sizes and designs to accommodate various body sizes and types. The femoral component can be cemented or uncemented and each part can be made of various materials including titanium, cobalt chromium, and steel. In addition, prosthetic femoral heads can be monolithic, with the stem and ball as one piece, or modular, consisting of different head dimensions and/or neck orientations, which can be attached via a taper to allow for additional customization in fit.

2.2.2.1 Cemented femoral stems

Cemented prostheses are seated within the femoral shaft surrounded by a mantle of bone cement, composed of polymethylmethacrylate (PMMA), for fixation. The cement mantle is designed both as a load-mediating compliant layer between the bone and the rigid prosthesis, and as a method of accommodating any geometrical inconsistencies. It has been suggested that the cement mantle provides greater ability to transfer load from the femoral implant to the surrounding endosteal bone [61]. In addition, creep or stress relaxation of the acrylic cement may accommodate long-term variations in the geometry of the bone due to remodelling or age related effects. Uniform load distribution can therefore be achieved over long periods of time.

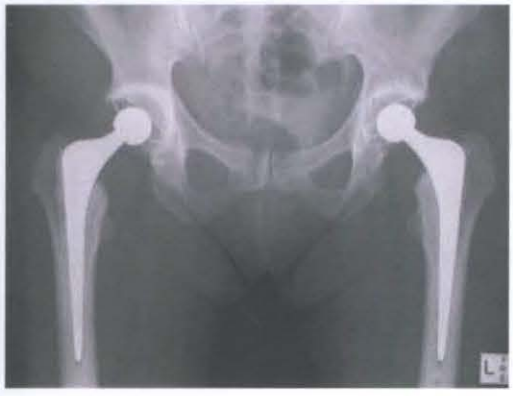

Figure 13 Bilateral cemented total hip replacement [62]

2.2.2.2 Cementless femoral stems

Cementless fixation for femoral stems is widely used in total hip arthroplasty, with all major companies offering products of this category. Without cement, the initial implant fixation wholly depends upon the tight apposition of the metal implant against the bone. The force with which the implant is initially compressed into the shaft of the femur is aimed to create the tight interference fit required for integration with bone. [63] This

tight interference fit in the initial period prevents large movements between the bone and prosthesis while the bone grows onto or into the implant surface.

Figure 14 Some cementless (press-fit) stems from (Stryker's website)

This process bone integration process takes several months and results in the long-term rigid fixation of the prosthesis into the bone. Some femoral stems designed for cementless mechanical press-fit hold within the proximal femur are shown in Figure 14. Several techniques are used to increase the long-term stability of cementless prostheses. Plasma-sprayed and hydroxyapatite (HA) coating on a grit-blasted surface implant are known to successfully encourage bony in-growth, which is essential for their long-term fixation [64]. Roughened surfaces, such as a plasma sprayed titanium surface, are designed to allow boney in-growth, where long term fixation is achieved because the new bone has grown into the roughened surface mechanically locking the prosthesis to the bone structure. HA (hydroxyapatite) surfaces work slightly differently. As HA (hydroxyapatite) is chemically similar to real bone (similar enough to trick the bone into thinking that it is actually bone) the new bone grows onto the HA (hydroxyapatite) coating. A direct comparison of these types of fixation is studied in Chapter 3. See Figure 15.

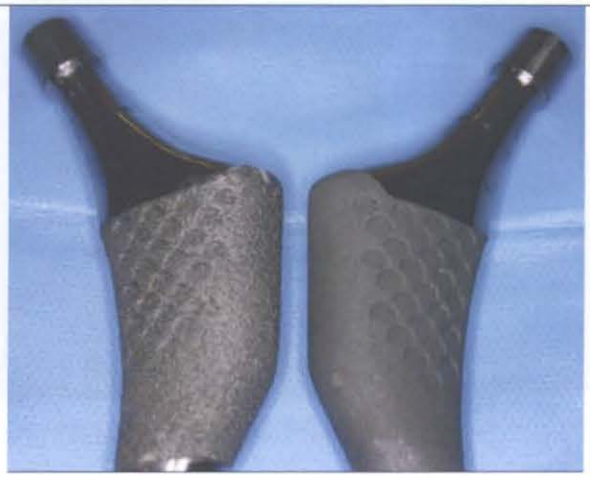

Figure 15 Porous coating only (left) vs HA coating only (implant samples used for testing in chapter 3)

There are designs available with both a roughened coating as well as a HA (hydroxyapatite) coating. For example, a commercially available coating described by Serekian [65] called "peri appetite" completely coats the entire three dimensional surface of the pouorus metal coating. Figure 16. This "three dimensional" HA (hydroxyapatite) coating of a metal coating was shown to dramatically increase the inteface shear (a measure of bonding strength), especially in the early post operative period in a canine model [65]. This superiority was verified in an Radiostereometric Analysis (RSA) human study, where a randomised prospective controled trial was conducted with periapatite coating on the femoral component of a total knee replacment. [66]

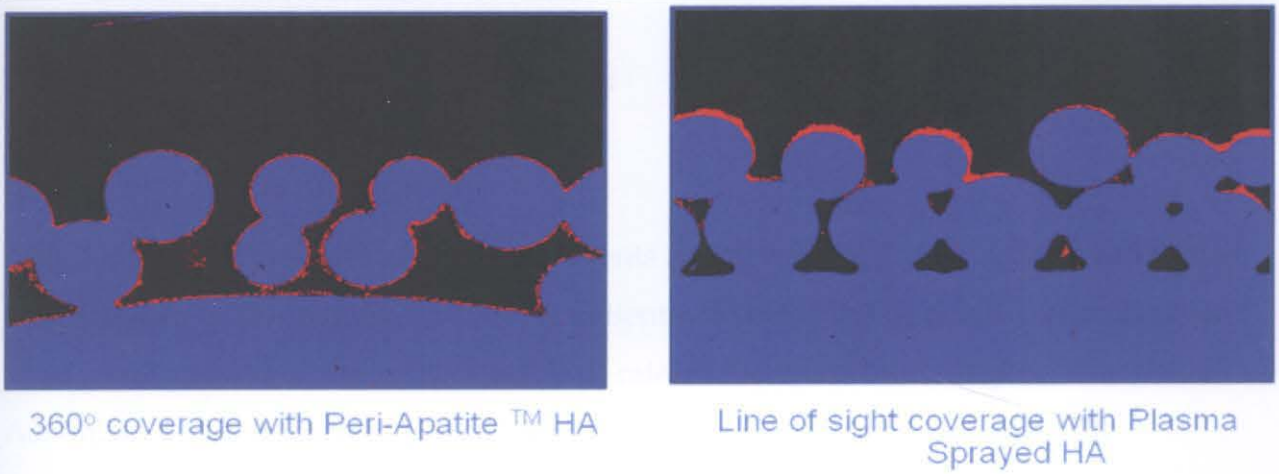

Figure 16 Peri-patite HA compared to a plasma sprayed HA on porous coating [65]

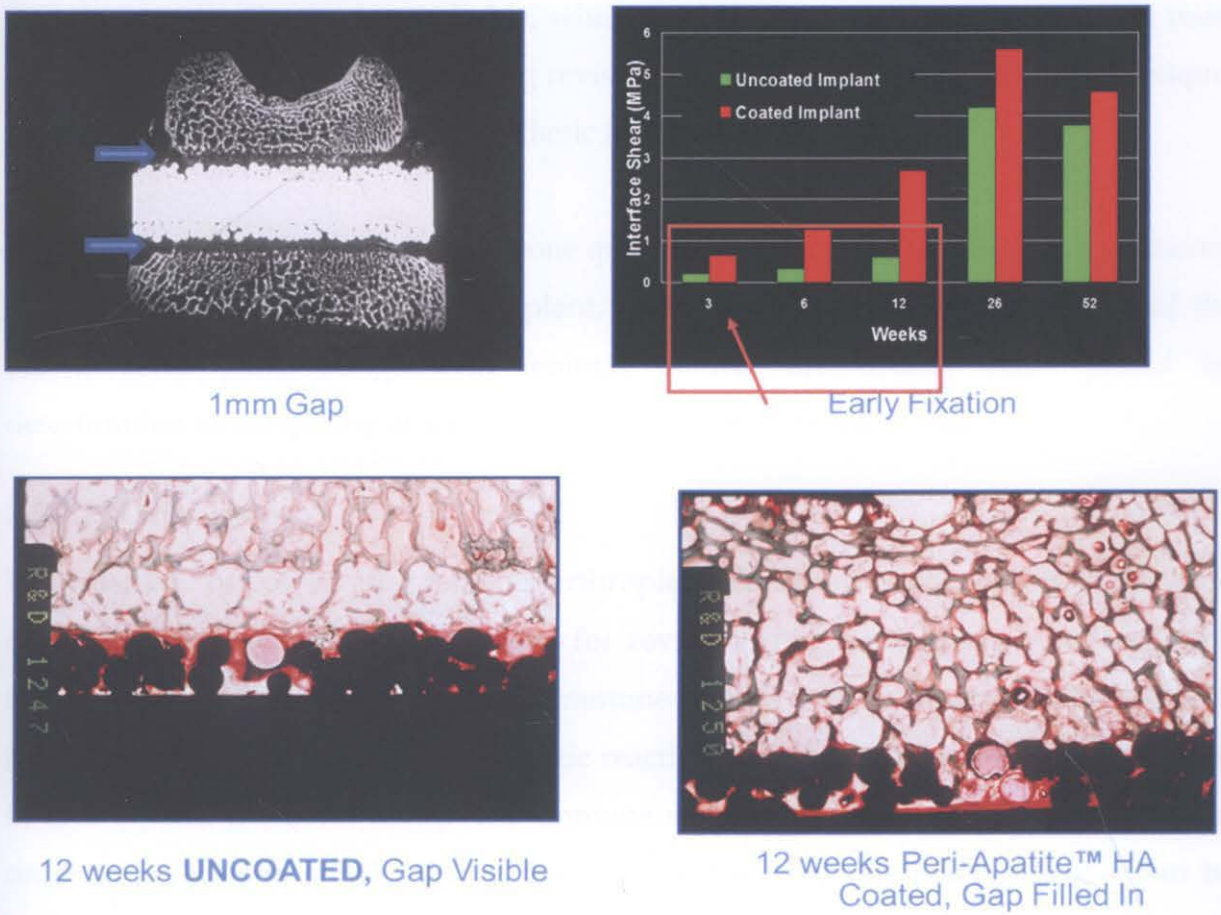

Figure 17 Peri-Apatite in a canine 1mm gap model from [67, 68]

2.3 Failure of hip replacements

2.3.1 Total hip replacements

Although the success rates of hip replacements are high, some 4 - 8 % still fail within the first ten years post-operatively. [69] As patients are often living much longer than ten years post operation, the overall revision rate is therefore much higher. The overall Australian revision rate for all total hip arthroplasty is estimated at 20–24%.[70]

Failure of implants can be categorized into short-term and long-term failures. Initial, short-term failures are considered to occur over a period of weeks or months postoperatively. On the femoral side, which is of most interest to this work, the most common early complications, causing revision, are due to infection, surgical technique, poor initial cementing, and peri-prosthetic fractures.

A wide variety of factors, including bone quality, levels of physical activity, age, obesity of the patient and design of the implant, all influence the long-term integrity of the reconstructed joint. Longer-term femoral failures are usually characterized by deterioration in the quality of the bone supporting the femoral implant.

2.3.1.1 Osteolysis

Periprosthetic osteolysis after total hip arthroplasty constitutes one of the most common complications and is a leading reason for revision after a primary hip replacement. Osteolysis is a condition in which the immune system triggers an attempt to reabsorb bone into the body. This adverse biologic reaction occurs in response to foreign bodies in and around the bone tissue. The immune system stimulates osteoctastogenesis in order to isolate and slowly absorb the material back into the body, where it can be converted into materials that pose no threat. Unfortunately, osteolysis can also begin to

deteriorate healthy bone tissue. This occurs when the immune system incorrectly identifies the nature of the so-called foreign material. [71]

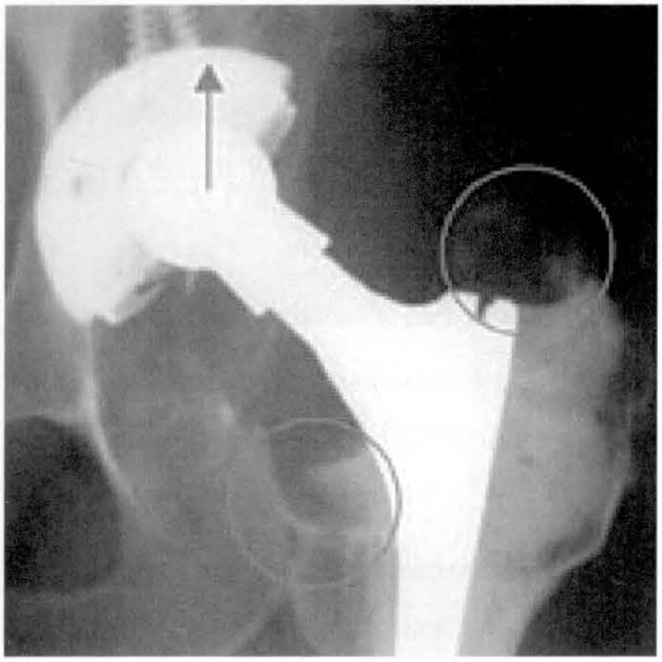

Figure 18 Polyethylene induced osteolytic lesions around femoral stem [72]

These foreign bodies have commonly been identified as Ultra High Molecular Weight Polyethylene debris particles that migrate around the joint causing a biologic reaction in the bone that results in osteolytic lesions. [71]. It is estimated that polyethylene wear greater than 0.2 mm annually results in focal osteolysis on radiographs within 5 years [73]. Ultra High Molecular Weight Polyethylene wear particles vary in size (usually 1 μm in thickness and 4 to 10 μm in length) and are best seen when viewed with transmitted polarized light [74]. Ultra High Molecular Weight Polyethylene wear particles induce a macrophage, or foreign-body, inflammatory response. Aged Ultra High Molecular Weight Polyethylene may show extensive pitting, cracking, delamination, and other deformities. Ultra High Molecular Weight Polyethylene failure can result in massive, aggressive granulomatous inflammation as shown in the hitological slide in Figure 19.

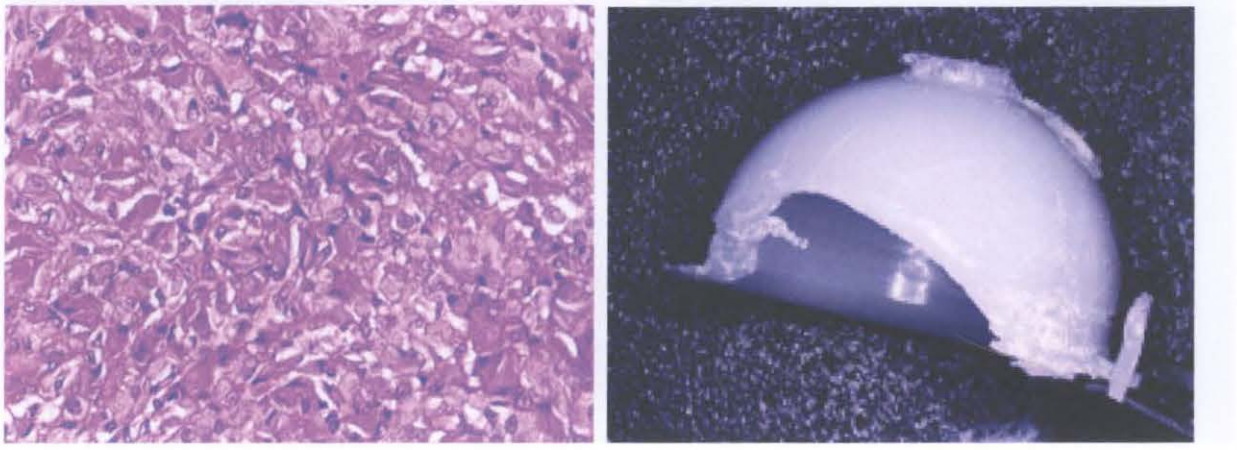

Figure 19 Periarticular granulomatous inflammation in response to ultrahigh molecular weight polyethylene (UHMWPE) wear debris (From Long 2008)

Efforts to reduce osteolysis caused by polyethylene particles led to the development of alternate bearing materials; such a ceramic on ceramic. The mechanics of this bearing result in reduced friction and therefore reduced wear. Osteolysis has also been reported in association with ceramic-on-ceramic bearing couplings [75] but the rate is much lower with ceramic bearings. Figure 20 shows that the histology seen when there is ceramic debris is quite different to what was seen above for poly debris.

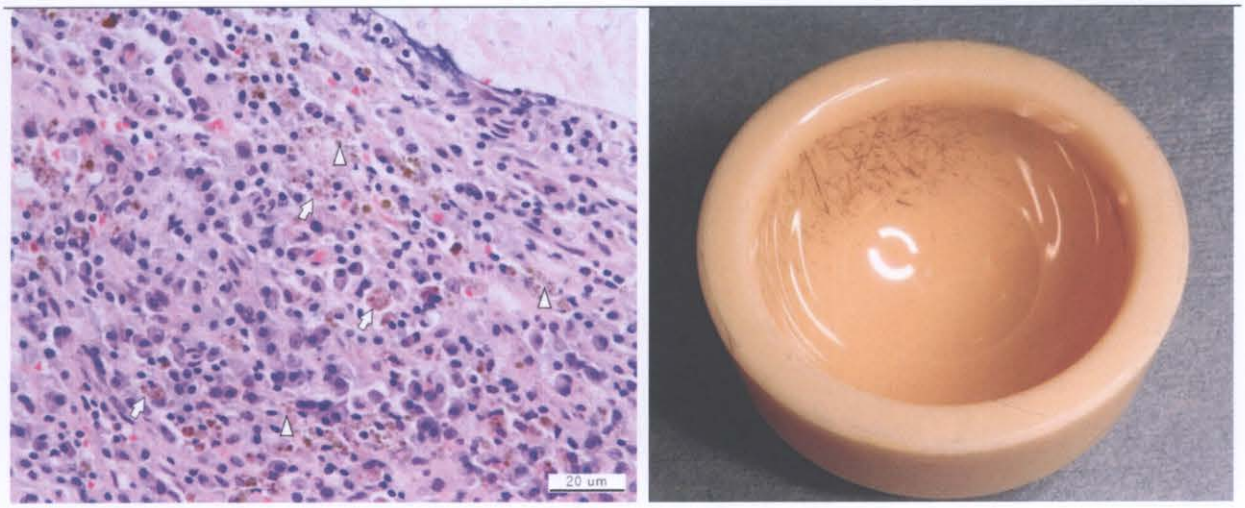

Figure 20 Osteolysis due to alumina ceramic wear [75]

2.3.1.2 Metal on metal articulations

Large diameter metal-on-metal articulations in total hip arthroplasty became popular in recent years because the bearing allows significantly larger diameter heads which offers the advantage of improved stability and increased range of motion, when compared with smaller diameter bearings [1-4]. The mechanical reasons for the increased stability and range of motion are discussed in detail in section 2.6.2.1 in relation to femoral head resurfacing. Another advantage of metal-on-metal articulations is the potential for lower wear rates and improved durability [5-8,10]. These proposed advantages have caused an increase in the use of large diameter metal-on-metal articulations worldwide. However many concerns still exist for metal-on-metal articulations. Metal ion levels, hypersensitivity, and pseudotumor reactions have been widely reported and continue to be an area of ongoing research [11-18]. Again, the debris in the tissue shown in the histology slide of Figure 21 differs from that seen for poly and ceramic.

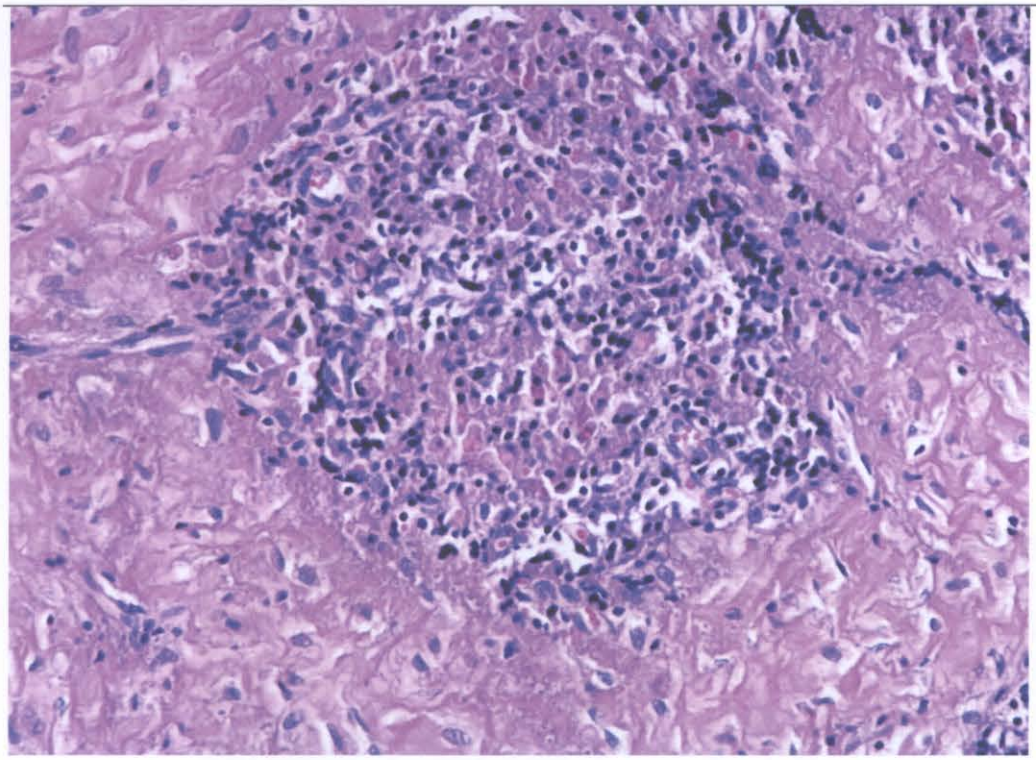

Figure 21 Histology of osteolysis due to metal wear from Kim 2004

2.3.1.2.1 Major concerns with metal- on- metal bearings

Adverse local soft-tissue reactions from metal ion debris are a relatively rare occurrence but are associated with devastating complications such as massive osteolysis and subsequent implant failure. Earlier in the story of hip resurfacing Hallab's [76] work on metal sensitivity suggested , firstly, that the incidence of dermatologic sensitivities to metals in arthroplasty patients is higher than in the general population. Secondly, the risk of sensitivity to orthopedic implants is minimal and it is unclear whether metal sensitivity contributes to implant failure. Recently there has been significant public attention to metal-sensitivity problems because of the recall by Depuy Orthopaedics (a Johnson and Johnson company) of the Articular Surface Replacement (ASR) metal-on-metal total hip replacement. The first description of a local reaction to metal bearings was provided by Evans and colleagues [77] in 1974 and was believed to be related to a hypersensitivity reaction to cobalt chrome alloys. Since the initial description, metal sensitivity has been further characterized by a predominantly lymphocytic immune

response and is histologically described by aseptic lymphocytic vasculitis-associated lesions (ALVAL) in both the presence and absence of excessive metal wear [78-80].

Clinically, soft-tissue changes due to metal-on-metal hypersensitivity are manifested through effusions or soft-tissue masses referred to as pseudotumors and lead to early osteolysis and failure. [81] Pseudotumor formation has been associated with higher circulating levels of cobalt and chromium [82] and has recently been linked to increased edge loading and increased combined anteversion. [83]

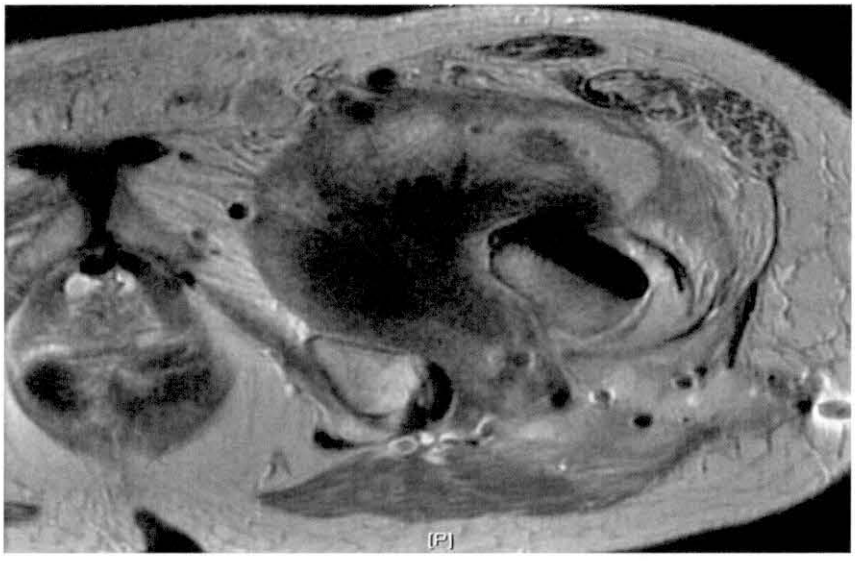

Figure 22 MRI image showing a larger pseudotumor resulting from metal sensitivity [84]

2.3.1.3 Bone remodeling

An unsatisfactory bone remodeling response around the implant is another cause of implant failure. This occurs when it is not possible to maintain sufficient bone mass around the implant. Abrupt changes in the local loading conditions can alter the growth patterns of the bone. This effect often occurs around implants when the density of the surrounding bone is altered, and is referred to as bone remodeling; non-anatomic load

transfer to the proximal femur causes this. The non-anatomic load transfer causes the bone to adapt by laying down new bone in the newly loaded areas and removing bone in unloaded areas. This eventually results in loss of stability of the implant in the bone.

Over longer periods of time, this effect plays a crucial role in bone loss and can lead to loss of support and therefore loosening of the prosthesis. If the process continues, total failure of the joint can occur. Figure 23 demonstrates both osteolysis (previously described) and remodelling around a cemented femoral stem.

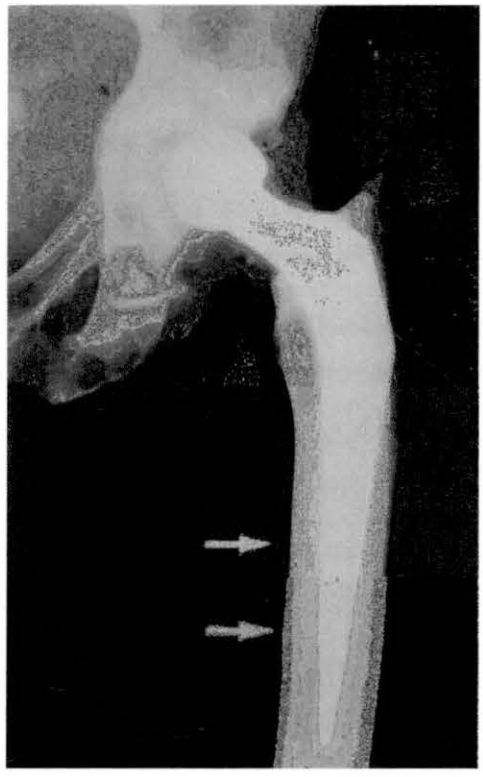

Figure 23 Radiograph showing results of long-term remodeling with bone resorption proximally and increased bone mass distally [85]

It is important to notice the deposition of bone matrix on both the periosteal and endosteal surfaces of the medial femoral shaft. This is a result of long-term remodeling, which is often seen around this design of stem. It is possible to use the evidence of this

sclerosis to validate the clinical relevance of modeling predictions. In addition, cortical reabsorption is seen in the areas surrounding the greater trochanter. This remodelling effect is especially significant in the modes of failure of modern implants. Reduction in bone mass around, or total reabsorption away from the surface of an implant can affect or even initiate tipping or pivoting of the prosthesis. Bannister compared the modes of failure of the Muller straight stem (small collar), the Muller curved stem (larger collar) and the Exeter (collarless) prosthesis that had survived a 10 year period or greater [86]. The most notable difference in the stem designs concerned the neck of the femoral component. It was found that the integrity of the stem was directly related to the X-Ray lucency at the bone-cement interface. The formation of osteolytic cysts and migration of the implant into the varus position were strongly associated with the need for revision surgery. In addition, the occurrence of cement mantle subsidence within the bone (or pistoning of the cement mantle at the bone-cement interface) was five times as frequent in the revision hips. Perhaps the most notable observation, however, was that subsidence of the implants within the cement mantle (at the stem-cement interface) was five times as common in the prostheses that survived. It was suggested that the allowance of this subsidence of the stem influenced the modes of failure of the implants. The analysis showed that failure due to pistoning of both the implant and cement within the bone was observed in three times as many revision cases as controls. This mode of failure was seen 6 to 7 times more frequently in the Muller curved stems as in the Exeter prosthesis. This observation is supported by Fowler et al. who examined the history of the Exeter stem [61]. Subsidence of the implant within the cement mantle appeared to benefit the long-term integrity of the joint. It was suggested that the capability of the implant to transfer load to the surrounding bone was improved by the movement of the implant within the cement. The taper of the stem appeared to induce lateral creep of the proximal cement, resulting in continued engagement of the cement mantle with the bone. Experiments went on to show that the stem-cement interface friction in the matt version of the stem was greater than double that of the polished counterpart. The reduced performance of the matt stem was attributed to the resulting

lack of subsidence of the implant. As a result, the smooth polished finish replaced the implant matt surface. The study went on to imply that any device, which might interfere with the subsidence of the stem at the stem-cement interface and prevent distal movement from occurring, (e.g. collars, flanges, texturing of the surface) would alter the engagement of the taper. As a result, reduction of the load transfer capability would occur, especially in the proximal regions. Marston et al. carried out a long-term study evaluating the differences between the Charnley and the Stanmore cemented prostheses in order to investigate, amongst other things, the effect of the femoral head size on longevity [87]. A sample of 213 Stanmore and 200 Charnley implants were reviewed post-operatively at 5 to 10 years (mean 6.5). No statistically significant difference in the rate of revision surgery was recorded between the stems (both resulted in a revision rate of 4.0%), and no difference was found in the effect of the size of the femoral head. Surprisingly, approximately equal subsidence was reported in both stems, despite the large collar on the Stanmore.

2.3.1.4 Clinical differences between different implant designs in total hip arthroplasty

Due to the heterogeneity of patients receiving implants, together with differing study protocols, consistent evaluation of the long-term success of hip prostheses and reliable assessment of innovative new stem designs and new materials is somewhat impractical and inefficient in vivo [88-91].

Revision rates for different implants can vary widely. Some designs have been reported to have very low rates of revision, for example a 0-5% revision rate after 10 to 15 years [88, 89] whilst others have been reported to be as much as 27% after 8 to 10 years. [90, 91] However, for the vast majority of available designs there is surprising little discernable difference between revision rates. A look at the 2010 Australian Joint Registry report shows that surgeons face a difficult choice when selecting which

prosthesis design to use. Even when considering very different design philosophies, such as cemented or cementless fixation the choice is confusing. The revision rate for cementless stems in the early years after a total hip surgery is slightly higher than that for cemented fixation. However, at around eight years the cumulative revision rate for cemented stems rises relatively sharply and overtakes that of cementless fixation. When the surgeon is concerned with longevity, this creates an unanswerable paradox.

Figure HT11: Cumulative Percent Revision of Primary Total Conventional Hip Replacement by Fixation (Primary Diagnosis OA)

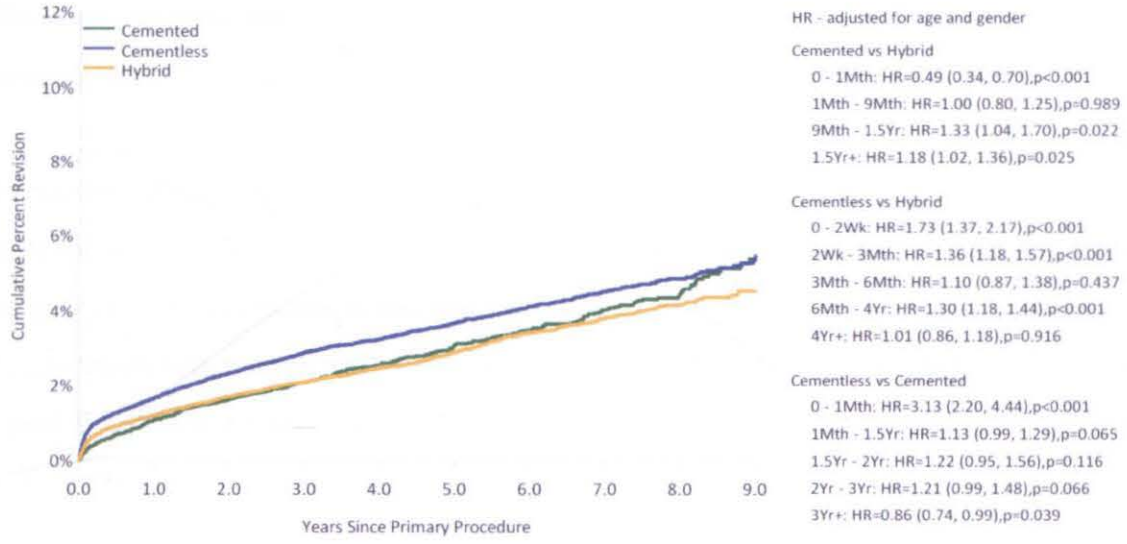

Figure 24 Cumulative percent revision of femoral component by fixation from the Australian Joint registry

When considering less profound design differences the problem becomes even more confusing. Some variations in the revision rate may be attributable to differences in prosthesis design; however, the population of patients in which each design is used may bias the results. As a hypothetical example, a certain newer prosthesis may have a higher revision rate than an established alternative design but this may be because this newer prosthesis has certain advantages, which mean it is more suitable for use in more

challenging patients. These more challenging patients will invariably have a higher likelihood of revision for reasons unrelated to the implant. In this circumstance, judging the efficacy of the prosthesis by revision rate alone would not be appropriate.

2.3.1.5 Increasing usage of cementless stems for total hip arthroplasty

Considering the above-described paradox, deciding on which types of prosthesis should be used by surgeons and should be studied further with the highest clinical relevance is not easy. One way to determine if a course of study will be clinically relevant is to consider implant usage trends. This will ensure that the results of studies are widely applicable and will therefore have a high impact on clinical practice.

Despite the good results of cemented stems, the trend in Australia and much of the western world is towards cementless fixation for stems. See Table 1. Knowing that the usage of cementless stems is increasing and that peri-prosthetic femoral fracture is more of a problem when cementless fixation is used. It is clear that efforts to reduce the risk of peri-prosthetic femoral fracture would be most effective if cementless fixation is the focus of the study.

Fixation	*Unipolar Monoblock*		*Unipolar Modular*		*Bipolar*		*All Patients*	
	N	*%*	*N*	*%*	*N*	*%*	*N*	*%*
Cemented	3038	13.7	2692	12.2	5044	22.8	10774	48.8
Cementless	9568	43.3	767	3.5	990	4.5	11325	51.2
Total	**12606**	**57.0**	**3459**	**15.7**	**6034**	**27.3**	**22099**	**100.0**

Table 1 Frequency of cemented and cementless hip replacements in Australia, 2006

2.4 Peri-prosthetic femoral fracture

Peri-prosthetic fracture of the femur after total hip arthroplasty is a major complication with high morbidity [92]. First described by Horwitz and Lenobel [93] , the prevalence of peri-prosthetic femoral fracture is on the rise due to both the increased number of

joint replacements and the high number of revisions as a result of demographic changes; such as increased age, and changes in lifestyle [94-96]. The success of total hip arthroplasty has led to a broadening of the indications for surgery, with both younger and more elderly patients eligible for surgery. The younger, more active patients are prone to fracture due to high energy trauma events. Whilst the elderly population are at risk from minor falls and stumbles, as well as an increased risk of loosening due to poorer bone quality as a result of osteolysis, osteoporosis, or multiple revision procedures [97-103]. Moreover, with hip arthroplasty now in its seventh decade, there are an increasing number of patients with revised and re-revised hips.

Peri-prosthetic fractures can be classified as either intra-operative or post-operative fractures, with post-operative fractures further classified as early or late. Risk factors for peri-prosthetic femoral fracture include female gender and increased age, although these may be confounded by medical co-morbidities including osteoporosis and rheumatoid arthritis, although the latter may be confounded by osteopenia; as well as treatment with corticosteroids and the presence of diseases, which may affect bone morphology or the healing process [16, 95, 101, 104].

Fracture risk is also increased in the setting of revision hip arthroplasty due to the effect of surgery-related osteopenia and osteolysis, and the presence of stress-risers related to previous procedures. Although revision is not investigated in this thesis. In addition, the risk of intra-operative peri-prosthetic femoral fracture is associated with technical problems such as damage to the proximal femur, under reaming of the femoral cortex, use of a large-diameter femoral stem, and a low ratio between the diameters of the femoral cortex and canal [105]. Postoperative peri-prosthetic femoral fracture, particularly early fractures, have been associated with inappropriate weight-bearing post-surgery.

Treatment of peri-prosthetic fractures represents a considerable challenge, with reported complication rates ranging between 31 and 52% [98, 106, 107]. As described in more detail below, it is recommended that treatment of both intra-operative and post-operative fractures be determined by the classification of the injury. The classification of which is often based on radiological appearance [108, 109]. In the case of peri-prosthetic fractures of the femur, the most widely used classification system is the Vancouver system [99, 110].

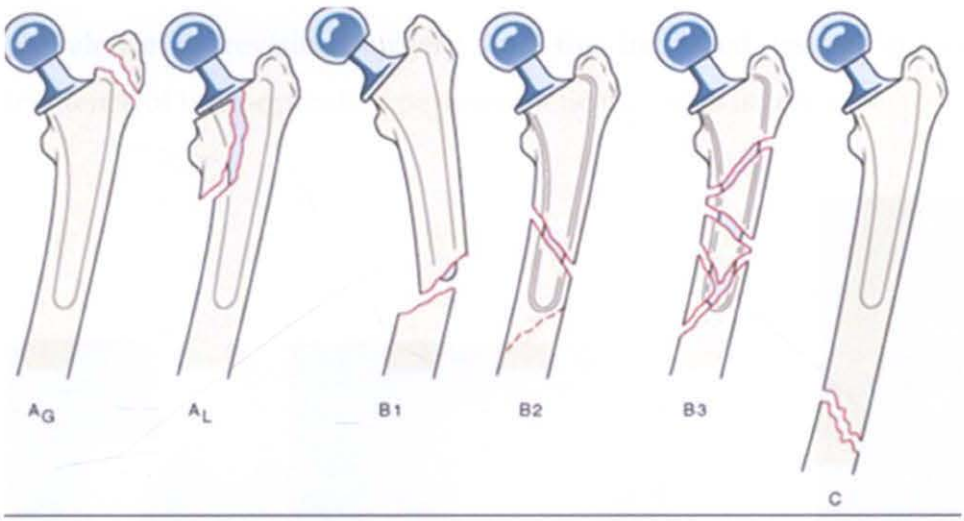

Figure 25 Vancouver classification for peri-prosthetic femoral fracture [111]

This system takes into account the location of the fracture, stability of the implant, and the quality of the surrounding bone stock, and has been used by a number of authors to define treatment algorithms [94, 109, 112]. Regardless of the treatment strategy, recovery is associated with a number of factors including concomitant morbidities and circumstances, such as local and generalized osteopenia, osteolysis, and endosteal ischaemia from metal or bone cement [113, 114].

2.4.1 Intra-operative peri-prosthetic femoral fracture

Intra-operative fractures most frequently occur during insertion of the femoral stem, with different fracture rates reported with different types of fixation method. Cemented stems have the lowest reported fracture rate with an incidence of 0.1-1% [115], whilst fracture rates of up to 5.4% [96] have been reported with uncemented stems. The higher incidence with uncemented stems has been suggested as being related to the effort required to obtain a sufficient press-fit to gain initial stem stability. [63] Intra-operative fracture rates are also higher in revision surgery, with reported incidences of 3.6% with cemented stems, and 20.9% with uncemented stems [116]. With the increased prevalence of revision surgery and the increased use of cementless fixation, the incidence of intra-operative periprosthetic fractures is rising.

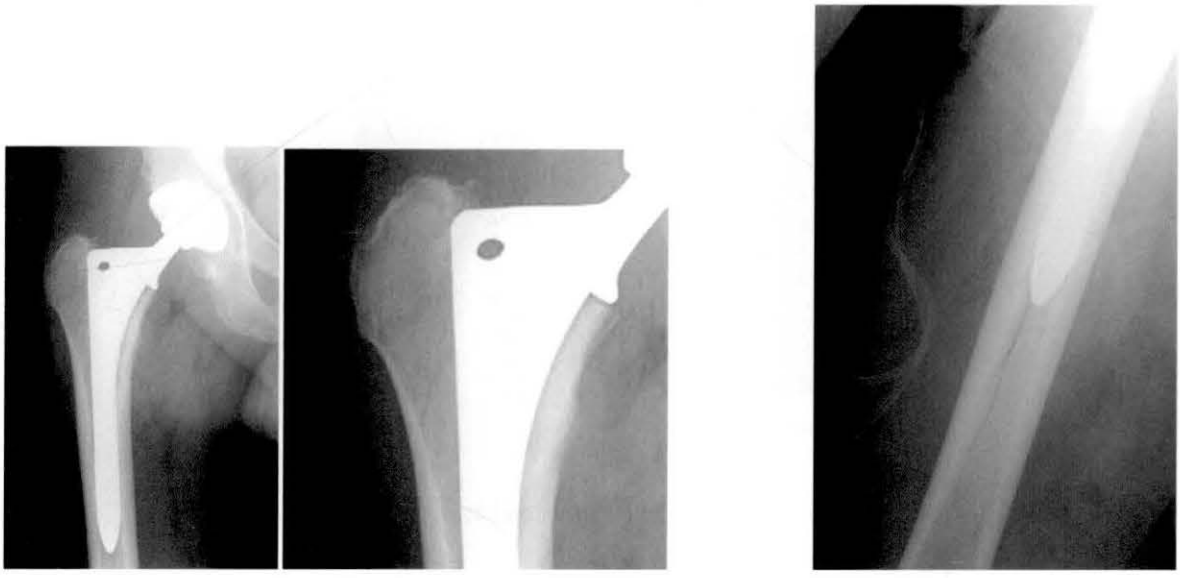

(a) (b)

Figure 26 (a) Intraopearative peri-prosthetic Femoral Fracture in metaphyseal region

(b) Intra-operative Peri-prosthetic femoral fracture in the diaphyseal region [117]

Intra-operative peri-prosthetic femoral fracture typically occurs in the metaphyseal or diaphyseal regions see Figure 26, in response to the surgical procedure. The fracture

occurs when the instruments or implant generates hoop stresses on the bone that are too great for the femur to resist [14, 96, 104] and it most frequently occurs during stem insertion. This is as a result of the need for the surgeon to achieve a firm initial press-fit of the implant against the bone to ensure long term prosthesis fixation [118, 119].

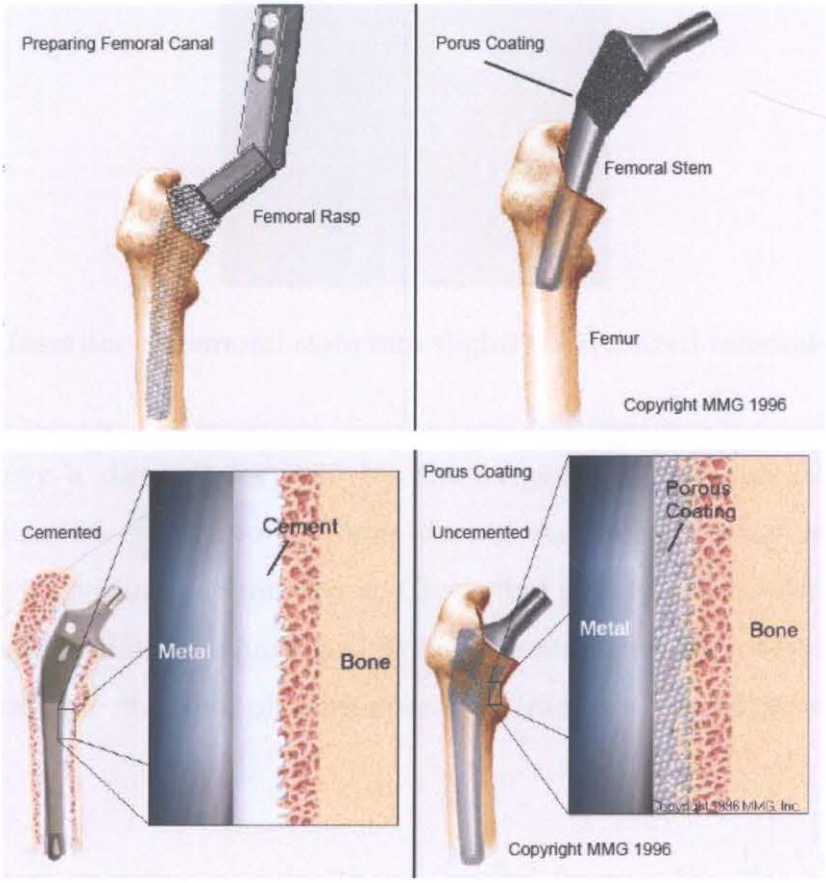

Figure 27 Insertion of femoral stem press fit against bone [120]

This initial press fit is typically achieved using a slightly undersized femoral canal preparation, and insertion of the prosthesis with the aid of a heavy mallet [14].

Figure 28 Insertion of femoral stem into slightly undersized femoral canal [14]

This is obviously a difficult scenario for the surgeon, as they need to balance the necessary application of load to the bone during the procedure against the strength capacity of the individual patient's bone. Given that patient's bone quality is variable and much of the population requiring a hip replacement have diminished bone strength, strategies to mitigate the risk of intra-operative fractures would be of considerable benefit.

Incidence of intra-operative peri-prosthetic femoral fracture has also been associated with design of femoral stem, varus positioning of the femoral component, and malposition of the prosthesis [121]. Intra-operative femoral fractures include many types and extents of fracture. Some fractures are recognized intra-operatively, while others are detected postoperatively with radiographic line or fracture displacement. Implant survival depends upon fracture pattern and, ultimately, implant stability. Accurate classification of intra-operative peri-prosthetic femoral fracture enables the appropriate clinical management to be determined [108, 122]. Classifications by location, displacement, and implant stability have been reported.

All classification systems label location proximal to distal, with complexity increasing as fractures move distally. In addition, most classification systems sub classify "A" as non-displaced and "B" as displaced fractures. Examples of classification systems for intraoperative peri-prosthetic femoral fracture include those by Mallory [123], which described type 1 fractures in the proximal femur, type 2 around the stem, and type 3 at or below the tip of the prosthesis; [124], which described type 1 fractures proximal to the prosthesis tip, type 2 at the region of the tip of the prosthesis and type 3 below the prosthesis; and Stanching [125] who described type 1 fractures as proximal, type 2 as long spiral fractures near the tip, type 3 propagating from stress points in the femur, and type 4 as unclassified.

Although all femoral classification systems generally grade based on location and displacement for description of fractures, the Vancouver system has become the most accepted [108, 122]. Modified to accommodate intra-operative fractures, the Vancouver system describes fractures in the same proximal-to-distal fashion with attention to configuration and stability of the fracture. Type A fractures are in the proximal femoral metaphysis, type B fractures extend or include the diaphysis but not distal diaphysis, and type C fractures extend distal and beyond long-stem fixation length. Each of these groups is further subdivided into type 1, 2, and 3. Type 1 includes perforations, type 2 represents linear non-displaced fractures, and type 3 includes displaced and unstable fractures. See Figure 29.

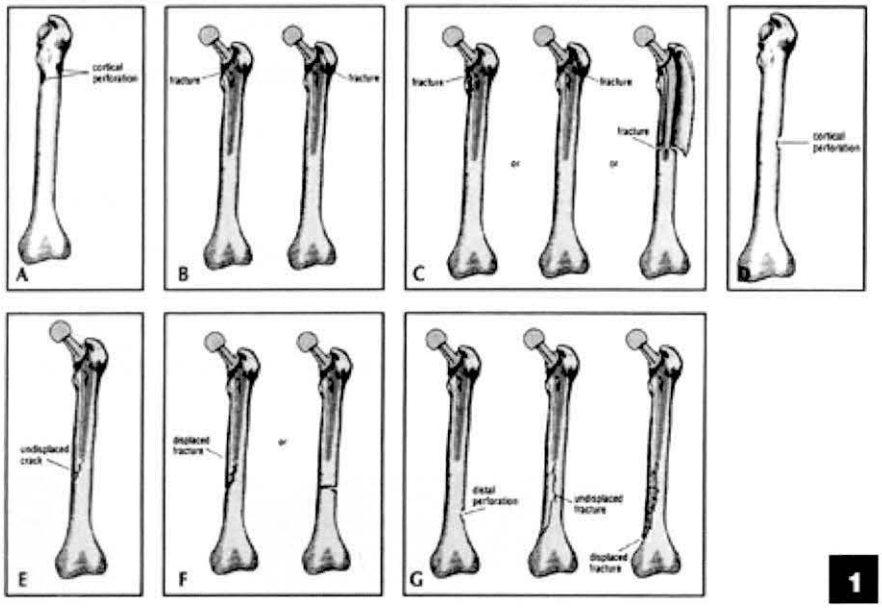

Figure 29 Intraoperative periprosthetic fractures of the femur – Vancouver classification [126]

Treatment of intra-operative peri-prosthetic femoral fracture aims to stabilize the components of the total hip arthroplasty and the fracture, prevent fracture propagation, and maintain component position and alignment. The methods for fixation of intra-operative fractures include cerclage wiring, plate osteosynthesis, and cortical allograft strut augmentation, depending on the site, prosthetic stability, and bone stock. Type-A1 fractures are generally stable and can, therefore, be treated with bone graft alone. Whilst less stable type-A2 fractures, risk of fracture propagation can be reduced by placement of cerclage wire before the insertion of a proximally coated stem [127]. Alternatively a porous-coated stem can be used, in which case the fracture may be ignored since there is no distal propagation of the fracture. Type-A3 fractures can be treated with a porous-coated disphysis-fitting stem or a tapered fluted stem. Type-B1 fractures, which usually occur during cement removal, and type-B3 fractures, which usually occur during hip dislocation, cement removal or final stem insertion, can be treated by bypassing the fracture with a longer stem [128]. If detected intra-operatively, type-B2 fractures, which usually result from increased hoop stress during implant placement, can be managed

by placement of cerclage wire. However, these fractures are often not diagnosed until after surgery, in which case treatment involves protected weight-bearing and close observation. Type-C1 fractures, which usually occur during cement removal or canal preparation, can be treated with morselized bone, bypassing the fracture site, or with cortical onlay allografts. Type-C2 fracture treatment involves the use of cerclage wires and augmentation with an allograft cortical strut whilst type-C3 fractures can be treated with open reduction and internal fixation [127].

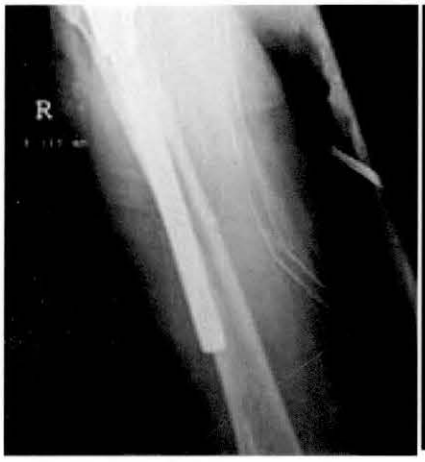

Figure 30 Intraoperative B1 fracture. [126]

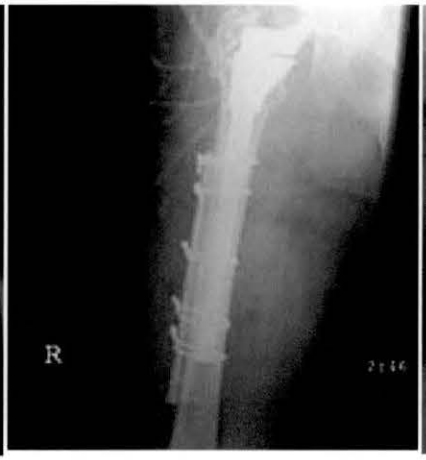

Figure 31 Intraoperative B1 fracture with strut and cerclage wires. [126]

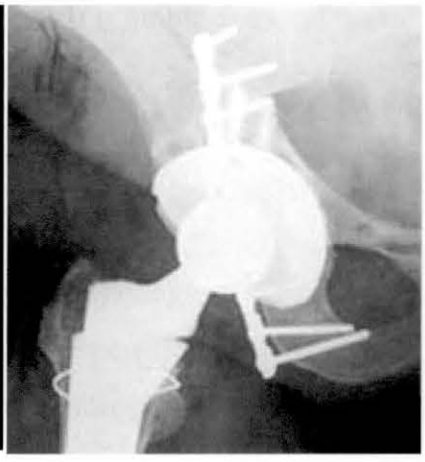

Figure 32 Intraoperative acetabular fracture treated with buttress plate. [126]

Comparison of intraoperative fracture management strategies is complex due to the different fixation strategies used, a lack of consistency in fracture classification, and a lack of robust comparative studies. The largest comparative study to date evaluated 211 patients undergoing revision total hip arthroplasty [105] with an extensively coated femoral stem for which a diaphyseal fit was obtained for all patients. Intraoperative femoral fractures were sustained in 30 per cent of patients, with the most prevalent type

being type-B2. A wide variety of treatment modalities were used including cerclage wire fixation and allograft cortical strut. No significant difference in functional outcome was noted between the different treatment strategies and no significant difference in the prevalence of stable fractures was found between bowed and straight stems or between stems of different length. Biomechanical studies have also compared fixation constructs, with cables reported to be stronger than cerclage wires; dynamic plates were found to be better than Ogden plates, with double plates providing greater stability than a single plate with wires; and a lateral plate supplemented with an anterior allograft cortical strut was reported to be the ideal construct for a fracture with a stable femoral stem [129-132].

2.4.1.1 Peri-prosthetic femoral fracture management

The method for fixation of intraoperative fractures includes cerclage wiring, plate osteosynthesis, and cortical allograft strut augmentation, depending on the site, prosthetic stability, and bone stock. Long term fixation of a non-cemented hip stem within the femur is achieved through bone ingrowth into a porous or textured stem surface. Because initial prosthesis stability and intimate bone to prosthesis apposition are required for bone ingrowth, non-cemented prostheses are typically press fit within a slightly undersized canal within the femur. Multiple impact loads are applied to a broach with a mallet to create the canal. The hoop stresses that develop within the proximal femur during broaching and stem insertion are capable of splitting the bone, with the reported incidence of intraoperative fracture ranging from 3% to 25%.

The medial and anteromedial proximal femur are the most commonly observed fracture sites. Both clinical and animal studies have shown that a large percentage of fractures go undetected. Undetected fractures dramatically decrease the stability of the hip stem and may increase the risk of short-term failure. Extracting the stem, applying cerclage wires, and re-implanting the stem is the typical treatment for fractures that are detected.

The influence of treated fractures on stem function is unclear. Canine studies have shown that both treated and untreated fractures hinder early bone ingrowth into the prosthesis. Some clinical investigators indicated that treated fractures do not adversely influence recovery time or failure rate, whereas others indicated that fractures can lead to an increased risk of prosthesis loosening and a prolonged recovery period, even when treated intraoperatively. One previous in vitro study examined the influence of prosthesis and canal size on the strains that develop within the proximal femur during non-cemented total hip arthroplasty. Increasing the size of the prosthesis relative to the canal increased the maximum hoop strain.

2.4.2 Post-operative peri-prosthetic femoral fracture

Post-operative peri-prosthetic femoral fracture following total hip arthroplasty is a serious complication that is difficult to treat, has a high likelihood of re-operation, a high rate of post-operative complication, and poor functional outcomes [16, 96, 104, 108, 133, 134] [63]. The incidence of post–operative periprosthetic fracture is reported to vary from 0.1% to 2.1% in primary procedures, and increases in a revision setting, with the Mayo joint registry reporting an incidence of 4%[108].

As previously described, the prevalence of peri-prosthetic femoral fracture after total hip arthroplasty appears to be increasing for many reasons, including a growing population of patients with hip arthroplasties in place, and a growing population of patients with compromised femoral bone around hip arthroplasties as a result of osteolysis or revision operations [15, 16, 96, 104, 108, 133, 134]. Also with more younger, more active patients receiving total hip arthroplasty, the pool of young active patients (who are at greater risk for high-energy trauma events) is also growing. Notably, low-energy trauma falls are the most frequent events linked with post-operative peri-prosthetic femoral fracture, with 75% of periprosthetic fractures in the Swedish registry database attributed to minor trauma [135].

As with intra-operative peri-prosthetic femoral fracture, the risk of fracture in the early post-operative period is higher when cementless fixation is used. With the growing trend for primary and revision cementless femoral component usage in many regions, peri-prosthetic femoral fracture will continue to be a growing problem [104, 136] and efforts to combat it are therefore essential.

Classification systems for post-operative peri-prosthetic femoral fracture have been described by a number of authors, including Morrey [137], Whittaker [138], Mont and Marr [107], using a combination of prosthetic stability and location as identifiers for the fracture. As with intra-operative fractures, the most commonly used classification system is the Vancouver system, which classifies fractures according to location, stability, and bone quality. Fractures involving the trochanteric area are categorised as type-A (AG, greater trochanter and AL, lesser trochanter), fractures around the tip or stem of the implant are categorised as type-B, and are further divided into subtype- B1 when adjacent to a well fixed stem, type-B2 in the presence of a loose stem and type-B3 when associated with osteopenia or loss of bone substance. Fractures distal to the tip of the stem are classified as type-C.

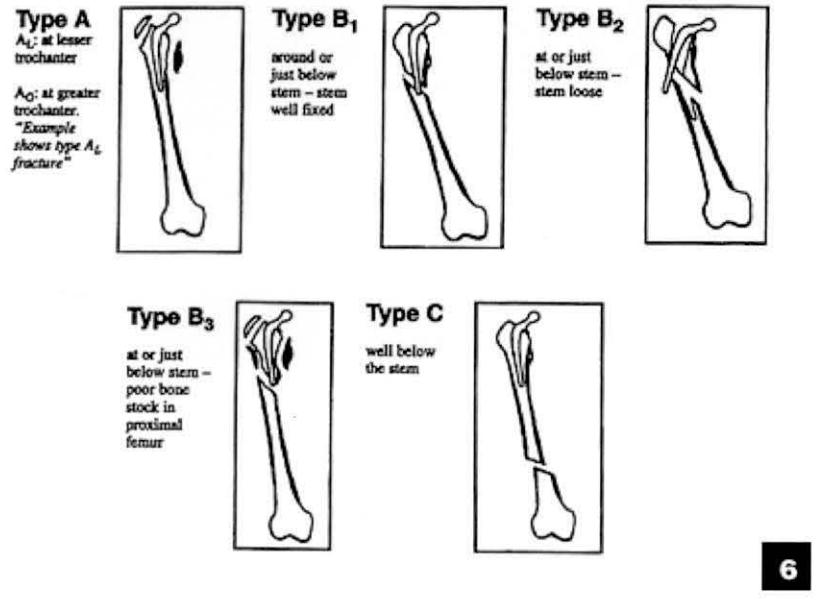

Figure 33 Postoperative peri-prosthetic fractures – Vancouver classification [126]

The majority of post-operative peri-prosthetic femoral fractures require surgical intervention, with the choice of treatment based on the type of fracture, integrity, and quality of bone stock and stability of the original implant [108, 139]. Type-A fractures are often related to osteopenia and associated with osteolysis in the proximal femur. If non-displaced, non-operative care is preferred and has good functional outcomes[140]. However, if the greater trochanter is displaced, fixation is generally achieved using cerclage wires supplemented by screws or plates in order to restore functional leverage of the glutei muscles.

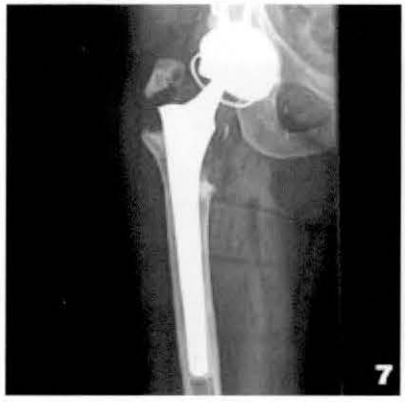

Figure 34 Displaced type A-G fracture.

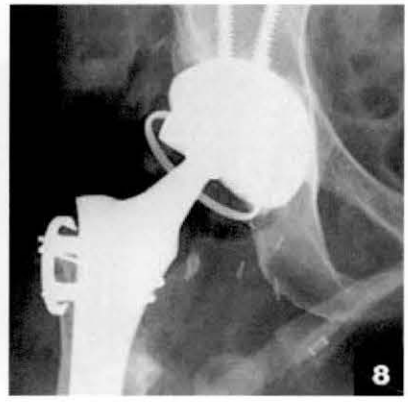

Figure 35 Type A-G fracture treated with trochanteric clamp.

Similarly, non-displaced type- B1 fractures can be treated non-operatively, however, the potential for displacement in non-operative care is high and poor outcomes have been reported [141]. If any displacement is present, then type-B1 fractures are treated with fixation or revision, often with the use of a trochanteric plate and where there is local osteolysis, the use of a cortical structural allograft to improve the implant's stability.

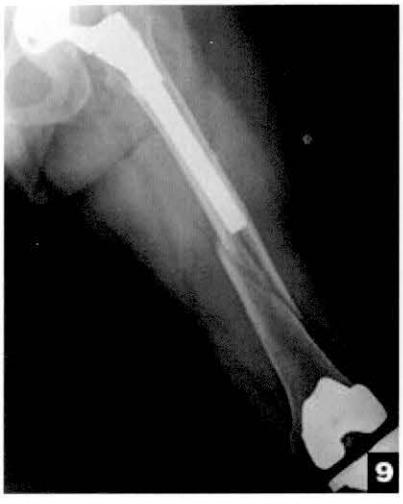

Figure 36 Displaced type B1 fracture.

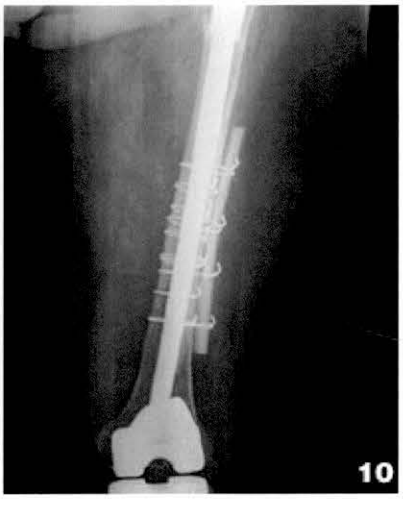

Figure 37 Type B1 fracture treated with revision to long-stem prosthesis.

Type-B2 fractures, and all other fractures associated with a loose femoral component are best treated with implant revision. Good outcomes have been reported with the use of long stems, which bypass the fracture site, with the additional use of cerclage cables, wires or straps for long oblique or spiral fractures, and plates and/or onlay grafts to provide stability in short oblique or transverse fractures. Either cementless or cemented stems can be used. However, cemented stems are generally reserved for infirm elderly patients with poor bone stock [142].

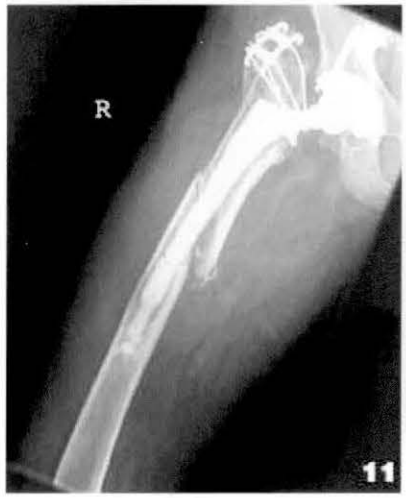

Figure 38 Displaced type B2 fracture.

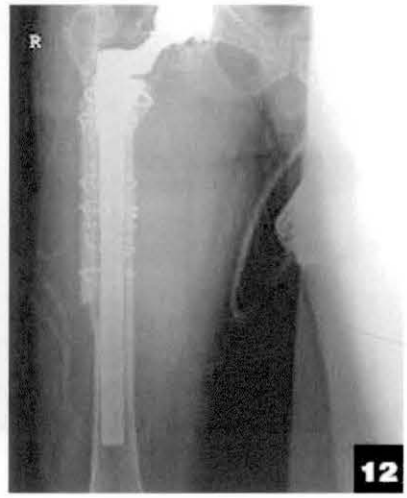

Figure 39 Type B2 fracture treated with revision to long-stem prosthesis.

Type-B3 fractures are the most difficult to treat due to the presence of grossly deficient proximal femoral bone stock and loose stems. As such, aggressive fixation techniques are required and revision of the component is essential. Revision surgery is often augmented with cancellous bone impaction grafting or strut-grafting with cerclage wires in order to enhance the stability of the entire construct. Type-C fractures can be managed in a similar manner to any distal femoral fracture and in general are treated with open reduction and internal fixation, using plates with screws and cerclage wires.

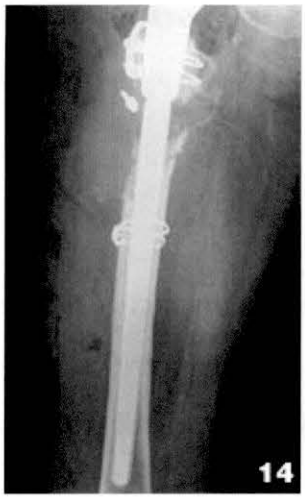

Figure 40 Type B3 fracture revised to distal fit Wagner style stem.

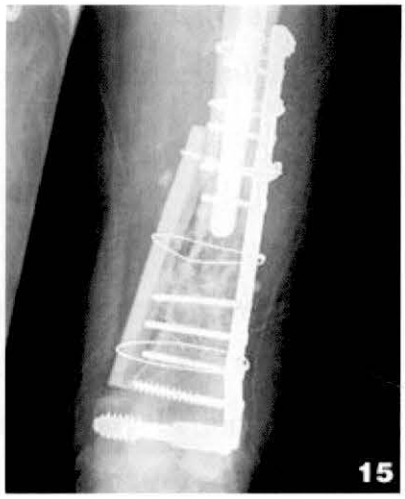

Figure 41 Type C fracture treated with ORIF plate and strut with cerclage wires.

For periprosthetic fractures with a loose stem, there is general consensus for stem replacement as the treatment strategy of choice and a number of studies have demonstrated this to be an efficient option [64, 122, 143]. For stable prosthesis, there is less consensus with some authors recommending stem revision[144] and others using conventional plate fixation, retrograde nailing or non-operative treatments such as traction, although with high complication rates [94, 145]. More recently, the less invasive stabilization system (LISS) has been reported as a useful treatment option for periprosthetic fracture. This system has favorable biomechanical characteristics and has been successfully applied to general fracture treatment [146-149]. In a study of 36 cases, Muller et al. found that patients treated with LISS (less invasive stabilization system) had similar clinical outcomes to those treated with stem revision [146-150]. Despite a slightly increased risk of implant failure, LISS (less invasive stabilization system) may be a preferred option for the management of stable stem periprosthetic fractures given the associated drawbacks with the major surgery required for stem revision. Such

drawbacks include an increased risk of intraoperative fracture, additional soft tissue damage, prolonged operative time, increased intraoperative blood loss and a higher mortality rate.

Post-operative peri-prosthetic femoral fracture can occur within a variable window after surgery. Early post-operative fractures often occur due to inappropriate mobilization and rehabilitation in the immediate post-surgery period [151]. Unambiguous advice concerning weight-bearing is therefore essential to reduce fracture risk. Changes to medication and the home environment to reduce fall risk should also be considered [122]. Early post-operative fractures have also been associated with notching of the femoral cortex leading to weakening of the femoral cortex [152]. The most common cause of late post-operative peri-prosthetic femoral fracture is osteolysis and the associated aseptic loosening of the stem [109, 153, 154] [63]. Localised femoral bone loss in association with a loose cemented stem was initially thought to be mediated by failed cement [155], however, it is now recognized to be the result of a response to wear of particles. In addition, late post-operative peri-prosthetic femoral fracture has been associated with different implants and with surgical technique. Countries using cemented stems have the largest incidence of late post-operative peri-prosthetic femoral fracture Data from both the Swedish and Finnish registry demonstrates a higher association of fracture incidence with the Exeter stem, the Swedish registry also found high incidence rates with the Charnley stem [95, 134].

Surgical technique can also have a significant impact on peri-prosthetic femoral fracture risk since any factor that decreases bone strength is a risk factor for late fracture. These may include screw holes and stress risers from adjacent implants [102, 156], and cortical perforations associated with reaming of the femoral canal, osteoporosis, osteotomy or previous prosthesis, and a narrow medullary canal [157]. A number of clinical studies have demonstrated a relationship between localized compromised bone and late post-

operative fracture. Fractures have been observed to localize with cortical stress risers, previous cortical breaches including old screw holes and at the tip of the stem through a cortical defect [103, 158-162]. Prevention of late periprosthetic fractures is best achieved through regular clinical and radiographic follow-up to enable early detection of osteolysis and aseptic loosening and thus timely revision surgery [102, 163].

2.4.2.1 Analysis of post-operative peri-prosthetic femoral fracture from the "Sydney Hip and Knee Surgeons" Database

For this thesis, with the permission from Dr William K Walter, a review of the "Sydney Hip and Knee Surgeons" extensive clinical database was undertaken. The analysis focused on cementless femoral stems where a post-operative peri-prosthetic femoral fracture was observed. In a six year follow-up period looking at 1152 primary cementless anatomic total hip arthroplasty (ABGI) performed in 1036 patients, 37 (3%) periprosthetic fractures occurred in 36 patients. Three fractures (0.2%) occurred during the first two months post-operatively, two identified on the post-operative radiograph, and one presented with groin pain following a minor stumble. All three fractures ran from the cut neck of the femur to the medial femoral diaphysis at a point 5 to 6 cm distal to the lesser trochanter. Thirty-four fractures (2.9%) occurred between 2-127 months post-surgery, and were caused by low, moderate or high-energy injuries. All late fractures involved the lateral aspect of the femur, and had two distinct phenotypes. The first type of fracture, which occurred 56 months post-operatively on average, ran from the lateral aspect of the femur just above the elbow of the prosthesis and extended distally in a long spiral manner into the femoral diaphysis 5 to 12 cm distal to the lesser trochanter. A second fracture line was also often present, extending proximally from the elbow to the neck of the femur so that the greater trochanter was a separate fragment. Fractures in this group were generally associated with loosening of the femoral stem. The second subset of fractures occurred later (an average of 81 months post-operatively) and ran from the lateral aspect of the femur just above the elbow of the prosthesis. They

extended a variable distance distally in a transverse or short oblique fashion, exiting the medial aspect of the femur within 2 cm of the lesser trochanter. In a few cases a second fracture line extended proximally into the neck of the femur. Due to the fractures location proximal to the metaphyseal-diaphyseal junction, the femoral stems in this group remained stable in the distal femur and therefore most of these fractures could be treated non-operatively.

Of significant interest, from this analysis a distinct pattern related to the timing of the fracture post-surgery and the patient age was found in the analysis. Observing a plot of the fractures on a graph with the horizontal axis being the time after surgery that the fracture occurred and the vertical axis being the patients age, two distinct areas can be identified on the plot. Firstly, the early fractures appear to be concentrated within the first 3 months. This is in the period where bony in-growth into the proximal coating and therefore rigid interlock of the stem with the femoral bone is occurring. Then a noticeable gap exists in the plot where no fractures have occurred for younger patients and only a limited number of fractures have occurred for patients over 80. See Figure 42.

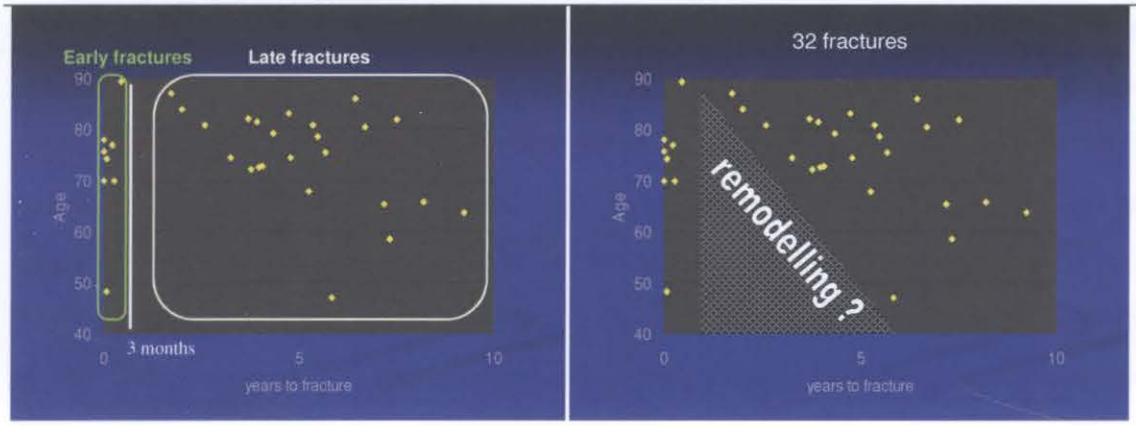

Figure 42 peri-prosthetic femoral fracture age vs years to fracture after total hip replacement Early vs Later fractures

The prosthesis-bone interface mechanics in the early postoperative period differ from those in the late postoperative period [104]. During the early postoperative period, bony in-growth has not yet occurred and the frictional loads arising from the initial press fit is the only support for the prosthesis. If these supporting frictional loads are overcome, the prosthesis may wedge further into the canal, increasing the hoop strains on the femur, thereby leading to a fracture. The mechanics of the construct are quite different once bony in-growth occurs. A much greater load is required to overcome the prosthesis-bone interface, which can only be achieved by fracturing the bone at the interface. Often, late-stage peri-prosthetic femoral fracture occurs in conjunction with loosening of the prosthesis or loss of bone due to osteolysis or unfavorable remodeling responses [116, 164, 165].

The ABGII press fit anatomic stem

The majority of press fit stems are straight, and as a result, the contact with the curved femoral shaft is incongruent and occurs unevenly at points of contact. To address this issue anatomic shaped femoral components were designed. One such anatomic stem is

the Anatomique Benoist Girard (ABG) stem that was supplied by Howmedica, Allendale, NJ. In its original form, the ABG femoral component was anatomically shaped, with mirrored geometries for left and right hips. The stem is made out of titanium alloy (Ti6A14V), and the proximal one third of the stem length is coated with Hydroxyapetite. The anterior and posterior faces of this coated region have a slightly structured morphology See Figure 43. Whereas the distal stem has a smooth matte finish. (See Figure 43) The design objectives of the stem were to create direct postoperative stability, proximal osseous integration, and load transfer. This shape promotes proximal fill in metaphyseal trabecular bone, and the distal stem is a fail-safe feature against excessive bending and has a loose fit in the diaphysis, which us promoted by over reaming. [166]

This stem reported excellent clinical results in a large multicenter study with a five to seven-year follow-up. [167] In that study, involving 398 patients, a component survival rate of 99.2% after five years was observed. [166] However, somewhat unfavorable patterns of bone remodeling were observed radiographically [167]. This was in the form of; endosteal apposition and cancellous bone densification in the mid stem section; bone resorption in the most proximal sections; and the formation of radiolucent lines around the distal stem. This seemed to signify a lack of stem bonding. [166] The results further showed approximately 4% distal cortical thickening and 27.1% calcar resorption after 5 years. [166] [167] Similar observations have since been reported by Herrera et al. [168] and confirmed with Dual-energy X-ray absorptiometry DEXA by Panisello et al. [169].

In an attempt to improve the proximal transfer of loads and reduce the phenomenon of stress-shielding the stem was redesigned and is now referred to as the ABG-II. The main differences between both stems concern geometrical design and material. The overall length was reduced by 8% and the proximal and distal diameters by 10%. The prosthesis shoulder has been modified, extending the HA zone over the proximal

shoulder, to promote in-growth where the shoulder comes into contact with the canal near the trochateric region. The material has changed from Wrought Titanium (Ti 6Al-4V) alloy to TMZF (Titanium, Molybdenum, Zirconium and Ferrous) alloy. [170] This beta titanium alloy offers 25 percent greater flexibility than Ti-6Al-4V alloy, yielding a modulus of elasticity that more closely resembles that of bone. In addition, TMZF (Titanium, Molybdenum, Zirconium and Ferrous) maintains a 20 percent higher tensile strength than Ti-6Al-4V alloy. [171]

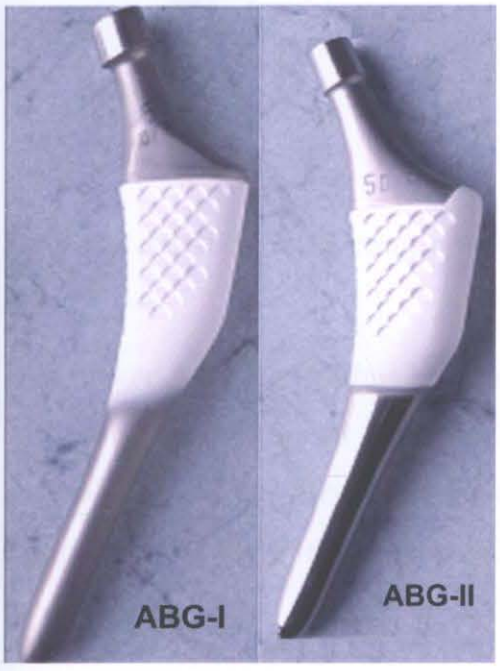

Figure 43 ABG I vs ABG II showing differences in design features [170]

Figure 44 ABGII femoral component (Stryker internal presentation)

This newer ABG II stem has been used extensively in Australia and in Europe and has had a successful clinical history. [172] [173] [174]. The results published in the 2010 Australian Joint Registry report show that the medium term results of the ABG II stem compare favorably to the other available stems. See Figure 45.

Table HT54: Yearly Cumulative Percent Revision of Primary Total Conventional Hip Replacement with Cementless Fixation

Femoral Component	Acetabular Component	1 Yr	3 Yrs	5 Yrs	7 Yrs	9 Yrs
ABGII	ABGII	1.7 (1.3, 2.3)	3.0 (2.4, 3.8)	4.1 (3.4, 4.9)	5.3 (4.4, 6.3)	5.5 (4.6, 6.6)
ABGII	ABGII (Shell/Insert)	1.7 (1.0, 3.0)	2.3 (1.5, 3.8)	3.1 (2.0, 4.7)	4.1 (2.7, 6.3)	
ABGII	Trident	2.2 (1.6, 3.0)	4.0 (3.2, 5.1)	5.0 (4.0, 6.3)	6.5 (5.0, 8.4)	
Accolade	Trident	1.5 (1.2, 1.9)	3.0 (2.5, 3.5)	4.0 (3.3, 4.7)	5.0 (3.7, 6.8)	
Adapter	Bionik	2.7 (1.5, 4.6)	5.8 (3.7, 9.1)			
Alloclassic	Allofit	1.6 (1.2, 2.0)	2.6 (2.1, 3.1)	3.3 (2.8, 4.1)	3.4 (2.8, 4.2)	
Alloclassic	Durom	1.4 (0.7, 2.7)	5.1 (3.4, 7.6)	6.2 (4.2, 9.0)		
Alloclassic	Fitmore	2.3 (1.6, 3.2)	3.6 (2.7, 4.7)	4.3 (3.3, 5.6)	4.9 (3.8, 6.4)	
Alloclassic	Trabecular Metal Shell	1.7 (1.0, 3.2)	1.7 (1.0, 3.2)	1.7 (1.0, 3.2)		
Alloclassic	Trilogy	0.6 (0.2, 1.9)	0.9 (0.3, 2.3)			
Anthology	R3	1.7 (1.0, 2.9)				
Anthology	Reflection	1.2 (0.6, 2.4)	1.6 (0.9, 2.8)			
CLS	Allofit	1.6 (0.9, 3.0)	3.1 (2.0, 4.9)	3.4 (2.2, 5.3)	5.2 (3.2, 8.4)	
CLS	Fitmore	2.0 (1.1, 3.6)	4.2 (2.7, 6.4)	4.4 (2.9, 6.7)	5.2 (3.4, 7.8)	
Citation	Trident	1.8 (1.2, 2.8)	2.5 (1.7, 3.7)	3.2 (2.1, 4.7)	3.2 (2.1, 4.7)	
Citation	Vitalock	0.5 (0.2, 1.7)	2.2 (1.3, 3.8)	2.8 (1.7, 4.6)	3.7 (2.3, 5.9)	5.1 (3.1, 8.4)
Corail	ASR	2.1 (1.6, 2.7)	6.4 (5.3, 7.6)			
Corail	Duraloc	1.4 (0.9, 2.2)	1.9 (1.3, 2.9)	2.7 (1.8, 4.0)	3.6 (2.4, 5.3)	
Corail	Pinnacle	1.7 (1.4, 2.0)	2.3 (1.9, 2.8)	2.9 (2.3, 3.7)		
Epoch	Trilogy	2.3 (1.5, 3.6)	3.1 (2.0, 4.7)	3.1 (2.0, 4.7)	3.6 (2.3, 5.7)	
F2L	SPH-Blind	3.1 (2.0, 4.8)	4.9 (3.5, 7.0)	6.2 (4.5, 8.4)	7.1 (5.3, 9.6)	
Mallory-Head	Mallory-Head	1.8 (1.3, 2.5)	2.3 (1.8, 3.1)	3.1 (2.4, 4.0)	4.3 (3.3, 5.5)	6.6 (4.9, 8.9)
Natural Hip	Fitmore	1.1 (0.6, 2.1)	1.5 (0.8, 2.6)	2.1 (1.3, 3.4)	3.0 (1.9, 4.9)	
Omnifit	Secur-Fit	3.2 (1.9, 5.1)	5.0 (3.4, 7.3)	6.7 (4.8, 9.3)	7.8 (5.7, 10.7)	
Omnifit	Trident	1.7 (1.1, 2.7)	2.8 (1.9, 4.0)	3.9 (2.8, 5.3)	4.4 (3.2, 6.0)	
Quadra-H	Versafit	2.8 (1.7, 4.7)				
S-Rom	Option	1.5 (0.8, 2.8)	2.4 (1.5, 3.9)	3.4 (2.2, 5.1)	3.9 (2.6, 5.9)	
S-Rom	Pinnacle	1.9 (1.4, 2.7)	3.1 (2.4, 4.1)	3.7 (2.8, 5.1)		
SL-Plus	EPF-Plus	1.8 (1.3, 2.5)	3.4 (2.6, 4.4)	4.6 (3.4, 6.1)		
SL-Plus	R3	2.5 (1.2, 4.9)				
Secur-Fit	Trident	1.3 (1.0, 1.7)	2.1 (1.7, 2.7)	2.6 (2.1, 3.2)	3.5 (2.8, 4.3)	
Secur-Fit Plus	Trident	1.3 (1.0, 1.7)	2.1 (1.6, 2.6)	2.6 (2.1, 3.2)	2.8 (2.3, 3.5)	3.0 (2.4, 3.7)
Stability	Duraloc	0.7 (0.2, 2.3)	2.3 (1.2, 4.3)	2.5 (1.4, 4.6)	4.8 (2.9, 7.8)	
Summit	ASR	1.2 (0.7, 2.0)	4.8 (3.5, 6.5)	7.1 (4.3, 11.5)		
Summit	Pinnacle	1.2 (0.8, 1.8)	1.6 (1.1, 2.3)	2.0 (1.4, 2.9)		
Synergy	BHR	1.2 (0.7, 2.4)	2.2 (1.3, 3.8)			
Synergy	R3	1.5 (0.9, 2.5)				
Synergy	Reflection	1.5 (1.2, 1.8)	2.3 (2.0, 2.7)	2.6 (2.3, 3.1)	3.3 (2.8, 3.9)	4.9 (2.9, 8.1)
Taperloc	M2a	1.7 (0.8, 3.3)	3.5 (2.1, 5.8)	5.5 (3.5, 8.5)		
Taperloc	Mallory-Head	1.7 (1.0, 2.9)	2.4 (1.5, 3.8)	2.8 (1.8, 4.4)	3.5 (2.3, 5.4)	
Taperloc	Recap	2.2 (1.2, 4.1)	3.3 (1.9, 5.8)			
VerSys	Trilogy	2.2 (1.8, 2.7)	2.9 (2.4, 3.5)	3.4 (2.9, 4.1)	3.9 (3.3, 4.7)	4.7 (3.3, 6.8)
Other (778)		2.0 (1.9, 2.3)	3.7 (3.4, 4.0)	4.9 (4.5, 5.2)	6.0 (5.5, 6.4)	7.0 (6.2, 7.9)

Note: Only prostheses with over 400 procedures have been listed.

Figure 45 From the Australian Joint Registry 2010 report: yearly cumulative percent revision of primary total conventional hip replacement with cementless fixation

However, Australian surgeons who have experience with the ABG II stem anecdotally noticed a relatively high number of peri-prosthetic femoral fracture with the ABG II stem, when compared to other stems designs. As such, in 2007 Stryker asked the Australian Joint Registry to conduct a more detailed analysis on revisions due to peri-prosthetic femoral fracture around the ABG II. The results were illuminating.

When looking at the ABGII stem there is a difference when it is compared to all other stems combined independent of time in-situ. The ABGII stem does have a higher overall revision rate (ABGII- 3%; all other stems-2.3%). Isolating peri-prosthetic femoral fracture as the cause for revision highlights the concern (ABGII-1.1%; all other stems-0.3%). Clearly, efforts to reduce the risk of peri-prosthetic femoral fracture for this stem design would be welcomed.

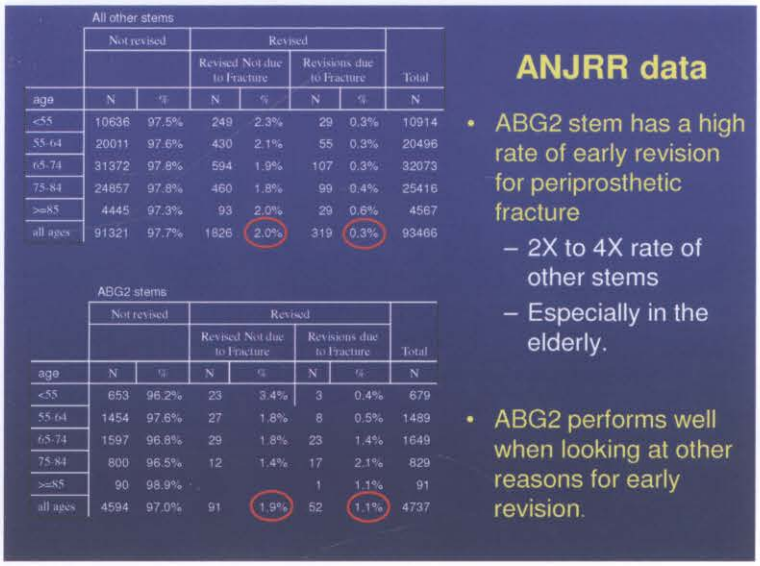

All other stems

	Not revised		Revised				
			Revised Not due to Fracture		Revisions due to Fracture		Total
age	N	%	N	%	N	%	N
<55	10636	97.5%	249	2.3%	29	0.3%	10914
55-64	20011	97.6%	430	2.1%	55	0.3%	20496
65-74	31372	97.8%	594	1.9%	107	0.3%	32073
75-84	24857	97.8%	460	1.8%	99	0.4%	25416
>=85	4445	97.3%	93	2.0%	29	0.6%	4567
all ages	91321	97.7%	1826	2.0%	319	0.3%	93466

ABG2 stems

	Not revised		Revised				
			Revised Not due to Fracture		Revisions due to Fracture		Total
age	N	%	N	%	N	%	N
<55	653	96.2%	23	3.4%	3	0.4%	679
55-64	1454	97.6%	27	1.8%	8	0.5%	1489
65-74	1597	96.8%	29	1.8%	23	1.4%	1649
75-84	800	96.5%	12	1.4%	17	2.1%	829
>=85	90	98.9%			1	1.1%	91
all ages	4594	97.0%	91	1.9%	52	1.1%	4737

Table 2 Data requested from the Australian Joint Registry provided courtesy of Stryker South Pacific

When looking for reasons as to why the stem has a higher fracture rate, comparison of the incremental designs is an obvious place to start, considering there was an incremental design change in the stems history. Unfortunately, the Australian Joint

Registry is a relatively modern initiative so the original ABG prosthesis cannot be analyzed adequately using the registry. Fortunately, the Sydney hip and knee surgeons who have extensive experience with both iterations of the ABG stem design have a detailed database that was analyzed as part of this thesis work.

Looking at the ABGII vs the ABG original stem in 2003, it is immediately clear that the iterative design changes appeared to have a favorable effect on the overall fracture rate. Over similar lengths of time, the ABG II Stem has a lower fracture rate than the original ABG. See Table 3

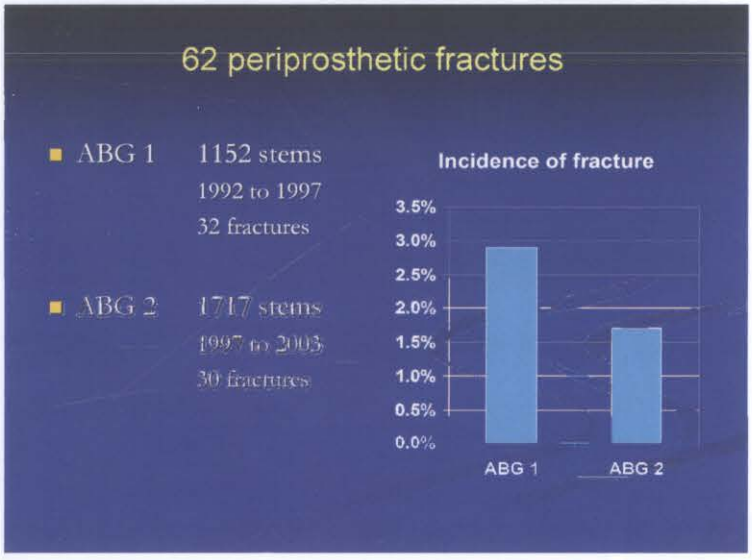

Table 3 ABGI vs ABGII incidence of fracture (Courtesy of the Sydney Hip and Knee Surgeons)

Considering the ABG was redesigned to best optimize against unfavorable bone remodeling, this result could be expected. It is anticipated that unfavorable bone remodeling (stress shielding) would increase the rate of later postoperative fracture, as was previously described.

What is most interesting is that a deleterious effect was observed. Although the overall fracture rate was reduced with the ABG II, the rate of early fracture appears to have increased with the ABGII. A smaller number of late stage fractures are observed with the ABG II but unfortunately a greater number of early stage fractures are also observed. See Table 4

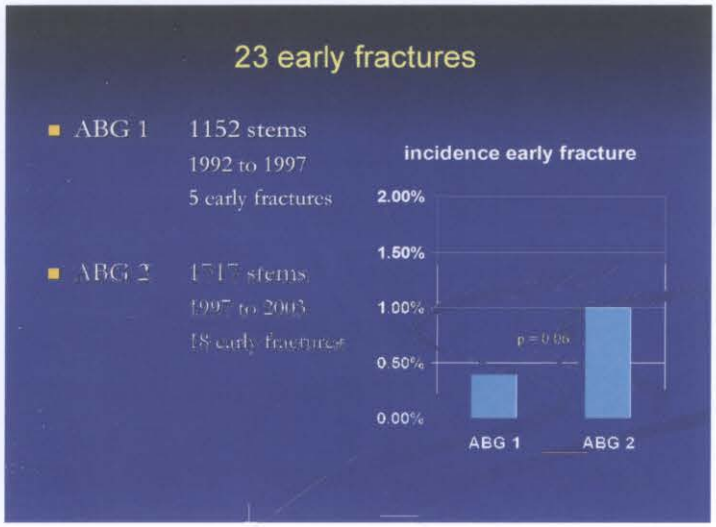

Table 4-ABG I vs ABG II incidence EARLY fracture (Courtesy of the Sydney Hip and Knee Surgeons)

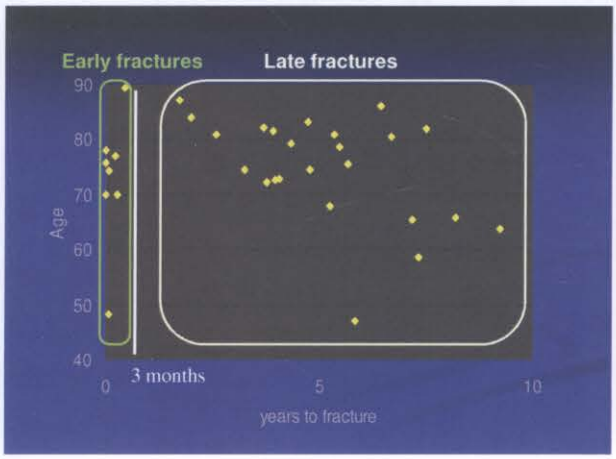

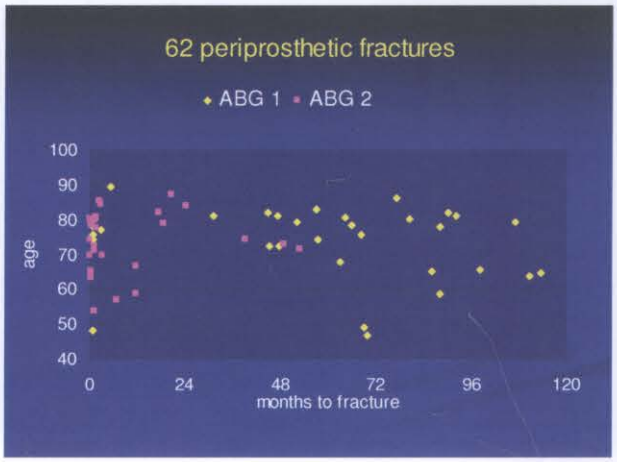

2.4.3 Surgical technique - cementless ABG II [175] and [176]

An understanding of the surgical technique used for hip surgery is of relevance to the work in this thesis. In this review, an emphasis is placed on the stages during surgery were the risk of peri-prosthetic femoral fracture is at its highest, namely broaching and stem insertion.

The techniques used by surgeons to implant total hip replacements are not uniform. The techniques vary according to the surgical approach preferred by the surgeon, the implant system chosen, the instrument set chosen, and the individual preference of each surgeon. However, generally there are similarities and many of the concepts are transferrable between surgical techniques. The posterior lateral technique is the technique recommended by the manufacturer,[175] for the ABG II stem this is the technique that detailed in this section.

2.4.3.1 ABG II Posterior Lateral Approach

2.4.3.1.1 Preoperative Planning

Pre-operative radiographs should be analysed using the manufacturer's templates to determine the correct leg length, centre of rotation of the hip joint, femoral offset and the size of the prosthesis. The patient is placed on the operating table in a lateral decubitus position (laying on their side).

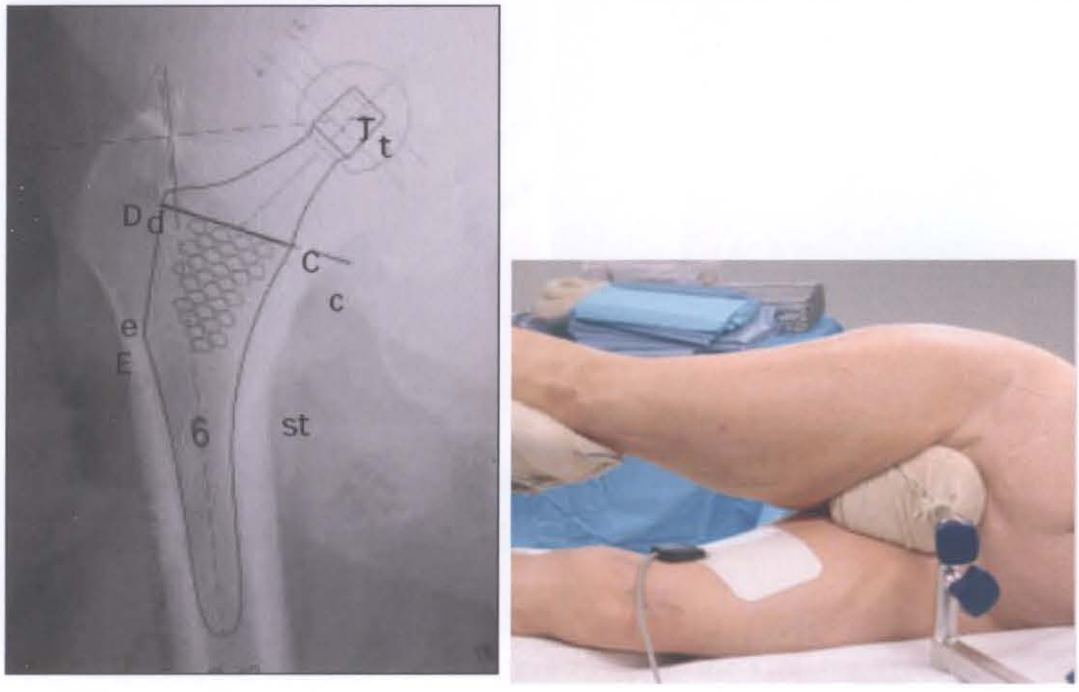

Figure 46 Left-Femoral X ray template Right- Patient positioned in lateral decubitus position on the operating table (ABG Surg tech, 2004)

The skin incision for a mini postero-lateral approach is placed slightly more posteriorly and obliquely than a standard incision. The incision extends 4cm proximally and distally to the tip of the Greater Trochanter. The fascia lata is divided in line with the skin incision and the gluteus maximus muscle is split along the line of its fibres. See Figure 47. A deeper incision is made, revealing the posterior aspect of the Greater Trochanter (1) and the trochanteric bursa, which must be reflected with the sciatic nerve (2) at the bottom to expose the short external rotators (3). The leg is placed in extension, abduction, and internal rotation to better expose the short external rotators.

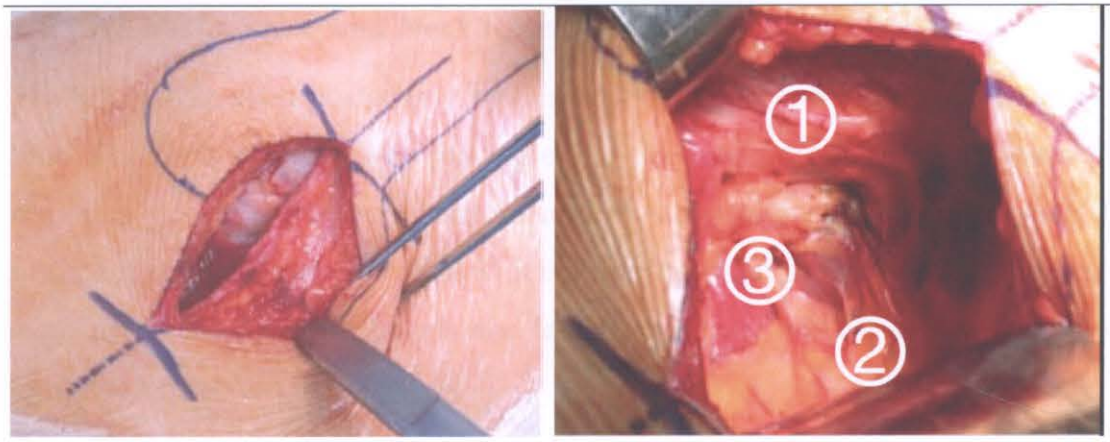

Figure 47 Left- Initial incision Right- Deeper incision revealing 1-Trochanter, 2- sciatic nerve 3- short external rotators [176]

The surgeon cuts the external rotators close to the Greater Trochanter and the fossa piriformis (preserving the piriformis muscle attachment (4) if possible). These may be raised with the posterior capsule as a composite flap or they may be raised separately. In both cases they will be repaired at wound closure. The capsule is split proximally along the axis of the piriformis muscle (5), the femoral neck, and the acetabular rim. The surgeon has the distally aim to be as close to the trochanteric attachment as possible (6). The external rotator muscles and capsule (7) will protect the sciatic nerve during the rest of the operation.

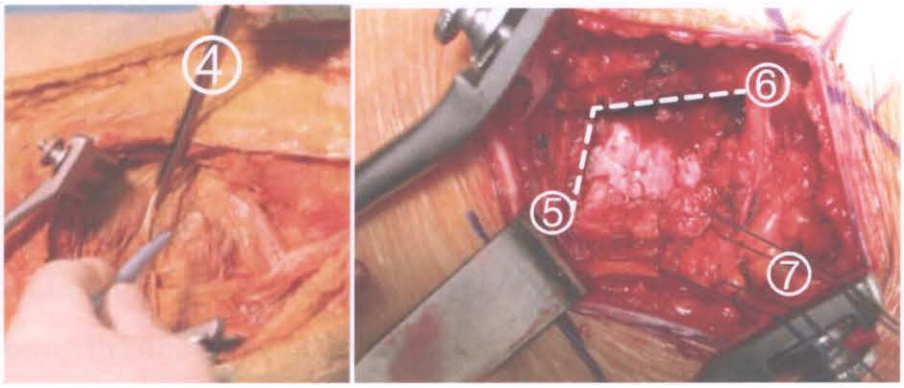

2.4.3.1.2 Dislocation and Neck Resection

The hip is dislocated posteriorly by flexion, adduction and internal rotation of the lower limb. The neck is exposed by placing either the autostatic retractor between the gluteus minimus and the external rotators and the capsule; or by placing two Hohmann retractors around the femoral neck. It is important that the surgeon remember that good exposure of the fossa piriformis and lesser trochanter will allow you to follow the pre-templated resection line.

The flexed knee is carefully orientated to prevent incorrect version of the neck. The femoral neck is resected using the anatomic landmarks (8) and the neck line resection drawn from the fossa piriformis (9). The femoral head is removed using either the corkscrew instrument or forceps.

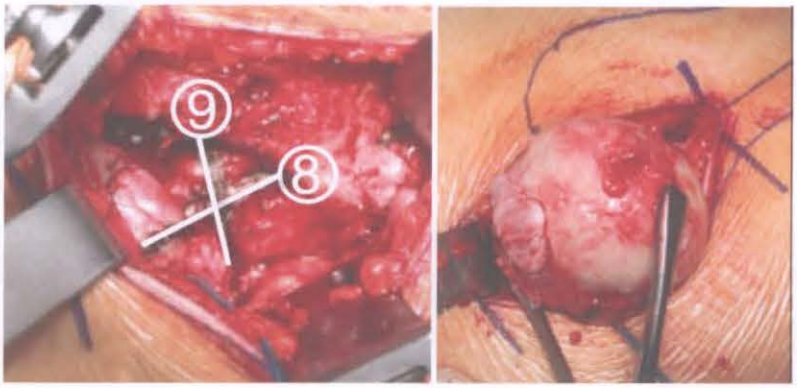

2.4.3.1.3 Acetabular Reaming and Cup Insertion

The acetabulum is prepared with cylindrical reamers until the required size is reached. The surgeon knows that the size is correct if bleeding bone is observed all the way around the hemisphere. The acetabular component is then impacted into the acetabulum using the dedicated instrument.

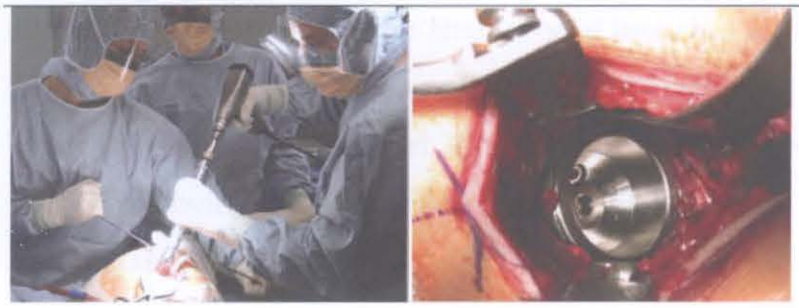

2.4.3.1.4 Femoral Exposure and Preparation

The acetabular retractors are removed and the operated leg is placed into maximum adduction and into internal rotation. This position ensures that the knee of the non-operated leg does not obstruct it, and a femoral elevator is placed beneath it displaying the entry to the femoral canal to the surgeon. See Figure 48. A box chisel is used to resect a piece of cancellous and remaining cortical bone from the lateral femoral neck to allow direct access to the femoral canal and avoid reaming in a varus position. Flexible reamers are then used to ream the distal canal to accept the pilot of the femoral implant.

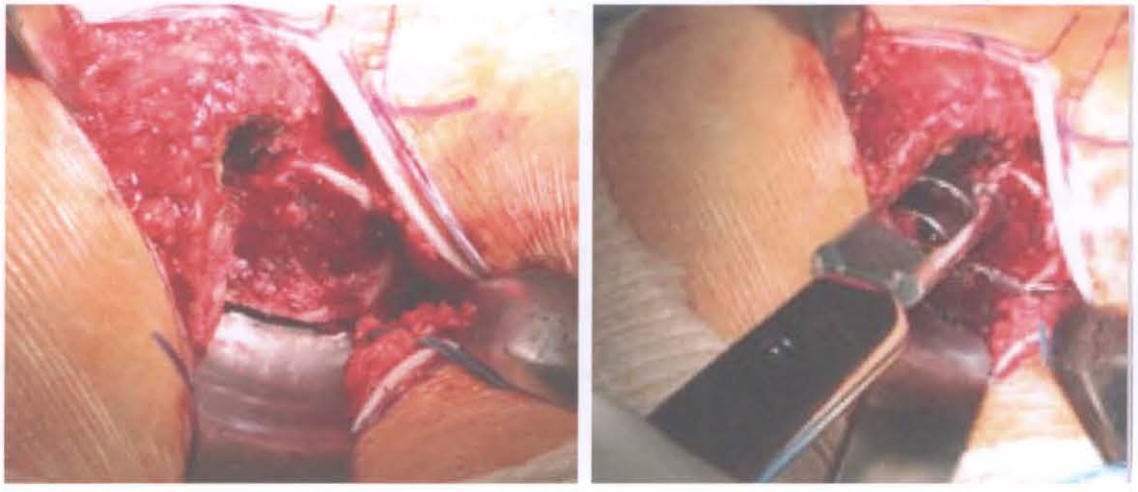

Figure 48 Femur exposed (Left) Femoral canal opened up by the box chisel (Right)

The surgeon starts with the smaller size broaches and working upwards, inserts the broaches into the canal. Cancellous bone is removed by rasping and impacting the broaches with a heavy mallet. The surgeon then progressively increases the size of the broach removing more cancellous bone until the broach is sitting firmly on cortical bone and is stable.

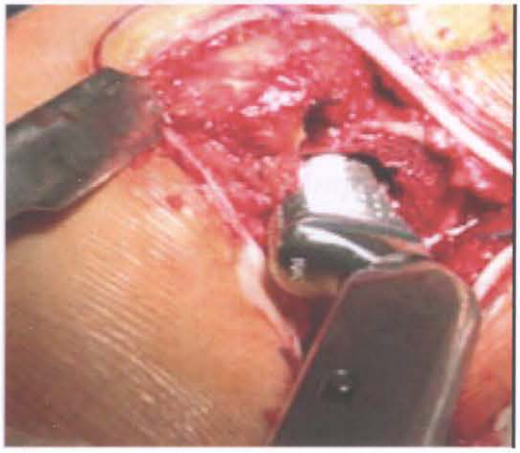

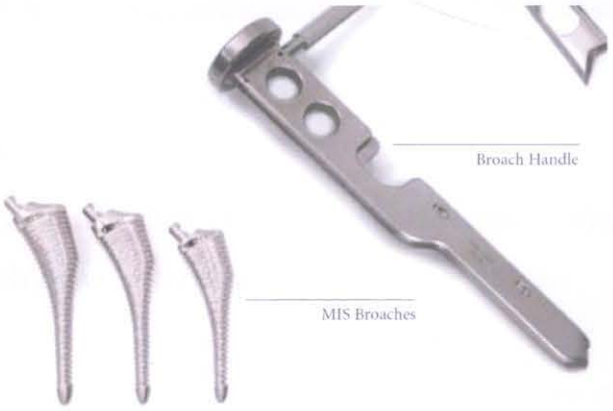

Rotating the broach in the canal and observing a firm fit with little movement between the broach and the femur allows the surgeon to judge broach stability. After inserting the final broach the broach handle is removed. The offset forceps are placed on the broach the modular trial neck and head with appropriate neck length, the trial acetabular liner is inserted and a trial reduction is performed. At this stage, the surgeon may trial many different options for neck length by using different sizes of femoral head offset or, if the stem has a modular neck (which is available in an ABGII stem), different neck offsets as well. The surgeon is aiming to select an offset that does not increase the patient's leg length but also tensions the soft tissue, thereby optimizing the patient's hip biomechanics appropriately.

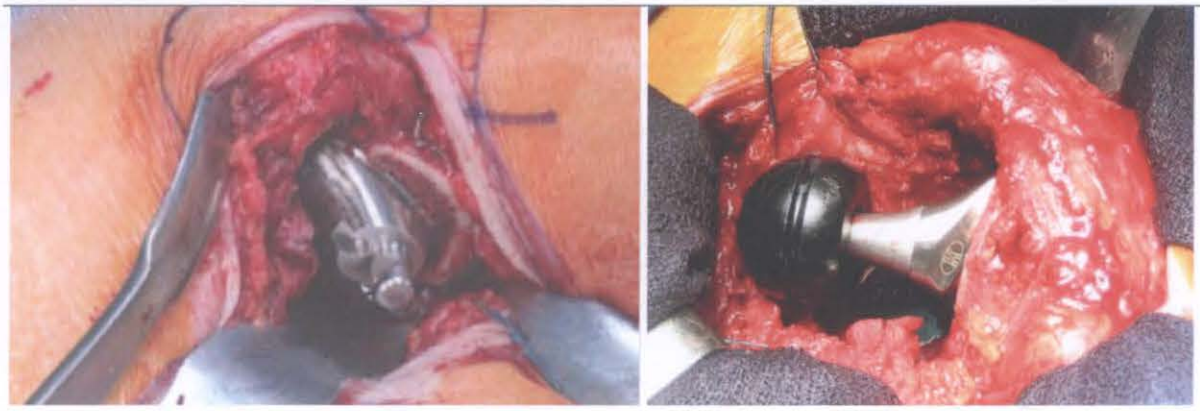

2.4.3.1.5 *Definitive Implant Insertion*

The trial insert is removed from the acetabular shell piece, the cup interior is cleaned and dried, and then the definitive polyethylene or ceramic insert is put in place.

The definitive stem is inserted; firstly by the surgeon pushing the stem into the canal. Then, to fully seat the stem, an insertion instrument is placed into the punch pad on the superior section of the stem. See Figure 49. The stem is then seated by firmly impacting the insertion tool with a mallet. It is important to note that this must be done carefully as this is the stage where the highest risk of intra-operative peri-prosthetic femoral fracture is seen.

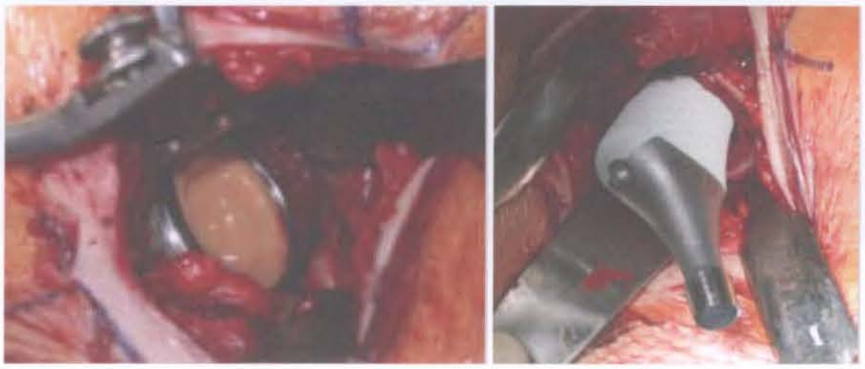

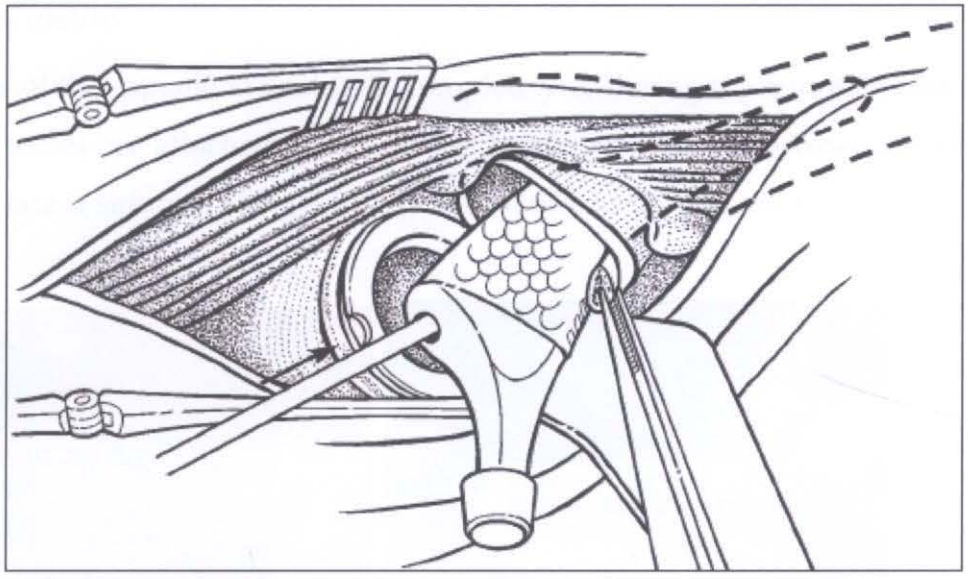

Figure 49 Femoral stem insertion

The taper is dried and the definitive femoral V40 head implant is impacted onto the stem neck with slight torsion. The hip is reduced and stability is checked again, both in extension and external rotation and in flexion, adduction and internal rotation.

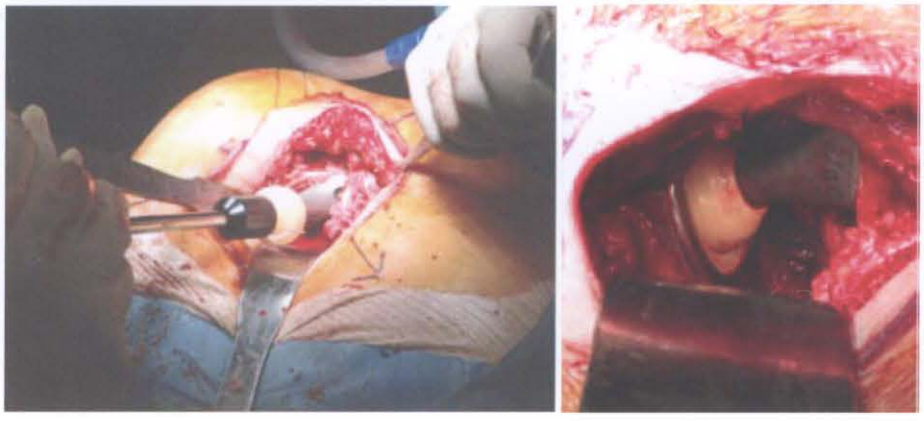

2.4.3.1.6 Closure

Both sides of the capsule are sutured, completely enclosing the femoral head. The short rotator muscles are attached to the greater trochanter with transosseous sutures, then the fascia lata is sutured, along with the subcutaneous tissues and the skin.

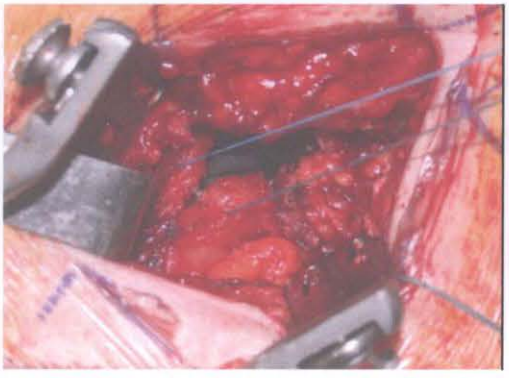

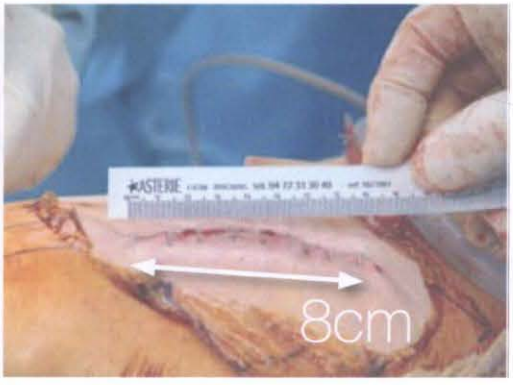

2.5 Computer assisted orthopaedic surgery

Surgical navigation systems provide positional information about surgical tools or implants relative to a target organ (bone), enabling the formulation of a surgical plan. Surgical navigation can use volumetric information provided by Magnetic Resonance Imaging, Computerized Tomography, or ultrasound scans (volumetric image-based navigation), intra-operative fluoroscopic images (fluoroscopic navigation) or intra-operative kinetic information about joints/morphometric information about bones (imageless navigation) [19, 21, 177-180].

Although initially developed to locate brain tumors based on stereotactic principles[181], computer-assisted surgery, utilizing robotic or image-guided technologies has been successfully expanded to a number of other surgical specialties, including computer-assisted orthopedic surgery. Computer assisted orthopaedic surgery aims to improve the perception that a surgeon has of the surgical field and the operative manipulation that they are undertaking. Conventional surgical handwork requires competences such as dexterity or fine motor skills, which are complemented by visual and tactile feedback. [182] Current computer assisted orthopaedic surgery systems have the ability to enhance visualization by displaying a virtual model of the operated anatomy in conjunction with the relevant information about the position of a surgical instrument or implant. This is usually done on a computer screen visible to the surgeon whilst operating. This visualization improves the surgeon's visual feedback by complementing the direct visual impression of the operation site.

The navigation system presents greater details, three-dimensional views or sights of internal structures, which are invisible to the naked eye or are difficult to visualize in the necessary way during the procedure.[182] Computer assisted surgery can be used at a number of levels. Passive computer assisted orthopaedic surgery systems are designed solely to assist pre-surgical planning and simulation of surgery, semi-active

computer assisted orthopaedic surgery systems have the capacity to perform non-surgical actions such as moving a cutting jig and active computer assisted orthopaedic surgery systems are able to perform surgical activities that are programmed pre-operatively.

Utilization of a navigation system is expected to increase, or enhance, the visual perception of the operator leading to an increased perception with which surgical tasks can be carried out. Surgical manipulations, such as drilling, chiseling, sawing, or the placement of implants, can be performed more accurately and with greater confidence. This should reduce the risk of harming the patient by damaging sensitive structures intra-operatively. As a result, numerous studies have reported smaller variations of the outcome of patients who underwent navigated surgery, when compared to the corresponding conventional approaches. For example, during total hip replacement, it has been demonstrated that computer assisted orthopaedic surgery provides more precise acetabular cup placement when compared to unassisted manual surgery. [183]

2.5.1 Tracking in a Navigation System

Navigation systems utilize a device, called tracker, to determine the spatial 3D positions and orientations of objects in real time. Different physical modalities have been investigated and used to remotely sense the spatial location of objects, such as electromagnetic field sensing. However, optical tracking is by far the most commonly used tracking modality. [182]

Optical tracking systems utilize infrared light that is either actively emitted or passively reflected from the tracked objects. See Figure 50.

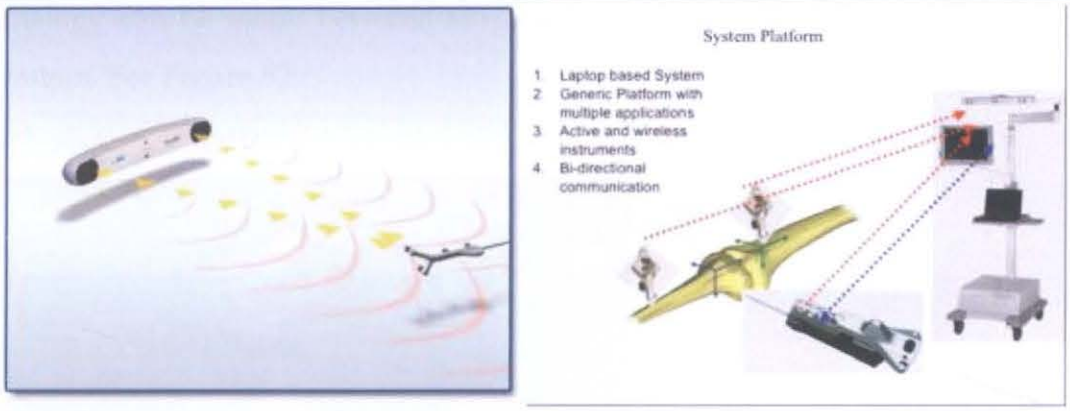

Figure 50 Optical tracking systems left passive right active (Stryker internal presentation)

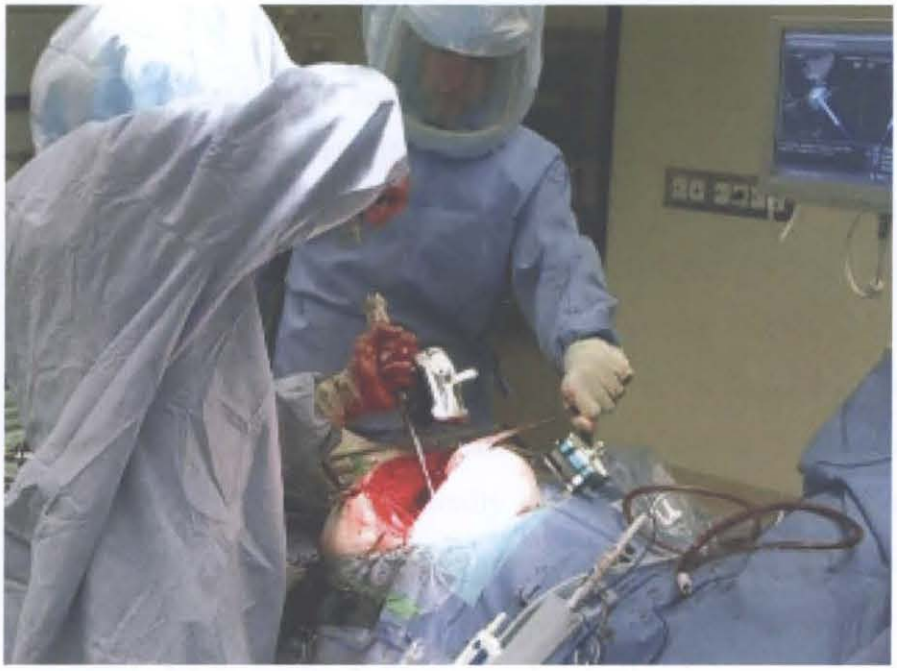

Figure 51 Instrument being tracked by an optical tracking system during a total hip replacement (Picture taken whilst observing surgery)

The basic principles of navigation are outlined in the following paragraphs using an optical tracking system but they apply for other physical modalities as well. A strong

analogy can be made between surgical Navigation systems and a Global positioning system. See Figure 52.

Figure 52 Optical Tracking analogous to a Global Positioning System. (Stryker internal presentation)

To track objects, such as surgical instruments or the patient's anatomy, light emitting or reflecting markers are rigidly attached to the tracked objects. A system consisting of an object to be tracked and markers rigidly attached to it is called rigid body. The optical trackers, also known as cameras, detect the reflected or emitted light signals and reconstruct the corresponding marker's 3D positions in the camera's coordinate system. From mathematics it is known that the positions of three non-collinear marker positions are required to uniquely define the 3D position and orientation of an object in space. Therefore, the markers are usually grouped in rigid constellations of three or more, forming their own local coordinate system. By increasing the number of markers, together with an optimized spatial arrangement, the visibility of a tracked object can be improved. Additionally, it has been shown that increasing the number of markers on a rigid body up to six significantly improves the navigation accuracy. With an increasing number of markers, the accuracy gradually converges against a maximum.

By means of calibration or registration, the real object geometry will be defined in the local rigid body coordinate system. Knowing the individual marker positions of a rigid body and the orientation of the real object within the local rigid body coordinate system,

the absolute position and orientation of the real object in the camera coordinate system can be computed. If the camera tracks more than one object simultaneously, the relative positions of all tracked objects can also be determined. (See Figure 53) [182]

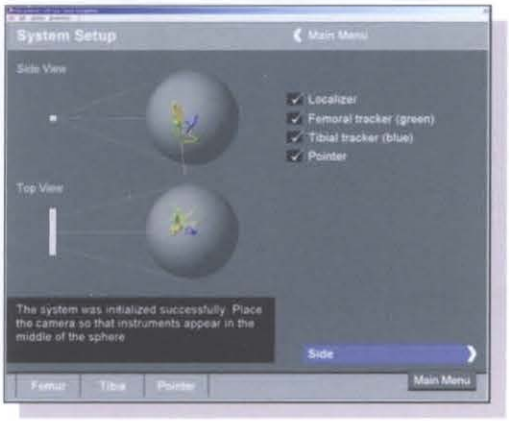

Figure 53 Instruments being tracked by a Navigation system (Stryker internal presentation)

For tracked patient anatomies, identical mechanisms are used. However, the instrument that is being tracked is rigidly attached to the patient, then that anatomy segment is tracked via the instrument. This instrument is referred to as the dynamic reference frame, or patient tracker. As long as the marker arrangement stays rigid in relation to the anatomy the rigid body concept is not violated and the relative position between patient anatomies and/or surgical tools can be computed. Figure 54 illustrates this tracking concept by showing the individual transformations between the camera coordinate system (C-cos), the tool coordinate system (T-cos), and a DRB attached to a patient anatomy forming a rigid body and defining a local coordinate system (A-cos). [182]

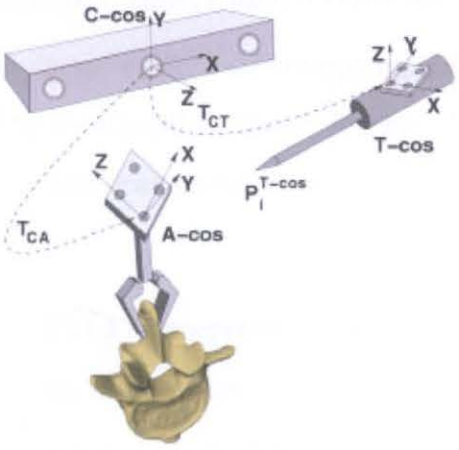

Figure 54 Tracking concept from [182]

2.5.2 Components of a computer assisted orthopaedic surgery System

The core of each computer assisted orthopaedic surgery system presents virtual representations of the operated anatomy and the performed surgical action. By linking this virtual model to the operated patient, it ensures that the replayed scene matches with what is performed at the surgical sites [182, 184]

2.5.2.1 Representation of Patient Anatomy-The Virtual Object

Operating with the support of a surgical navigation system requires an image of the treated anatomy to be used as the virtual object. The virtual object is predominantly represented on a computer screen after the image has been processed. The processing changes the patient image into the virtual object.

2.5.2.1.1 Image based representation

A large variety of image modalities have the potential to be used for this purpose. Predominantly, these images have been acquired preoperatively; however, intra-operative acquisition is also possible.

2.5.2.1.1.1 Preoperative Image Acquisition

These modalities could include Computerized Tomography, Magnetic Resonance Imaging , Preoperative X ray, or even Proton Emission Tomography. Each modality has its own advantages and disadvantages.

2.5.2.1.1.1.1 Computerized Tomography

Computerized Tomography is an almost ideal preoperative image modality for the needs of computer assisted orthopaedic surgery. It presents the outer shape and inner structures of bone anatomy with high resolution, good contrast and without any geometrical distortions. [182]

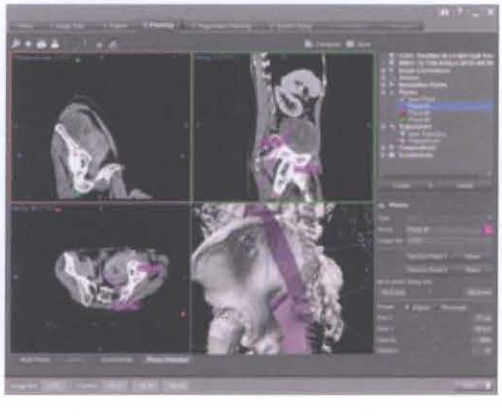

Figure 55 CT image used for Navigation of Pelvic Anatomy (courtesy of Stryker South Pacific)

2.5.2.1.1.1.2 Magnetic Resonance Imaging

In contrast, Magnetic Resonance Imaging suffers from poor hard tissue representation and sometimes considerable geometric distortions. Although special acquisition protocols have been suggested to, at least partially, overcome these difficulties, Magnetic Resonance Imaging are not widely used in orthopedic navigation [185] However, the use of Magnetic Resonance Imaging is almost standard for Cranial Navigation where visualization of the soft tissues, such as those of the brain, is essential.

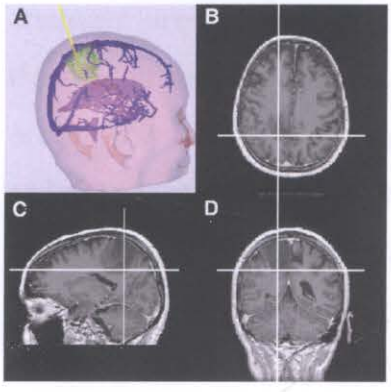

Figure 56 MRI Image used for Cranial Navigation

2.5.2.1.1.1.3 Preoperative X-Ray

Pre-operative X-ray is rarely used because of its geometrical imprecision and the fact that they only capture a two-dimensional (2D) perception of a three-dimensional (3D) scene. These issues have made developers refrain from building navigation systems based on X-rays. [182]

2.5.2.1.2 Image based Requirement for Image Registration

Where a preoperative image serves as the virtual object, a so-called registration or matching procedure is required to align the operated anatomy with its preoperative

image, assuming that the represented topology of the bone has not changed between image acquisition and surgical intervention.[182]

Numerous registration approaches have been described, which will register the preoperatively acquired image (or now the virtual object) to the patients anatomy [186]. Each of these registration techniques requires certain features to be interactively or semi-automatically identified. They must first be identified in the processed image and then the patient's anatomy. The spatial relation between virtual object and operated anatomy are extrapolated from the inherent knowledge of correspondence between these acquired feature sets. [182] Another way of describing this is to say that the co-ordinate system of the virtual object is identified and transformed to align with the co-ordinate system of the patient reference frame. Resulting in the virtual object being aligned with the patients anatomy.

One way of achieving this is by paired point registration. Using fiducial markers that attach to the patient before the preoperative image are acquired; a set of easily identifiable points can be defined both in the image and on the patient during the procedure. Then it is matter of identifying and mathematically describing these locations on the patient image, which is now the virtual object. Then, at the beginning of the procedure, these landmarks are touched and paired relative to the patient reference frame. See Figure 57. Then the two reference frames are processed with an iterative solver that tries to find the transformation matrix, which minimizes the mean error between all of the paired points.

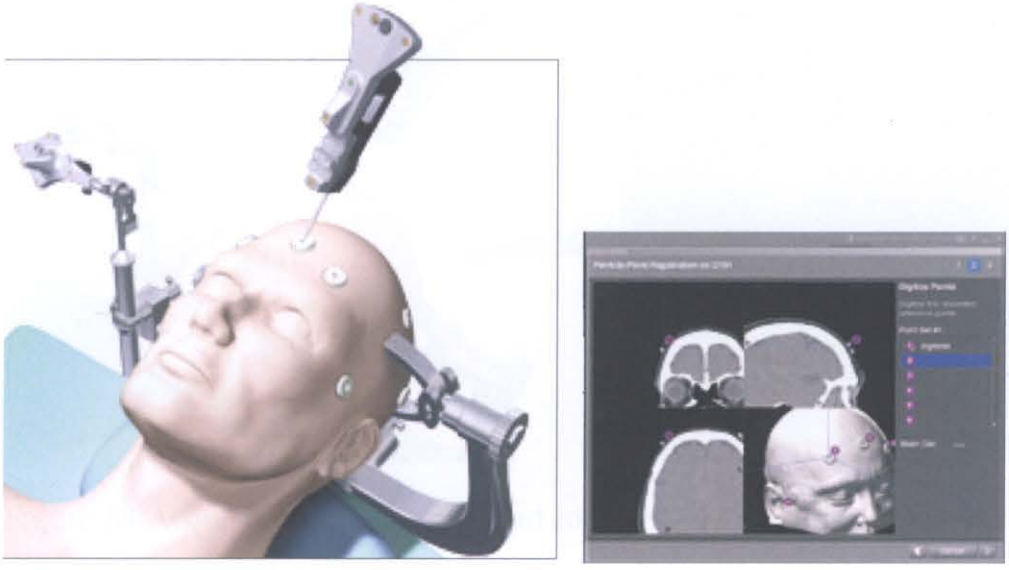

Figure 57 Point to Point registration of image to virtual object (images courtesy of Stryker South Pacific)

Since the perfect alignment of image and reality is crucial for the accuracy of the subsequently available navigation feedback, this usually interactive step requires careful execution and, as an element of safety, subsequent verification of the achieved result. [182] This procedure is far from perfect, and large errors in the registration can often be observed. There is often a need to improve the registration procedure with more refined techniques. One of these is that of a so-called surface matching. This is practically achieved by digitizing many indiscriminate points on the surface of the patient. This point cloud is then used to match to a processed surface from the virtual object.

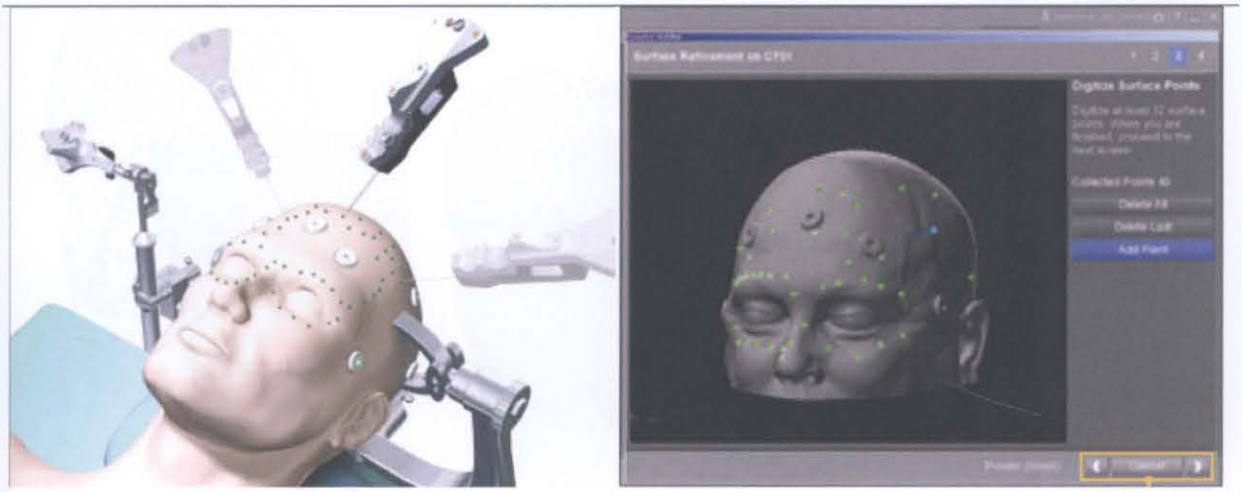

Figure 58 Acquisition of a point cloud for surface matching (Image courtesy of Stryker Navigation internal presentation)

There is a large body of literature in computer vision concerned with the surface-based registration problem. The approach normally used in the medical image processing community (and which is referred to in computer vision as the "free-form" surface matching problem) is to search for the transformation that minimizes some disparity function or metric between the two surfaces. The disparity function typically used for surface-based image registration is the mean squared, and optionally weighted, distance between points on one surface (the "data" point set) and corresponding points on the other surface (the "model" surface). The principal difference between point-based registration, which minimizes the mean squared distance between two sets of corresponding points, and surface-based registration is the availability of point correspondence information. Whereas point-based registration can be solved using any of several algorithms with closed-form solutions, the lack of exact point correspondence information causes surface-based registration algorithms to be based on an iterative search. Most algorithms calculate approximate point correspondence information for the current transformation at each iteration of the search.[187]

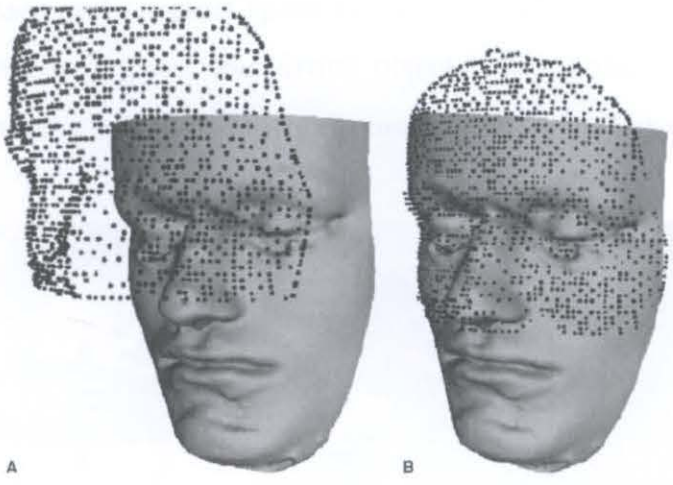

Figure 59 Surface based registration of the head[187]

2.5.2.1.2.1 Intra-operative image acquisition

Intra-operative imaging using 2D or 3D fluoroscopy can be used to build the virtual object in place of a preoperatively acquired image. [188] Utilization of an intra-operatively acquired image has some distinct advantages over other imaging modalities:

Using an intra-operative image allows for intra-surgical image update when the operated morphology does not any more correspond to what is frozen in the preoperative image. For example; in cases of fracture reduction or repositioning osteotomies. [182]

It is much more convenient, as there is no requirement to collect or process preoperative imaging to build the virtual object. It is acquired and processed during the procedure.
Intra-operative image allows for a much simpler registration of the patient image (virtual object) to the patient. Using an intra-operative means of image acquisition permits the imaging device to be integrated into the coordinate space of the navigation system. Provided a pre-calibration of the device has been done, the link between image

space and surgical space can be determined automatically. This effectively makes the need to register the virtual object to the patient obsolete. [182] These intra-operative imaging solutions may gain much more acceptance in the future.

Figure 60 Intraoperative 3D image from a flouroscopy being utilized with a Navigation Solution (From Siemens Website)

2.5.2.1.3 *Imageless Representation of the Virtual Object*

As another alternative, which goes entirely without any form of radiological image is the so-called image-free systems. These construct virtual models of the operated anatomy based exclusively on interactively acquired position data. Such data is either recorded by intra-operative palpation of anatomy or derived from the kinematic analysis of joint motion [189], which lets the computer assisted orthopaedic surgery system determine, for example, the rotation centre or axis of a joint. Resulting models are rather abstract since they are constructed from very sparse data [190]. To improve the realism with which the surgical field is represented on the screen, statistical shape atlases can be combined with the recorded data. [182]

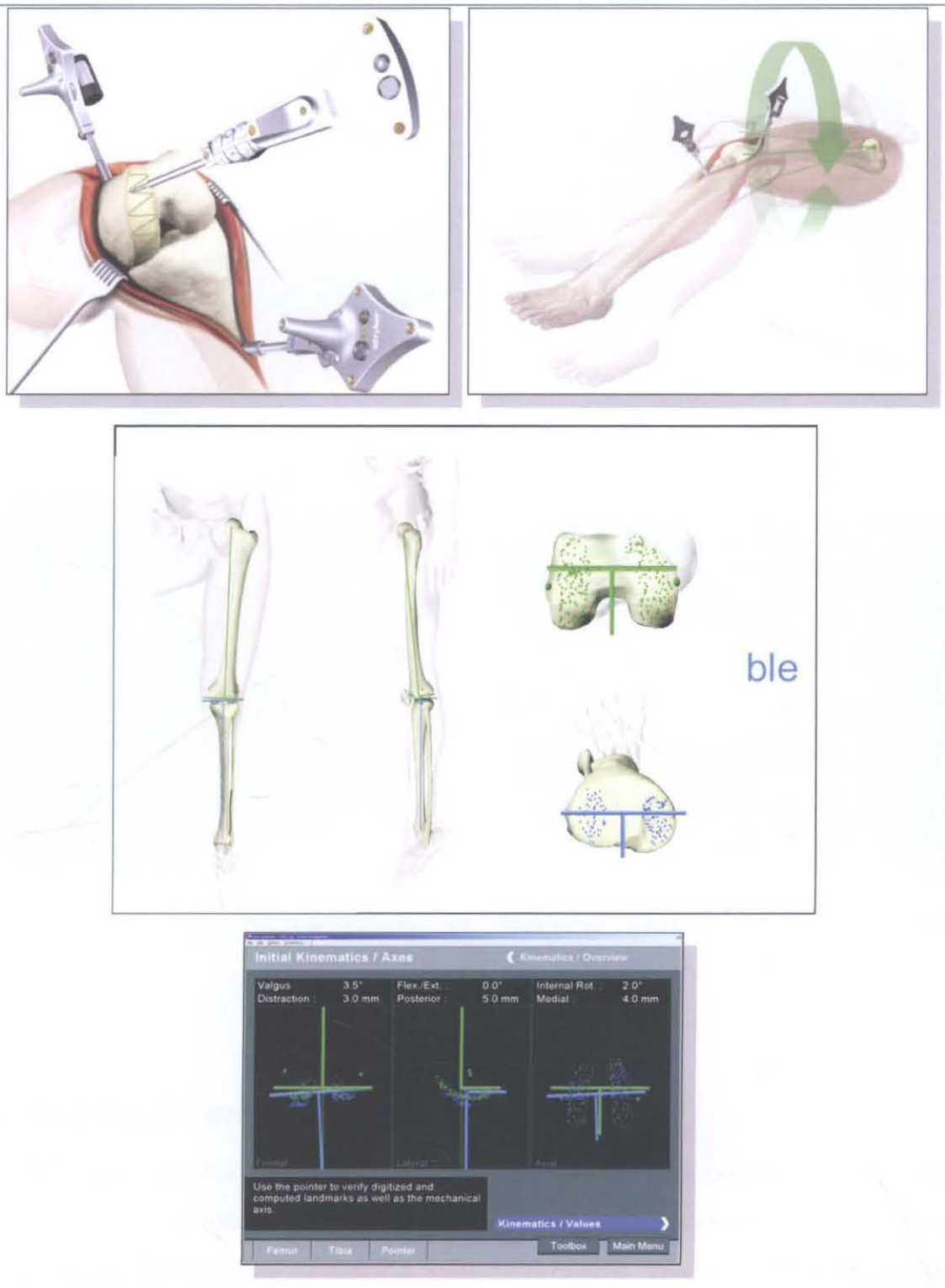

Figure 61 Imageless Digitization of Landmarks to build virtual object (From Stryker Navigation internal presentation)

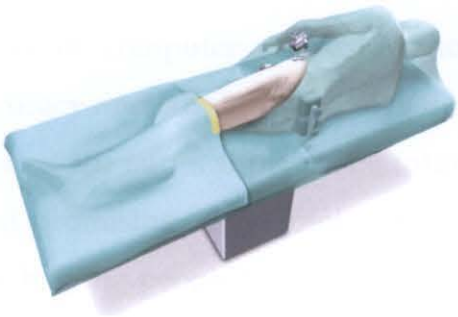

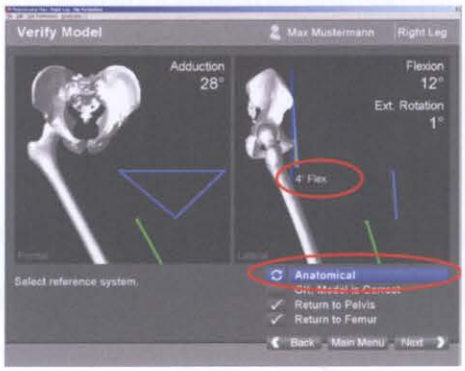

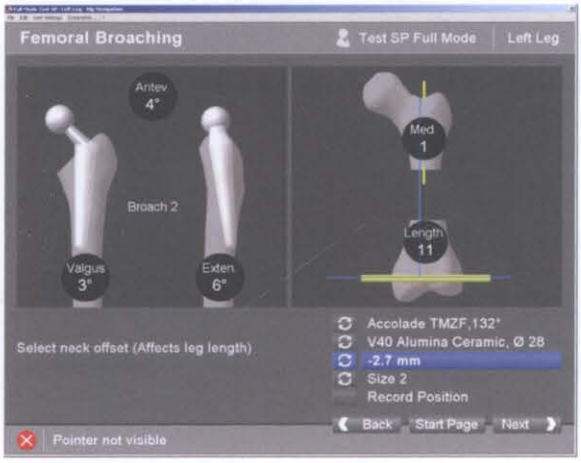

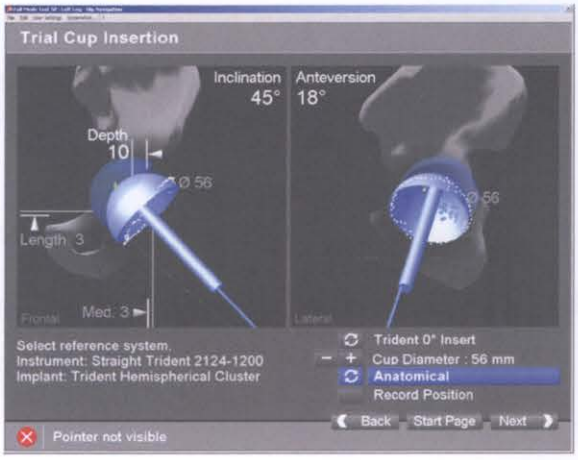

Figure 62 Imageless representations of Anatomy (Stryker Navigation internal presentation)

2.5.3 Robotic Surgery

Robotic surgery involves visualizing the surgical plan and the positions of the surgical tools. Three types of robotic systems have been designed to overcome the inaccuracy of hand-controlled positioning of surgical tools by surgeons. Two of the systems are semi-active: The first is free moving as it guides the tools into place to enable precise execution of a surgical action by the surgeon. The other constrains the movement of

surgical tools so that the surgeon can only move it within a preprogrammed range [191]. The third system is an active one, which automatically moves a milling device according to pre-surgical planning [192, 193].

Early studies of computer assisted orthopaedic surgery suggest that it improves surgical accuracy and surgical outcomes through enhanced pre-operative planning and optimization of the surgical plan. The future of computer-assisted surgery is therefore exciting and promising. Total joint replacement is a proven procedure that has been successfully helping people live with less pain and greater mobility for decades. With the use of computer assisted orthopaedic surgery, total joint replacement can continue to evolve and improve, with the development of new, rapid surgical procedures with minimal invasiveness that surgeons are currently not technically able to perform.

2.5.4 Total hip replacement- using the Stryker Navigation System

To utilize the Navigation system at this stage the unit must be placed opposite to the surgeon with the camera pointing at the operative site.

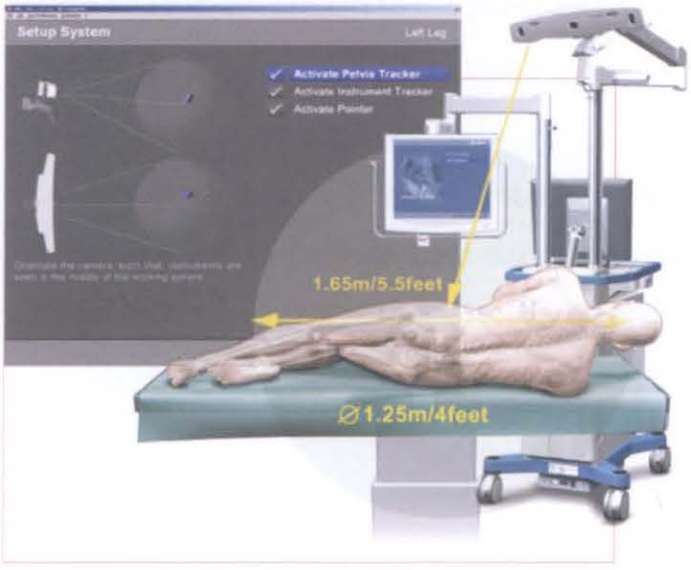

Then the navigation system's pelvic tracker must be attached to the patient's pelvis, in order to provide a stable reference frame, from which all future measurements can be made from. This is achieved by inserting two percutaneous pins into the superior iliac crest of the patient. Attached to these pins is a device, which is then attached to the tracker itself. The Navigation tracker must then be orientated so that it points directly at the Navigation systems camera so that the infrared light emitted from the LEDs on the tracker can be received by the camera for the entirety of the procedure.

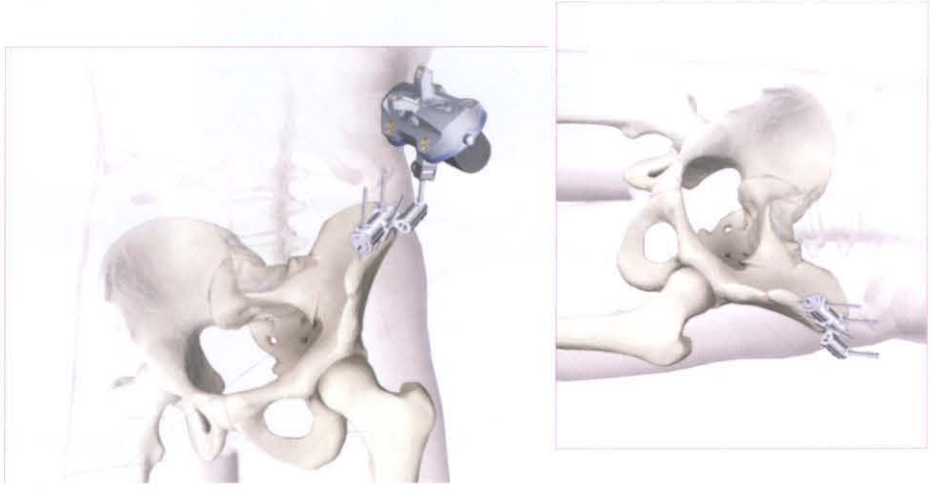

Figure 63 Trackers affixed to the patient's pelvis during navigated total hip replacement surgery.

A registration process is then undertaken which involves utilizing the Navigation systems pointer to palpate landmarks and record the, x, y, z co-ordinates of these landmarks relative to the reference frame attached to the patient (the patient tracker).

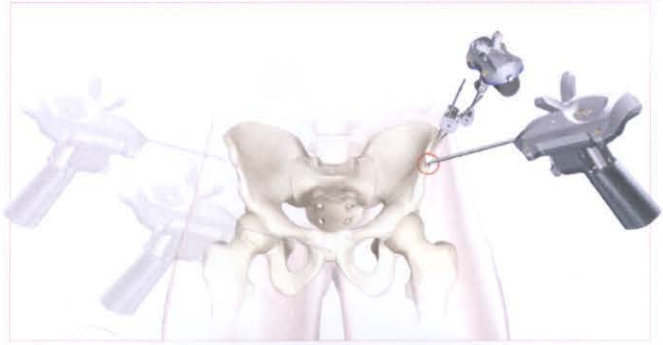

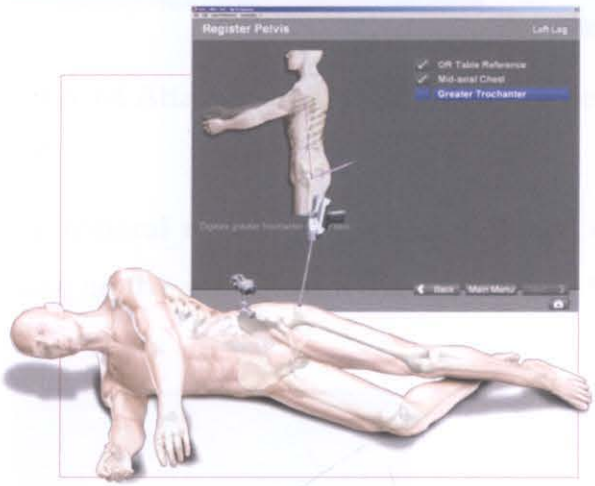

If navigation is being used for the femoral portion of the surgery only (it is possible to only navigate the acetabular cup position) at the stage before the hip is dislocated, then the femoral reference frame must be attached to the patient's femur. This is achieved by affixing two or three pins into the patient's distal femoral epiphasis. These pins then attach to the tracker, which is orientated toward the camera. See Figure 64.

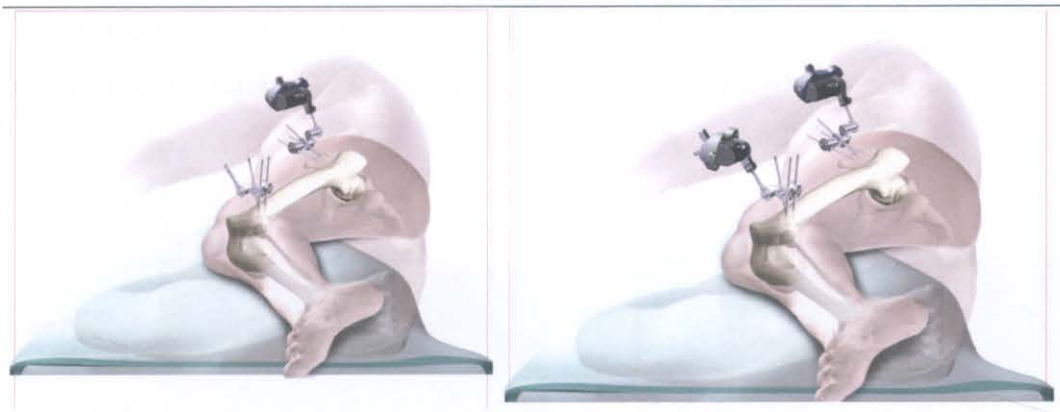

Figure 64 Attachment of the femoral tracker to the femur

The femoral reference frame is digitized using the pointer to digitize landmarks that make up the axes of the femur. See Figure 65.

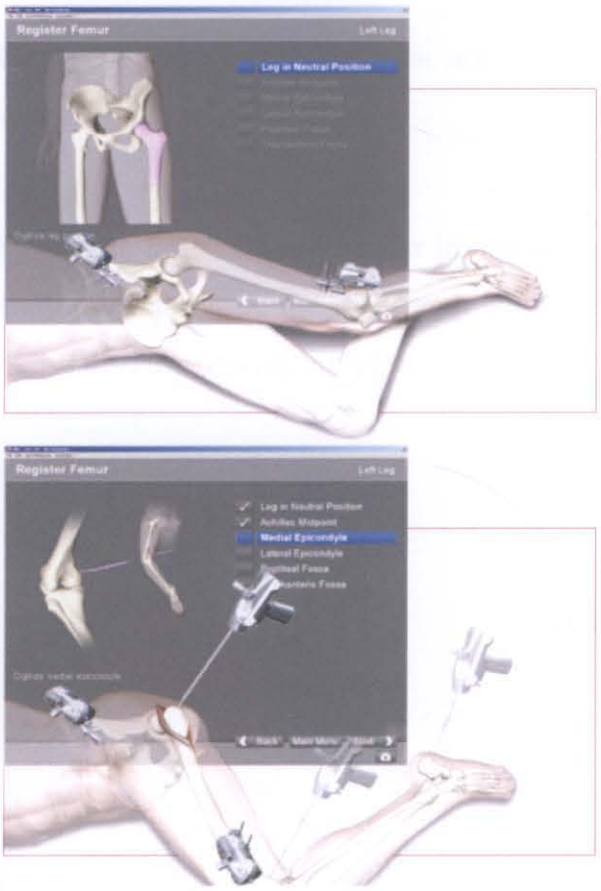

Figure 65 Femoral landmarks are digitized to define the femoral limb axes

The surgical approach is then undertaken and the femoral head is dislocated exposing the acetabular surfaces. These surfaces are digitized with the poitner. See Figure 66.

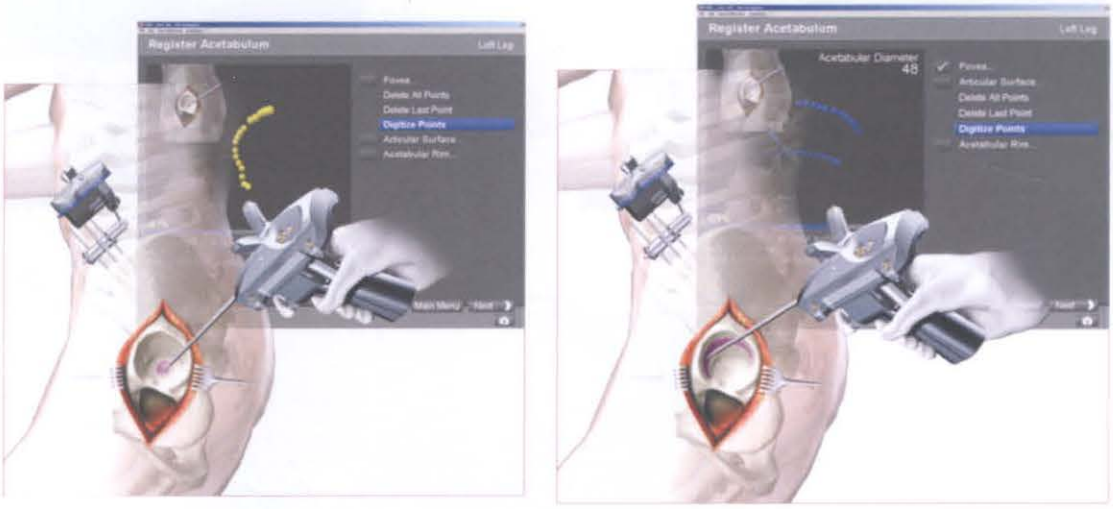

Figure 66 Acetabular surfaces are digitized during navigated total hip replacement surgery

Now with both and acetabular image and a femoral image, made up from the digitized anatomy relative to the trackers it is possible to measure and characterise the positions of the instruments and implants relative to the anatomy. See Figure 67 and Figure 68.

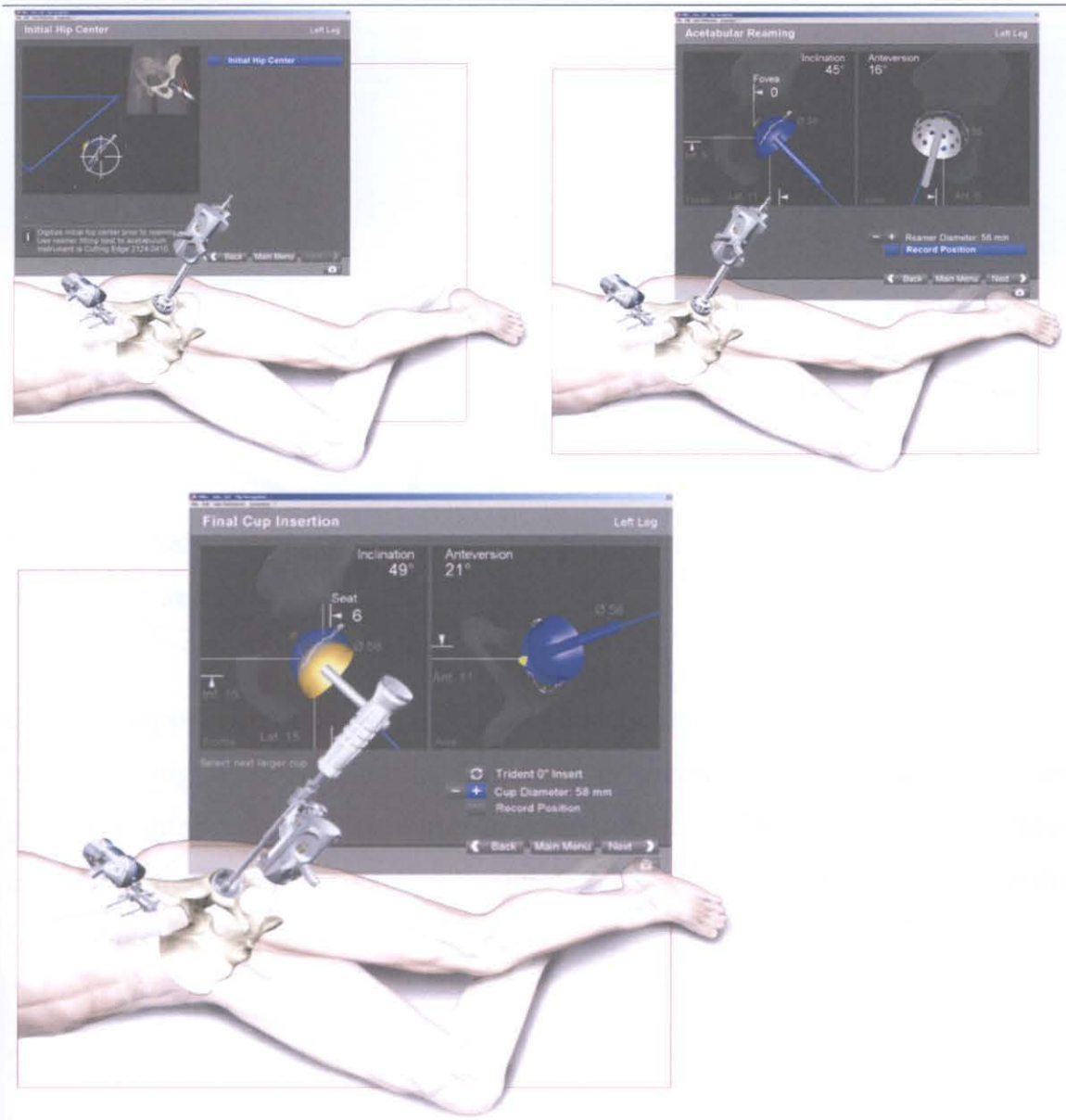

Figure 67 Positions of instruments and implants can be characterized with reference to the acetabular anatomy

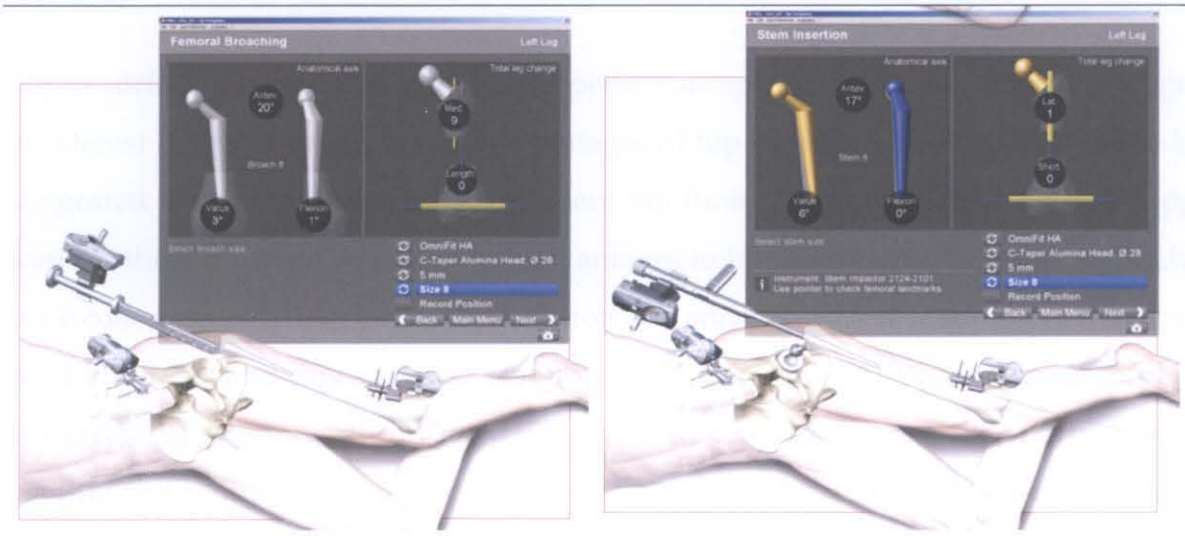

Figure 68 Positions of instruments and implants can be characterized with reference to the femoral anatomy

Of most importance to the work in this thesis, the instruments can be tracked whilst the stem is being inserted into the femur as is shown in Figure 68. Combining this positional information with a dynamic subject specific finite element model allows for a characterization of intra-operative loading. This novel approach to subject specific finite element modeling is detailed in Chapter 4.

2.6 Hip resurfacing

Hip resurfacing is considered by many as a viable alternative to conventional total hip arthroplasty, especially in younger and more active patients. In this procedure, the socket is replaced in a similar manner to a total hip replacement. The femur, however, is covered or "resurfaced" with a hemispherical component. This fits over the head of the femur, and spares the bone of the femoral head and the femoral neck. It is fixed to the femur with cement around the femoral head, and has a short stem that passes into the femoral neck. Hip resurfacing is most commonly performed on younger or more active patients.

Hip resurfacing surgery is an old orthopedic concept that has undergone a resurgence of interest in recent times. Several advantages of hip resurfacing arthroplasty have been suggested in the literature; however, there are limited or inconsistent data to support some of these claims. The purported advantages to hip resurfacing arthroplasty include: bone conservation [194]; improved function as a consequence of retention of the femoral head and neck and more precise biomechanical restoration [195]; decreased morbidity at the time of revision arthroplasty [196]; reduced dislocation rates[197]; normal femoral loading and reduced stress-shielding. Simpler management of a degenerated hip with a deformity in the proximal femoral metaphysic (after trauma or osteotomy) [198], an improved outcome in the event of infection, and a reduced prevalence of thromboembolic phenomena as a consequence of not using instruments in the femur [199] have also been proposed as advantages. While the data is limited or inconsistent to substantiate these claims, I will nevertheless review the available evidence.

2.6.1 History

The concept of hip resurfacing is not new. Contemporary designs have evolved directly from the original arthroplasty mold introduced by Smith-Petersen in 1948 [200]. Despite being a hemi-arthroplasty, with no means of stable fixation to the femoral head, some have survived for many years, although the outcomes were unpredictable. The first total resurfacing arthroplasty was developed by Charnley [201] in the early 1950s using a Teflon-on-Teflon bearing. This implant was associated with a high rate of early failure that Charnley ascribed to avascular necrosis of the femoral head. Charnley subsequently recognized the poor wear characteristics of Teflon when he used it as the bearing of a total hip replacement.[202]

In 1960, Townley [203] attempted a hip resurfacing procedure using a metal-on-polyurethane articulation. However, this came to be associated with catastrophic wear

and was later replaced by a metal-on-polyethylene articulation. In 1967, Muller [204] designed a metal-on-metal articulation. Despite excellent early clinical results, Muller abandoned the use of the metal-on-metal articulation in favor of a metal-on-polyethylene articulation. Six of the initial 18 all-metal articulations were revised after functioning for up to 25 years.

In 1970, Gerard [205] introduced a bipolar metal-on-metal resurfacing system, which consisted of a Luck cup inserted into an Aufranc Vitallium cup; with this system, movement occurred between the prostheses and between the outer cup and the bony socket. The Aufranc cup was later substituted, in 1972, with a polyethylene cup in an attempt to decrease the friction between the two implants. However, it was later discovered that the convex surface of the polyethylene component, which articulated with the acetabulum, wore rapidly and this combination was abandoned in 1975 in favour of a metal bipolar combination with a polyethylene inlay. Starting in 1976, a cementless alumina ceramic-on-ceramic resurfacing was used by Salzer [206] in Vienna but was soon abandoned because of high rates of early loosening

Eicher and Capello [207], in the United States, developed a cemented hip resurfacing system, in 1972, using a metal femoral and a polyethylene acetabular component, which was reinforced with a metal backing in 1982. Cemented hip resurfacings using polyethylene acetabular components and metal femoral components were implanted in 1971 by Paltrinieri and Trentani in Italy and again in 1974 by Freeman [208] in the United Kingdom. Wagner, also in 1974, introduced a hip resurfacing system in Germany, which became widely used in Europe [209]. The acetabular components of his system had a thickness of only 4 mm but head preparation was crude. Freeman had used a HDP femoral component and a metal acetabular component earlier, but this was associated with rapid wear of the convex surface.

In Japan, Furuya [210] performed 13 hip resurfacings using a stainless steel acetabular component with a high density polyethylene (HDP) femoral component fixed with cement, and then subsequently reversed the material combination, using a metal or ceramic femoral component. In 1972, Nishio [211] combined an Urist acetabular component with his own femoral component made from Vitallium and in 1975, Nishio substituted the acetabular component with a polyethylene-lined cementless socket. In 1974, Tanaka, introduced a hybrid system with a cemented eccentric socket and a metal head.

Amstutz introduced the THARIES (total hip articular replacement using internal eccentric shells) in 1975, at the University of California–Los Angeles. The prosthesis was cemented and consisted of a Co-Cr femoral component and an all-polyethylene acetabular component. Both components were eccentric, with a maximum polyethylene thickness of 3.5 to 5.5 mm. A plasma-sprayed metal-backed polyethylene acetabular component for use with cement was introduced in 1982 [197]. In 1983, Amstutz implanted the first cementless resurfacing arthroplasty with a Ti-6Al-4V femoral component, modular ultra high molecular weight polyethylene acetabular liners, and pure titanium mesh porous backing. Initially, the sockets were hemispherical with screws, and later, the first chamfered cylinder socket with an interference fit was developed.

The renaissance of metal-on-metal articulations for total hip arthroplasty began in 1988. Amstutz, in 1988, developed another porous-coated cementless system with a Co-Cr femoral component, a modular liner, and a Ti-6Al-4V hemispherical acetabular component. In 1989, Buechel and Pappas [212] introduced a cementless resurfacing system with a modular acetabular component and a titanium nitride ceramic-coated titanium alloy femoral component. [213] Weber, in collaboration with Sulzer Orthopedics (Winterthur, Switzerland), developed the Metasul bearing, a precisely engineered, high carbon-containing, wrought Co-Cr alloy with excellent wear

characteristics. Large numbers of these bearings were used in Europe with good early results. The availability of a durable low-wear bearing that could be used in a large diameter articulation enabled Wagner [209], in Germany, to introduce a second-generation hip resurfacing in 1991. This system was cementless. The acetabular component was a titanium alloy shell with a Metasul inlay. The thickness of the construct and the extensive macro features on its external surface made it difficult to implant. There were only four sizes available and the instruments for the preparation of the femoral head were crude. The first design was screwed onto the reamed femoral head, but because of insertion difficulties, a press-fit version was developed. Only small numbers of the Wagner metal-on-metal resurfacings were used, and no long-term results are available.

In the same year, McMinn [214], in the United Kingdom and in collaboration with Corin Medical (Cirencester, United Kingdom), introduced a hip resurfacing based on a cast Co-Cr alloy. The initial design was smooth surfaced and press fit on both sides. The acetabular component was a modification of the Freeman finned cup. This design was associated with high incidence of early failure due to aseptic loosening of both components. The following year, the components were coated with hydroxyapatite (HA), but only a small number of these implants were inserted. McMinn then introduced a system in which both components were cemented. This system had a high incidence of early acetabular loosening due to cement-cup debonding, which led to the introduction of a hybrid system in 1994 with a cementless HA-coated acetabulum. This implant was withdrawn in 1996, apparently due to manufacturing problems.

By the end of 2004, most of the main implant manufacturers had introduced metal-on-metal hip resurfacing systems. All of these systems have a number of features in common, including (1) a bearing made from high carbon-containing Co-Cr alloy, (2) cementless fixation of the acetabular component, and (3) cemented fixation of the femoral component. There are, however, important differences between these implants,

particularly relating to the metallurgy and geometry of the bearing and to aspects of the fixation of the acetabular and femoral components.

2.6.2 Concepts for hip resurfacing

2.6.2.1 The 'small ball' and 'large ball' paradigms, metal-on-metal and resurfacing

Clarke et al [215] describes an important concept that must be understood in regard to resurfacing and femoral head size that being the 'small ball' and 'large ball' paradigms. One of the most significant advantages for hip resurfacing over traditional total hip arthroplasty is that resurfacing uses larger anatomical sized femoral heads whereas traditional total hip replacement utilizes smaller heads. Larger femoral components are inherently more stable and reduce the risk of dislocation, a serious complication of total hip arthroplasty. The reason larger femoral heads are more stable is because the distance to dislocation is larger when the head size is larger providing mechanical resistance to dislocation. See Figure 69.

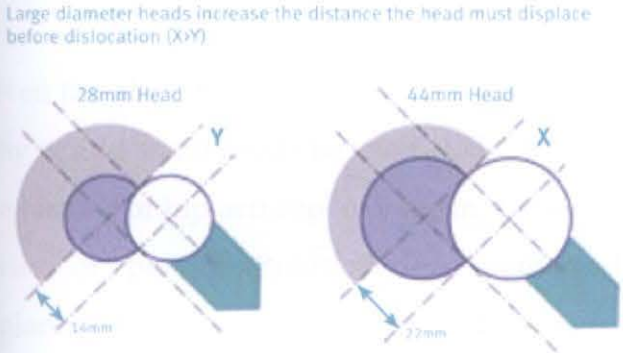

Figure 69 Distance to dislocation is greater when the femoral head size is larger (Stryker internal presentation)

The use of anatomical sized heads for modern resurfacing is possible because the material used for both the head and cup is metal. The metal material has sufficient strength to support the geometrical restrictions that the resurfacing design has. That is, the requirement for a relatively thin walled hollow femoral head and a thinned walled acetabular cup. Hip resurfacing has the requirement to produce a thin acetabular shell of between 3 and 5 mm. This measurement limits the material of choice to metal-on-metal bearings. See Figure 70. Other modern bearing options such as ceramic or cross linked polyethylene generally lack the required strength to be a viable material option for the design.

Figure 70 A typical resurfacing hip design: A thin walled cup and thin walled hollow femoral head. (Stryker internal presentation)

Given the abovementioned advantages of larger femoral heads, the obvious question is why would small heads be used at all? To illustrate this it is important to look back into the history of hip arthroplasty again. Observations of revision components from earlier series of polytetrafluoroethylene cemented total hip replacement (Total hip replacement) in the 1960s, noted that progressively downsizing the femoral ball (41.5 to 22.25 mm) led to noticeably less wear in vivo. [216]. This concept is illustrated in Figure 71. It was clear that larger femoral heads increased wear, and that with the bearing materials available early in the development of hip arthroplasty, a compromise was needed to increase the longevity of the prosthesis.

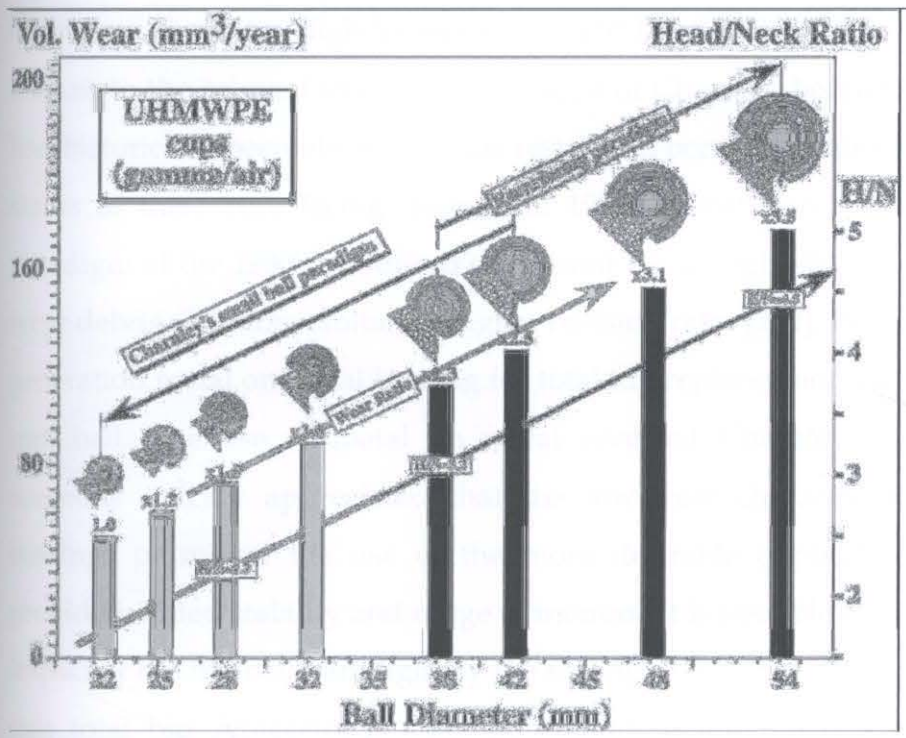

Figure 71 Wear rates of Ultra High Molecular Weight Polyethylene cups indicated with 1.8-fold wear increase over the 22 to 32 mm range of total hip replacement ball sizes. [215]

Consequently, Charnley et al [217] introduced the concept of a uniquely small ball (22.25 mm) in a cemented ultra-high molecular weight polyethylene (UHMWPE) cup. With improved bearing surfaces such as ceramic on ceramic and metal on metal the wear problem was minimized and larger femoral head size became possible. It was much easier to balance dislocation risk against wear issues when wear was so significantly reduced. [218] The resurfacing concepts launched in the 1970s and 1980s used even larger diameter anatomic sized heads and introduced the thin-walled Ultra High Molecular Weight Polyethylene cup. [215]

Over time, the Ultra High Molecular Weight Polyethylene cups restricted the surgeons' choices to the original small-ball paradigm of Charnley because wear was increased as had historically been observed. This restriction occurred after Clarke [219] reviewed the status of these resurfacing designs in 1982. Unfortunately the resurfacing's big-ball paradigm of the 1980's produced significant Ultra High Molecular Weight Polyethylene wear debris with concomitantly higher revision rates [220]. In the late 1980s, the second-generation metal on metal bearing for total hip replacement was launched using the 28-mm ball. The use of metal on metal reversed Charnley's small-ball paradigm as surgeons quickly appreciated that the low-wear characteristics of metal on metal bearings permitted the use of the more desirable big-ball concept. Together these provided added stability and range of motion. It is possible to visualize the tremendous impact of the big-ball paradigm by the scaling of ball diameters. Compared with the 28-mm total hip replacement size, the 38-and 54-mm resurfacing added 30% to 90% additional range of motion (approximately 1_ range of motion added per 1 mm of diameter). The design of the "thin" acetabular cup combined with the now standard, porous-coating layer for fixation was facilitated by the high-strength cobalt chromium (CoCr) alloy.

Wear rates of Ultra High Molecular Weight Polyethylene cups indicated with 1.8-fold wear increase over the 22 to 32 mm range of total hip replacement ball sizes. Prior clinical experience with polytetrafluoroethylene cups led to a downsizing in femoral balls from 41.5 mm to 22.25 mm, concluding that Charnley's 'small ball' paradigm produced the least Ultra High Molecular Weight Polyethylene wear. The range of total hip replacement balls (22– 32 mm) and femoral resurfacing shells (38– 54 mm) is evidence of the dramatic size of the scale. Also shown in Figure 71 the nominal head/neck ratios (H/N; 12 mm diameter neck assumed) increasing from 2.3 with 28 mm ball to 4.5 with 54 mm ball, thereby conferring greater range of motion and stability with the 'large ball' paradigm.

2.6.2.2 Patient selection for hip resurfacing

The ideal candidate for a hip resurfacing procedure is currently believed to be a young (<60 years) active man with normal proximal femoral bone geometry and bone quality who would be expected to outlive any current conventional prosthesis. Preoperative diagnoses can be varied and include osteoarthritis, osteonecrosis, and degenerative conditions secondary to developmental hip dysplasia, slipped capital femoral epiphysis, and Legg-Calve´-Perthes disease [151].[221]

2.6.3 Failure of hip resurfacing

During the late 1990's and early 2000's there was a rapid increase in the number of resurfacing procedures being performed and previously recognized complications began to reoccur. [222]

Problems that have been encountered can be divided into two main groups: (1) those associated with any type of hip arthroplasty; for example, dislocation, thromboembolic disease, heterotopic ossification, nerve palsies, and vascular damage; and (2) those that are more specifically related to the hip resurfacing procedure, namely, femoral neck fractures, avascular necrosis, raised metal ion levels.

2.6.3.1.1 Metal ion levels

As previously discussed in section 2.3.1.2 metal-on-metal articulations have recently become a major source of concern. This is not exclusively a hip resurfacing issue. In fact, recent evidence suggests that the issue is more of a concern for total hip replacement with a *large* diameter metal-on-metal femoral head. The metal ion levels observed in blood serum following hip resurfacing are less than those observed following a total hip replacement with a *large* diameter metal-on metal bearing [223]. Further, The 7th Annual report of the National Joint Registry for England and Wales revealed that *large*

diameter metal-on-metal total hip replacement has failure rates above those of resurfacing, and in fact the highest of all hip replacement procedures.[224]

It has been suggested by Bolland et al [225] that the increased metal ion levels observed in the blood serum following *large* metal-on-metal total hip arthroplasty is the result of an increased torque at the modular head-neck taper junction. This increased torque a higher demand on the head-neck junction than is placed on the same junction in smaller metal or ceramic femoral heads [225]. This possibility can be visualised looking at Figure 72- which is actually a diagram intended to show the greater range of motion with larger femoral heads.

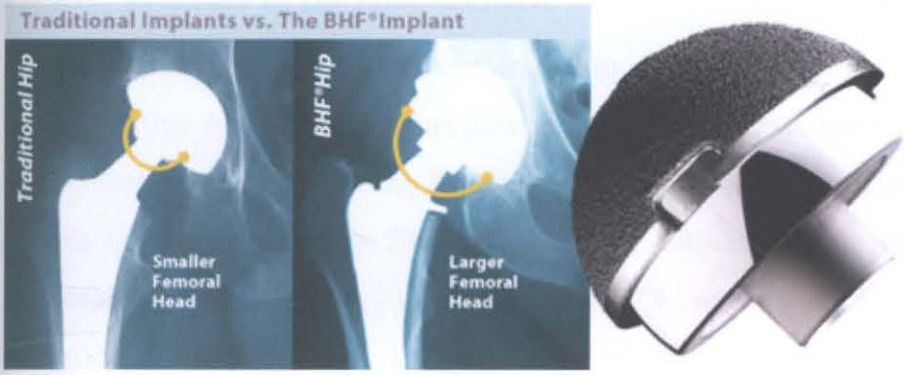

Figure 72 Traditional implant vs. large diameter metal-on-metal femoral head: Greater ROM [226] (but also possibly greater torque on the junction [225])

2.6.3.1.2 Avascular necrosis of the femoral head

The required preparation of the femoral head can cause avascular necrosis, which could ultimately lead to failure of the prosthesis due to loosening or peri prosthetic fracture. The arthritic hip undergoes changes in the vascular supply of the femoral head, with the blood supply being predominantly intraosseous in arthritic hips rather than subsynovial vessels [227]. Current studies report a low incidence of avascular necrosis as a cause of implant failure at a mean of 3 years [214, 228, 229]. Studies on isolated

primary hemiresurfacing of the femoral head report an absence of avascular necrosis on retrieval specimens [230]. These series appear to support Freeman's [227] theories.

Other possible reasons for the small incidence of avascular necrosis with resurfacing procedures may reflect that it is the neck rather than the head that is being resurfaced. Considering that the technique involves resecting a portion of the zenith of the head and pressurizing cement for several millimeters into the prepared surface, it may be that there is not much remaining of the bone proximal to the fused epiphyseal plate [222].

2.6.3.1.3 Fracture of the femoral neck

The most common early complication of hip resurfacing arthroplasty, and one which is unique to this type of hip arthroplasty, is peri-prosthetic fracture of the femoral neck. The Australian National Joint Registry reports the early revision rate (<1 Year) for hip resurfacing arthroplasty in 2004 was 1.9%[11]. This is well above the early revision rate for total hip arthroplasty. Of this 1.9%, 67% were due to femoral neck fracture. Retention of the femoral neck exposes the patient to the risk of femoral neck fracture in the immediate postoperative period and in the future as per the general aging population [222].

According to Steffen [231], fracture rates reported by ten different surgeons who performed hip resurfacing arthroplasty ranged from 0% (in a study by Daniel [229], who analyzed 446 hips resurfaced with metal-on-metal implants) to 12% (in a study by Capello [207], who reported on sixty-eight hips resurfaced.

Morlock et al [232], in an analysis of fracture patterns and histological characteristics in association with fifty-five failures of femoral resurfacing established that many of those failures were considered to have a dual-phase mode. The original trauma to the bone

occurred at the time of the operation; healing was initiated, but the actual failure occurred several weeks or months later. This suggests that fractures that occur in the short-term may be related to patient selection or biomechanical or technical factors, whereas those occurring later may be associated with other factors such as impaired healing.

Beaule et al [221] carried out extensive implant retrieval studies on ninety-eight metal-on metal hip resurfacing prostheses, including twenty-eight that were associated with a fracture of the femoral neck. The conclusions were similar to the abovementioned Morlock et al. study [232]. The majority of the fractures in the Beaule et al. study were noted within two months after the operation and had occurred through an area of active bone repair at the femoral neck-component junction. In contrast, in seven cases with an average time to fracture of fifteen months, a substantial proximal segment of the head was fully devascularized and necrotic and the fracture had occurred between the interface of the dead and viable segments of bone, within the area covered by the femoral component.

Consistent with the biomechanical principles suggested by Freeman and by Paul E. Beaule [233] are the technique-associated factors including notching of the superior part of the femoral neck and varus femoral placement relative to the anatomical neck . With the femoral component in the varus position, there are increased tensile forces in the superior-lateral aspect of the femoral neck, increased shear stresses at the head-neck junction of the prosthesis, and increased compressive forces on bone that is likely to be weak under compression.

A multi surgeon national audit of the first 3429 metal-on-metal hip resurfacing arthroplasties performed in Australia over a four-year period demonstrated a fracture rate of 1.46% at a mean of 15.4 weeks (range, zero to fifty-six weeks) postoperatively.

Important patient, surgical, and postoperative factors with regard to the risk of fracture were identified from this review. [222]

In view of the prevalence of femoral neck fractures, a period of protected weight bearing should be considered in some or all cases to allow the operatively machined femoral neck time to heal and remodel [222] [234]. Displaced femoral neck fractures require conversion to a conventional total hip replacement.

Intraoperative factors such as poor exposure, incomplete seating of the femoral component, and inaccurate direction of impaction on the implant may also contribute to fracture risk.[233]

2.6.4 Implant positioning and femoral neck fracture

One goal of hip resurfacing arthroplasty is to reproduce, as closely as possible, the normal anatomy of the proximal part of the femur and the hip joint, and it has been suggested that implant positioning may have a greater impact on implant survivorship and patient function than it does in a conventional hip replacement [235]. It has been generally recommended that surgeons strive for a relative valgus placement of while avoiding notching of the superolateral cortex of the femoral neck in order to minimize the risk of peri-prosthetic femoral fracture. However positioning of the femoral component is a complex balance for the surgeon. Valgus positioning may sometimes lead the surgeon to compromise on femoral offset which may have a deleterious effect on hip biomechanics but also longevity.

2.6.4.1.1 Femoral offset and resurfaced hip biomechanics

The fact that some femoral necks have naturally a more varus orientation must be taken into account when positioning the femoral component in resurfacing. Although relative

valgus orientation is favorable to implant survivorship (which is discussed in more detail below), it results in a decreased femoral offset. [233]

Although a decreased femoral offset with a stemmed device is associated with increased polyethylene wear and instability of the hip, the clinical implications of a reduced femoral offset in hip resurfacing has yet to be defined. Both Silva [236] and Loughead et al. [237] have shown that femoral offset is reduced with hip resurfacing, when compared with a stemmed replacement. With hip resurfacing, the lack of modularity on the femoral side requires the use of other means to optimise the femoral head/neck offset. Optimum positioning of the femoral component and correction of any underlying abnormality to maximize the femoral head/neck offset ratio will minimize the risk of impingement and maximize the functional range of movement. Because the femoral head overlaps with the cortex of the neck and projects most prominently posteriorly, it is necessary to identify the neck axis or else there will be a tendency to place the femoral component more posteriorily on the neck. This will add to the deficient anterior offset already present, which, it left uncorrected, can result in persistent pain secondary to impingement.

Although the larger diameter of the femoral head with hip resurfacing may provide a greater functional range of movement, Chandler et al. [238] compared the range of movement of normal and prosthetic hips and demonstrated that bony contact eventually becomes the limiting parameter, so that an increase in the diameter of the head no longer contributes to increased movement.

Silva et al.[236] and Loughead et al.[237] documented an average decrease in femoral offset ranging from 4.5 to 8 mm. This, combined with a limited capacity to correct a limb-length discrepancy of >2 cm, has put into question the capacity of hip resurfacing arthroplasty to properly restore hip biomechanics. However, it is important to note that both of these studies were retrospective. In a more recent prospective randomized

clinical trial by Girard et al. [239], comparing hip resurfacing arthroplasty with conventional total hip replacement, found that a greater percentage of resurfaced hips had the offset reconstructed to within 4 mm of that on the normal, contralateral side. The lack of modularity of the femoral component represents a major difference between hip resurfacing prostheses and conventional total hip replacement devices. This is especially apparent when the surgeon attempts to optimize the femoral head-neck offset in order to minimize the risk of impingement and maximize the range of motion. The best method for optimizing the head-neck offset during hip resurfacing arthroplasty is still not known. One technique, to restore femoral head sphericity, optimizing component sizing and facilitating accurate guidewire placement, involves the removal of prominent osteophytes on the anterior aspect of the head and neck. Although, if done too aggressively, osteophyte removal could weaken the femoral neck the arthritic femoral head is usually enlarged and thus the surgeon may tend to favor the use of a larger femoral component if the osteophytes are preserved. This will also result in the implantation of an acetabular component that is larger than what might have been used in a conventional total hip replacement [239].

2.6.4.1.2 *Justification for valgus positioning of the femoral component*

Freeman is believed to have been the first to emphasize the importance of a valgus orientation of the femoral component relative to the native femoral neck [233] (See Figure 73 Figure 74), and this has been supported by more recent studies.

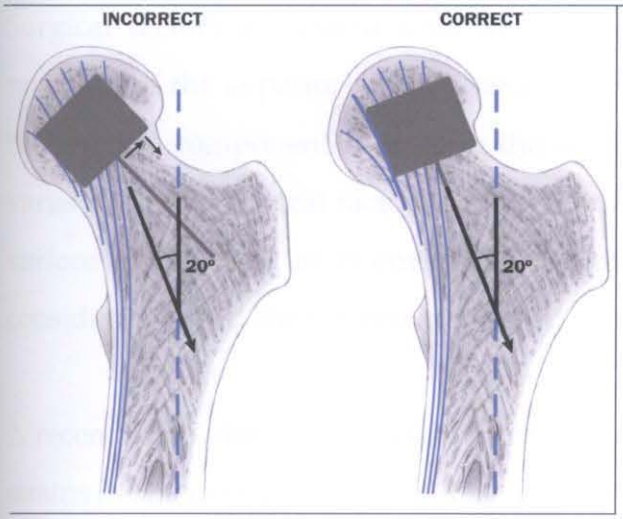

Figure 73 Diagrammatical representation of incorrect and correct implantation of the femoral component in hip resurfacing arthroplasty.[233]

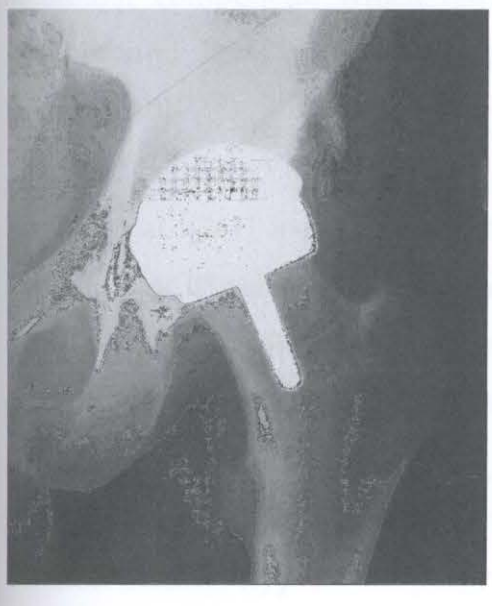

Figure 74 Anteroposterior radiograph showing the ideal position of the femoral component of the hip resurfacing arthroplasty [233]

Surgical factors associated with an increased risk of femoral neck fracture include notching of the superior femoral neck cortex when combined with varus placement of the femoral component relative to the anatomic femoral neck shaft angle [222]. In the varus position, surgical factors include: tensile stresses appear in the bone of the lateral surface of the neck as it enters the prosthesis; the medial compressive stresses rise considerably; and sheer stresses develop at the mouth of the prosthesis.

A recent finite element analysis reported valgus positioning reduced compressive bone strains near the implant rim, had little effect on tensile bone strains, and reduced tensile cement stresses when reamed cancellous bone was exposed [240]. Further this article describes another point of interest to femoral positioning is the notion that more vertical positioning of the component can theoretically result in the need for a larger femoral component to avoid notching. A larger femoral component necessitates a larger acetabular component, which requires more bone to be removed from the socket; whether and how often valgus positioning would result in such an upsizing is unclear.[240]

Anglin et al. [241] loaded 10 notched cadaveric femur pairs to failure; one side was implanted at 0° relative to the femoral neck and the other at 10° valgus. All 20 were dual-energy x-ray absorptiometry scanned. Failure load correlated with bone mineral density. Valgus placement increased the fracture load by an average of 28% over neutral for specimens with normal bone mineral density but had no effect on fracture load in specimens with low bone mineral density. For specimens with normal bone mineral density (typical of patients undergoing resurfacing arthroplasty), neutral-valgus placement had a greater effect than bone mineral density, explaining 54% of the fracture load variance. Component placement greater than 10° valgus is likely undesirable because this can lead to an increase in component size and a greater likelihood of notching.

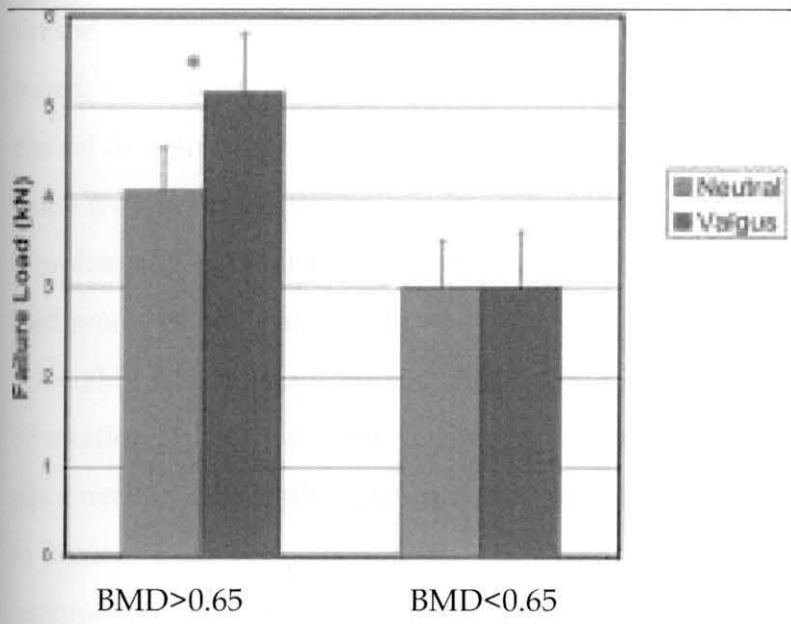

Figure 75 The effect of neutral versus valgus stem placement (mean ± standard deviation) differed according to the bone mineral density bone mineral density.

Valgus placement resulted in a 28% increase ($p < 0.05$, marked with an asterisk) in failure load compared with neutral placement in femurs with higher bone mineral density typical of the patient undergoing hip resurfacing patient.

A study by Vail [242] looked at surgical techniques that might increase the risk of a failed implant due to femoral neck fractures. This study was the first time scientists measured changes in the load on the femoral neck caused by different positions of the implant after resurfacing. They used sixty-four cadaver *femora* to examine the load and shear strain placed on the femoral neck using different positions of the implant. The results showed that resurfacing with placement of the implant in good alignment protects or shields the femoral neck from strain and this article explicitly links this decreases in stress to a decrease in unfavorable bone remodeling around the femoral neck. .

On the basis of anatomic and mechanical considerations, Freeman[227] discussed the benefit of a valgus orientation of the femoral component nearly thirty years ago. Recent clinical data strongly supports this benefit, with some authors advocating the placement of the femoral neck component in 140^0 of valgus while avoiding notching and ensuring complete coverage of the reamed femoral head. Finite element, and mechanical failure load analyses such as that by Anglin et al [241] also suggest that valgus alignment is preferable to varus alignment. Although there appears to be a consensus for valgus orientation, it is not clear if this is to avoid varus placement or whether valgus placement is inherently desirable. The results of Anglin et al.[241], with femora loaded to failure show that, in femora with normal bone density, valgus placement of the femoral component increases the fracture load strength in the proximal portion of the femur.

Richards et al [243] performed a biomechanical investigation of neutral oriented and valgus-oriented hip resurfacing femoral components to determine the ultimate load required to achieve a femoral neck fracture. The investigation also assessed if there were any advantages associated with valgus positioning of these components. Richards blindly assigned twenty fresh-frozen cadaveric femora, to be implanted with a neutral or valgus-oriented hip-resurfacing femoral component. Bone mineral density scans were acquired for all femora. All specimens were loaded axially to failure at a rate of 0.21 mm per second. Radiographs of the specimens were measured in order to determine the relative valgus orientation of the femoral components and the change in offset.

The biomechanical results of Richards[243] and Anglins et al [241] reveal a significant increase in the ultimate failure load for the valgus oriented components in the cadaveric femora, in comparison to that seen with the neutral-oriented components. The higher ultimate load suggests that the valgus-oriented components have a lower risk of developing a periprosthetic femoral neck fracture.

Although significant emphasis in the literature has been placed on the orientation of the femoral component in the coronal plane and its impact on biomechanical reconstruction and peri-prosthetic femoral fracture, little is known about its placement in the sagittal plane and how this relates to the femoral head/neck offset or fracture.

In conclusion, the findings from the discussed studies suggest that a valgus orientation of the femoral resurfacing component decreases the risk of periprosthetic femoral neck fracture. Obtaining the maximum possible valgus angle, while avoiding notching, may in fact provide the optimum protection from periprosthetic femoral neck fractures. However the surgeon must be careful not to compromise on femoral offset by orientating the component into valgus. It is clear that controlling the version of the femoral component may affect anterior posterior offset. No real work has been done to quantify the effect that version has on femoral neck fractures. Nor is there any work that specifically relates a patient's natural bone state before surgery to the risk of fracture. That is to say, it is not clear if it may be acceptable to place a component into less than the maximum amount of valgus to minimize potential offset issues if the patient has sufficient bone stock and bone quality to resist fracture.

2.6.4.2 Surgical technique for hip resurfacing

2.6.4.2.1 *Patient preparation*

The patient is positioned on his or her side with the pelvis stabilized by padded supports in a neutral position on the pubis, the sacrum, and the anterior and posterior aspects of the thorax and with the table tilted slightly anteriorly. This enables maximum rollback of the patient during acetabular reaming. The lower extremity must allow ≥90° of flexion at the hip and be adducted for the femoral head to be delivered through the

split in the gluteus maximus. Most metal on-metal surface arthroplasties are performed with the use of epidural, supplemented with general hypotensive, anesthesia.

2.6.4.2.2 *Templating*

Preoperative planning is considered essential when a hip resurfacing prosthesis is used. [244] Twenty percent magnified templates are placed over both the anteroposterior and the horizontal lateral radiographs of the hip. The anteroposterior template is oriented to provide a 140° stem/shaft angle. A series of 5-mm dotted lines radiating from the centre of the head assists in positioning the pin in the optimal position with respect to the ligamentum teres. The dotted lines that are parallel to the neck indicate how much bone the reamer will remove and how close the reamer will come to the external surface of the femoral neck. The template on the lateral radiograph shows the position of the stem, which should be translated anteriorly and directed slightly posteriorly to clear the anterior osteophyte, which is invariably present.[244]

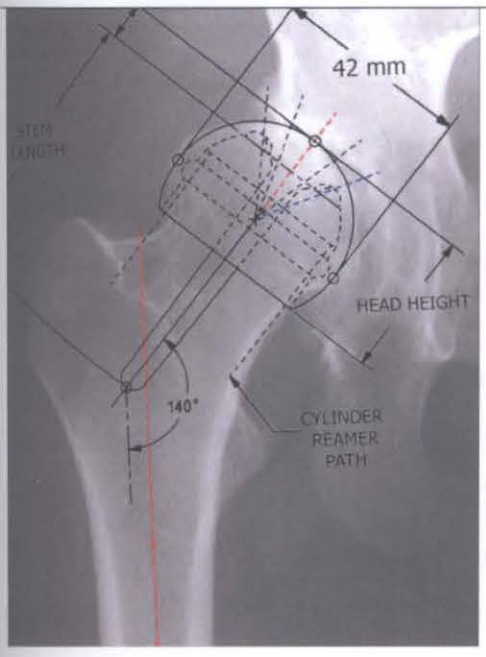

Figure 76 The template, when placed on the anteroposterior radiograph at 140°, allows visualization of the entry point (red dotted line) of the pin with respect to the location of the ligamentum teres (blue dotted line).

2.6.4.2.3 *Approach*

The posterior approach is preferable because no important muscle groups are transected. There is no release of the abductor muscles, which play the most important role in stabilizing the hip during walking and other bipedal activities. The only muscle groups that are released are the short external rotators, which are repaired at the conclusion of the procedure. No important gait disturbances result from a release of the external rotators, even if they are not repaired, because other muscles can accomplish external rotation. The incision starts 6 to 8 cm distal to the top of the greater trochanter, continues along the centre of the shaft, and then angles posteriorly from the tip of the trochanter for about 4 to 6cm where the short external rotator muscle fibers are divided and may be tagged for reattachment. The capsule is then incised posteriorly and the hip is dislocated by flexion, adduction, and internal rotation. A subtotal capsulectomy is

performed superiorly and anteriorly. Adduction and internal rotation of the lower limb beyond 90° cause the interval between the head and neck and the acetabulum to widen, facilitating resection of the anterior aspect of the capsule and then release of the capsule inferiorly. This inferior release is performed, by the surgeon, with a scalpel along the anterior aspect of the neck. The capsule needs to be released inferiorly to deliver the head and to allow the insertion of the neck elevator, which is necessary for the placement of the pin-centering guide. It is not necessary to excise the entire posterior aspect of the capsule, which can be retracted by a pin inserted into the pelvis to facilitate acetabular preparation. The femoral head is debulked to facilitate capsular removal, and the head is translocated superiorly and anteriorly for preparation of the acetabulum and implantation of the acetabular component.[244]

2.6.4.2.4 *Pin centering*

The pin-centering guide is positioned with use of the angle finder, which has a range of 135° to 145°, so that the pin forms an angle of approximately 140° with the femoral shaft and the entry point of the pin is consistent with the position determined by templating. The pin should be centered in the middle of the neck in the frontal plane (on the anteroposterior radiograph) and anterior to the neck centre and directed slightly from posterior to anterior in the coronal plane (on the cross-table lateral radiograph) to avoid reaming into the anterior osteophyte. A 3.2-mm Steinmann pin is inserted by the surgeon, to a depth of 3 to 5 cm, with the use of the guide to prevent the pin from moving off line during insertion. The cylindrical reamer gauge for the anticipated final femoral head size is then used to check the positioning of the pin; it should be able to rotate freely with sufficient clearance around the neck to ensure that cylindrical reaming will not result in notching of the femoral neck. If the cylindrical reamer gauge impinges on the neck at any location, the pin needs to be repositioned with use of the relocator guide. It is especially important to protect the superior cortex, which is thinner than the

inferior side and undergoes tensile loads, to decrease the risk of creating a femoral neck fracture.[244]

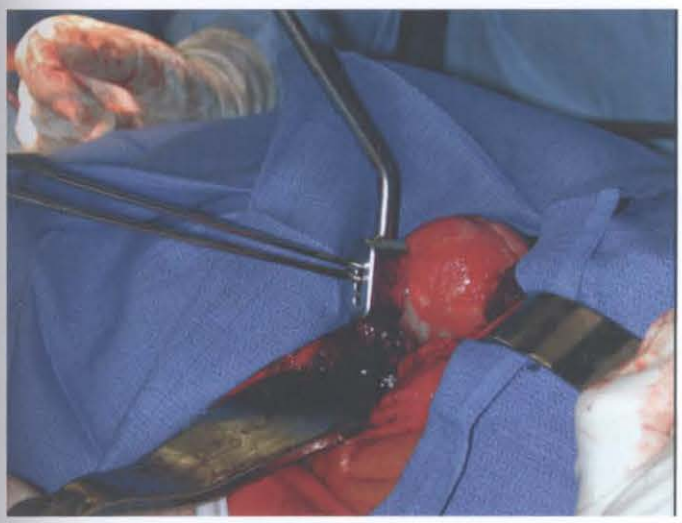

Figure 77 The template, when placed on the anteroposterior radiograph at 140°, allows visualization of the entry point (red dotted line) of the pin with respect to the location of the ligamentum teres .

2.6.4.2.5 *Cylindrical reaming*

Reaming commences with an oversized reamer, generally two or three sizes larger than the final anticipated size of the femoral head, with copious irrigation to avoid seizing. It is important to start the reaming with intermittent repetitive pressure directed parallel to the axis of the pin so as not to bend the pin. (The pin rarely travels through the centre of the head, and consequently the teeth of the reamer often engage the femoral head asymmetrically.) Smaller reamers are similarly used, with the last reamer being one size greater than the final templated and anticipated size. One should be careful to stop reaming at the head-neck junction and to avoid notching of the superior aspect of the neck. This is essential because the reaming at 140° is generally at a higher neck-shaft angle than the native anatomical condition. After this initial reaming, the interval between the anterior aspect of the femoral neck and the acetabulum is increased so that

the remaining anterior aspect of the capsule can be excised more easily. This will facilitate the positioning of the femoral head into a muscle pocket superiorly and anteriorly, as the lower limb is brought into extension and neutral or slight internal rotation to provide wide access to the acetabulum. A right-angle Hohmann retractor (Innomed, Savannah, Georgia) is placed over the anterior wall of the acetabulum to retract the femur anteriorly. A malleable retractor is useful to retract the muscles inferiorly and facilitate resection of the inferior aspect of the capsule. A double-pointed inferior acetabular retractor (Innomed) is inserted to visualize the entire acetabulum.[244]

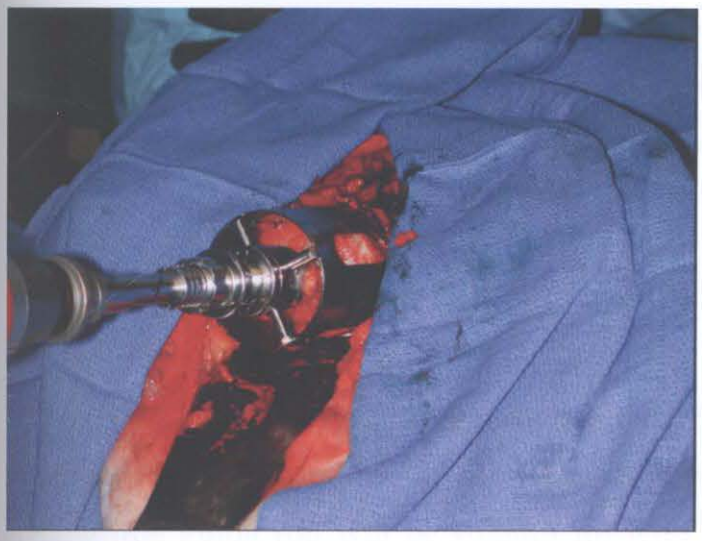

Figure 78 Cylindrical reaming of the femoral head during hip resurfacing operation

2.6.4.2.6 *Acetabular preparation*

Acetabular preparation starts with a careful assessment of the anterior and posterior walls. The soft tissues and the cartilage lying on the floor of the cotyloid foramen are removed. Reaming is performed in a manner similar to that used for a total hip replacement, with use of hemispherical reamers of increasing sizes until some cancellous bone is exposed. It is not necessary to ream to the acetabular floor in most

patients. The final reamer size should be 1 mm less than the final outside diameter of the acetabular component. Acetabular cysts are curetted and then grafted with fragments obtained by the reaming of the femoral head. The final size, roundness, and especially depth of the reamed acetabulum are checked with use of translucent acetabular gauges. A final check in three planes is then performed, with the surgeon using metallic rigid ring gauges. For the thin shells, reaming is performed "line to line" (e.g., to 58 mm for a 58-mm thin-walled 3.5-mm-thick socket, which is actually 59 mm in diameter). The 58-mm ring gauge should seat to the floor of the acetabulum. If surgeon finds that the gauge does not reach the floor, or is difficult to insert, the cause is probably a ridge rim of bone at the acetabular entrance that was created posteriorly because the cutting teeth of the reamers are less than a full hemisphere. The 59-mm gauge should not go completely to the floor in order to provide a pressfit of about 1 mm. The press-fit is achieved in the anterior-to-posterior direction between the anterior and posterior columns of the acetabulum.[244]

2.6.4.2.7 *Acetabular implantation*

The surgeon inserts the acetabular component after a final jet lavage and antibiotic irrigation. The outriggers on the handle of the inserter should be set on 42° of lateral opening (the guide rod will be straight up with the patient in the lateral decubitus position) and 15° of anteversion. The surgeon holds the inserter, and the technician or assistant impacts it until the acetabular component sits firmly. It is important that the surgeon checks the fixation of the implant at this point. This is achieved by rocking the pelvis with use of the inserter still engaged in the socket. If the fixation is insufficient, the component should be removed and the acetabular cavity should be reamed more deeply. Mallet taps on the rim can accomplish minor degrees of correction with an impactor. To disengage the insert, the surgeon should pull up on the release, have the assistant rotate it counterclockwise a few degrees, and remove the inserter by bringing the handle cephalad. The new inserter design has a lower-profile holder and is much

easier to release, making this process simpler and easier to achieve. The insertion is the completed using a ball impactor. Protruding osteophytes are removed by the surgeon with an osteotome from the posterior, and especially the anterior, wall of the acetabulum within 1 to 2 mm of the socket, and the remaining wall is chamfered with a high-speed burr.[244]

2.6.4.2.8 *Final femoral preparation*

The femoral head is again delivered, and internal rotation is aided by a towel pack held between the thigh of the assistant surgeon and the patient's leg. The surgical team repositions the neck elevator, and the pin is reinserted through the last cylindrical reamer that was used. A final check is conducted to assess pin orientation, and, if necessary, a correction is done before reaming to the final size is carried out. The saw cutoff guide is positioned so that its inferior margin covers all of the reamed bone at the head neck junction. The surgeon then inserts two or three short pins into the guideholes to maintain the position of the cutoff guide during the resection of the dome, which is performed with a saber or an oscillating saw. All debris must be removed so that the tower alignment guide is positioned flush with the top of the cutoff guide, and it is then rotated until snug. The surgeon then centers the final hole for the tapered metaphyseal stem reamer using the starter drill. The depth of drilling depends on the chosen method of stem fixation: it should be one or two sizes deeper if the stem is to be cemented and one size shallower if the stem is to be press-fit. [244]

After the removal of the tower alignment and cutoff guides, the appropriate chamfer guide is inserted into the drilled hole, and the final shape of the femoral head is obtained with the chamfer reamer. When the bone stock is good, it is possible to chamfer with a larger chamfer reamer (up to three sizes larger than the size corresponding to the final cylindrical reamer) to remove less bone. A plastic drape sheet with a hole in it placed over the femoral head prior to chamfer reaming can be used to

collect bone debris. It is recommended that the surgeon removes the superior sclerotic bone with the chamfer reamer. A final check of the femoral head shape is made by rotating the trial femoral head component. The trial component should rotate freely to ensure a cement mantle of about 1 mm all around the femoral head. All cystic material and soft tissue is then removed by the surgeon from the prepared femoral head with a sharp curet and burr, and additional fixation holes should be made in both the dome and the nonporous chamfered areas with use of a 1/8-in (3.2-mm) drill bit. Generally, six, seven, or eight holes are made in the dome and twelve, thirteen, or fourteen holes are made in the chamfered area.[244]

2.6.4.2.9 Femoral head cementation

Before cementation, the femoral head is jet-lavaged free of any fat or debris and is irrigated with antibiotic solution. The surgeon then inserts a suction tip through the stem hole and is connected to wall suction, with an additional tapered suction cannula inserted into a 3.2- mm drill hole in the lesser trochanter. The tapered stem of the suction cannula is then tapped in for a tight fit. It is important that the surfaces and then cleaned and dried. A CO_2 blow-drier is useful to dry the field and to identify any tissue that would prevent intimate contact of the cement with the bone. One package of bone cement is then mixed and the surgeon pours the cement into the femoral component to just below the recessed groove. The cement is then hand-pressurized into the cylindrically reamed portion of the head. All excess cement should be trimmed carefully with a scalpel and/or dental tool so that it is not pulled away from the interface. A mirror can assist in the removal of excess cement from the anterior cup-bone margin.[244]

If the stem is to be cemented, the cement is hand pressurized down the central hole after cleaning and drying. The femoral component is then inserted with the cement in the early dough stage, with care taken to make sure that the component is fully seated.

(If needed, the impactor and mallet are used.) Pressure is maintained until the cement has cured. [244]

2.6.4.2.10 *Hip reduction and closure*

After careful removal of all visible or palpable loose pieces of cement and bone debris, the hip is reduced and a complete range of motion is performed. The surgeon then checks for anterior impingement by internally rotating the hip in 90° of flexion. It is desirable to have ≥40° of internal rotation, and 40° of external rotation in extension. With the hip and knee extended, the hip should be pushed anteriorly to make sure it is stable. Final irrigation is performed using 2000 or 3000 mL of saline solution and 1000 mL of antibiotic solution. The surgeon, with number-1 Vicryl suture, repairs the gluteus maximus tendon and the short external rotators, and the wound is closed over one Hemovac-type drain. [244]

2.6.5 Implant positioning with computer assisted surgery

Attempts have been made to use computer-assisted surgery to improve the implant position of the femoral component during hip resurfacing.[245-248] Others have shown that the learning curve of inexperienced surgeons in hip resurfacing is reduced by the use of navigation.[249]

A navigation system in computer assisted surgery gives visual information on the precise positioning of the acetabular component, the optimal placement angle of the femoral component, and the hip geometry. This information is vital for the correct placement of a hip surface replacement. E. T. Davis's [250] and C. Schnurr [251] have both demonstrated that computer navigation used with femoral head resurfacing was more accurate and more consistent in its placement of the femoral component than standard instrumentation. These findings suggest that image-free computer-assisted

navigation may have an application in aligning the femoral component during hip resurfacing.

2.6.5.1 Surgical technique for navigated femoral head resurfacing

In this section, the use of a Brainlab (Feldkirchen, Germany) Navigation system for femoral head resurfacing is discussed. Other similar commercial Navigation systems are available for positioning the femoral component in hip resurfacing.

In order to establish a coordinate on the femur for real-time tracking during the CAS procedure, a tracker must be attached to the femur by a pin placed in the lesser trochanter. The following landmarks are registered using the navigation pointer: medial and lateral epicondyles, tip of the greater trochanter, piriformis fossa, and intended cap edge. These points for the axes of the femur. Clusters of points of the femoral head, as well as the superior, inferior, ventral, and dorsal femoral neck are also taken (See Figure 79).

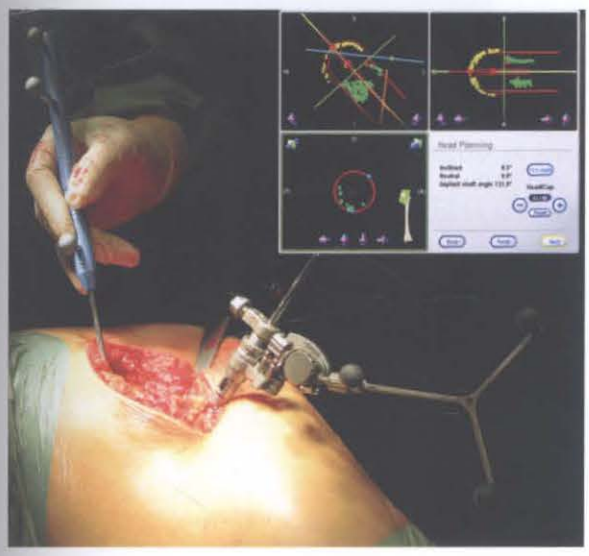

Figure 79 Collection of points on the femoral neck and head with the navigation pointer. The optical unit is attached in the lesser trochanter.

Now that the femoral axes and the outer surfaces of the proximal femur have been defined relative to the femoral tracker, the instruments can be tracked relative to the femur and be used to correctly align the instruments and implants during the surgery and avoid notching or varus placement of the component. The 2.4-mm guide wire was inserted into the femoral head and neck using the navigated drill guide (See Figure 80). Thereafter, the femoral head is prepared using the standard instrumentation and the final implant position can be verified using a dedicated instrument. See Figure 81.

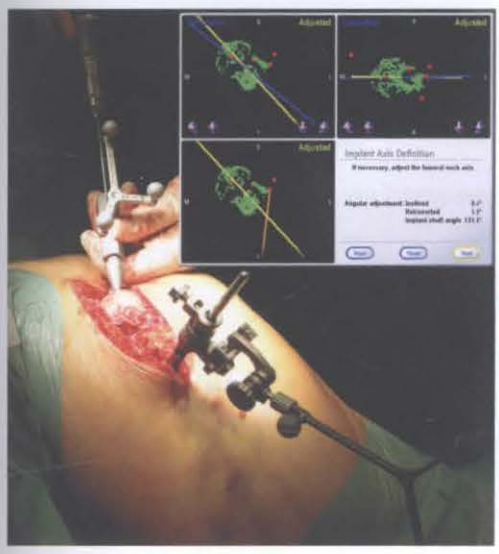

Figure 80 The navigated drill guide is inserted into the femoral neck and shaft. On the navigator screen the planned axis is shown (yellow).

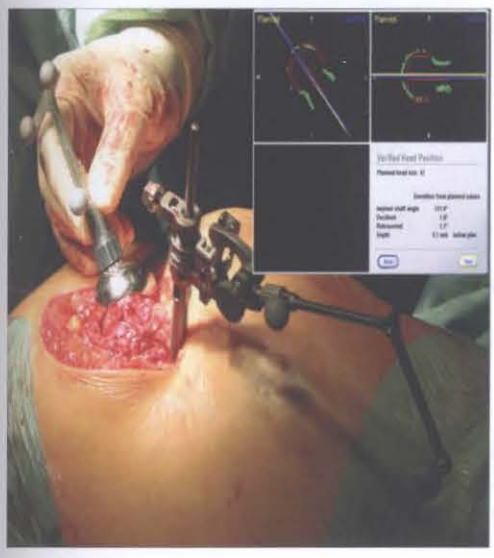

Figure 81 The implanted position of the femoral component is verified with the navigation tool. Differences between planning and implanted position are shown on the navigator screen

In C. Schnurr et al's [251] series, the navigation resulted in an extremely accurate placement of the femoral component. There were discrepancies between planning and implantation below 1° for CCD angle, circa 1° for anteversion, and about 1.5 mm for depth. These discrepancies were found to be superior to other studies. Other reports include: CCD angle errors of 2.6° and 3.3° in cadaver studies using computer tomography-based navigation systems, 2.2° in image-free cadaver studies, and 2.8° in a clinical fluoroscopic study.

In conclusion, computer-assisted navigation allows for an extremely accurate implantation of the femoral component, avoiding the pitfalls of hip surface replacement such as femoral notching, or leaving reamed cancellous bone uncovered. Hence, navigation may improve the possibility for the long-term survival of the implant. From my point of view the optimal placement of the femoral component outweighs the disadvantage of a longer operating time. Ongoing prospective follow-up studies are

necessary to evaluate the benefit of computer-assisted navigation of hip surface replacement.

2.7 Hip joint loading

Many of the muscles, which influence the position of the hip and leg, have been discussed in Section 1.1.3, but what is of most interest to this body of work is the loading environment that they transfer to the proximal femur that. There is still a great deal of discussion in the literature regarding the loading conditions on the proximal femur during recognized actions such as one-legged stance and stair climbing. There is, however, general agreement that the hip withstands loads of many multiples of body weight during these simple tasks. Figure 82 shows the general trends of force variation that occurs in the hip of a normal male during walking. The values of hip joint load were adapted from Berme [252].

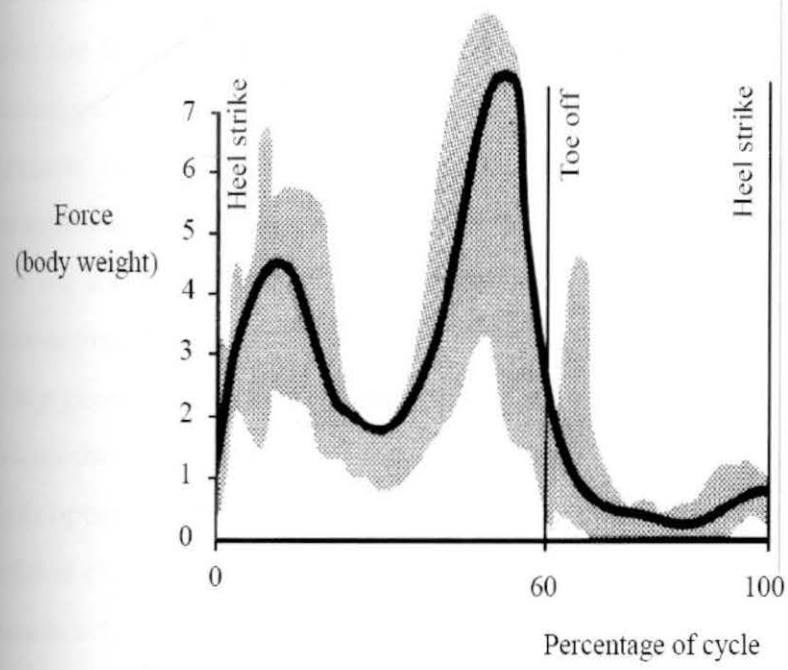

Figure 82 Variation in hip joint loading during walking

In terms of the longevity of implants, one of the most significant studies into the loading of the hip was conducted by Lu et al [253], who examined the influence of muscle activity on the loads measured by in vivo prostheses [254]. Massive femoral implants in two patients were capable of relaying force data, additional information was provided by force plates and EMG signals from surface electrodes attached to the muscle groups. The subjects were exposed to isometric and gait tests, and the results showed that the force in the femoral implant was up to 3.5 times as large as that seen by the force plates. Corresponding axial forces of up to 2715N were seen by the prosthesis. Bergmann et al [255] extended the work by monitoring the load on an in situ prosthesis during routine activities characterizing the load through a full gait cycle [254].

To predict muscular forces and joint loading in a noninvasive way, musculoskeletal models can be used together with inverse dynamic analysis. Studies have shown that the calculated hip contact force is strongly affected by the activity of the muscles that span the hip joint. Lu et al [253] has shown that the axial force exerted on the femur during gait is highly influenced by muscle activity [254]. Hurwitz et al [256] reported an increase in hip contact force of 0.2 times body weight with a 10% increase in antagonistic muscle force [256]. Later studies demonstrated how biomechanical factors and the configuration of muscle models influence hip loading and consequently, bone remodeling. Lenaerts, G , et al [257, 258] analyzed the effect of subject-specific modeling of hip geometry on muscle activation patterns and hip contact forces during gait. They did so through the use of musculoskeletal modeling, inverse dynamic analysis, and static optimization [259, 260]. They first used sensitivity analysis to analyze the effect of isolated changes in femoral neck-length (NL) and neck-shaft angle (NSA) on calculated muscle activations and hip contact force during the stance phase of gait. A deformable generic musculoskeletal model was incrementally adjusted to adopt a physiological range of neck length and neck-shaft angle. In a second similar analysis, they adjusted hip geometry to the measurements from digitized radiographs of twenty subjects with primary hip osteoarthrosis. Finally, they studied the effect of hip abductor weakness on

muscle activation patterns and hip contact force. This analysis showed that differences in neck length (41–74mm) and neck-shaft angle (113–140) affect the muscle activation of the hip abductors during stance phase and hence hip contact force by up to three times body weight. In conclusion, the results from both the sensitivity and subject-specific analysis showed that at the moment of peak contact force, altered neck-shaft angle has only a minor effect on the loading configuration of the hip. Increased neck length, however, results in an increase of the three hip contact-force components and a reduced vertical loading.

Jonkers et al [261] demonstrated that inclusion of subject-specific loading conditions drastically influences the calculated stress distribution, and thus influences the correlation between calculated stress distributions and changes in bone mineral density bone mineral density after total hip replacement. For two patients who received cementless total hip replacement, personalized finite element models of the proximal femur were generated representing the pre- and post-operative geometry. In the prediction of bone remodelling processes after total hip replacement, modeling of the subject-specific geometry is now state-of-the-art. They found subject-specific differences in the stress distribution induced by specific loading conditions, as interchanging of the loading also interchanged the patterns of the stress distribution. The correlation between the calculated stress distribution and the changes in bone mineral density were affected by the two-dimensional nature of the bone mineral density measurement. Jonkers [261] results confirmed the hypothesis that inclusion of subject-specific hip contact forces and muscle forces drastically influences the stress distribution in the proximal femur. In addition to patient-specific geometry, inclusion of patient-specific loading is, therefore, essential to obtain accurate input for the analysis of stress distribution after total hip replacement.

ISO 7206-4 specifies a test method for determining the endurance properties of stemmed femoral components of total hip joint prostheses, and stemmed femoral

components used alone in partial hip joints under specified laboratory conditions. It defines conditions of testing so that the important parameters, which affect the components, are taken into account; the specimen is correctly set up for testing; the value of the endurance limit tests forces and the corresponding number of load cycles are specified according to physiological conditions. Development of an in vitro model for physiologically adapted cyclical loading (according to ISO 7206-4 parameters) performed using a hip simulator has allowed for the reproducibility of physiological loading, enabling experimental comparison of stem designs.

The ISO standard simplifies the anatomic and gravity loads into a single resultant load that is orientated 9 degrees out of plane in the sagittal plane and 10 degrees out of plane in the coronal plane. This simplification is convenient for lab testing setups. (See Figure 83)

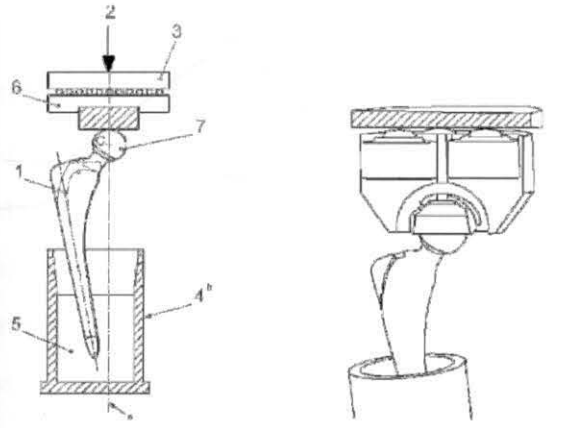

Figure 83 ISO 7206 loading (taken from ISO-7206 part 4 standard document)

2.8 Developing subject-specific finite element models of the femur

2.8.1 Finite element analysis in biomechanics

Finite element analysis was first introduced to the field of orthopaedics in 1972 [262]. Since that time, finite element models have been increasingly used for three main purposes: (i) for design and pre-clinical analysis of prostheses (ii) to obtain fundamental knowledge about musculoskeletal structures and (iii) to investigate time-dependent adaptation processes (i.e., tissue growth, remodeling and degeneration) in tissues. Successful three-dimensional finite element modeling has been applied to several different prostheses such as the hip, [263-266] the knee, [267-269] the ankle, [270] the metacarpophalangeal joint, [271] and the shoulder. [272-274]

The finite element method is a standard tool used in the engineering sciences to precisely assess local stress–strain distributions in geometrically complex structures. Precision in the results can be achieved once geometry, material properties, and boundary conditions have been carefully provided. Due to the complex and irregular shapes that normally characterize biological structures, the finite element method has become widely used in all biomechanical fields, especially for assessing stresses and strains in normal bone and in bone around implants. In early studies most of the models were just two-dimensional constructions, [275] this was due to computer limitations and simplicity in the way that finite element models were made. Although this could be sufficient in some cases (finite element parts with simple geometry and/or good symmetry), it was soon realized that a true three-dimensional finite element model was the only method to assess realistic stress fields whenever an irregular and non-symmetrical object was to be studied [262]. There have been a number of attempts to develop an automated method for generating finite element models. Keyak and coworkers developed an efficient and robust automatic mesh generation (AMG)

method [276] that has proved to be useful in many research areas [277-279]. Viceconti and coworkers also developed an automatic method that generates patient-specific finite element models of different types of various bones, other than the femur [280].

The quality of an finite element model and its accuracy of predicted stresses and strains depend on the quality of representation of the finite element model, as compared to the actual conditions (normal bone or a bone with implant). The accuracy is highly dependent on element selection-type and size and allocation of material properties based on CT scan data. A thorough experimental validation, though a very difficult and tedious procedure, is the best tool to assess the quality of finite element predictions [281]. Strain gauge measurements were used for stress analysis of bone, and sometimes, for the purpose of validation of the finite element models. The studies of Keyak J H [282] and Dalstra M. [283] based on the femur and the pelvic bone respectively, are significant contributions towards strain gauge validations of finite element modeling of bone. The goal of these studies was to validate a three-dimensional finite element model, by comparing calculated stresses and strain with those measured on a bone, in vitro.

2.8.1.1 Subject-Specific/Patient-Specific finite element modeling

Subject-specific/patient-specific finite element modeling (referred to from now on as subject-specific finite element modeling) is becoming a tool that is used extensively for the numerical analysis of the biomechanical behaviour of human bones. By combining imaging data with finite element modeling, numerical models can be built to incorporate both the geometry and material properties of individual femurs. As such, subject-specific finite element modeling can be used to compare different implant geometries in one particular femoral geometry, and also analyze one particular implant geometry in different femoral geometries. Great attention is posed to the automation of the modeling strategy to make it compatible with the clinical practice [280, 284]. The method of choice for the generation of those models is to derive information on both

bone geometry and its material properties from CT data. In reality, CT data provides quantitative information on the attenuation coefficient of the bone tissue that can be related to its density, provided the CT scanner has been properly calibrated. [285] Density can, in turn, be related to the mechanical characteristics of the bone tissue, using one of the many experimental relationships available in the literature [45]

2.8.1.1.1 *Creating the geometry-meshing*

To create a subject-specific finite element model, a three-dimensional representation of the patient's femur is produced through digital extraction of segmented femoral slices from grayscale CT scan images. To produce accurate models, images must be broken down into small and manageable elements. This so called 'meshing' can be achieved through voxel-based meshing or geometry-based meshing.

2.8.1.1.1.1 **Voxel based meshing**

A voxel (volumetric pixel or Volumetric Picture Element) is a volume element, representing a value on a regular grid in three dimensional space. This is analogous to a pixel, which represents 2D image data in a bitmap (which is sometimes referred to as a pixmap). As with pixels in a bitmap, voxels themselves do not typically have their position (their coordinates) explicitly encoded along with their values. Instead, the position of a voxel is inferred based upon its position relative to other voxels. That is to say that, its position in the data structure that makes up a single volumetric image). Voxels are frequently used in the visualization and analysis of medical and scientific data. Some volumetric displays use voxels to describe their resolution. [286]

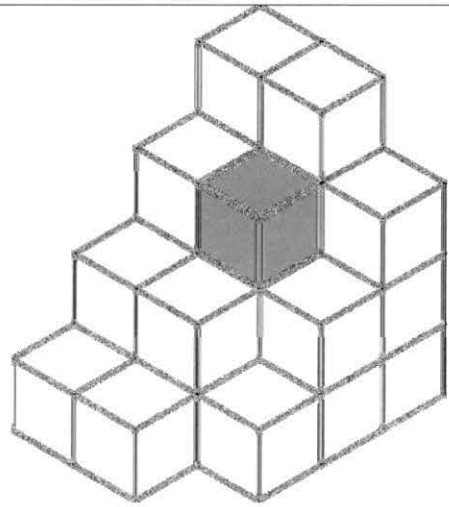

Figure 84 A series of voxels in a stack with a single voxel highlighted [286]

Voxel-based meshing is a single-step method where the segmented voxel data are converted into an finite element model with brick elements. The elements take on the size of the , which enables the rapid generation of meshes. See Figure 85. Voxel-based meshing has a number of advantages, including trivial implementation, optimal elements, guaranteed conformity of meshes at interfaces, and easy assignment of inhomogenous material properties to elements.

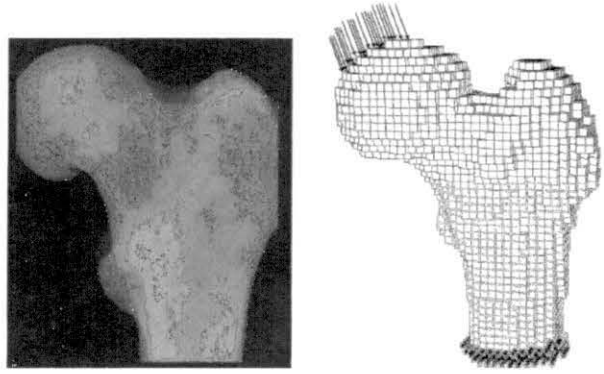

Figure 85 Voxel based meshing used for Finite Element Analysis used by Keyak et al [287]

This method has been used to study the mechanical behavior of cancellous bone, with some success [288]. Although voxel-meshing is a simpler, automated and more rapid technique compared to geometry-based meshing, it is less able to deal with curved surfaces that are not easily represented by brick elements. A number of smoothing algorithms have been developed to alleviate problems of peak stresses and strains and inaccuracies in surface area calculations caused by the typical jagged-edged surfaces in a voxel-based mesh [289, 290]. In addition, voxel-based meshing does not allow for the adaptation of element size to features or allow for localized mesh refinement. [291]

2.8.1.1.1.2 Geometry based meshing

Geometry-based meshing is a two-step procedure in which the contours of the femur are first extracted from the CT scan, a 3D cad model of some description is created then an finite element mesh is created from this CAD representation, that is based on the model shape, the surface of the bone is reconstructed by building an finite element mesh with tetrahedral [292] or hexahedral [293, 294] elements.

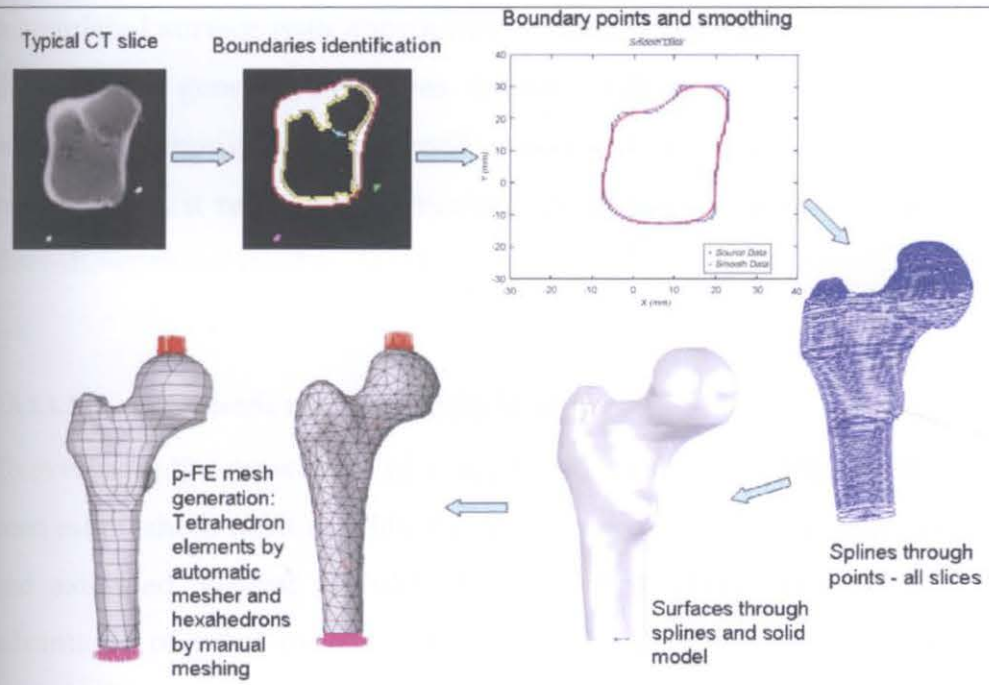

Figure 86 finite element Meshes of the proximal femur created using geometry based modeling workflow. The bottom left shows both tetrahedron and hexahedron mesh options. [295]

In contrast to pixels and voxels, points and polygons are often explicitly represented by the coordinates of their vertices. A direct consequence of this difference is that polygons are able to efficiently represent simple 3D structures with lots of empty or homogeneously filled space, while voxels are good at representing regularly sampled spaces that are non-homogeneously filled. [286]

Comparisons between tetrahedron meshes and hexahedron meshes have found little difference between the respective models, so long as the meshes are sufficiently well refined. [296-298] Tetrahedron meshes have much more flexibility to accommodate for variable geometry which makes them more suited to AMG and subject specific models. The principal drawback of geometry-based meshing is that the success of the technique in generating meshes with low distortion is dependent on an initial high-quality

triangulated surface with appropriately sized surface element distribution. In addition, this method generally involves manual editing, with possible associated loss of accuracy. Although only a small percentage of mesh surface nodes may require repositioning, it remains a particularly daunting and time-consuming task with large three-dimensional meshes. [291]

2.8.1.1.1.3 Volumetric marching Cube Meshing

To overcome the drawbacks of voxel-based meshing, further meshing techniques have been established, most notably the technique of Volumetric Marching Cubes (VoMaC) and extended VoMaC (EVoMaC) approaches. [291] These techniques combine the advantages of voxel-meshing effectively but with the issue of having stepped mesh surface definition. This is achieved by adaptation of the marching cubes approach [299] to generate volume meshes so that for every base case, instead of simply determining surface triangulations, there is a complete tetrahedralization of the hexagonal volume is pre-computed. In order to address disadvantages of the VoMaC approach, most notably its applicability to only nested or multiple spatially unconnected domains, suitable schemes and algorithms have been developed and implemented into a flexible mesher, +ScanFe (Simpleware Ltd. 2006), which is part of the integrated image processing and meshing environment ScanIP (Simpleware Ltd, Exeter, United Kingdom).

A number of studies have now validated the range of problems, which can be robustly treated using the VoMaC approach in conjunction with ScanIP (Simpleware Ltd 2006). In a single part meshing study, which compared traditional unstructured three-dimensional mesh generation with the EVoMaC approach implemented in +ScanFE (Simpleware Ltd 2006), the EVoMaC approach was able to produce a significantly better quality mesh. The mesh produced by the traditional method being of very poor quality with high element side ratios[300]. Similarly, in a multipart modeling study, the EVoMaC approach with +ScanFE produced a full volumetric mesh, which was smooth,

of high surface element quality, and highly conforming. Comparative meshing techniques failed to mesh the multi-part surface meshes with volume meshes [300].

Given these results, it is clear that the use of the Simpleware Scan FE package and the EVoMaC meshing capabilities within this software is a powerful and appropriate tool for the generation of subject specific bone geometry.

2.8.1.1.2 *Assignment of material properties*

A second consideration in the generation of subject-specific finite element models is the use of appropriate material properties. It is now commonplace when building subject specific finite element models to take into account in-homogeneity of bone.

Vose and Kubala [301] were possibly the first to quantify how much mechanical properties depend on composition, obtaining a correlation between ultimate bending strength and mineral content. One of the most cited works is Carter and Hayes [45], who found that elastic modulus and the strength of trabecular and cortical bone are closely related to the cube and square of the apparent wet bone density, respectively.

There is little agreement in the literature as to the correct, most accurate or best accepted way to assign material properties to subject specific finite element models. The approaches taken vary from basic simplified methods that discount heterogeneity and assign linear elastic isotropic homogenous material properties to the bone model, [302] through to complex representations of the bone accounting for material property heterogeneity throughout the volume and the anisotropy of bone [303].

2.8.1.1.2.1 Heterogeneous material property mapping

This can be achieved by utilizing the attenuation coefficient of the material present in each voxel. [291] A number of different relationships can be defined, including: the use of a linear or non-linear stress-strain relationship, the assignment of isotropic or anisotropic material properties, the conversion of CT number to elastic modulus, and the implemented failure theory. Provided the CT scanner has been properly calibrated, CT data can provide quantitative information on the attenuation coefficient of the bone tissue that can be related to its density. Density can, in turn, be related to the mechanical characteristics of the bone tissue, using one of the many experimental relationships available in the literature [304, 305]

2.8.1.1.2.2 Biphasic material property assignment

Are more simplified but often adequate approach is to divide the bone into cortical and cancellous regions assigning an averaged, distributed or generalized material property to each region. An example of this approach is seen by Bessho et al. [306] who assigns an homogenous cortical bone shell to the model, then applies a bone mapping function to the cancellous bone. See Figure 87 and Table 5.

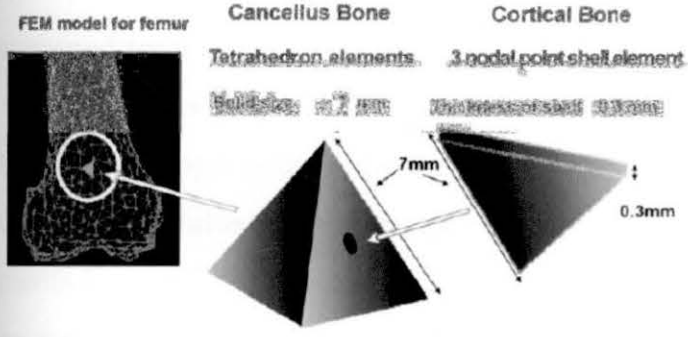

Fig. 1. Element types of the finite-element model (FEM): 7-mm tetrahedron elements are applied for cancellous bone, three-nodal-point shell elements are applied for cortical bone, and three-nodal-point shell elements are placed on the outer surface of the tetrahedron elements

Figure 87 Bessho et al. allocates cancellous bone and cortical bone regions to the finite element mesh [306]

Table 5 Mechanical properties of Cancellous bone used by Bessho [306]

Table 1. Mechanical properties

Ash density (ρ) (g/cm^3)	Yield stress (σ) (MPa)
$\rho \leq 0.2$	$\sigma = 1.0 \times 1020$
$0.2 < \rho < 0.317$	$\sigma = 137 \times \rho 1.88$
$0.317 \leq \rho$	$\sigma = 114 \times \rho 1.72$
Ash density (ρ) (g/cm^3)	**Young's modulus (E) (MPa)**
$\rho = 0$	$E = 0.001$
$0 < \rho \leq 0.27$	$E = 33900 \times \rho 2.20$
$0.27 < \rho < 0.6$	$E = 5307\,\rho + 469$
$0.6 \leq \rho$	$E = 10200 \times \rho 2.01$
Ash density (ρ) (g/cm^3)	**Poisson's ratio**
$1.8 \leq \rho$	0.22
$0.2 < \rho < 1.8$	0.15
$\rho \leq 0.2$	0.49

The elastic modulus and the strength of each element are calculated from the data according to Keyak et al.[15] and Keller,[13] and Poisson's ratio is also determined from the data according to Minamisawa[21]

Another approach to material property assignment that is attractive is to just assign two material phases to the bone, a single cancellous phase and a single cortical phase. Pastrav [307] applied this strategy successfully when simulating the vibration behavior of stemmed total hip replacement in situ. This approach is especially convenient when an implant is modeled alongside and interacting with the bone tissue. This is because utilizing a heterogeneous mapping property mapping strategy results in the allocation of very low modulus material properties to some of the lower stiffness cancellous bone elements in the mesh. When simulating a total hip replacement in contact with the bone, these very low modulus elements are often in direct contact with the relatively stiff elements of the metal implant. This dramatic stiffness differential in the mesh at the contact boundary between the implant and the bone causes numerical issues that make solution convergence extremely difficult to achieve.

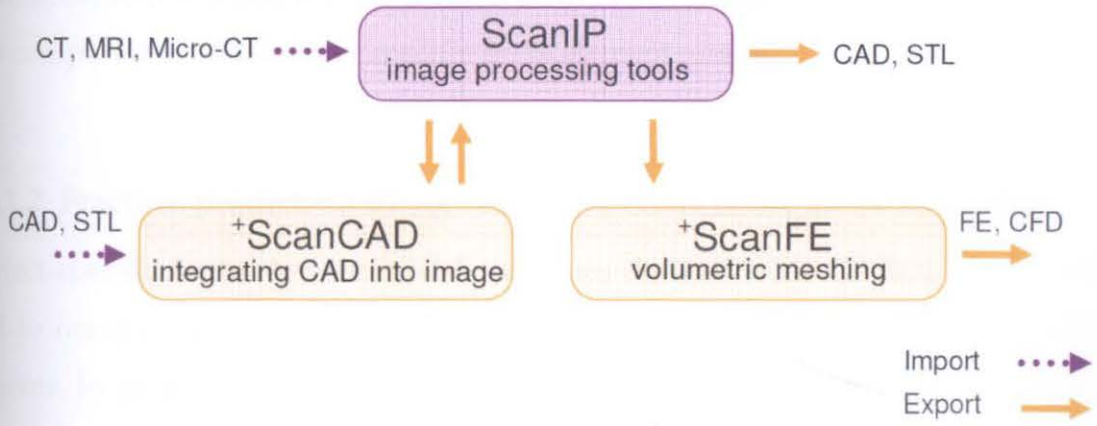

Figure 88 Simpleware Software Products interaction between modules

2.8.1.1.3 *Subject specific finite element analysis loads*

Finally, in addition to an accurate assessment of bone strength, information on loading conditions encompassing the greatest risk of fracture must be considered. Fractures occur when loading on the bone is greater than the strength of the bone itself. Most fractures occur by a fall to the side but a significant number of hip fractures are spontaneous. As such, finite element modeling must include modeling the impact of a fall to the side and/or modeling a single-legged stance [277, 293, 294].

The human femur, in physiological conditions is subjected to an instantaneous loading pattern that can be quite complex, which is due to the many muscles that insert in the femur and develop contractile forces. This loading pattern may change considerably with time and with the type of movement being performed. However, the overall structural effect of these loading conditions can always be seen as the superposition of an off-axis compression and torque moment around the long axis of the femur. The ISO 7206 part 4 loading scenario previously discussed in section 2.7 Hip joint loading, provides a standardized representation of the combined load vectors acting upon a hip

joint. Because it is standardized it has a distinct advantage when attempting to make a to b comparisons with subject specific finite element models.

2.8.1.2 Fracture prediction using subject-specific finite element models

Subject-specific finite element models of bones derived from CT data are a promising tool to non-invasively assess the stress-state and fracture risk of bones in individual patients. In general, bone strength can be characterized through internal (shape, bone tissue distribution and bone tissue properties) and external determinants (loading conditions) [278]. Subject-specific finite element models can be designed to include most of these internal parameters and to simulate the influence of external conditions [292, 308]. In principle therefore, subject-specific finite element models have the capacity to enable prediction of fracture risk for any specific bone segment under any generic loading condition. In practice, however, this still represents a considerable challenge.

The studies performed by J.H. Keyak et al. [287, 309-313]showed that CT scan-based finite element models of the proximal femur could predict fracture location and fracture type with moderate accuracy. Her studies showed that these computed tomography scan-based finite element models could be used to estimate the strength of femoral shafts with and without metastases. These models may be useful for assessing the risk of pathologic fractures of femoral shafts. She also worked on the comparison of in situ and in vitro CT scan-based finite element model to predict proximal femoral fracture load.

Finite element models have been demonstrated to outperform densitometric measurements in the explanation of the failure load variability among different subjects [278, 314]. However, although an accurate and consistent predictor of bone strength has been achieved this was only possible under a specific loading condition [315]. Hence,

although prospectively useful for comparative studies (for example, evaluation of a pharmacological treatment or screening of a target population [316], such finite element models are limited by their lack of generality. The development of more general models is needed to predict and localize fracture risk for a bone segment under a generic condition (for example, including muscles). In other words, the model should implement both a bone tissue failure criterion, and structural collapse criterion. Although several such studies have been performed, failure to include validation against experimental tests prevents definitive conclusions from being derived [308, 317-319]. Notably, although differing in the modeling strategy adopted and in the specific strength criterion chosen for the bone tissue, these studies were mainly based on stress parameters. Few validation studies on whole bones have investigated the possibility of applying strain-based criteria and compared their performance with stress-based ones Schileo et al, Keyak J H et al and Lotz et al [18, 282, 294]. This is important in the context of recent advances in basic bone biomechanics, which demonstrate the effectiveness of strain-based criteria to describe yield or failure of normal bone tissue. Moreover, there is evidence to suggest that bone failure is driven by deformation [320, 321] and there is growing agreement on the substantial isotropy of yield strain and its invariance to density [322-326].

Further support for the use of strain-based criteria stems from work by Ford and Keaveny who, in 1996, suggested that strain-based failure theories might be superior to stress-based ones. They argued that it is the loading conditions which decide the superiority of the failure theory [317]. Their studies demonstrated that strain-based failure criterion could identify the failure patterns of bones when implemented into subject-specific finite element models that are able to accurately predict strain levels. The appropriateness of a strain-based criterion can also be supported, as it has been received as a better experimental characterization. Furthermore, it directly descends from experimental observations on the invariance of limit strain with respect to density. While the adoption of a stress-based criterion in an inhomogeneous model implies the

inclusion of another empirical relationship (between limit-stress and density), which may bring in further uncertainties. Hence, it follows that strain-based criteria should be implemented in finite element models of bone for prediction of fracture risk.

In a recent combined experimental-numerical study by Schileo E., et al [18], the capacity for identification of the failure patterns of bones by strain-based failure criterion was evaluated using subject-specific finite element models able to accurately predict strain [18]. Three cadaver femurs were CT-scanned and subsequently fractured in a clinically relevant single-stance loading scenario. Load displacement curves and high-speed movies were acquired to define the failure load and the location of fracture onset, respectively. Subject-specific finite element models of the three femurs were built from CT data following a validated procedure. A maximum principal strain criterion was implemented in the finite element models, and two stress-based criteria selected for comparison. The failure loads measured were then applied to the models, and the computed risks of fracture were compared to the results of the experimental tests. Schileo E., et al [18] concluded that the proposed principal strain criterion managed to correctly identify the level of failure risk and the location of fracture onset in all the modeled specimens. While the Von Mises or maximum principal stress criteria did not provide significant information. A maximum principal strain criterion can thus be defined as a suitable candidate for the in vivo risk factor assessment on long bones.

The distortion energy (DE) failure theory, as used in this study, was originally developed for engineering materials such as steel. Such materials differ greatly from bone in both their microstructure and their mechanical behavior. As a result, the choice of failure theory may not have been optimal. Alternative failure theories include: Hoffman and a strain-based Hoffman analog, maximum normal stress, maximum normal strain, maximum shear strain, maximum shear stress, Coulomb-Mohr, and modified Mohr failure theories. Factors of safety, defined as the ratio of the allowable to the computed stress or strain according to a particular failure theory, were computed

for each element using several failure theories. By definition, a factor of safety less than 1 indicates element failure. The above mentioned failure theories were examined while assuming isotropy. The Hoffman, Coulomb-Mohr, and modified Mohr theories were developed for brittle materials and could account for differences in tensile and compressive strain The maximum normal strain and strain-based Hoffman analog could account for difference in tensile and compressive failure strain.

2.8.1.2.1.1 Prediction of bone adaptation

Subject-specific finite element computer models of the proximal femur in hip replacements could potentially predict stress-shielding and subsequent bone loss in individual patients. Before such predictions can be made, it is important to initially determine if the between subject differences in stress-shielding are sensitive to poorly defined parameters, such as the load and the bone material properties. Harrie Weinans [327] investigated if subject-specific finite element models provide consistent stress-shielding patterns in the bone, independent of the choice of the loading conditions and the bone density-modulus relationship used in the computer model. The analyses showed that for the four loading conditions and two bone density-modulus relationships the difference in stress-shielding between the two subjects was essentially constant (1% variation) when the same loading condition and density -modulus relationship was used for both subjects. The severity of stress-shielding within a subject was sensitive to these input parameters, varying up to 20% in specific regions with a change in loading conditions and up to 10% for a change in the assumed density-modulus relationship [327].

2.9 Literature review summary and direction

2.9.1 Summary

In the literature review, the natural hip joint is researched and described in detail. Important aspects about the biology of the bone along with relevant descriptions of the natural hip joints anatomy and physiology are presented. Further relevant mechanisms of natural hip joint failure are described. Review of these failure mechanisms demonstrates that Osteoarthritis is a dominant failure mechanism and that Osteoarthritis of the joint is a significant burden on the community. Replacement of the hip is an effective treatment choice for the condition.

Attention is given in the review to Osteoporosis which is a condition associated with aging that weakens the bone. This condition contributes to hip joint failure but is especially interesting for this work because it creates challenges for hip replacement patients such as weakened bone support for the prosthesis.

The review demonstrates that despite the success of hip replacement as a whole, there are failures, and these failures place a significant burden on the community. Many of the major failure mechanisms of total hip replacement are reviewed. When concentrating on femoral component failures, one of the more severe and less understood failure mechanisms is peri-prosthetic femoral fracture

The review demonstrates that peri-prosthetic femoral fracture after total hip arthroplasty is a major complication. Further, the prevalence of peri-prosthetic femoral fracture is increasing. The increased number of joint replacements in an ever-broadening population of hip replacement recipients can be summarized as the dominant drivers of this trend.

Peri-prosthetic fractures can be classified as either intra-operative or post-operative fractures, with post-operative fractures further classified as early or late. Risk factors for peri-prosthetic femoral fracture include gender and increased age. Fracture risk is also increased when the prosthesis is cementless and in revision hip arthroplasty setting. The review demonstrates that the usage of cementless primary implants is growing in much of the world.

Specific attention is given in the review to the history, surgical technique and clinical results of the ABGII femoral stem. Specifically the stem and its predecessor (the ABGI) are analyzed in detail. The Australian Joint Registry published clinical reviews and the Sydney Hip and Knee Surgeons database are reviewed. Although the overall results for the ABGI and ABGII stems are good the rate of post-operative peri-prosthetic femoral fracture for the ABGII stem is higher than the rate for other cementless stems.

Post-operative peri-prosthetic femoral fracture is divided into early and late and clinical evidence from the Sydney Hip and Knee Surgeons database is used to show that the rate of fracture changes both between the early (less than 3 months post op) and late period and also between the ABGI and ABGII. Design changes between the ABGI and II appear to have reduced the overall risk of post op peri-prosthetic femoral fracture but with the deleterious effect of increasing the rate of earlier fractures. This review highlights the importance of prostheses design on peri-prosthetic femoral fracture risk and shows that the ABGII is a good choice for further study of implant design to reduce the risk of peri-prosthetic femoral fracture.

A variant of total hip arthroplasty called femoral head resurfacing is reviewed in detail. femoral head resurfacing has many theoretical benefits over total hip arthroplasty however, this type of prosthesis has a much higher rate of peri-prosthetic femoral fracture than total hip replacement does. The history, technique and clinical results of femoral head resurfacing are reviewed in detail. The review highlights that the reasons

for the higher rates of peri-prosthetic femoral fracture are predominantly surgical technique (implant positioning) and patient specific factors. (Patient selection) The review highlights that this type of prosthesis design is a good choice for further study.

Computer assisted orthopaedic surgery is reviewed in detail, concentrating on important basic concepts and the current state of play in the discipline. A detailed review of a commercially available Navigation System that can be used with the ABGII femoral stem is undertaken as it relates to total hip replacement surgery. Further computer assisted orthopaedic surgery is also reviewed for femoral head resurfacing femoral component placement.

Methods for subject specific finite element analysis modeling are reviewed including the generation of subject specific geometry meshing techniques, material property assignment and load application. The review focuses on the methods for geometry creation and meshing that are available within the commercially available software package Simpleware.

Prediction of bone fracture using subject specific finite element analysis is reviewed demonstrating that the use of strain based failure criteria are state of the art. Studies modeling native femoral bone tissue fracture with finite element analysis are reviewed. However, no previous studies that attempt to predict bone fracture around femoral stems were not found. To model peri-prosthetic femoral fracture around femoral stems obviously this is an area where further study is required.

2.9.2 Direction

The review shows the importance of the prosthesis, the patient and the procedure to the risk of peri-prosthetic femoral fracture. Novel ways to consider all of these factors (in combination where possible) are now pursued.

Understanding that the ABGII prosthesis has an unsatisfactory rate of peri-prosthetic femoral fracture, it is appropriate to look at reducing the fracture rate through implant design. From the review it is clear that the rate of fracture observed clinically can be influenced by small design changes. (ABGI and ABGII). The rate of earlier peri-prosthetic femoral fracture with the ABGII is most concerning and it is hypothesised that a reasonably simple change to the proximal coating (the addition of a roughened plasma coating) may reduce the risk of early peri-prosthetic femoral fracture.
A cadaveric study where matched left/right pairs of cadaveric femurs are used to compare the effect of the design change (roughened proximal coating) is undertaken. This experimental comparison forms the body of work in Chapter 3 of this thesis.

Subject specific finite element analysis is an obvious choice to consider the abovementioned prosthesis and patient specific factors simultaneously and effectively. However no work was identified in the literature review where finite element analysis was used to specifically predict bone failure around prosthesis. A new finite element method must be developed. The cadaveric study along with being extremely valuable in its own right; had the added advantage that it facilitated the development of subject specific finite element modelling techniques by allowing for an experimental comparison. The development of an finite element method for predicting bone failure (or more specifically cracking) around a femoral stem forms the body of work in Chapter 4.

As shown in the review the procedure or the surgery itself is an important factor for the risk of intra-operative peri-prosthetic femoral fracture. However subject specific finite element analysis methods have not previously considered the loading from the procedure specifically. This is likely because the loading is dynamic in nature (not quasi-static as most finite element analyses are) and also it is quite impractical to measure the dynamic load experimentally. Looking at computer assisted orthopaedic

surgery systems it is clear computer assisted orthopaedic surgery methods have matured sufficiently in recent times. It is proposed in Chapter 5 that an optical tracking system or a Navigation system could be used in combination with a subject-specific finite element analysis to characterise the loads that the surgeon imparts onto the patient during a total hip replacement procedure. Further it is proposed that such a combination could be used clinically to regulate a surgeons behaviour and almost eliminate any risk of intra-operative peri-prosthetic femoral fracture.

The review demonstrates that the risk of peri-prosthetic femoral fracture for femoral head resurfacing is high. Further it shows that the risk is related to both the positioning of femoral component and patient specific factors or, subject specific bone strength. The surgeon undergoing a femoral head resurfacing has many possible positions that they could place the femoral component during surgery. To aid the surgeon to select a position for the femoral component all that is available is an understanding from clinical reviews and previous studies, that placing the femoral component into relative valgus should reduce the risk of peri-prosthetic femoral fracture. But there are no rules for how much valgus or further what version they should place the component to reduce the risk of peri-prosthetic femoral fracture. In Chapter 6 a subject specific finite element method is proposed that utilizes a Design of Experiments approach to investigate the impact of femoral position (both varus valgus and version) on subject specific peri-prosthetic strain in the femoral neck. The Design of Experiments approach allows for a goal driven optimisation that highlights the best options for the component to be placed for that subject.

Chapter 3

A Plasma-Sprayed Titanium Proximal Coating Reduces the Risk of Peri-Prosthetic Femoral Fracture in Cementless Hip Arthroplasty

3.1 Introduction

Periprosthetic femoral fracture is a serious complication of total hip arthroplasty and is often associated with poor outcomes [328]. As described in Chapter 2, risk factors for peri-prosthetic femoral fracture include osteoporosis, femoral stem design, and surgical technique [329, 330]. Higher rates of peri-prosthetic femoral fracture are observed with cementless fixation [104, 108, 331]. The use of cementless fixation is increasing in much of the world, and this trend may continue with cementless implants showing excellent long-term success rates [53-57] and decreased operating time [58]. Undoubtedly, this will result in an increased prevalence of peri-prosthetic femoral fracture. A further increased prevalence of peri-prosthetic femoral fracture will be observed as the patient population with hip replacements rapidly increases, which will be driven by an ageing population and a trend toward early intervention hip arthroplasty. Additionally, broadening of the indications for hip replacement has led to younger patients, who are at greater risk for high-energy trauma events, undergoing the procedure [104]. Overall the prevalence of peri-prosthetic femoral fracture will increase and efforts to reduce the risk are needed.

Based on the timing of the fracture, peri-prosthetic femoral fractures are classified as intra-operative, early postoperative, and late postoperative, with unique mechanics involved in each situation [104, 108, 141]. Intra-operative peri-prosthetic femoral fractures can occur at any time during the surgical preparation; however, they most commonly occur during implant insertion as the surgeon strives to obtain the firm initial press fit, which is required to promote bony in-growth and achieve long-term fixation [14, 63, 307]. To achieve the required firm press fit, the stem is pressed into the femur with considerable force, causing a wedging effect and the resulting generated hoop stresses can become too great for the bone to resist. [104]. A minor episode of trauma is cited as the most frequent cause for postoperative peri-prosthetic femoral fractures [136, 332]. Postoperative peri-prosthetic femoral fractures occur due to

anatomic forces resulting from the patient's own weight bearing and muscle loads. Mabry [333] suggested that early post-operative fractures (three months post-implantation) may be the result of an undiagnosed intraoperative fracture, which decreases the load-bearing capacity of the bone.

The ABG II prosthesis (Stryker Orthopaedics, Mahwah, NJ, USA) is a cementless implant with a grit-blasted hydroxyapatite-coated proximal on-growth surface with proximal medial scales and a polished distal stem, and has a successful clinical history [172-174]. For the purpose of my study sequential design changes were made to the ABG II-standard implant; the first was lack of medial scales (hereafter referred as ABG II-NMS) and the second was a high-friction titanium plasma-sprayed proximal coating (hereafter referred as ABG II-plasma). These implants were then compared to the ABG II-standard implant. Femoral fractures were simulated using biomechanical loading to determine if either of the changes to the ABG II femoral stem design would primarily increase the load-bearing capacity of the femur (decrease the proximal surface strains on the femur) during broaching, implant insertion, and early weight bearing; thereby improving implant longevity and durability.

3.2 Methods

3.2.1 Femoral specimens

The experimental testing procedure was approved by the Royal North Shore Hospital ethics committee. Twelve cadaveric femurs (6 left and 6 right, matched pairs) of donors with a mean age of 61 years (range, 39–77 years) were sourced from the International Institute for the Advancement of Medicine (IIAM Corporate, Jessup, PA, USA). The laboratory testing was conducted in a facility certified to operate within all requirements as per the NSW Anatomy Act 1977 and Human Tissue and Anatomy Legislation Amendment Act 2003." The femurs were subjected to x-ray (see Figure 89) and then computed tomography evaluation in the anteroposterior and mediolateral planes to

ensure that they were free of pathology and to allow preoperative templating to determine the expected prosthesis sizes for the ABG II femoral components.

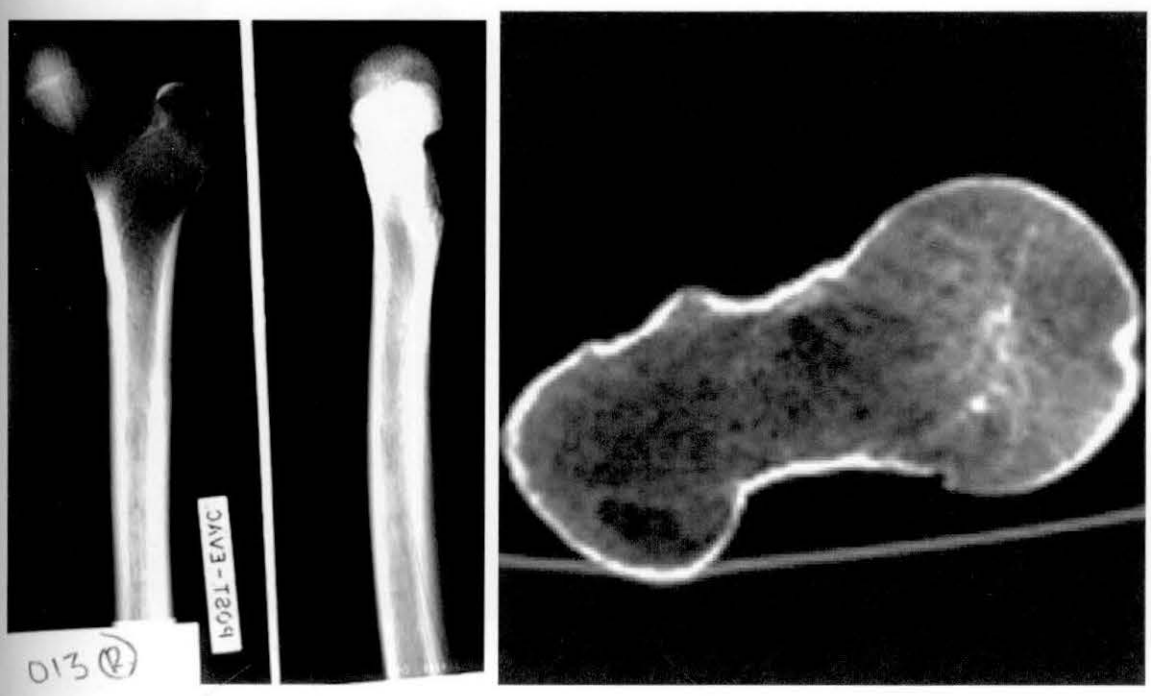

Figure 89-Representative X-ray of cadaveric femora (top) axial slice of cadaveric femur (bottom)

3.2.1.1 Cortical index:

Cortical index is a measure of the strength of bone. The cortical index of each bone was determined using the equation shown in Figure 90

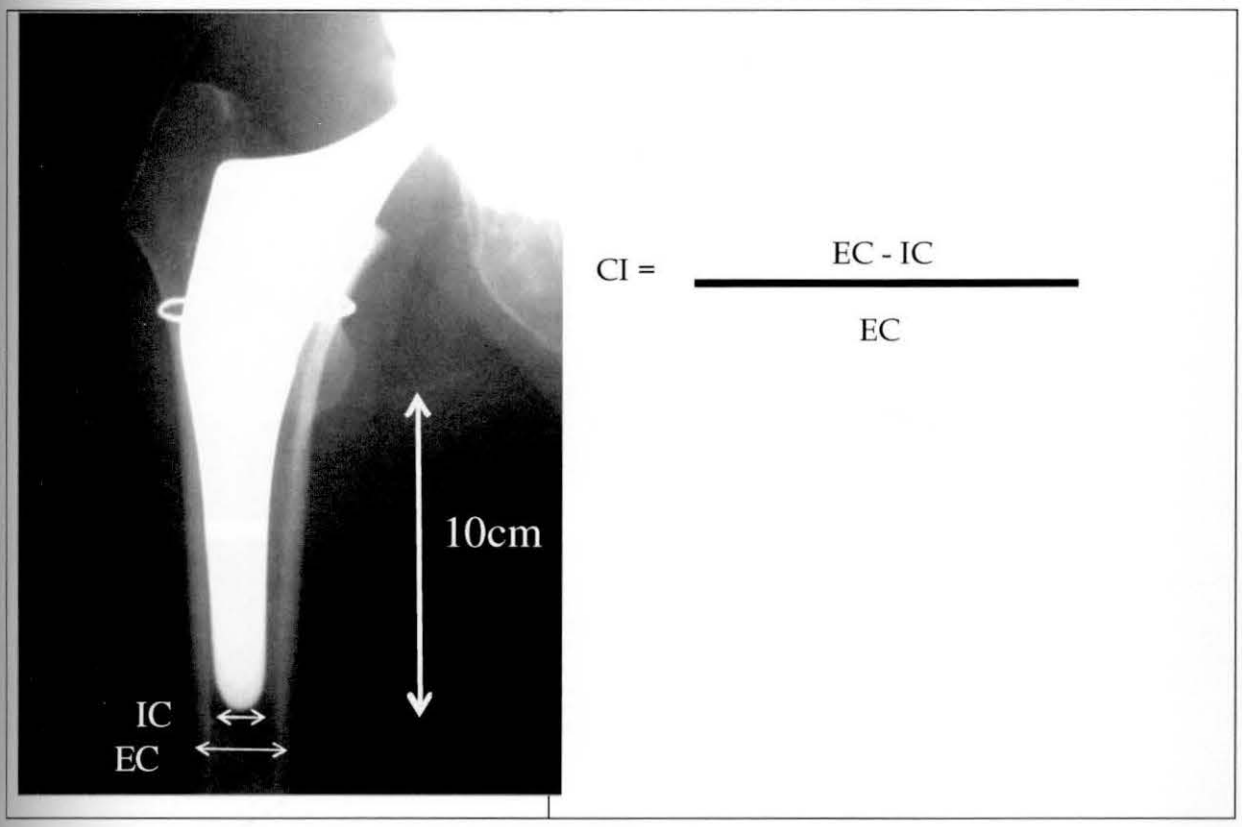

Figure 90 Calculation of cortical index measurements on the left and formula to the right

After templating, the femurs were sectioned and potted in a polymethylmethacrylate potting medium, 30 mm distal to the expected position of the distal tip of the prosthesis for the template size. Each femur was cleaned of all soft tissue. Strain gauge locations were prepared by defatting with propan-1-ol, sanding with fine grade sandpaper, re-defatting using propan-1-ol, and finally, neutralizing with a light detergent (See Figure 91).

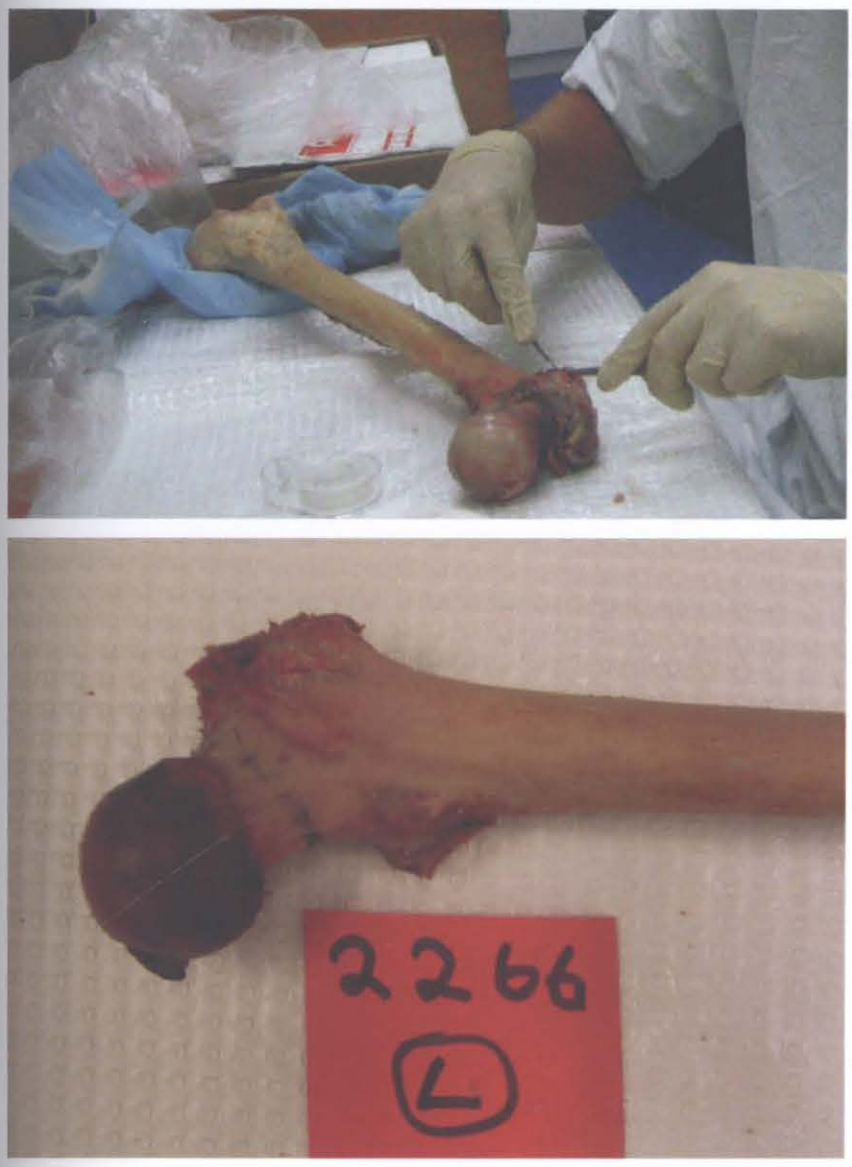

Figure 91 Preparation of cadaveric femurs removal of soft tissue

Five rosette strain gauges (TML Co. Ltd., Tokyo, Japan) were attached to each femur anterolaterally (AL), anteromedially (AM), medially (M), posteromedially (PM), and posterolaterally (PL) (See Figure 92 and Figure 94).

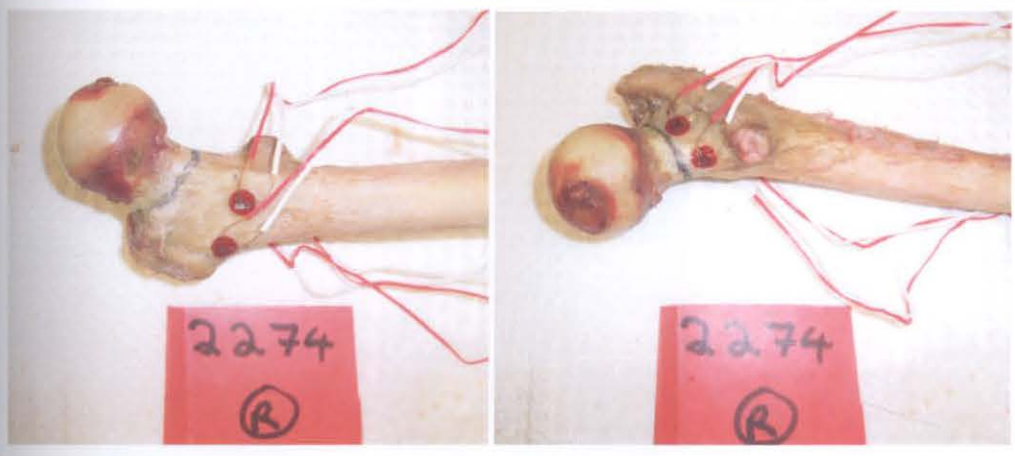

Figure 92 Representative strain gauge attachment to femur

A mechanical testing jig was prepared to orient the bone 9 degrees in the sagittal plane and 10 degrees in the coronal plane. This was in order to closely replicate the anatomic loading of femoral stems (ISO 7206-4, 2010 specifications) (See Figure 93).

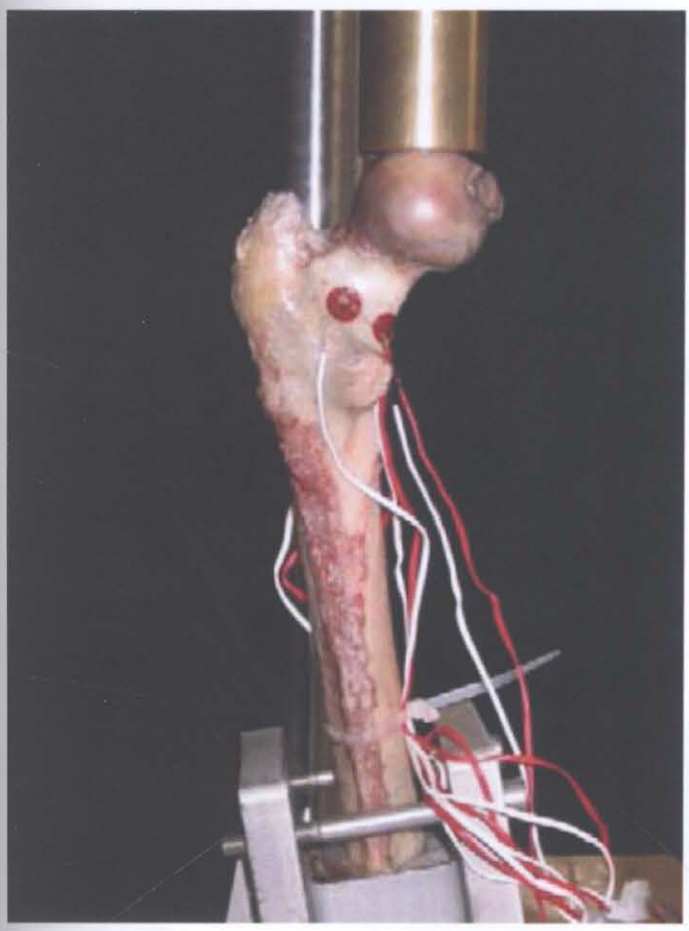

Figure 93 Representative potted femur loaded into testing jig in ISO-7206-4 2010 loading orientation

3.2.2 Strain gauge location

Strain gauge rosette 1 was placed at the thinnest edge of the osteotomy in the region of the trochanteric fossa. Gauge 2 was placed 23 mm posteromedially from gauge 1 at the edge of the osteotomy. Gauge 3 was placed on the anterior aspect of the femur 17 mm distal as well as lateral to the most medial aspect of the osteotomy. Gauge 4 was placed 22 mm lateral and 10 mm superior to gauge 3. Gauge 5 was placed on the inferior aspect of the femur (See Figure 92 and Figure 94). Each rosette gauge measured

the strain directly about 3 axes, which were oriented such that the axial, shear, and hoop strain were measured directly on each bone.

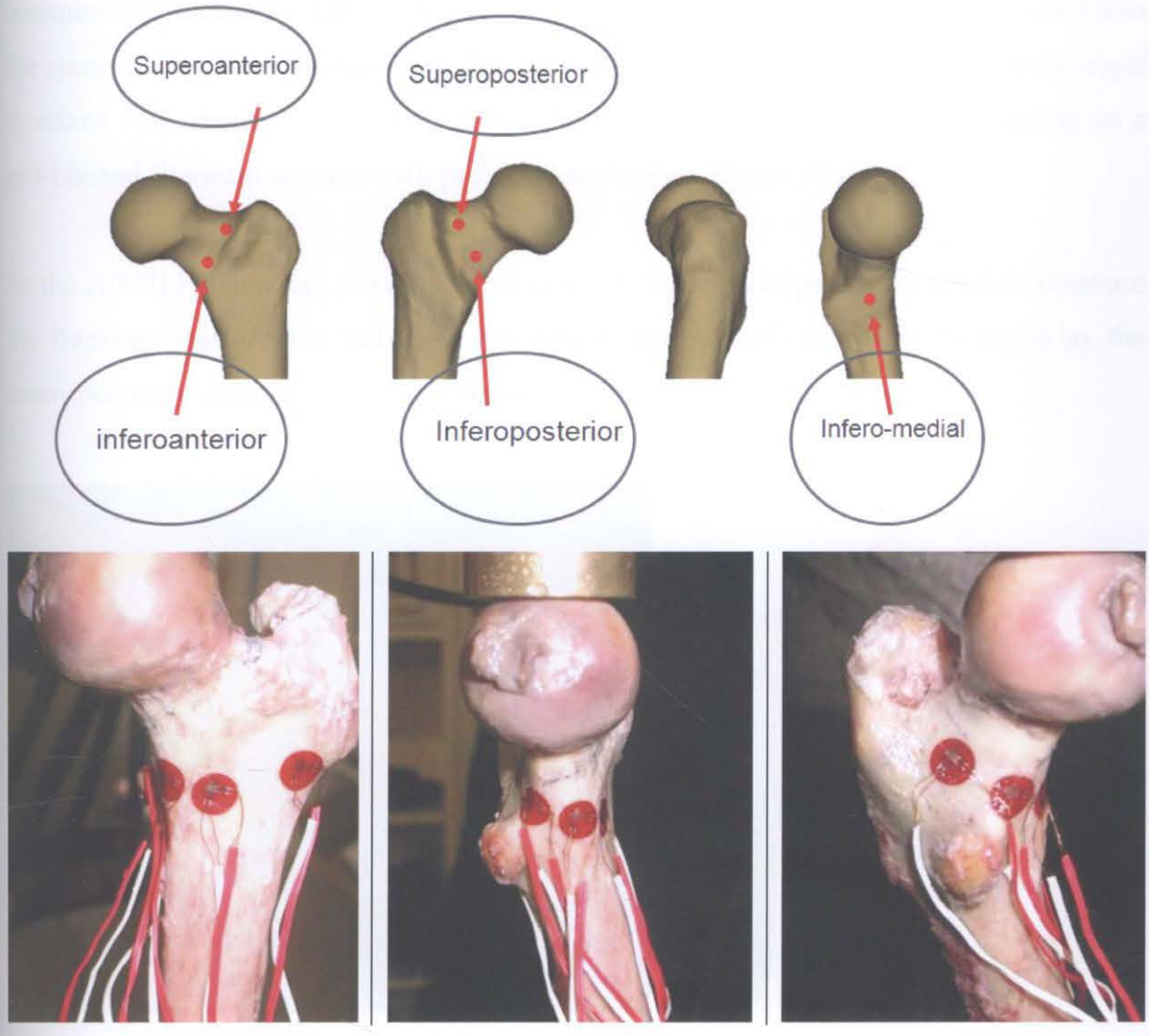

Figure 94 Planned locations of strain gauges (top) actual locations (bottom)

3.2.3 Prostheses

Two types of experimental prostheses were manufactured by Stryker Orthopaedics Mawah: (i) ABG II-plasma—an experimental ABG II femoral stem with a high-friction plasma-sprayed titanium proximal in-growth surface. This surface was not HA coated,

as is most common practice for other commercially available Stryker stems. (see Figure 95) and (ii) ABG II-NMS – an experimental ABG II femoral stem identical to the commercially available ABG II stems but without the medial scales being machined into the stem during manufacture (See Figure 95 and Figure 96). As controls, off-the-shelf standard ABG II stems were used as they have a proximal hydroxyapatite coating on a grit-blasted titanium surface with proximal scales (see Figure 95 right).

As the ABGII Plasma had the additional coating, Vernier calipers were used to measure the thickness differential between the ABGII plasma and the ABG II stems in the anteroposterior dimension at the line marked "limit HA" in Figure 96.

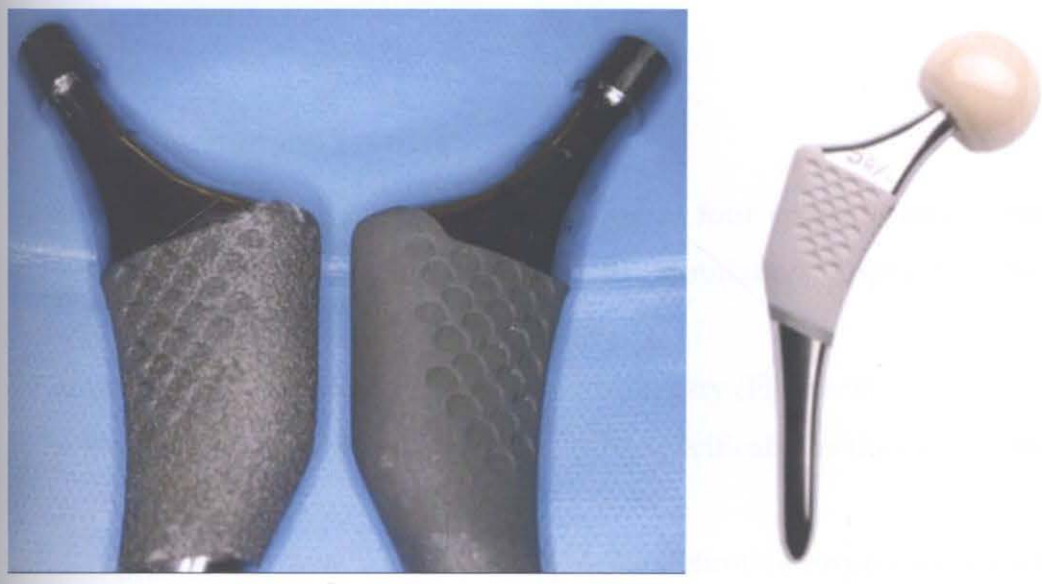

Figure 95 Experimental stems; ABGII Plasma (far left) ABGII NMS (middle left) ABGII Standard (right)

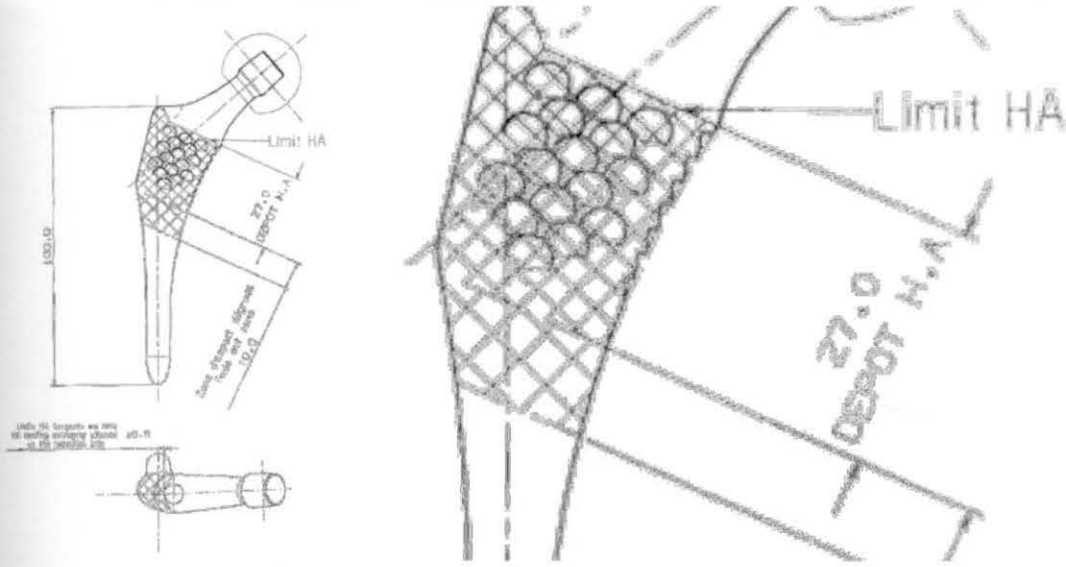

Figure 96 ABGII medial scales visible in region marked "DEPOT H.A"

3.2.4 Biomechanical testing

The strains across each gauge were measured at four separate time periods using an MTS 858 mechanical testing system and simulation apparatus (MTS Systems Corporation, Eden Prairie, MN, USA):

(i) Native femoral strain was recorded before surgery (Figure 93);

(ii) Surgical preparation strains were recorded specifically as the canal was broached to receive the prosthesis;

(iii) Stem insertion strains were recorded as the definitive prostheses were inserted into the canal; (See Figure 97)

(iv) Strains were measured following the insertion of each femoral stem (See Figure 98).

At the first and last time points, a cyclic load of 80–800 N was applied to the femur.

The femurs were then loaded to failure with the implants *in situ*. (See Figure 99)

Strains at failure were not recorded and the procedure and order of testing are depicted in Figure 100 .

Figure 97 Impaction of stem into femur during testing

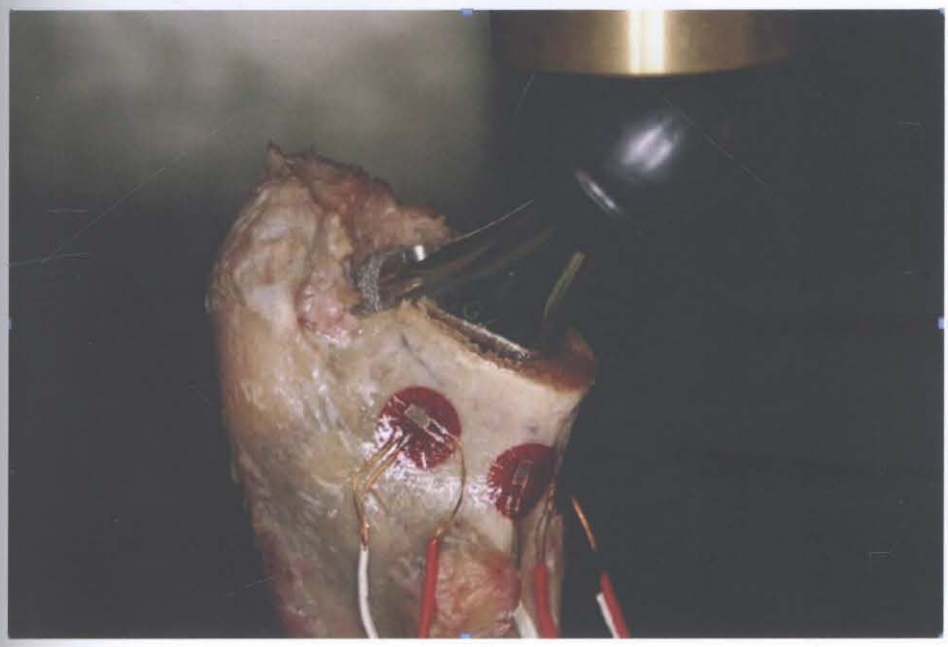

Figure 98 Implant loaded under compression in the MTS testing system

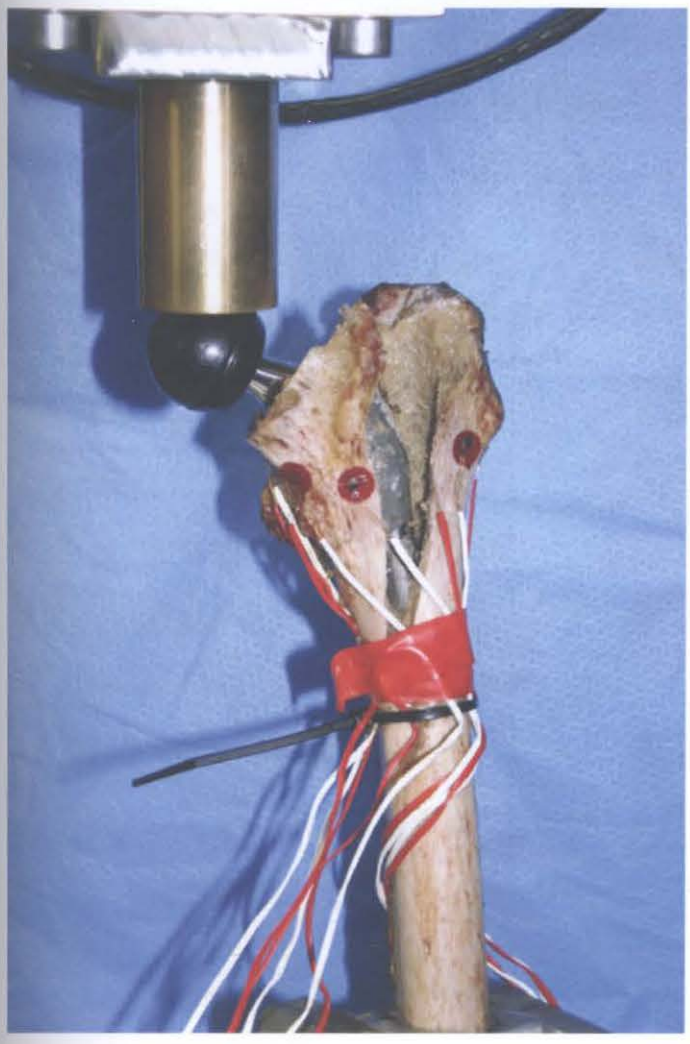

Figure 99 Implant femur loaded to failure fracture clearly visible superior to inferior

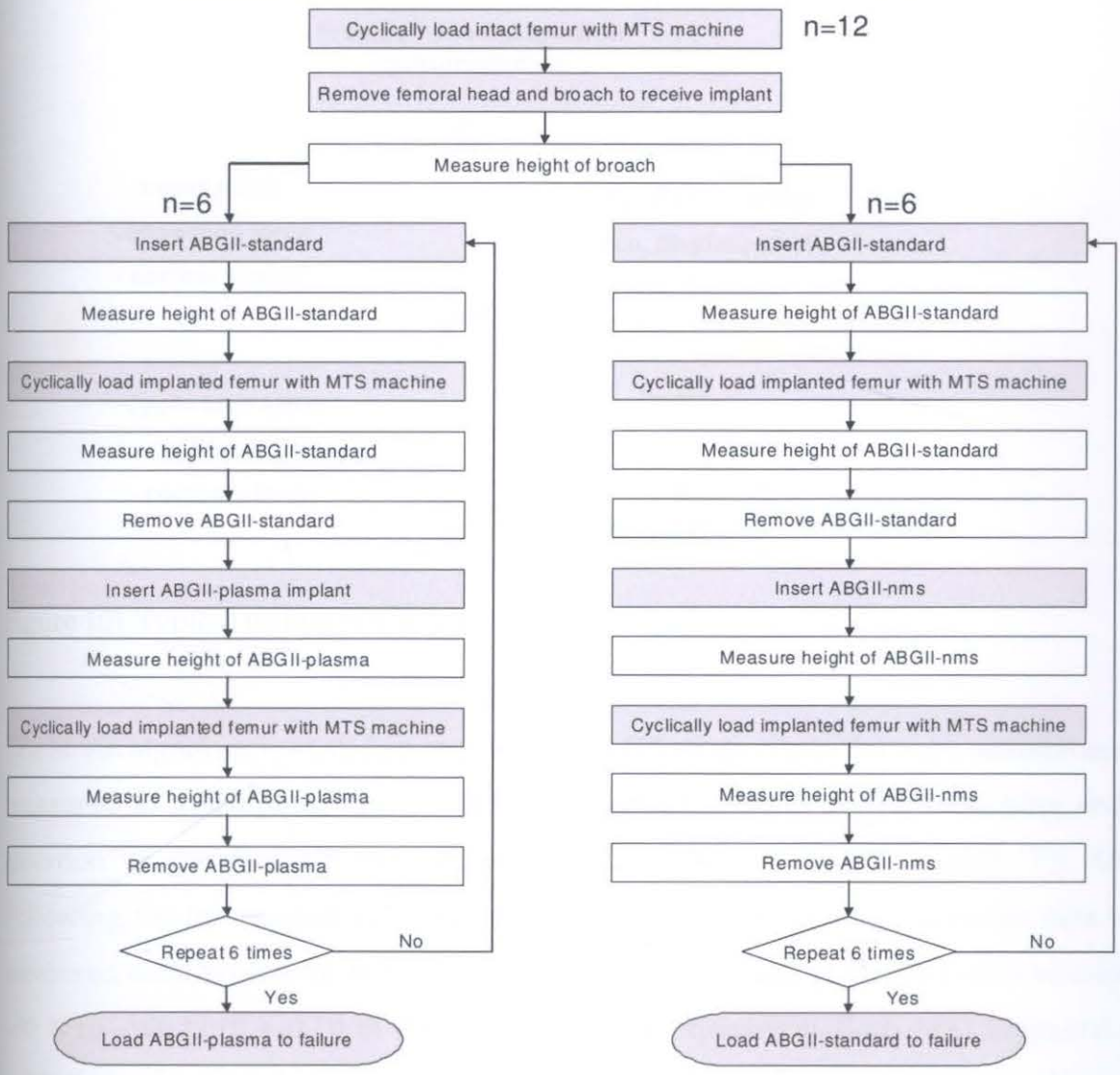

Figure 100 Sequence of testing -The grey boxes indicate the steps where the strain was measured

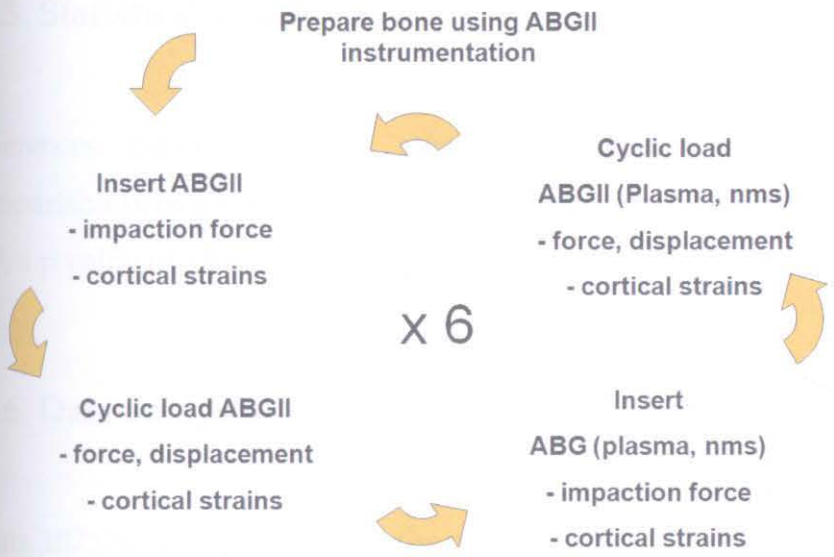

Figure 101 Typical testing sequence

The strain signals across all five rosette gauges (15 strain channels) were simultaneously measured at a sampling rate of 50 Hz for the intact bone during broaching and on insertion of the femoral stem (Labview; National Instruments, Austin, TX, USA). Following the insertion of each femoral stem, strain and force-displacement data were measured simultaneously during cyclic loading of the femur (1 Hz, 50 cycles, sinusoidal, -80 N to -800 N [R = 0.1]) in the ISO 7206-4 type orientation. Both ABG II-plasma and ABG II-standard implants were alternatively tested in a femur, six times under cyclic compressive loading. Similarly, the contralateral femur was used to test the ABG II-NMS and ABG II-standard implants six times. This testing regime was repeated with all of the paired femurs. On completion of the cyclic loading, the left and right paired femurs were implanted with ABG II-plasma and ABG II-standard, respectively, and loaded to compressive failure (bone fracture) under a constant ramp displacement of 1 mm/s. The force and displacement signal was again collected at 50 Hz. This procedure was repeated with all of the paired femurs.

3.2.5 Statistical analysis

Differences between groups were determined using an analysis of variance. Comparison between groups was made using a least significant difference post-hoc test, with a p value of <0.05 set as significant. Data will be presented as [median (range)].

3.2.6 Data analysis

Figure 102 shows an example of the cortical bone strain during implant impaction using a hammer. The series of sharp steps in each strain channel coincide with the change in bone strain generated with each impaction blow to the implant. This data was then used to determine the peak compressive or tensile strain of each channel during implant insertion, and the final strains after the implant was fully seated.

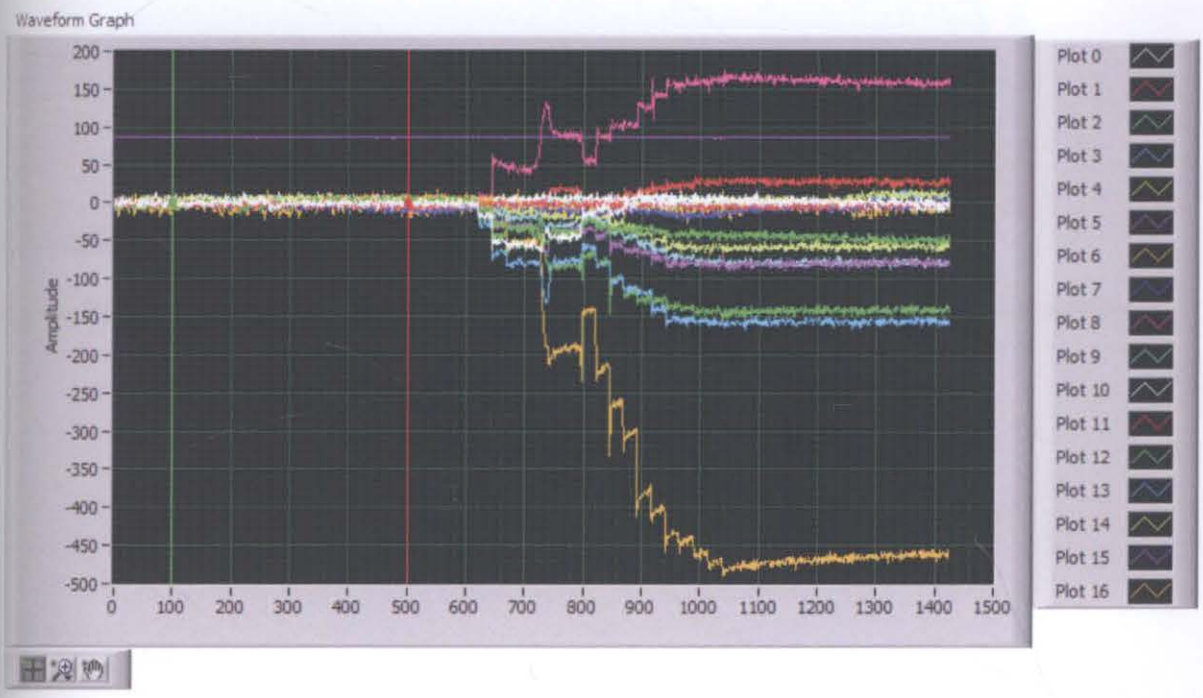

Figure 102 Example strain versus time plot during impaction stage of the testing

The Figure 103 shows an example of the strain, force and displacement versus time signals for one implant tested over the 50 sinusoidal loading cycles. To allow for implant settling and bone conditioning, only the last 20 cycles were used for analysis. Strains versus force plots were created and a linear trend line was fitted to each strain channel. (Figure 104) From this trend line both the slope and Y-intercept were extracted. The magnitude of the slope represented the cortical bone sensitivity to implant loading (strain/force) while the Y-intercept represented the residual strain remaining in the bone at zero load.

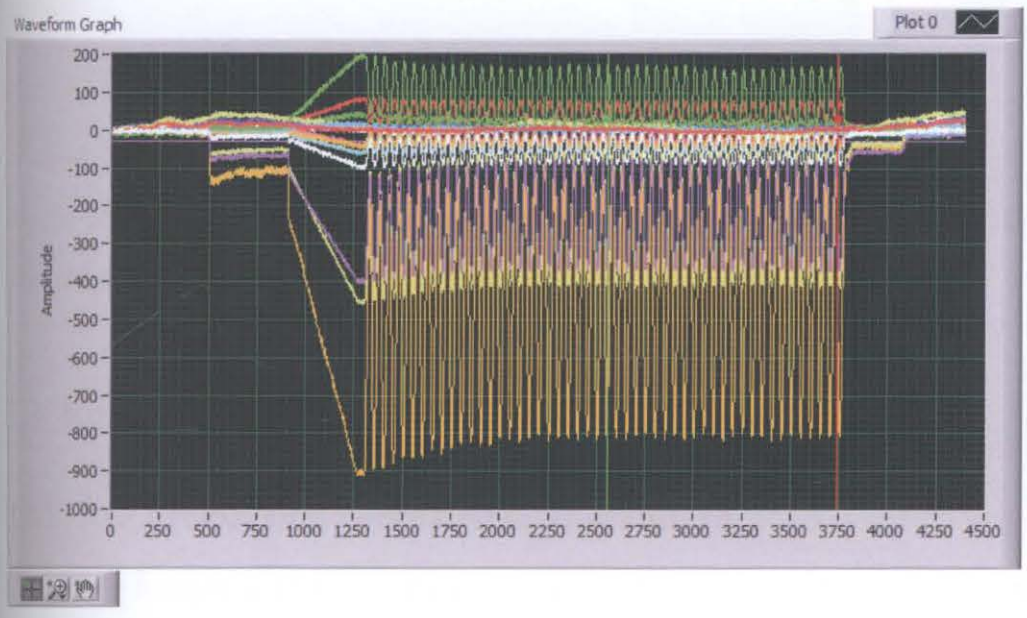

Figure 103 Example strain versus time plot for the cyclic loading part of the testing

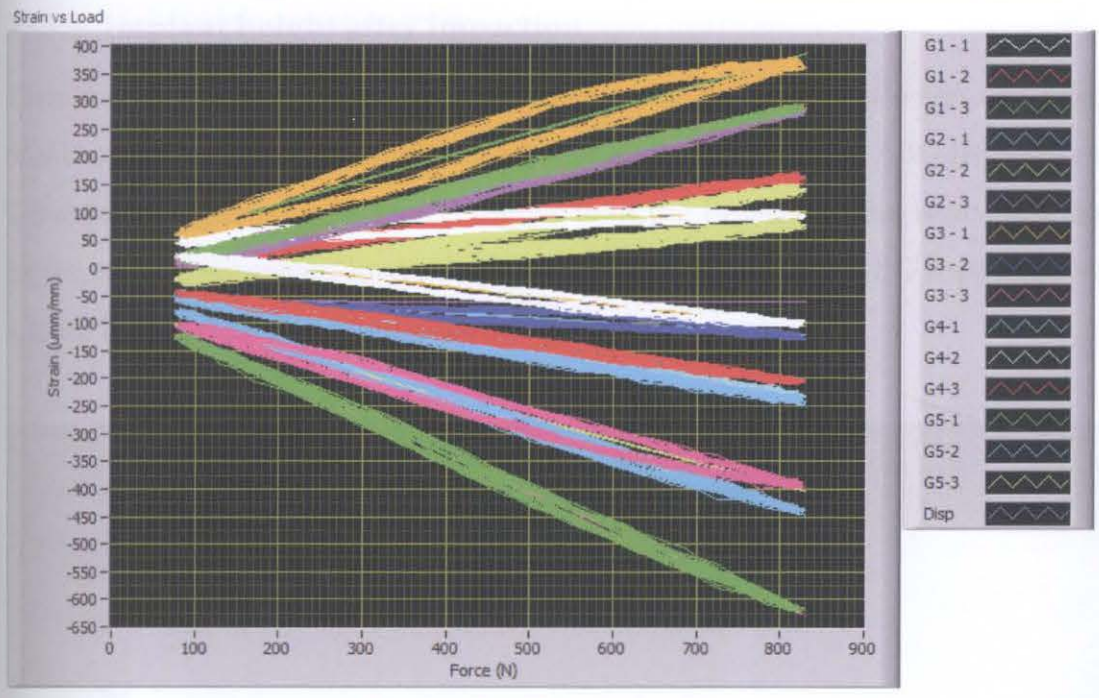

Figure 104 Example strain versus force plot. Note that most channels demonstrate a near elastic behavior with only a minimal hysteresis loop

3.3 Results

3.3.1 ABG II-plasma versus ABG II-standard

One of the femurs with the ABG II-plasma implant fractured during insertion; therefore, only five pairs have been reported for that group.

3.3.1.1 Comparison of implant sizes

ABGII-Plasma stem external dimensions were greater than ABGII-standard in all dimensions

mediolateral proximal - Size 5 by 0.5mm, Size 3 by 1mm

anteroposterior- proximal - Size 5 by 0.4 mm, Size 3 by 0.6 mm

anteroposterior distal - plasma 1.2 mm greater for both

3.3.1.2 Implant height after impaction

There was significant variation in the seating of the implants when compared to the final broach position. In 5 out of the 6 bones analysed, both the ABG II-plasma and ABG II-standard implants were seated higher than the broach. In the remaining bone, both the implants were seated lower than the broach. On average, ABG II-plasma was seated 0.3 mm higher than ABG II-standard (maximum, 1 mm).

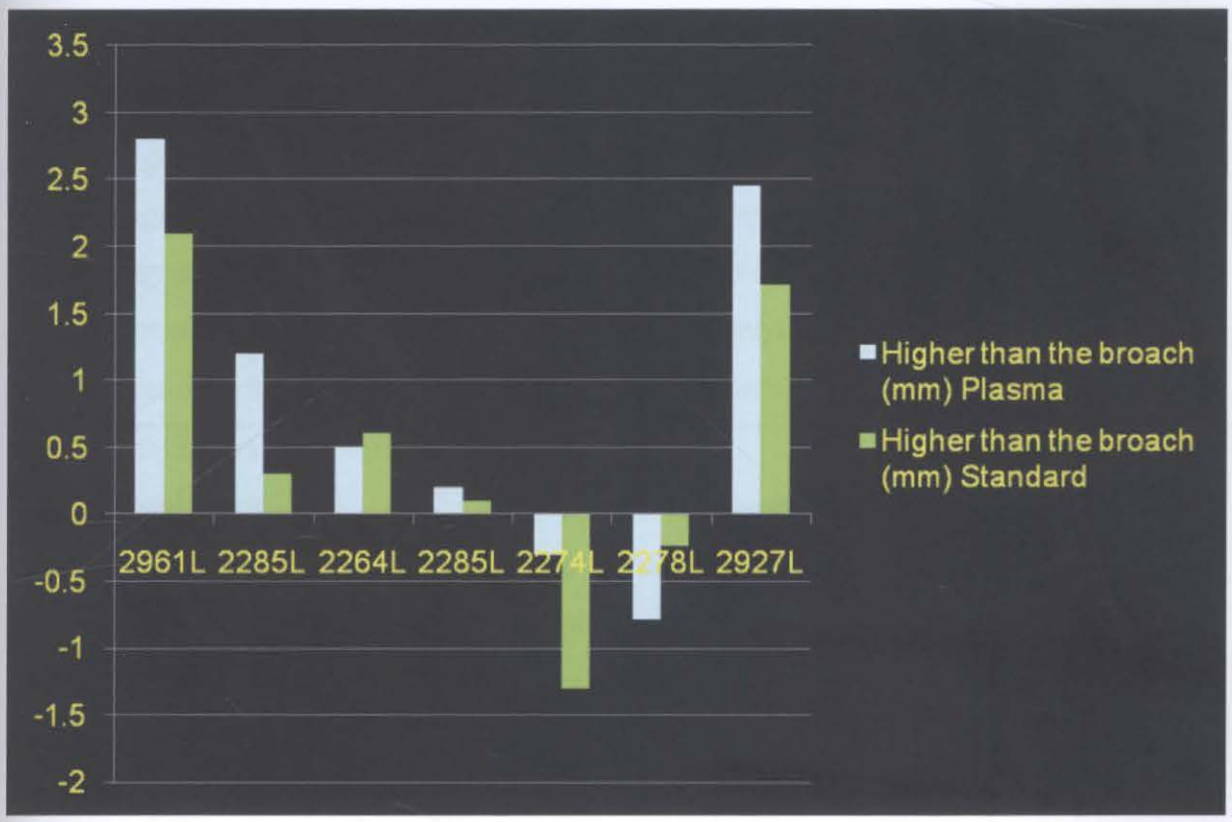

Figure 105 Implant heights after impaction measured with MTS machine

3.3.1.3 Implant impaction

The maximal impaction cortical hoop strain was lower across all the gauges (less tensile) with the ABG II-plasma stem than with the ABG II-standard stem. The

difference was significant in 4 out of 5 gauges, namely: the PM gauge (p = 0.0004), PL gauge (p = 0.0025), al. gauge (p = 0.0157), and M gauge (p = 0.0060).

The final impaction cortical hoop strain was lower across all gauges (less tensile) with the ABG II-plasma stem than with the ABG II-standard stem. The difference was significant in 3 out of 5 gauges, namely: the PM gauge ($p < 0.0001$), PL gauge (p = 0.0002), and M gauge (p = 0.0009).

Hoop - Maximal Impaction Strain		
PM	Significant	plasma less tensile than standard
M	Significant	plasma less tensile than standard
PL	Significant	plasma less tensile than standard
AM	not significant	plasma less tensile than standard
AL	Significant	plasma less tensile than standard
Hoop - Final Impaction Strain		
PM	Significant	plasma less tensile than standard
M	Significant	plasma less tensile than standard
PL	Significant	plasma less tensile than standard
AM	not significant	plasma less tensile than standard
AL	not significant	plasma less tensile than standard

Axial - Maximal Impaction Strain		
PM	Significant	plasma less tensile than standard
M	Significant	plasma less tensile than standard
PL	Significant	plasma less tensile than standard
AM	not significant	plasma less tensile than standard
AL	Significant	plasma less tensile than standard
Axial - Final Impaction Strain		
PM	Significant	plasma less tensile than standard
M	not significant	plasma more tensile than standard
PL	not significant	plasma more tensile than standard
AM	Significant	plasma less tensile than standard
AL	not significant	plasma less tensile than standard

Table 6 Impaction data(comparing ABGII Plasma and ABGII Standard)

3.3.1.4 Strain sensitivity

The hoop strain measured in the ABG II-plasma stem was closer to that of intact bone; the modified design was significantly less tensile than ABG II-standard based on the measurements from the M ($P < 0.0001$), AM ($P = 0.0173$), and al. ($P = 0.0009$) gauges (See Figure 106). The axial strain measured in the ABG II-plasma stem was significantly lower than those of the ABG II-standard implant and intact bone for the M gauge. No differences were noted in the other strain gauges for axial strain (See Figure 107).

Table 7 Hoop strain sensitivity

Hoop -strain sensitivity		
GAUGE	Standard vs Plasma	Trend
AL	Significant	plasma less tensile - closer to intact bone
AM	Significant	plasma less tensile - closer to intact bone
M	Significant	plasma less tensile - closer to intact bone
PL	Significant	plasma more compressive - closer to intact bone
PM	not significant	both compressive - similar to intact bone

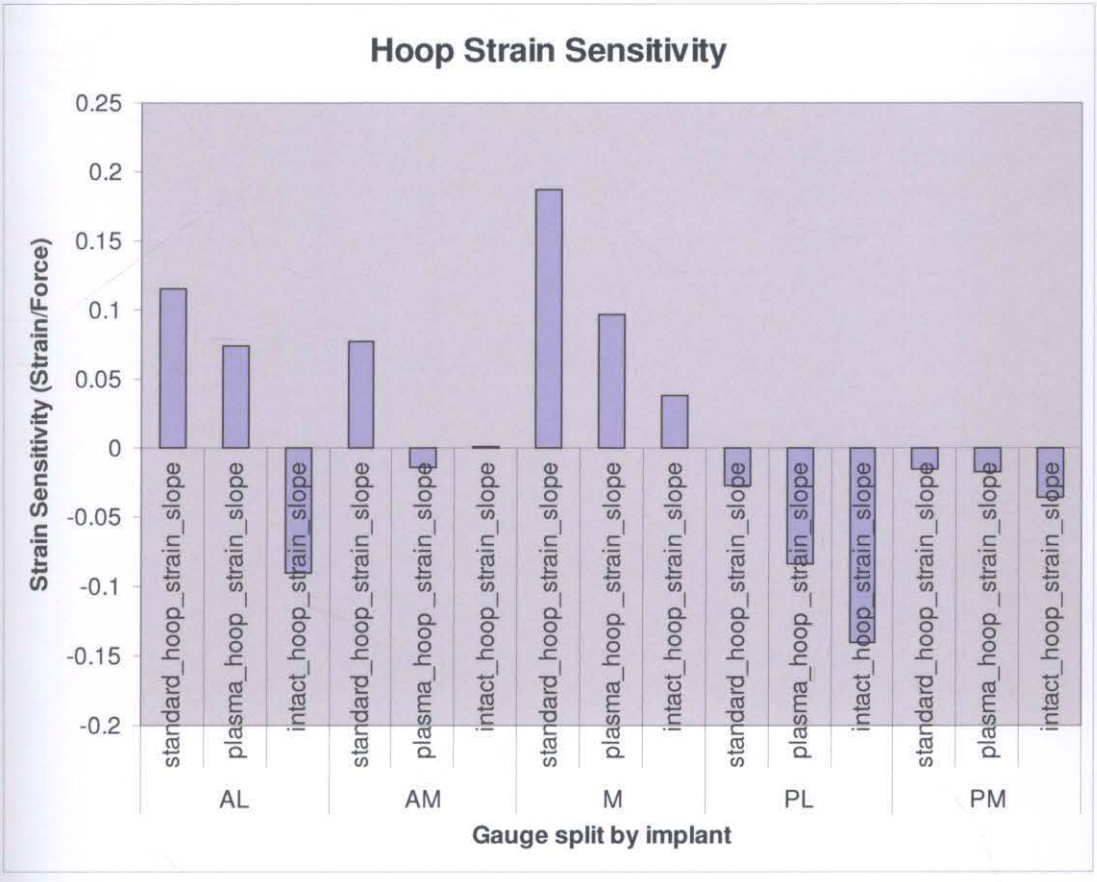

Figure 106 Hoop strain sensitivity

Table 8 Axial strain sensitivity

Axial -Strain sensitivity		
	Standard vs	
GAUGE	Plasma	Trend
AL	not significant	all similar
AM	not significant	all similar
M	significant	plasma less compressive than standard and intact
PL	not significant	all similar
PM	not significant	Plasma and standard less compressive than intact

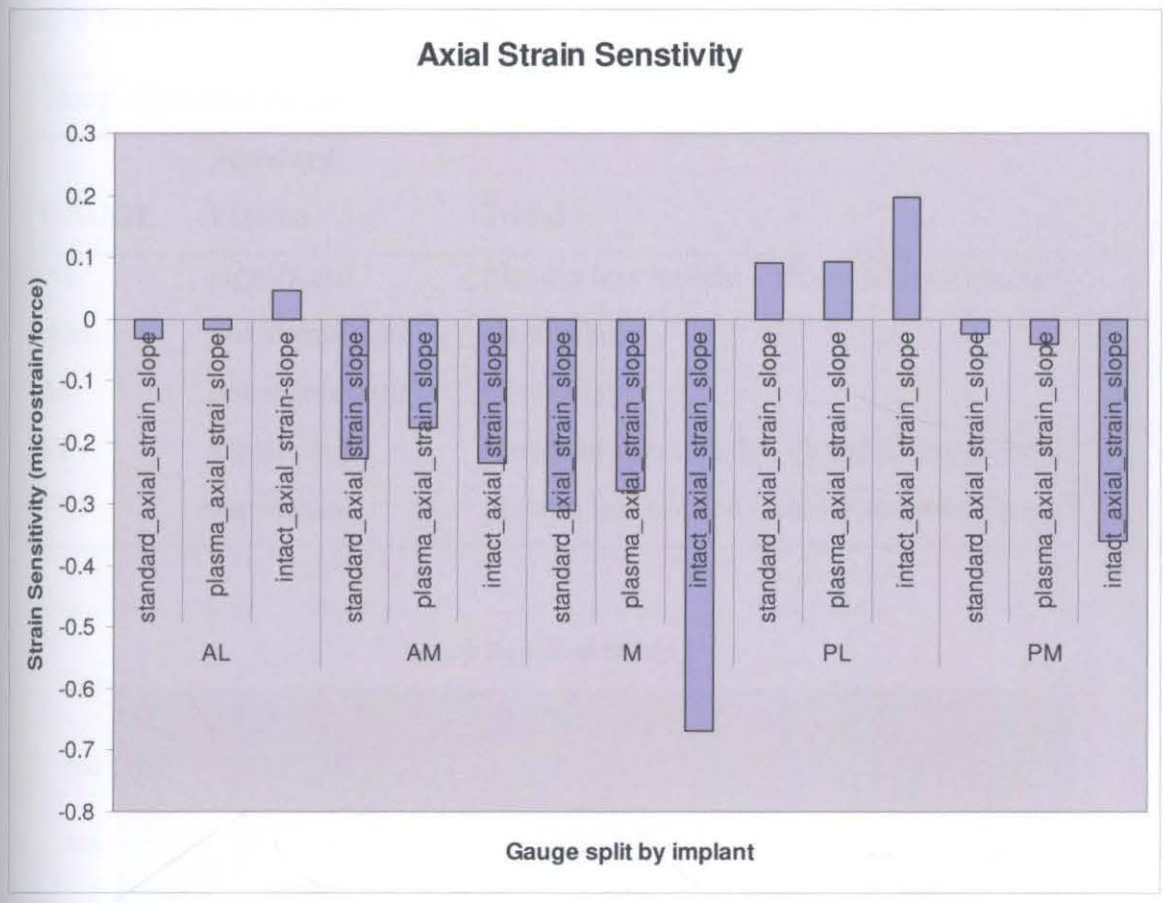

Figure 107 Axial strain sensitivity magnitudes

3.3.1.5 Residual strain

In 3 out of 5 gauges, the final residual hoop strains of the ABG II-plasma stem were lower than those of ABG II-standard and were also closer to those of intact bone. However, these values were only statistically significant for the al. (P = 0.0002) and PM gauges (P = 0.0068) (See Figure 107). In 2 out of 5 gauges, the axial residual strains of the ABG II-plasma stem were closer to those of intact bone as compared to ABG II-standard. These values were statistically significant for the AM and al. gauges (See Figure 108).

Table 9 Hoop residual strain signifiance

Hoop -Residual Strain		
	Standard v	
GAUGE	Plasma	Trend
AL	significant	plasma less tensile - closer to intact bone
AM	not significant	all similar
M	not significant	all similar
PL	significant	standard less tensile - closer to intact bone
PM	significant	plasma less tensile - closer to intact bone

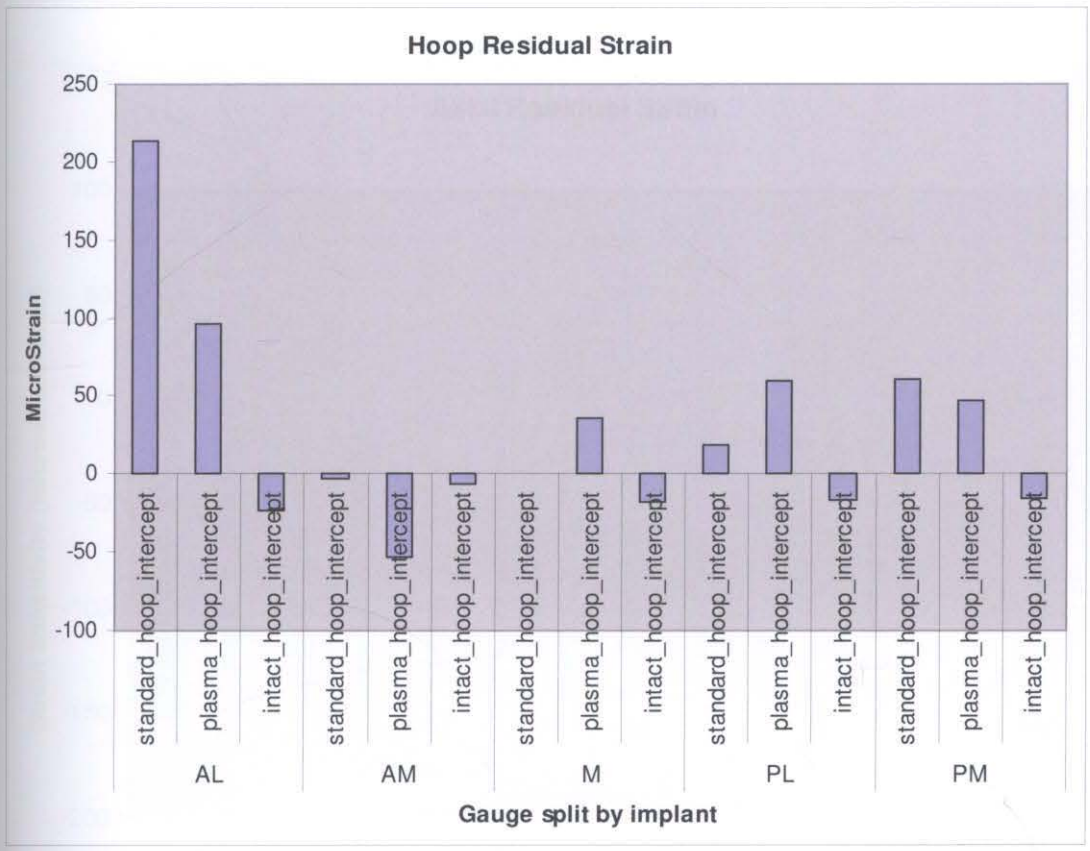

Figure 108 Hoop residual strain magnitudes

Table 10 Axial residual strain significance

Axial -Residual Strain		
	Standard v	
GAUGE	Plasma	Trend
AL	significant	plasma less compressive – closer to intact bone
AM	significant	plasma less compressive – closer to intact bone
M	not significant	all similar
PL	not significant	all similar
PM	not significant	Plasma and standard less tensile than intact bone

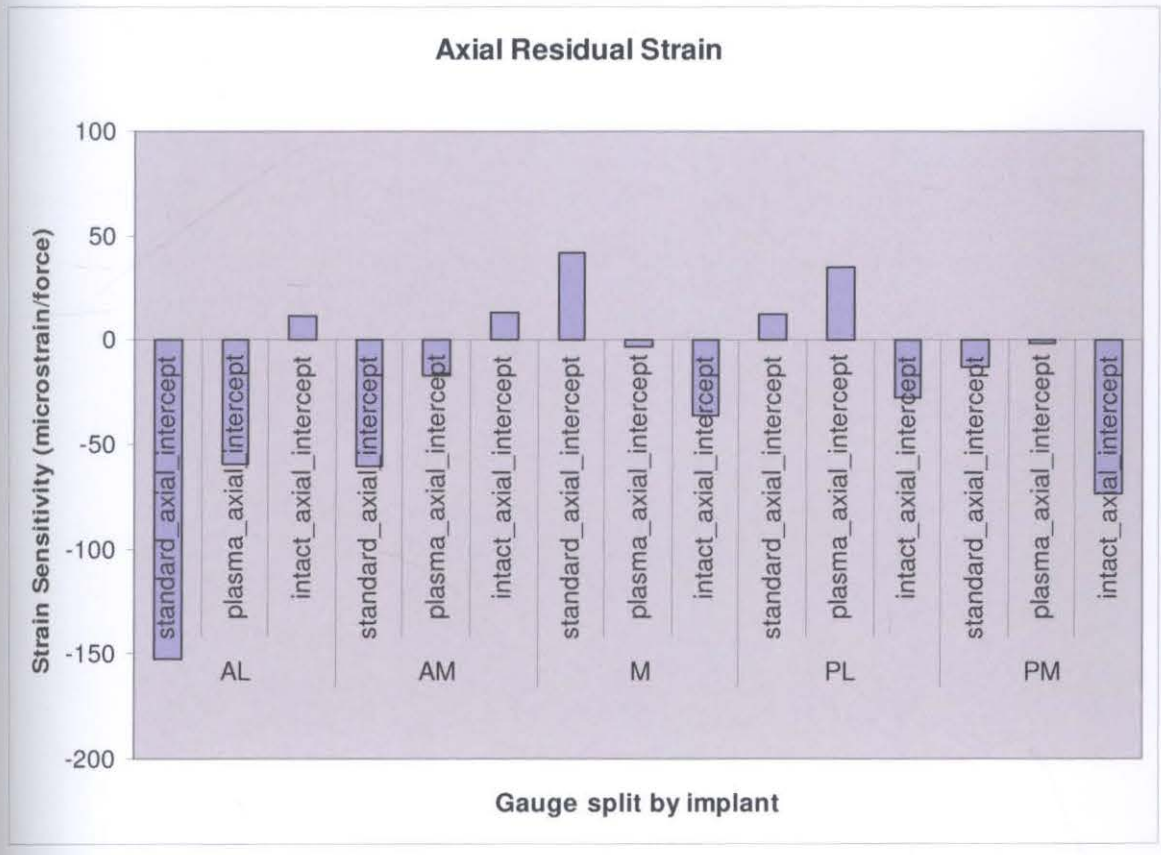

Figure 109 Axial residual strain magnitudes

3.3.1.6 Failure load

The ABG II-plasma, in all of the paired bones tested, showed a significantly higher load to failure, when compared to ABG II-standard.

ABG II- Plasma demonstrated higher load tolerance [32% (12% to 102%)] when compared to ABG II-standard ($p<0.05$) (Table 6).

Table 11 Failure Load ABG II-Plasma vs ABGII- Standard

ABG II-plasma		ABG II-standard		
Sample ID	Load (N)	Sample ID	Load (N)	% diff
2961L	-8635.5	2961R	-6550.8	32%
2285L	-10314.0	2285R	-9184.7	12%
2274L	-4510.4	2274R	-2236.5	102%
2278L	-3764.8	2278R	-3300.0	14%
2264L	-7604.0	2266R	-6479.9	49%
			Mean	42%
			P =	0.014

3.3.1.7 Failure load versus cortical index

A close correlation between the cortical index and the failure load was shown for both the ABG-standard and the ABG-plasma. For the same cortical index the ABG-plasma had a greater failure load than the ABG-standard. See Figure 110.

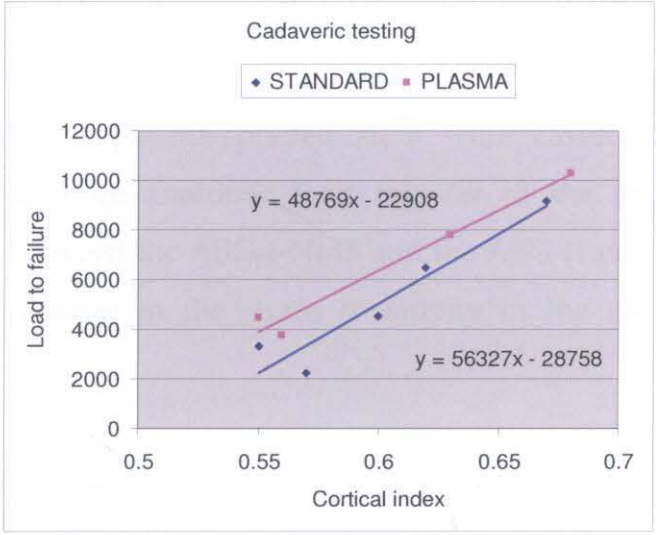

Figure 110 Failure load vs cortical index

3.3.2 ABG II-NMS versus ABG II-standard

There was no significant difference for the maximum impaction strains between the ABGII-NSM and the ABGII-standard across all five gauges. In addition there was no significant difference in the implant height between ABG II-NMS and ABG II-standard. There was also no statistically significant difference in the residual strain between the ABG II-NMS and ABG II-standard across all 5 gauges. Failure load was not tested in ABG II-NMS.

Strain sensitivity measurements did not show any difference between the two implants across the PL, AL, or AM gauges. However, the ABG II-NMS stem was significantly more tensile than ABG II-standard for the M gauge ($P < 0.0001$), and significantly less tensile for the PM gauge ($P < 0.0001$).

3.4 Discussion

In this study, two experimental cementless femoral designs were compared; the ABG II-plasma and ABG II-NMS, with the commercially available ABG II-standard cementless implant. Results show that the modified ABG II-plasma, with a high-friction titanium plasma-sprayed proximal coating, was associated with increased load-bearing capacity and lower surface strains as compared to the ABG II-standard. Additionally, the surface strains with the plasma-sprayed stem were closer to those of the native bone, suggesting a more anatomic load transfer to the proximal femur. Less dramatic differences between the ABGII-NMS and the ABG-II standard were observed with only a localized change in the strain sensitivity in the gauges immediately around the modification.

The most significant finding in this work was that the failure load of the ABG II-plasma-implanted bone was an average 42% (32% median) greater than that of the ABG II-standard-implanted femurs. Thus, the load-bearing capacity of the femur in the early

post-operative period would be greater when a plasma-sprayed stem is used, rather than a smooth stem. Clinically this would decrease the risk of early peri-prosthetic femoral fracture by creating a factor of safety against fracture.

The observed differences between the ABGII plasma and the ABGII standard can be explained by an increase in the frictional forces at the bone-implant interface. The increased frictional forces are due to the addition of the roughened plasma-sprayed coating, which increases the friction co-efficient at the interface. The increased frictional force at the interface can better resist the slippage of the implant into the femoral canal when the implant is forced into the femur under simulated anatomic loading. The resistance prevents a wedging effect that would expand the proximal femur and result in an increase in hoop strains in the bone. A strong analogy for the above-mentioned mechanism would be that a smooth sharp axe would split a log with considerably less effort than a rusty dull (higher friction) axe. This theory is supported by the finding that, when compared to ABG II-standard; the ABG II-plasma implant was on average seated higher in the femur after insertion.

The higher final seating with the ABGII- Plasma is, however, in itself a concern. A previous study by Fitzgerald [334] reported an increased incidence of intra-operative fractures with the Omnifit prosthesis (15.2%) and attributed the fractures to the oversizing of the femoral prosthesis relative to the instruments. The plasma-spray coating of the ABG II-plasma added thickness to the implant and did, therefore, result in an oversize of the implant relative to the broach. The thicker coating might lead the surgeon to inadvertently induce an intra-operative peri-prosthetic femoral fracture by trying to seat the thicker stem further into the canal. Despite the increased friction, the thicker stem would then cause higher hoop stresses in the bone at the same level due to further expansion of the bone canal. In this study, the additional thickness of the coating caused the plasma-sprayed stem to be seated higher on average than the other stems. Fractures during stem insertion were not observed; however, this may not be the case in

a wider clinical setting. It is conceivable that an increased incidence of intra-operative peri-prosthetic femoral fracture could be seen if the addition of a plasma coating to the implant was not accompanied by new broaching instruments and this must be a consideration.

It is, however, possible that the additional thickness could be advantageous. The addition of thickness will undoubtedly result in a tighter apposition of the implant against the bone. The common design principle for cementless femoral stems is to achieve a close fit of the prosthesis, to restore strains in the proximal femur, and obtain maximum stability of the implant. Aamodt A., et al and Kim Y.H., et al [63, 335] demonstrated that a closer proximal fit can produce closer to normal magnitude and patterns of stress. It was also observed that the experimental plasma-sprayed stem appeared to load the femur more anatomically; the surface strains on the specimens implanted with ABG II-plasma were closer to those of the anatomic femur as compared to the other comparative stems. This is advantageous, as anatomic load transfer would cause less pronounced stress shielding, thereby preserving the proximal femoral bone. To maintain bone stock, proximal anatomic stress transfer must be a prominent feature of the cementless implant system. Bone stock preservation is crucial while performing THA, especially in young patients who are more likely to require a revision procedure in their lifetime [336]. This may be crucial for implant longevity; if load transfer at the proximal prosthesis is too dissimilar from that at the physiological level, anomalous bone resorption could lead to failure of the bone-implant interface, resulting in instability and loosening of the prosthesis, as is noted in late peri-prosthetic femoral fractures [63].

It is important to point out, however, that the differences observed between the ABGII-Plasma and the ABGII-Standard may not persist beyond the early post-operative period. After approximately three months it would be expected that bony in-growth would have occurred into either surface. Therefore, either design would be rigidly attached at

the bone to implant interface. In this circumstance the friction co-efficient is much less relevant. Rather, the bond would rely on the bone strength at the interface. As bony in-growth cannot be simulated in a cadaveric study, no conclusions can be drawn from this work about the period after bony in-growth has occurred. It is likely that minimal or no clinical difference would be observed between these stems after bony in-growth has occurred. Several studies with the ABG II-standard implant have been associated with good long-term outcomes and favorable proximal bone remodeling responses [172-174]. This would support the assumption that the high-friction plasma coating may not be clinically significant beyond the early postoperative period.

The ABG II-NMS version was devoid of medial scales that are intended to promote proximal load transfer. The experimental results show that the removal of the medial scales did not appear to have a dramatic effect on the overall scenario. There was no observed difference in the maximum impaction strains, the seating heights, nor any difference for the residual strains. However, a localized difference was observed for the strain sensitivity measurements at the M and PM gauges. The ABG II-NMS stem was significantly more tensile than ABG II-standard for the M gauge ($P < 0.0001$), and significantly less tensile for the PM gauge ($P < 0.0001$). No strong conclusions could be drawn from this result, other than to say that the removal of the medial scales has a less dramatic effect on the strain state of the proximal femur than the addition of the plasma coating. In this study, alternate designs were inserted into the same femur progressively. This approach could be criticized as the successive impactions may leave a lasting change on each bone and therefore corrupt the results of further tests. This progressive approach was accepted after considering the results of a similar experimental set up by Elias J.J., et al who specifically analysed the effect of successive impactions and found and reported no difference. [14]. A further limitation must be acknowledged in that the friction co-efficient of the surfaces of the implants was not measured.

Chapter 4

Subject-specific Finite Element Modeling of Peri-prosthetic Femoral Fracture using Element Deactivation to Simulate Bone Failure

4.1 Introduction

Postoperative peri-prosthetic femoral fractures, following total hip arthroplasty, are difficult to treat and are associated with increased postoperative complications [104, 328, 332], and thus lead to poor functional outcomes [15]. The prevalence of postoperative peri-prosthetic femoral fracture ranges from 0.1%–2.1%, with a rate of 4% reported in a revision setting by the Mayo Joint Registry [340]. The apparent increase in its prevalence has been attributed to the growing population of patients with existing hip arthroplasties, increasing pool of elderly patients at risk of falls, and the increasing number of young active patients at risk of high-energy trauma events [340]. Despite a higher fracture risk being linked with cementless fixation, especially in the early postoperative period [341], the recent Australian National Joint Replacement Registry Report (2010) indicates a growing trend in the use of cementless prostheses as compared to cemented or hybrid prosthesis [69]. Risk factors for peri-prosthetic femoral fractures include patient-specific or procedure-specific (technical) factors [342].

Subject-specific finite element models developed from computed tomography data are a powerful tool to investigate bone strength in different simulated clinical settings non-destructively [18, 292, 343]. Three-dimensional finite element modeling is a better predictor of femoral strength than quantitative CT and dual energy X-ray absorptiometry [278], as finite element analysis techniques can model most of the parameters that contribute to bone fracture risk [279, 306, 344] and can also simulate the influence of general and variable boundary and loading conditions [279, 292, 345]. Therefore, subject-specific finite element models of bones, in principle, can help predict fracture risk for a bone segment under any generic loading condition (including muscles). However, this requires development of generalized models and implementation of bone tissue failure and structural collapse criteria [18]. Models that adopted both criteria based on stress were unable to provide definitive results, as the analysis was not validated against experimental tests [308, 346].

Previous studies have also adopted modeling strategies that utilized a specific strength criterion to assess bone failure based on stress parameters and compared their results with strain-based criterion [282, 293, 345]. However, recent advances in bone biomechanics have demonstrated that strain-based criteria are more effective than stress-based criteria in describing yield or bone failure. Therefore, it may be advisable to implement these criteria in bone finite element models to predict fracture risk [345]. The use of strain-based criteria can be further justified because they allow better experimental characterization and have been derived from experimental observations on the invariance of limit-strain with respect to density. In contrast, the use of stress-based criteria, especially in an inhomogeneous model, leads to inclusion of another empirical relationship between limit-stress and density, which may bring in further uncertainties [345].

Subject-specific models should be capable of predicting fracture risk in the clinical setting if the boundary conditions, loading, and failure criteria are well-defined. This study discusses the development of a strain-based subject-specific finite element analysis method using crack modeling techniques, which may be used to accurately characterize a patient's postoperative peri-prosthetic femoral fracture risk prior to hip arthroplasty.

As peri-prosthetic femoral fracture obviously occurs around an implant, the modeling of both the implant and the bone is essential. It should be noted that all of the previous studies of bone fracture have only included native femoral geometry and have been predominantly used to predict native femoral neck fracture. When the implant is introduced, unique challenges are presented resulting from the modeling of contact, at a boundary where there is a large stiffness discontinuity.

4.2 Methods

4.2.1 Experimental testing

One of the cadaveric femurs from the previous chapter was used for the development of the finite element models in this chapter. This allowed direct comparison of the finite element models to the experimental results. As the femurs were matched pairs the mechanical testing results of the matched pairs is of interest in this comparison. Thus, the experimental setup for this pair of femurs is briefly restated and summarized here.

A matched pair of cadaveric femurs donors was sourced from the International Institute for the Advancement of Medicine. (IIAM Corporate, Jessup, PA, USA) The laboratory testing was conducted in a facility certified to operate within all requirements as per the NSW Anatomy Act 1977 and Human Tissue and Anatomy Legislation Amendment Act 2003." The femurs were subjected to x-ray and then CT evaluation to ensure that they were free of pathology and to allow preoperative templating for determining the expected prosthesis sizes for the ABG II implants. After templating, the femurs were sectioned and potted in a polymethylmethacrylate (PMMA) potting medium, 30 mm distal to the expected position of the distal tip of the prosthesis for the template size. Each femur was cleaned of all soft tissue. Two experimental prostheses manufactured by Stryker Orthopaedics (Mahwah, NJ, USA), the ABG II-plasma and the standard ABG II stem, were implanted in the left and right femur, respectively, after a neck osteotomy. In order to closely replicate the anatomic loading of femoral stems, a mechanical testing jig was prepared to orient the bone 9° in the sagittal plane and 10° in the coronal plane (ISO 7206-4, 2010 specifications). An MTS 858 mechanical testing system and simulation apparatus (MTS Systems Corporation, Eden Prairie, MN, USA) was used to load the femurs to failure with the implants in situ.

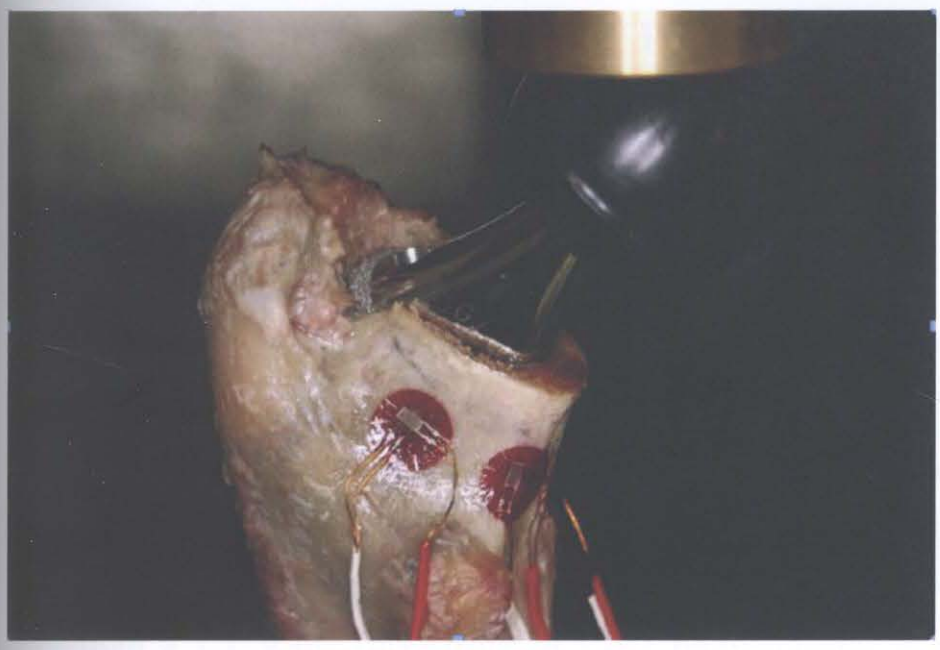

Figure 111 Mechanical testing setup implanted stem

4.2.2 Generation of a subject-specific finite element model

The CT scan of a left-sided femur (from the experimental study) was used for preparation of the finite element model. This was obtained prior to the mechanical testing being carried out.

4.2.3 Finite element model development

4.2.3.1 Summary of issues encountered in the model development

4.2.3.1.1 Simpleware standardized workflow was not appropriate

As discussed in the literature review, Simpleware is a commercially available set of software tools that allow for the conversion of 3D images into CAD and Finite Element

models. Simpleware offers three modules for processing and meshing 3D image data for the preparation of subject specific finite element models:

ScanIP Module: Core image processing platform

ScanCAD Module: Bolt-on module for CAD integration

ScanFE Module: Integrated module for Mesh generation

4.2.3.1.1.1 Summary of standardized workflow

The recommended way to utilize the Simpleware suite of products would be to flow from one module to the next in the order depicted in Figure 112 which would be to;

Create subject specific geometry by utilizing ScanIP to segment the 3D geometry from a CT scan. This creates a CAD representation of the subjects' bone geometry.

After creating the patient specific geometry in ScanIP, the model of the native femur should be imported to ScanCAD for the simulation of the surgery by introducing and placing the CAD files of the implants in the required location and removing the surgically removed bone by performing Boolean operations.

After the surgical intervention is simulated with the implant CAD files in place, the models are exported to ScanFE, where a finite element mesh is created and material properties are assigned.

With all of the pre-processing undertaken in Simpleware, an input file to the finite element solver is generated from ScanFE and this input file is transferred to the finite element solver pre-processor where boundary conditions and loads are added.

The model is then submitted to the solver and post-processed in the post-processing application of the finite element solver.

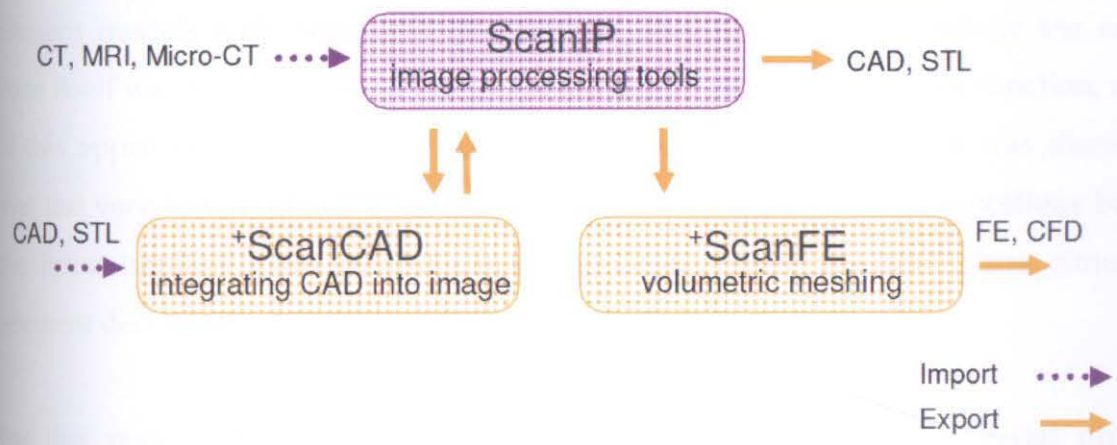

Figure 112 Relationship between Simpleware modules and workflow

Unfortunately, this standardized method was not suitable for this specific problem and following this standardized workflow resulted in some issues. The issues were predominantly around the interface between the CAD model of the implant and the bone where inadequate meshing boundaries between the implant model and the bone model caused either convergence issues or localized strain discontinuities. These were not acceptable to the failure simulations adopted in this study. To overcome these issues, a modified workflow was adopted. The modified workflow and justification for these modifications is described below.

4.2.3.1.2 *Heterogeneous material property mapping causes mesh discontinuities*

A further, but related issue encountered was to do with material property assignments. As mentioned above, the finite element models were created from a CT scan of one of the cadaveric femurs that was then used for the mechanical testing described in the previous chapter. This obviously has the distinct advantage that the simulation results could be compared with the mechanical testing results for verification and validation. However, at the time the CT scans were taken no calibration phantom was available. This would have allowed for the assignment of material properties in a straightforward way. Other authors Turner., et al [347] have had success creating subject specific finite

element models with heterogeneous material mapping strategies, where the cortical bone itself was used for the calibration of a material property mapping function. A trial of this approach was attempted and is described below. However, it was discovered that the very low modulus bone material properties applied to the cancellous bone at the bone implant interface did cause significant issues for the failure simulation (element deactivation) that was adopted.

For this reason, it was decided to utilize another approach to material property assignment, which has also been adopted by other authors [307] where the bone material property assignment was divided into two regions, the cancellous and the cortical bone regions. This was much more suitable to the crack modeling approach that was adopted for failure modeling.

4.2.3.2 Workflow adopted for Modeling

The following is the methodology that was used to create the finite element models in this chapter.

4.2.3.2.1 *Segmentation of geometry from CT scan*

Simpleware Scan IP was used to segment the geometry of the femur from the CT scan. A DICOM (Digital Imaging and Communications in Medicine) file, which is the standard file format for all medical imaging files, that contained the CT scan data of the femur was obtained on an external USB drive.

This file was imported into ScanIP and visualized using the standard tools available in the import module. See Figure 113.

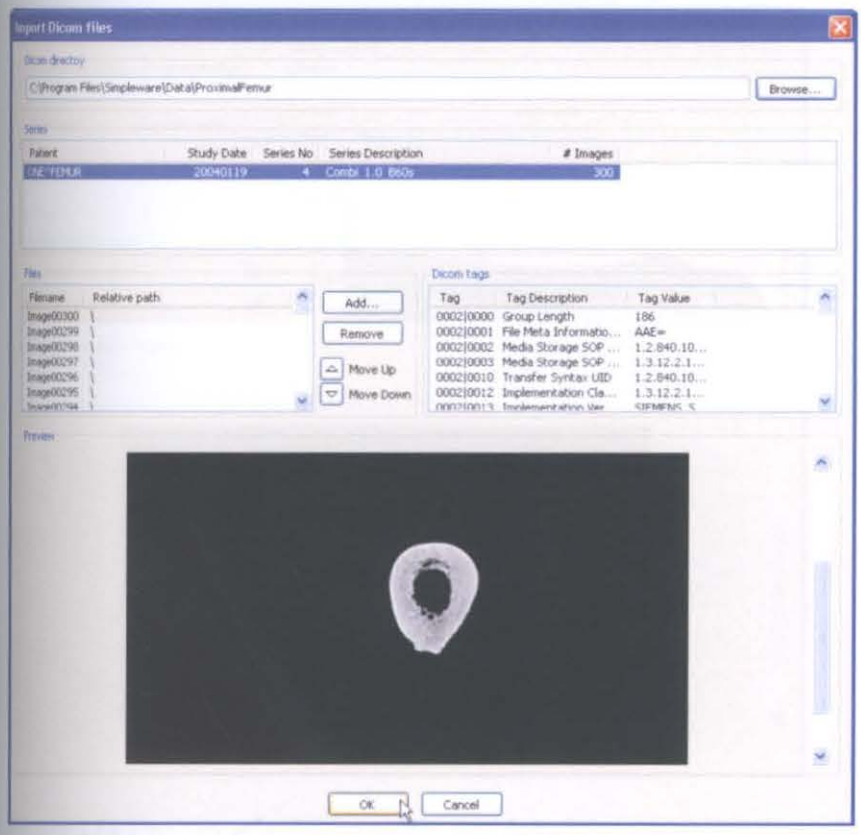

Figure 113 Import DICOM file into Scan IP

The window width and level controls allow the user to change the grayscale appearance and contrast to visualize the CT scan to be segmented. A preset for bone is available and this was chosen for the segmentation. See Figure 114.

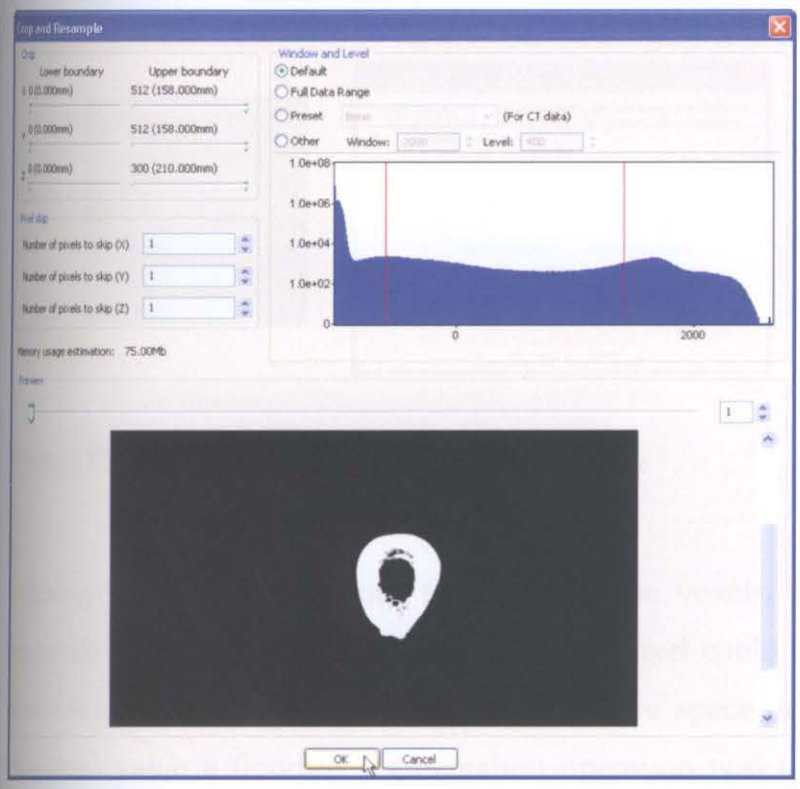

Figure 114 Pre-set window width and level for visualisation of CT scan slices

Next, the size of the volume that was of interest was isolated and irrelevant volume from the CT scan was removed. That is volume not representing proximal femoral bone was removed. See Figure 115. This has the effect of significantly reducing the size of the file for the segmentation. That is because the number of voxels in the volume are reduced. See section 2.8.1.1 for a description of voxels.

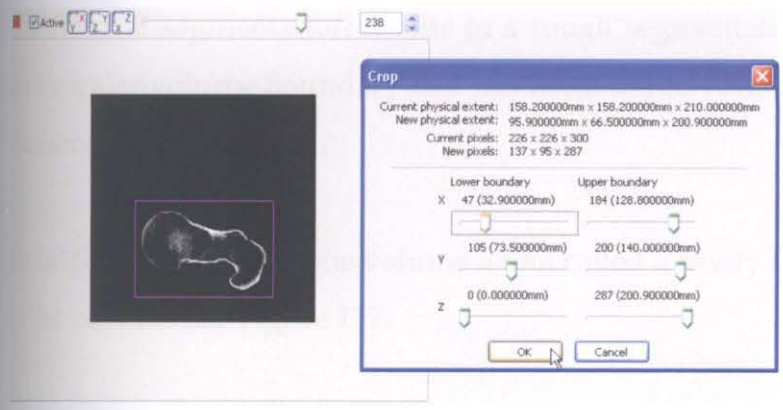

Figure 115 Crop region of interest in Simpleware

Utilizing the grayscale values from within the voxels; firstly a threshold value of grayscale was determined; below which the voxel could be assigned to be bone and above which the voxel could be assigned to be space or softer tissue. Utilizing this threshold value a floodfill segmentation operation was used on the bone volume to roughly segment the bone from the surroundings. See Figure 116.

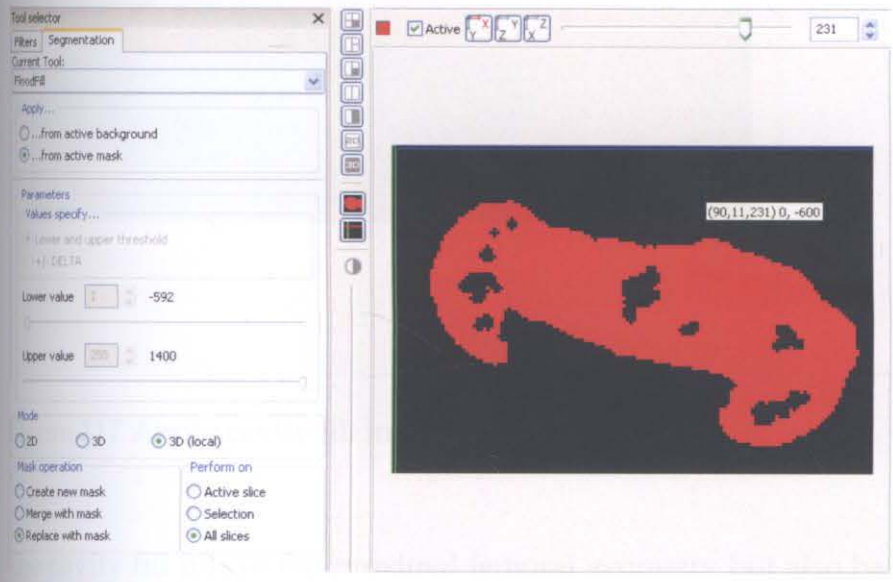

Figure 116 Floodfill segmentation in Simpleware

The floodfill segmentation results in a rough segmentation of the volume. It results in an irregular volume boundary and has holes in the volume that are not captured by the threshold.

To fill the holes in the bone volume a tool called a cavity fill is used that fills in the holes in the volume. See Figure 117.

Figure 117 Apply cavity fill in Simpleware

The cavity fill fills in the proximal femoral geometry but also has the effect of filling in the intra medullary canal. The canal is in reality filled with bone marrow and should not be included in the geometry mesh of the bone. To remove the marrow, a second segmentation threshold is set up. It is set to only capture the marrow volume in the

threshold. See Figure 118. After segmenting the marrow with a threshold, another operation called a Morphological Close to unite the marrow volume is required. See Figure 119. To remove the bone marrow volume, a Boolean operation is performed that subtracts the marrow volume away from the proximal femoral bone volume. See Figure 120.

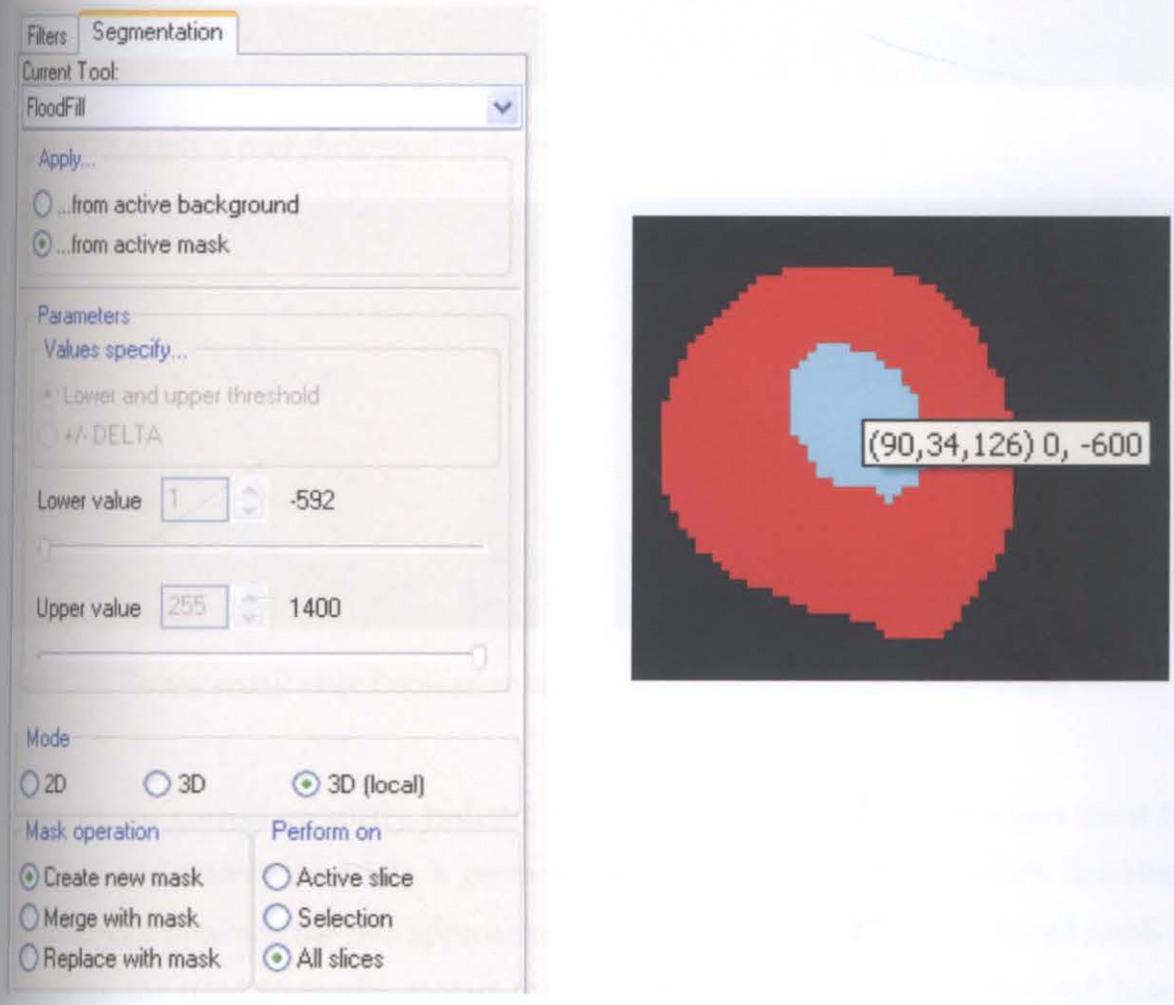

Figure 118 FloodFill tool panel and segmented marrow in Simpleware

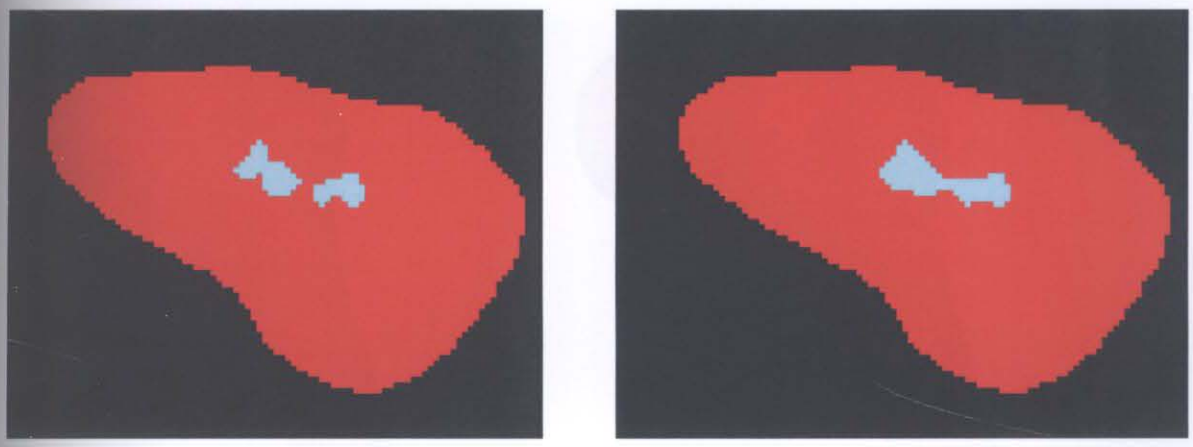

Figure 119 Apply a morphological close on marrow in Simpleware

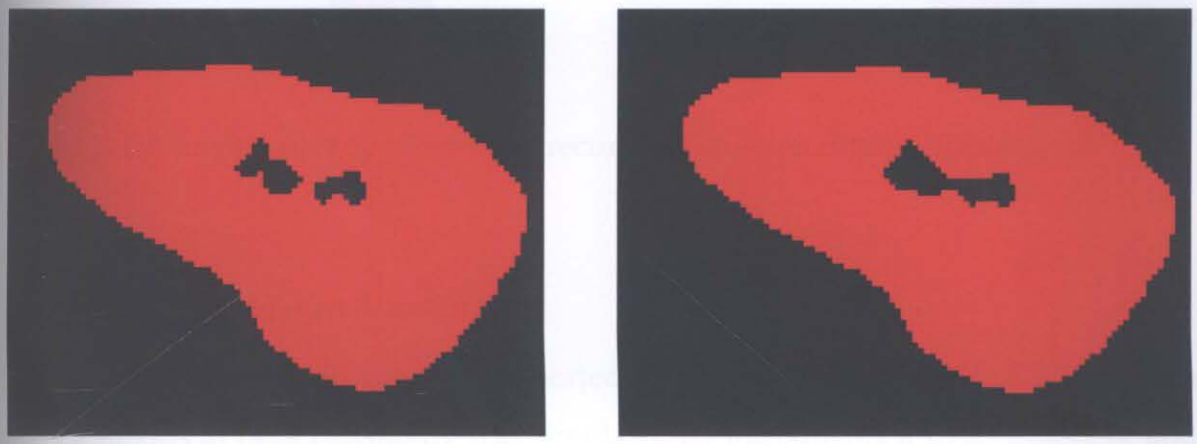

Figure 120 Femur mask after Boolean subtraction of the marrow in Simpelware

Now with the correct geometry isolated, the voxel mesh with irregular edges must be smoothed and transformed into a geometry mesh. See section 2.8.1.1 which describes the difference between the two approaches. The necessity for a geometry based mesh is because of the need to model contact at the implant to bone interface. A voxel based mesh, having a jagged surface would be inappropriate for contact modeling. It would cause stress concentrations and solution convergence issues. To smooth and transform the mesh, a Gaussian filter is chosen and good results are achieved. See Figure 121.

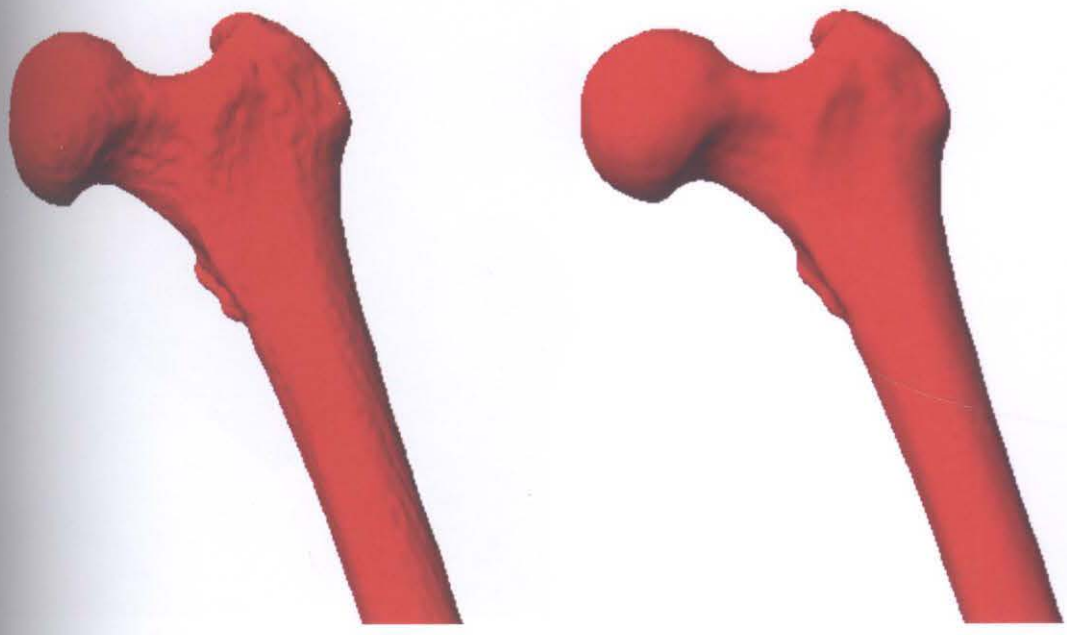

Figure 121 Difference after application of recursive Gaussian filter in Simpleware

4.2.3.2.2 *Export model to ScanCAD*

The Femur model ALONE was then exported to the ScanCAD module of Simpleware where a single-cut neck osteotomy was simulated by introducing a CAD primitive and performing a Boolean operation. See Figure 123 CAD model of ABG II stem,
a) With scales. b) Without scales. CAD models of the definitive ABG II prostheses in .stl file format, with some minor geometrical simplifications (removal of small cut-outs in the proximal region), were provided by Stryker Orthopaedics. See Figure 124 Anterior, lateral and 3D views of the model in ScanCAD. The removal of the small cutouts simplified the mesh generation and contact modeling.

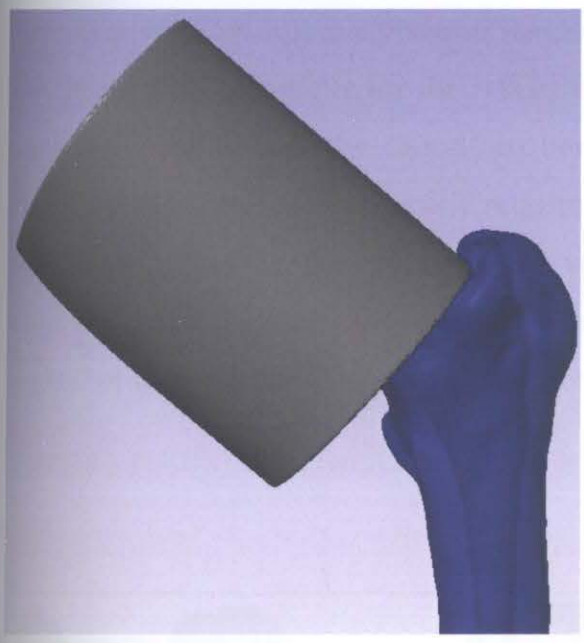

Figure 122 Femoral neck osteotomy with CAD primitive in Simpleware Scan CAD

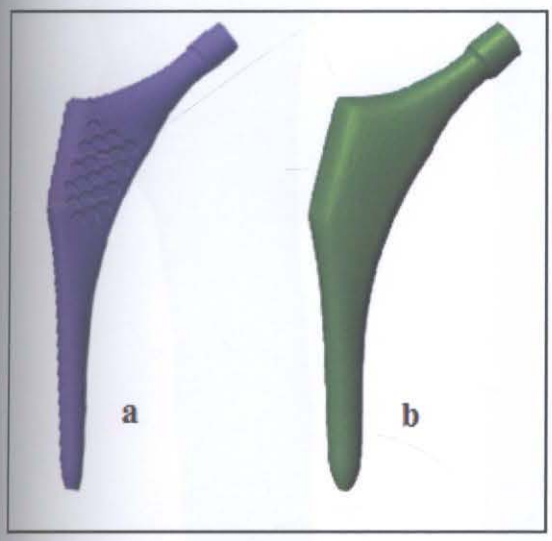

Figure 123 CAD model of ABG II stem,

a) With scales. b) Without scales

In the Simpleware ScanCAD module, a size 4 ABGII femoral stem (The correct size for this femur) was virtually positioned into bone to simulate the surgical preparation as in

the experimental testing. It's position was verified by a company representative familiar with the surgical technique for the ABGII implant. Boolean operations were applied to simulate the removal of the cancellous bone by broaches and the distal reaming step around the distal stem, as surgically required for the insertion of the prosthesis. Further, a CAD primitive and a Boolean operation were used to section the femoral shaft 30 mm below the tip of the stem and perpendicular to the shaft axis to represent the potting height that was used in the experimental setup.

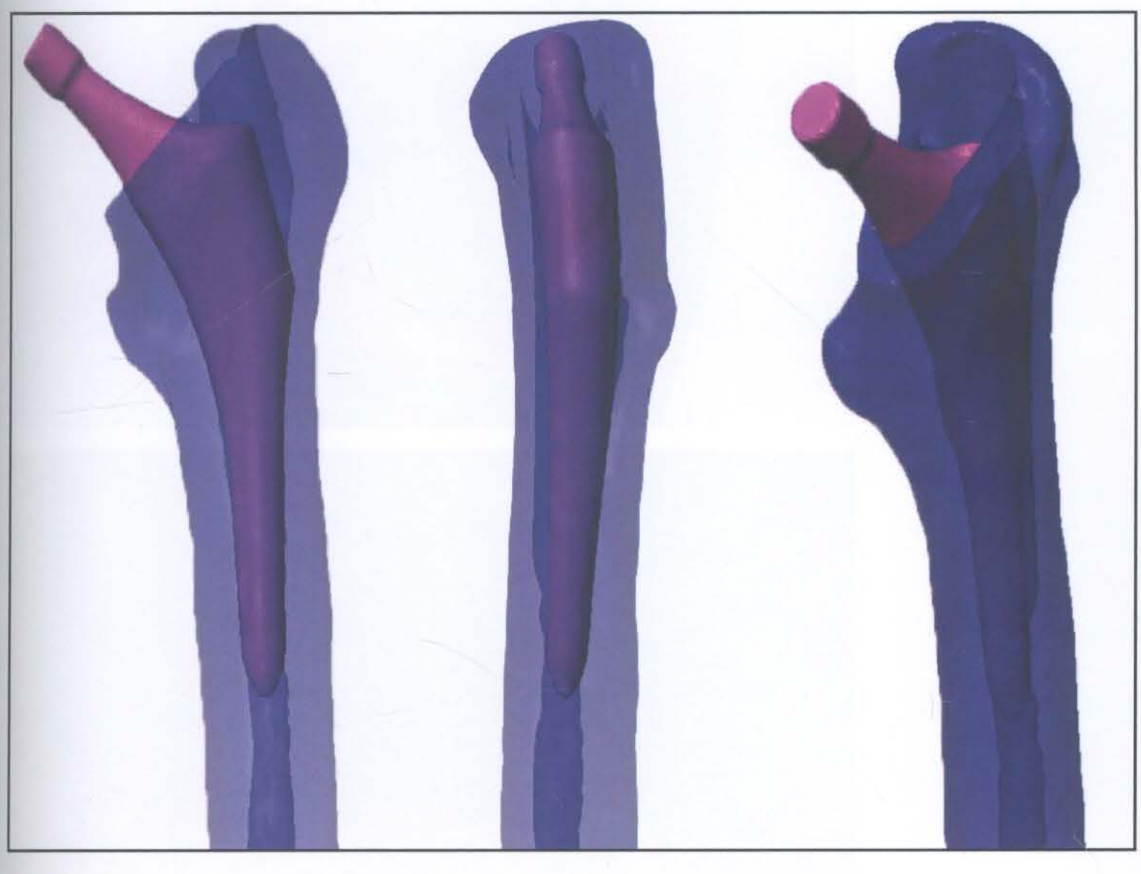

Figure 124 Anterior, lateral and 3D views of the model in ScanCAD

4.2.3.3 Generation of finite element mesh

4.2.3.3.1 Summary of mesh inconsistency problems

As mentioned, when using the standard workflow of Simpleware there were issues when meshing occurred at the boundary between the implant and the bone. Examples of these issues are depicted in Figure 125 through to Figure 127. It was not possible to overcome this problem using the mesh control tools available in Simpleware.

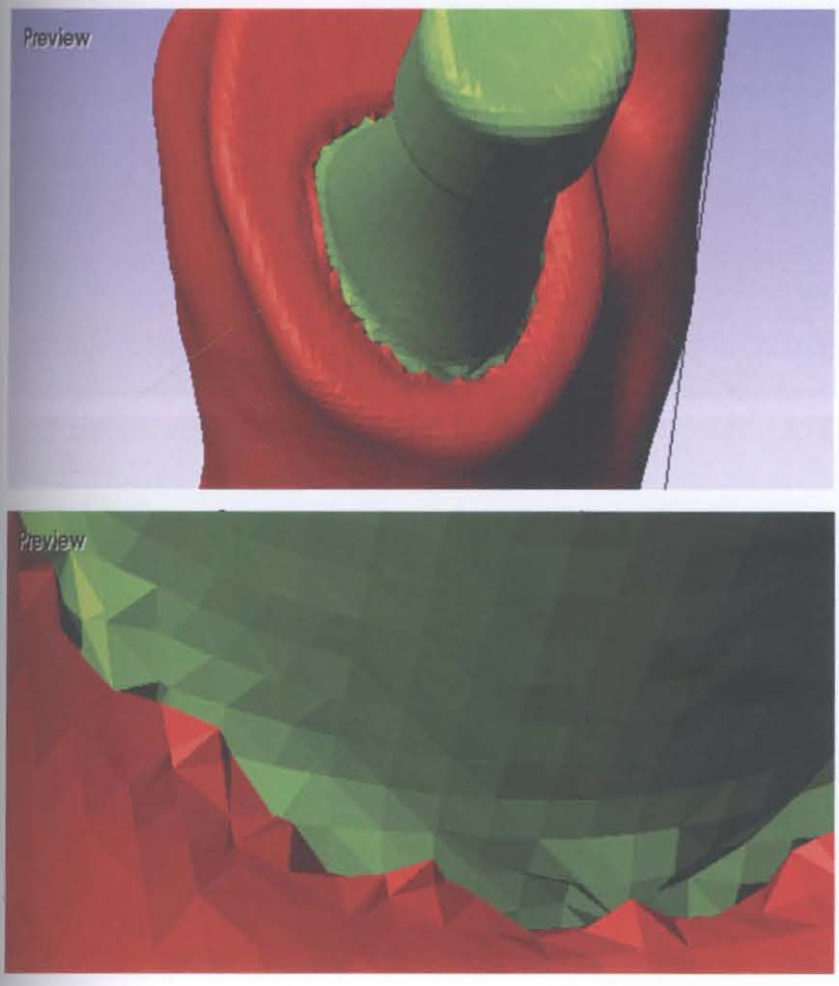

Figure 125 Inadequate mesh boundary between implant and bone using Simpleware mesh control tools.

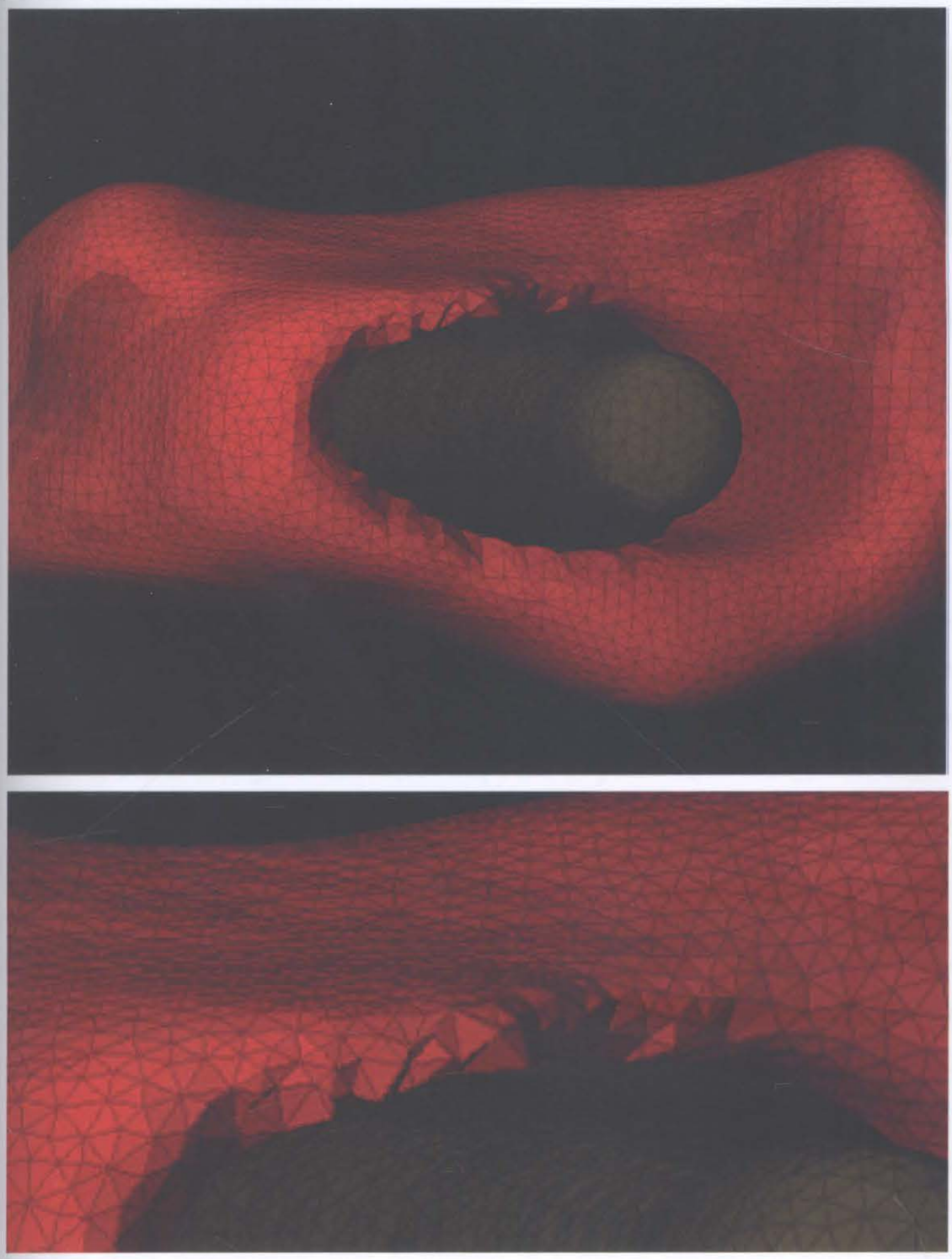

Figure 126 Inadequate mesh boundary between implant and bone using Simpleware mesh control tools

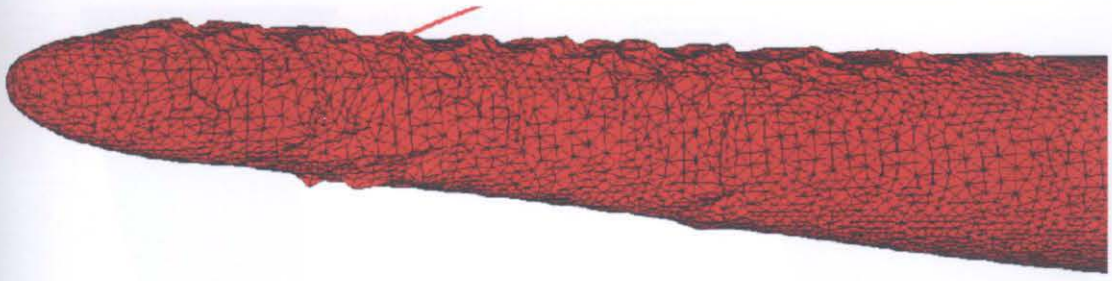

Figure 127 Inadequate mesh boundary between implant and bone using Simpleware mesh controls

It was discovered that the mesh control issues in Simpleware were primarily due to the attempts by the automatic meshing algorithms to keep an interlocked mesh across the boundary between the two parts. Unfortunately, there was no ability to simply mesh the parts as individual entities in Simpleware. Discussion with the Simpleware development team, in an attempt to resolve these issues revealed that these issues were not being encountered by other users of the software. This was due to other users only modeling the anatomy itself without implants in place. Alternately, they were not as concerned with the mesh quality at the implant boundary because their regions of interest were distant to the interface.

Given the approach to failure modeling being undertaken in this work (crack modeling with element deactivation) there was no ability to ignore the mesh inconsistencies. The mesh inconsistencies caused local strain concentrations that caused element failure (element deactivation/deletion), which in turn causes the mesh to be altered and a cascade of strain concentrations occur around the mesh defect causing an erroneous crack path to be generated. For example, in the model depicted in Figure 127 and Figure 128, the crack propagation was beginning in a region where the mesh inconsistency caused this cascade of events to occur and an unrealistic crack simulation resulted.

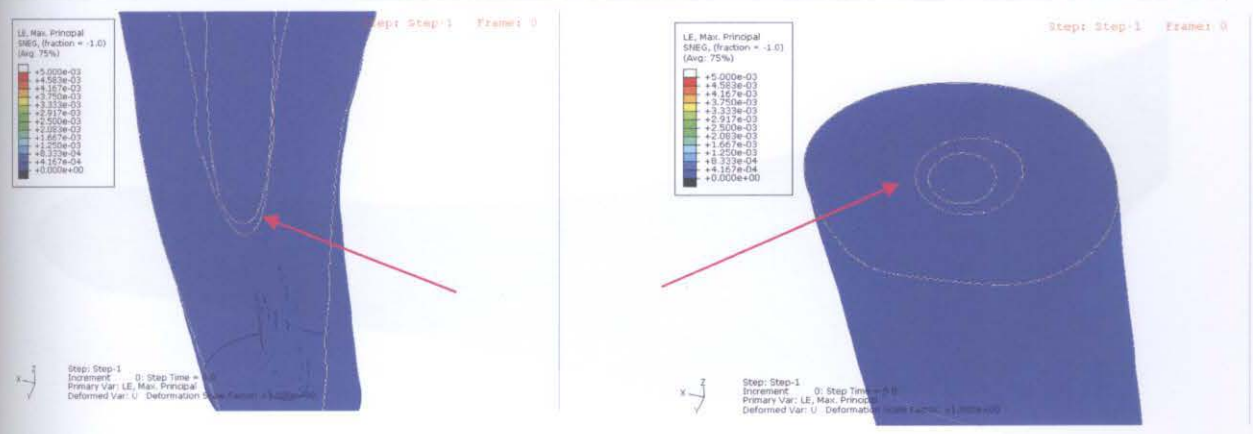

Figure 128 High strain area resulting from mesh inconsistency a the implant bone boundary

4.2.3.3.2 *Overcoming mesh inconsistency problems by altering workflow*

As described above, those users of Simpleware who were not modeling implants in place did not get the mesh inconsistency problems at the surface of their meshed models. To overcome these meshing issues, a different approach was adopted.

When the meshed bone model alone (after the Boolean operation to remove the bone material to accommodate the implant) was exported to Scan FE and meshed alone the boundary was smooth and consistent. See Figure 129.

Figure 129 Meshing implant in ABAQUS CAE gives consistent mesh boundary at the interface

The meshed bone model alone was transferred to Simpleware Scan FE (Simpleware Limited) where it was meshed using the automatic meshing capabilities of the software with 226,362 C3D10M elements. No mesh convergence study was performed as the elements were limited by the voxel size of the CT scan, and the mesh was at its highest density possible.

The element type C3D10M was used for the bone model, due to its excellent contact properties. This element type is a second order ten node modified quadratic tetrahedron. This "modified" element is designed for use in complex "hard" contact simulations, which allow for accurate calculation of contact pressures [348-350]. The specialized element is robust for large deformation and contact problems, compared to regular tetrahedral elements (C3D10), which have zero contact force at the corner nodes, thus giving inaccurate predictions of contact pressures [350]. A basic tetrahedral mesh and ten node tetrahedron element are shown in Figure 130 .

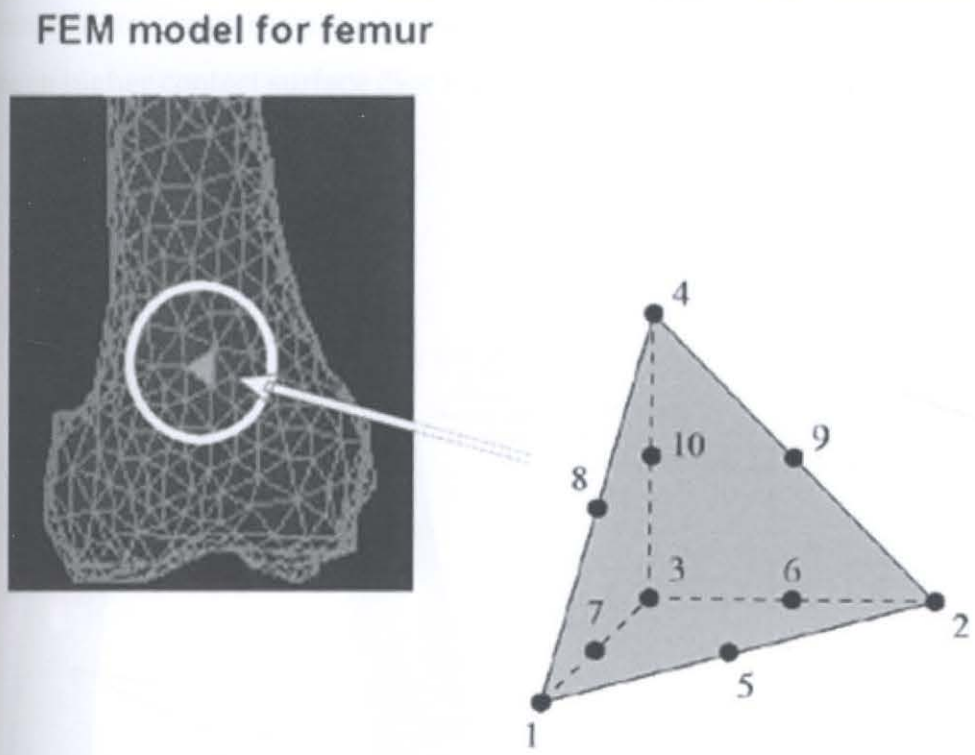

Figure 130 Ten node tetrahedron element used in the mesh of a femur model. [306]

As this model only contained the bone with the femoral cavity prepared, it was required to combine the stem and bone mesh together in the finite element Solver pre-processor, ABAQUS CAE (ABAQUS Inc., Providence, RI, USA). The CAD model of the ABG II size-4 stem, (The same size stem that was implanted in the mechanical testing) was re-introduced and placed in the femoral cavity of the bone, which had been previously prepared in Simpleware Scan CAD.

Further, a 28-mm femoral head was assembled on the proximal taper in accordance with the experimental testing setup. The implant model was meshed in ABAQUS CAE using the automatic meshing capabilities of the software with 16,938 R3D3 elements. This approach produced a consistent mesh boundary that was adequate for the failure approach being undertaken. Evidence of this superior meshing can be seen when the

initial contact surfaces are visualized side by side. With the second approach giving a much higher contact surface (See Figure 130).

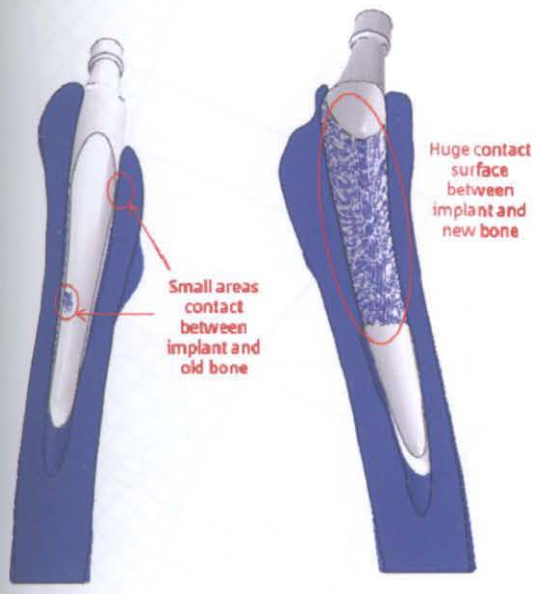

Figure 131 New approach (right) provided more constant initial contact between the bone and the implant than previous approach (left)

4.2.3.4 Adequate boundary conditions

4.2.3.4.1 Contact Boundaries

To represent the implants geometry correctly, the area representing the grit blasted hydroxyapatite zone (Figure 132) was isolated and designated as the friction zone (see Figure 133).

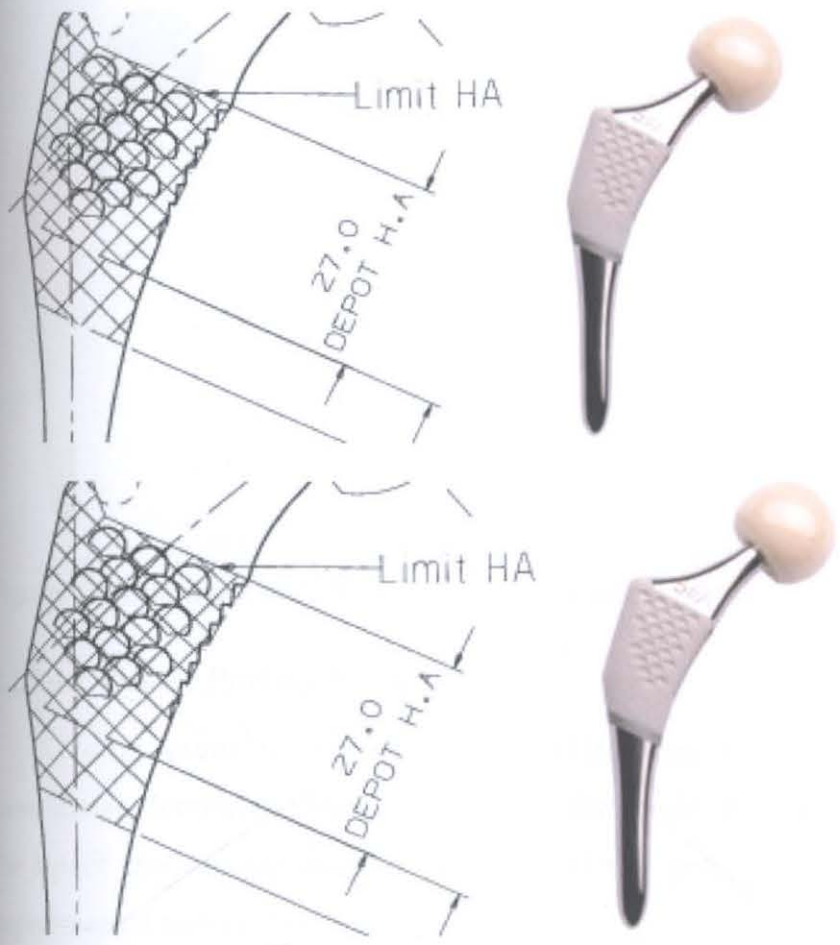

Figure 132 Higher friction zone on the implant labeled "DEPOT H.A"

The contact boundary for the loading of the femoral head is described below in 4.2.3.5.

Figure 133 Friction Zone (Red) Frictionless Zone (Green)

4.2.3.4.2 *Distal Potting Boundary*

To represent the potting medium, a fixed boundary condition was applied to the most distal elements of the bone mesh as the model had been sectioned 30 mm below the tip of the prosthesis. This represented the potting height that was used in the experimental testing. See Figure 134.

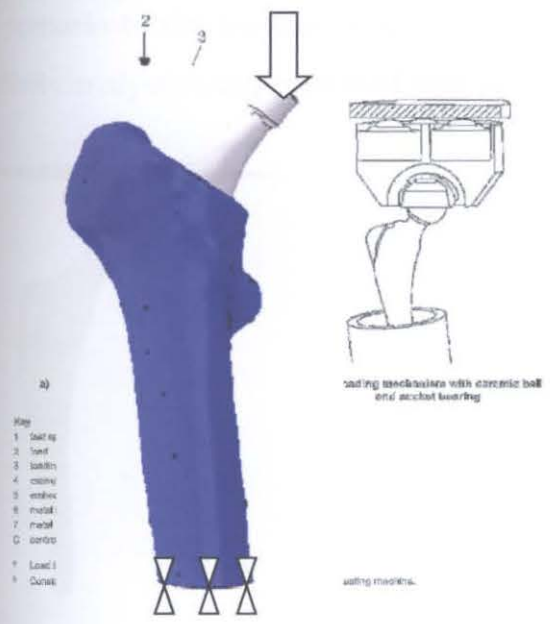

Figure 134 Fixed distal boundary conditions and load orientation (left) set to resemble ISO 7206-4 (right)

4.2.3.5 Loading scenario

To represent the loading in the experimental setup, a plate was modeled just in contact with the femoral head and angled to represent the loading direction of the mechanical testing setup. This loading direction was orientated as per the ISO 7206-4 specifications (2010) as 10° varus in the coronal plane and 9° flexed in the sagittal plane (See Figure 135).

4.2.3.5.1 Exploration of ISO 7206-4 compliant loading scenarios

Whilst setting up the loading scenario it was noted that there was some ambiguity and flexibility in the ISO 7206-4 loading specification. To demonstrate this, both loading scenarios below would conform to the ISO 7206-4 loading specification. In reality, the friction that exists between the testing jig and the femoral head would be difficult to control. Therefore, both loading scenarios were tested to determine the sensitivity of

each scenario to the friction at the interface by performing a sensitivity analysis. The sensitivity analysis was performed only on the biphasic material assignment model.

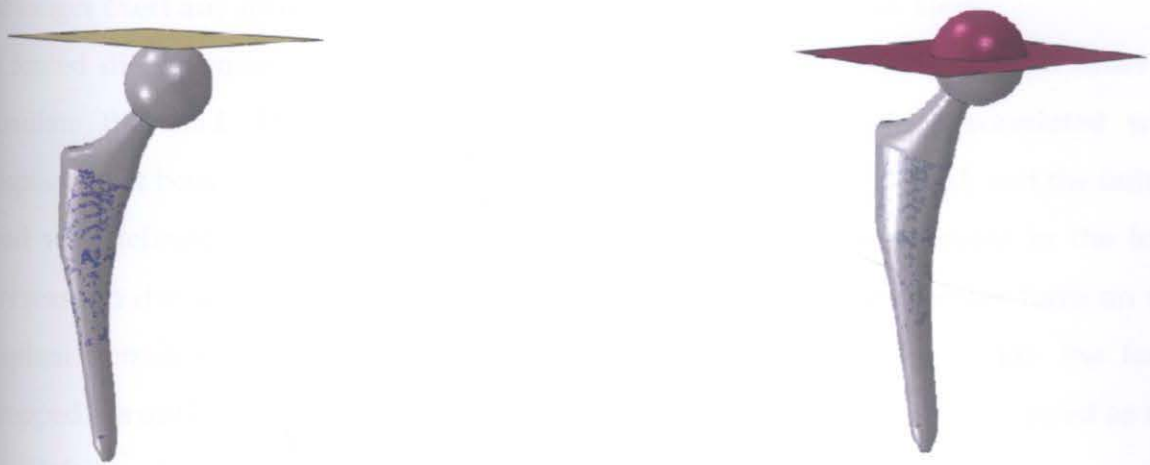

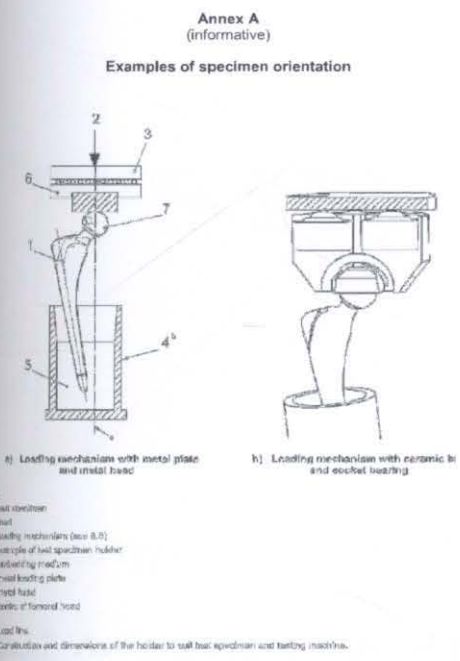

Annex A
(informative)

Examples of specimen orientation

Figure 135 ISO 7206-4 compliant loading scenarios

4.2.3.6 Failure modeling approach

As previously mentioned, the element deletion capability available in ABAQUS 6.9 was used to simulate a crack path in the bone tissue, based on a threshold of strain. Brittle

element failure mode was assumed, whereby an element with a strain value of 0.01 was considered to have failed and was "deactivated." After deactivation, the element could no longer exert any influence on the analysis in the subsequent time steps.

A forced displacement was applied to a plate along the axis of the bone in order to simulate the load. The resultant force value versus time (which correlated with displacement because the displacement was constant) curve was plotted, and the failure load was defined as the point on the curve where a dramatic decrease in the load (increase in displacement) was recorded. For all simulations, the reaction force on the implant versus the displacement was recorded. As the crack developed, the force dropped abruptly and the peak force was defined just before the curve dropped as the "crack failure load". See Figure 136 for typical failure plots.

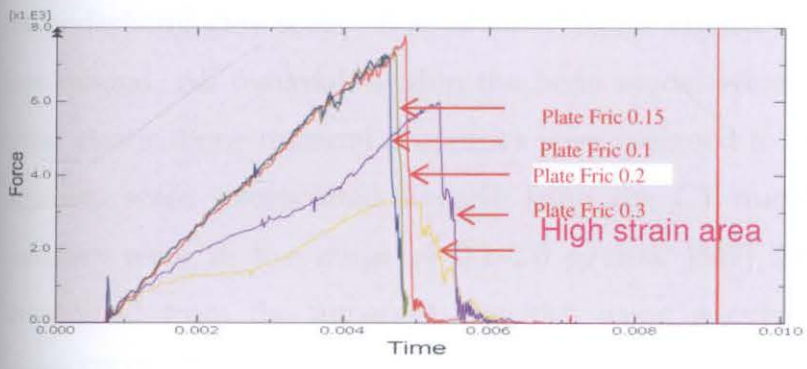

Figure 136 Typical force vs time plots for failure characterization

4.2.3.7 Assignment of material properties

Three strategies were investigated for the assignment of material properties to the bone model. In all three approaches the implant material was considered homogenous, isotropic, and linear-elastic.

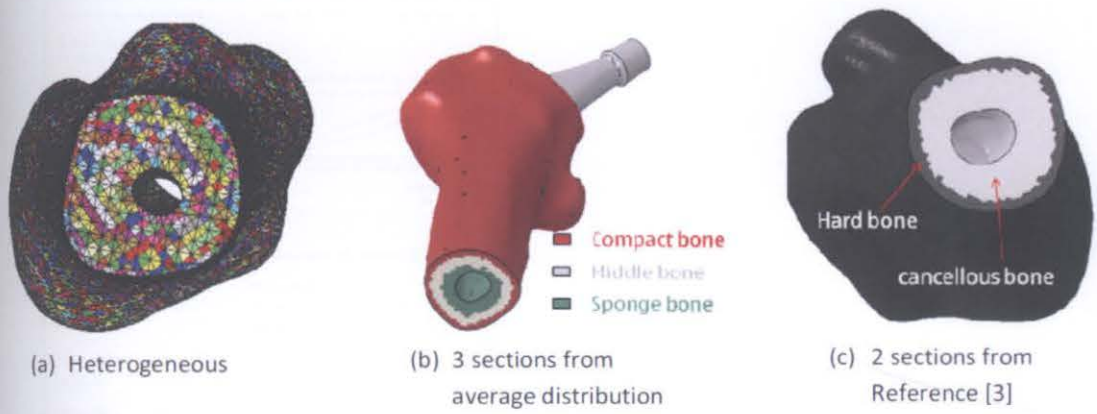

(a) Heterogeneous

(b) 3 sections from average distribution

(c) 2 sections from Reference [3]

Figure 137 Different material property assignments used in this work

4.2.3.7.1 *Heterogeneous Material Mapping*

Simpleware ScanFE assigns heterogeneous material properties to each element based on the underlying gray scale value obtained from original CT scan from which the model was created. All materials within the bone model were assumed to be isotropic and linear elastic. Bone material properties were assigned to each element, where apparent densities were interpolated linearly from the CT numbers by assuming the bone densities were in the range of 0.1–2.0 g/cm3. [347] The elastic moduli were then determined from the apparent densities using a cubic relationship of Carter and Hayes,[351]

$$E = 2875\,\rho^3.$$

This mapping function is applied through the Simpleware ScanFE export feature, which designates a material property for each element immediately prior to export into ANSYS CAE. See Figure 138.

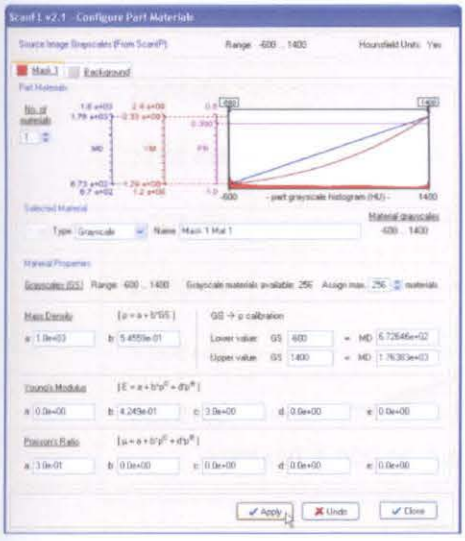

Figure 138 Simpleware Scan FE material property assignment for applying heterogeneous material properties to the bone model

4.2.3.7.2 *Biphasic material assignment*

Within the bone model mesh, there are two separate bone material properties: one for cortical bone, and one for cancellous bone. The bone was modeled as an orthotropic, linear-elastic material in which the cortical and cancellous bone properties were assigned to the outer and inner layers of elements, respectively. This approach was similar to that of Pastrav [352].

4.2.3.7.3 *Triphasic material assignment*

A triphasic model that included the compact, middle, and cancellous bone. The material properties were obtained from the CT scanned femur model by calculating the average density of the three layers of bony material. The assignment was done in the ANSYS CAE pre-processor. Beginning with the heterogeneous material property mesh with material property assignment, already done using ScanIP, the modulus of elasticity was extrapolated from the elastic modulus versus the density graph. See Figure 139.

The elastic moduli pertaining to different types of bone are shown in Table 12.

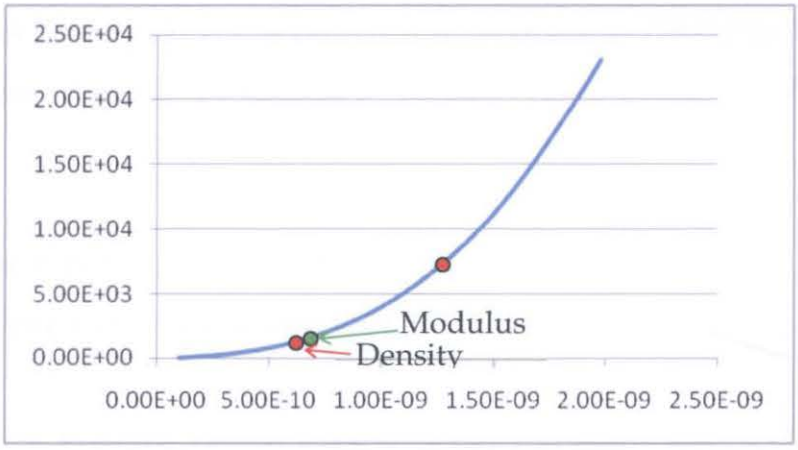

Figure 139 Elastic modulus vs density for triphasic bone

Table 12- Modulus of elasticity of various components of bone in biphasic and triphasic finite element femur models

	Elastic modulus (MPa)		
Models	Compact bone	Middle bone	Cancellous bone
Biphasic model	6000	N/A	375
Triphasic model	7610	2060	1830

4.2.3.8 Finite element solver used

All simulations were carried out using the explicit solver ABAQUS V6.9 (Dassault Systèmes, SIMULIA, Providence, RI, USA) because of its powerful contact and large scale model processing capability. The ability of the Abaqus Explicit solver to effectively handle severely nonlinear behaviour, such as contact, makes it very attractive for the simulation of many quasi-static events [348]. Furthermore, its ability to fully utilize parallel processers to significantly decrease computational time was a distinct advantage over the Abaqus standard solver.

4.2.3.9 Computer and simulation times

Processor: Intel Xeon 5450 Quad-Core 3.0GHz 12MB Cache 1333MHz FSB
2x 3.0GHz, Quad-Core, (8 processors in parallel) 12MB Cache, 1333MHz FSB, Socket 771, 45nm

Memory: 8 x 4GB PC5300 ECC FBDIMM (32 GB Total)
667MHZ, 240-pin, ECC Fully Buffered, CL5

Hard Drive: 2 X Western Digital Raptor 150GB 10000rpm with RAID Configuration: RAID 0 - Disk Striping, Enhanced Read/Write Performance,
10,000rpm, 16MB Cache, 4.5ms Read, SATA/150 Interface

Operating System: Microsoft Windows Vista Ultimate 64-Bit
Simulation times varied significantly, Typically two or three simulations could be run in a 24-hour period, depending on the time that they were commenced. No Simulations utilizing Abaqus explicit solver ran longer than 24 hours.
Early in the project whilst attempting to use the Abaqus Standard solver simulations would routinely run for three or more days. Utilization of the standard solver was abandoned in favor of the explicit solver because of these issues.

4.3 Results

4.3.1 Crack propagation/failure mechanism

4.3.1.1 Experimental testing

The left-sided and the right-sided femoral specimens showed a failure load of 4510.4 N and 2236.5 N, respectively. A sudden fracture process was detected (a sharp decrease in load after reaching the peak value) with no noticeable decrease in the slope

of the curve immediately before failure. This is suggestive of generalised yielding. Both left-sided and right-sided femoral specimens demonstrated a similar failure mechanism.

The prosthesis first displaced into the femoral canal with a brittle crack suddenly emanating from the neck osteotomy on the medial and the lateral side, and the medial calcar of the bone was displaced. Although the internal structures were not seen, it is believed that the crack initially propagated through the upper cortical layer (See Figure 140). However, this could not be confirmed. The crack propagation appeared to be very rapid and the thorough separation of the fracture surfaces lasted for a very short time period.

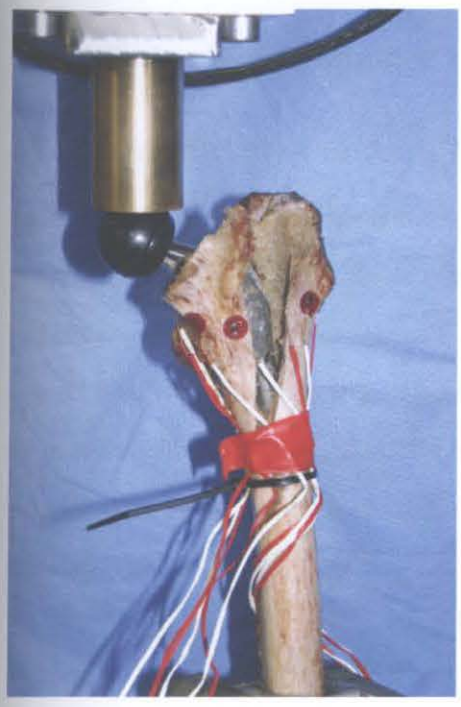

Figure 140 Typical failure of bone during experimental testing.

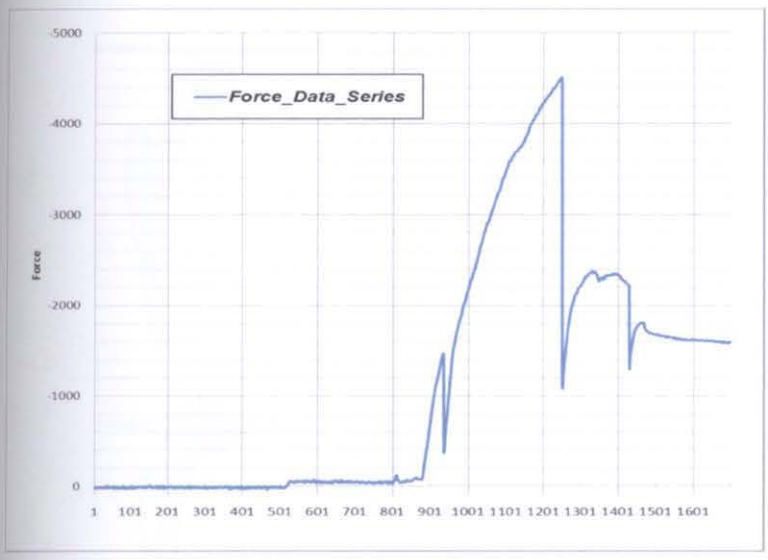

Figure 141 Force vs time plot for failed bone

4.3.1.2 Finite element model

4.3.1.2.1 Sensitivity analysis of ISO 7206-4 compliant loading scenarios

As mentioned in the methods section, both of the loading situations that were permissible under ISO 7206-4 were investigated with a sensitivity analysis where the friction co-efficient at the femoral head to plate interface was varied for both scenarios. The results were surprising. The first test method appeared to be very sensitive to the friction co-efficient; whereas the second test method did not appear to be as sensitive (See Figure 142). Therefore the second test method setup was used for subsequent simulations.

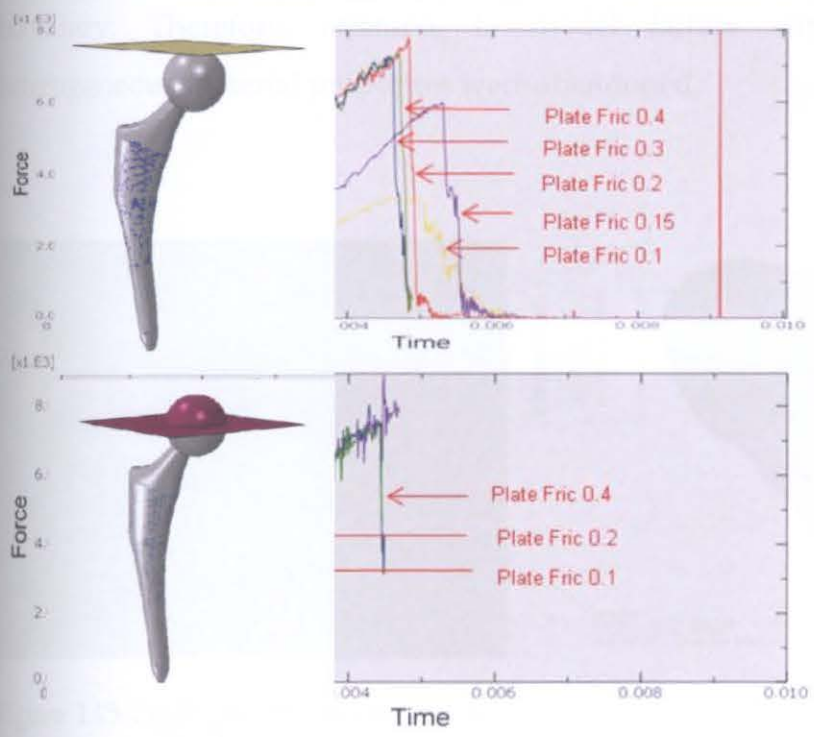

Figure 142 Sensitivity of failure load to friction at the loading plate to femoral head contact interface

4.3.1.2.2 *Results of heterogeneous material property modeling*

Modeling heterogeneous material properties was attempted. However, the models were inherently unstable and would not solve. This appeared to be a problem when the failure of very low modulus bone occurred at the implant to bone interface or contact surface. Two problems existed.

Firstly, deleting an element in contact situation means that formerly interior faces (behind the deleted element) become exterior faces. Thus, the contact algorithm has to calculate new contact surfaces, and new contact forces, and sometimes it can cause numerical instabilities. Without element deletion, the contact calculation is obviously much easier and the same models would converge, just with very high strain areas (See Figure 143). Secondly, there is a large stiffness discontinuity at the implant to bone

boundary. Therefore, attempts to model failure with element deletion and heterogeneous material properties were abandoned.

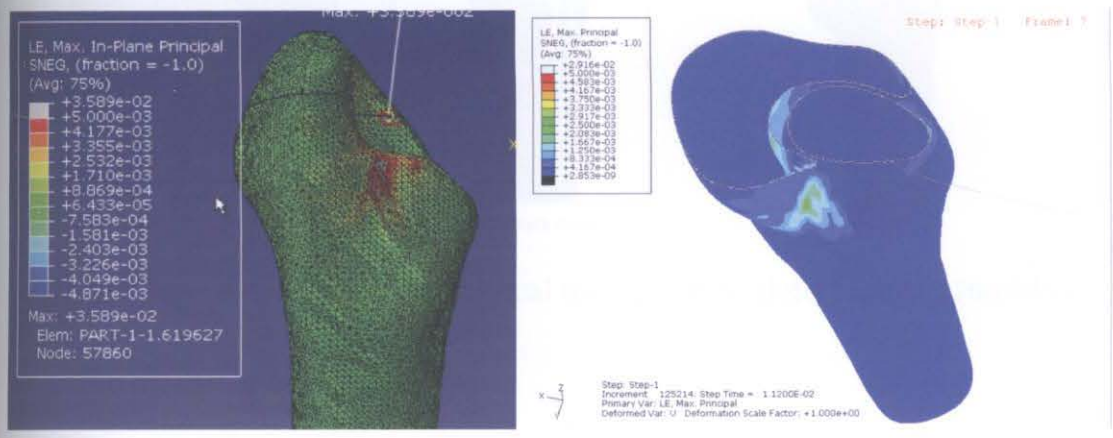

Figure 143 High strain area in models that would not converge with element deletion- these models converged when element deletion was not used.

4.3.1.2.3 *Results of biphasic and triphasic material property modeling*

Compared to the triphasic models, the biphasic models more closely replicated the failure mode of the experimental specimens, but there were some noticeable differences (Figure 144 middle and right). In both models, the prosthesis was initially displaced into the femoral canal, with a brittle crack suddenly emanating from the midline of the neck osteotomy on the medial and the lateral side. In the biphasic model, the crack then moved distally and unlike the experimental specimen, it did not fully displace the calcar region of the bone. Later, the crack progressed laterally and out through the lateral diaphysis before a secondary crack emanating distally from this crack line progressed medially and displaced the medial calcar. However, in the triphasic model, the initial crack progressed distally and laterally and also displaced the trochanter away from the femur, quite unlike the experimental specimen.

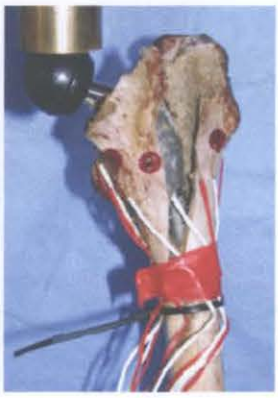

Physical test crack mode

Simulation crack mode

Figure 144 Typical failure mode physical test specimen (left) biphasic (middle) triphasic (right)

4.3.2 Failure load

The triphasic models showed a considerably higher failure load than the biphasic ones (See Figure 145). In both models, an increase in the friction coefficient at the implant-bone interface led to a corresponding increase in the failure load (See Figure 146). This suggests that failure was sensitive to the friction coefficient. However, over-prediction of the failure load was observed in the models with the higher friction coefficient. The finite element analysis showed that the triphasic bone models were much stiffer than the experimental femoral specimens (See Figure 146).

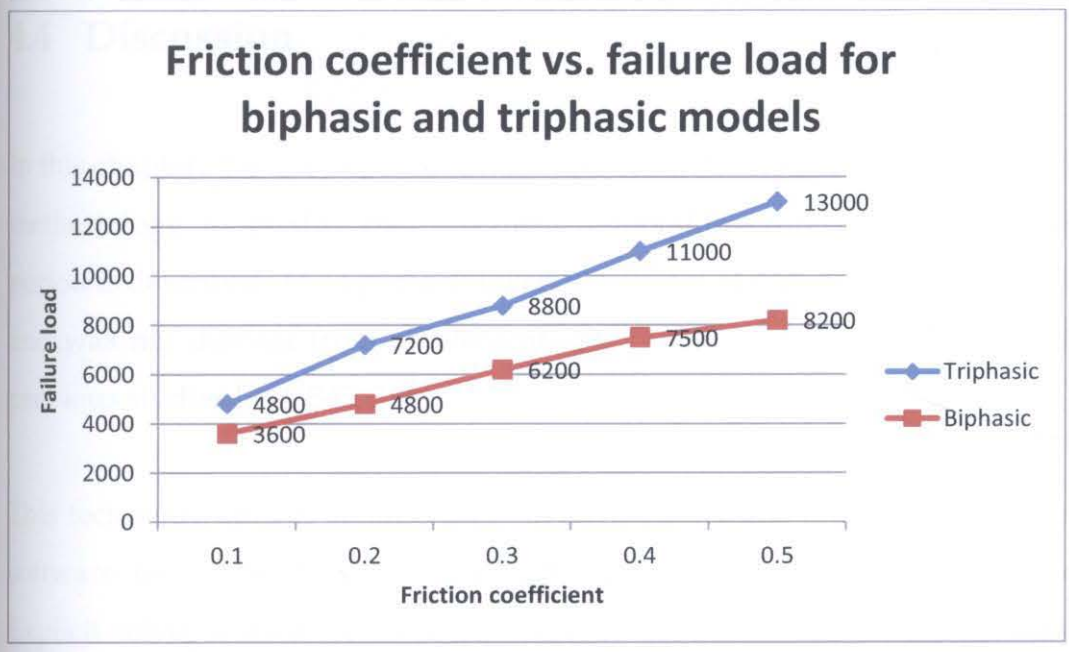

Figure 145 Friction coefficient vs failure load for biphasic and triphasic models

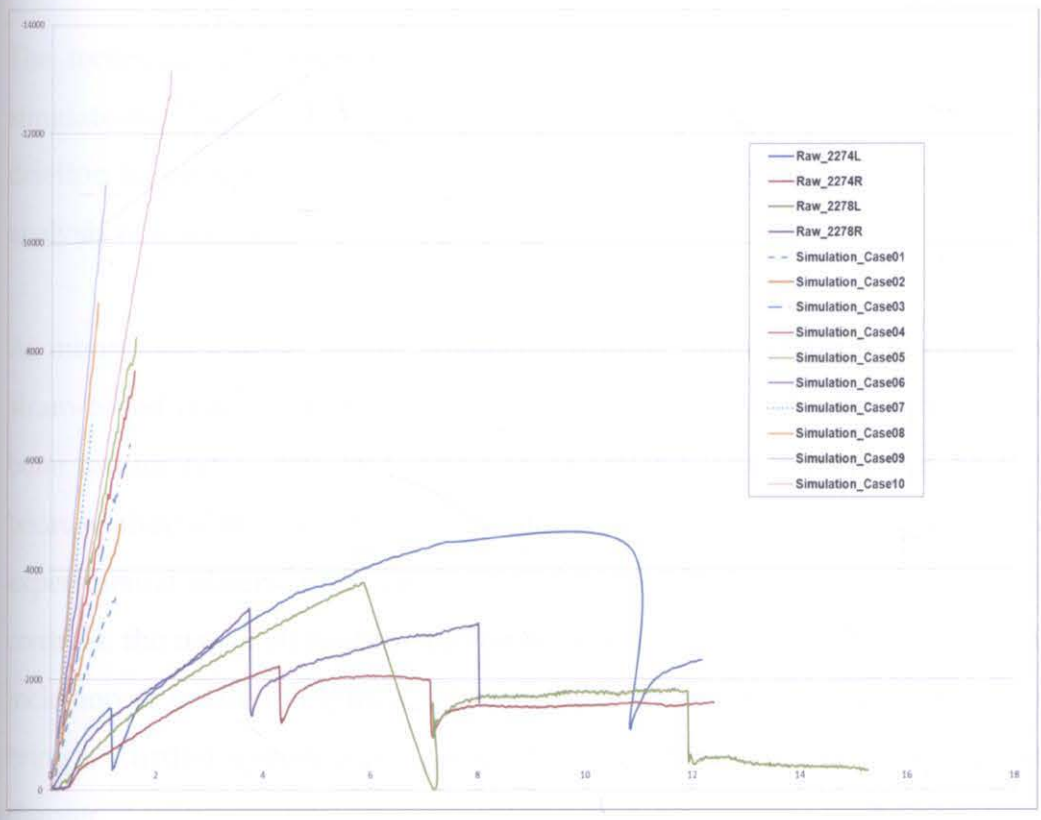

Figure 146 Comparison of force vs. time (also displacement) plots

4.4 Discussion

In this chapter, the development of a simplified patient-specific finite element modeling methodology to predict peri-prosthetic femoral fracture in the early postoperative period is described. The approach taken used a novel technique to simulate bone failure and was not derived from an element-specific failure risk calculation as described in previous studies [344, 345, 353].

This technique utilizes commercially available software, namely the Simpleware set of software tools and ABAQUS CAE 6.9, for pre and post processing. The ABAQUS Explicit solver is used for all of the analyses which allowed for significantly decreased computational time over the Standard solver.

The technique utilizes a newly available feature in the ABAQUS CAE module to simulate the failure of the bone. That is the capability to set element deactivation or deletion based upon a threshold field value. The threshold field value chosen for this analysis was strain.

As mentioned earlier, recent advances in bone biomechanics have demonstrated that strain-based criteria are more effective than stress-based criteria in describing yield or bone failure [282, 293, 345]. The use of strain-based criteria can be further justified because they allow better experimental characterization and have been derived from experimental observations on the invariance of limit-strain with respect to density. In contrast, the use of stress-based criteria, especially in an inhomogeneous model, leads to inclusion of another empirical relationship between limit-stress and density, which may bring in further uncertainties [345]. Therefore, these criteria were implemented in this chapter.

When preparing the models, ambiguity in the ISO 7206 - 4 testing standard was discovered. This was investigated with a sensitivity analysis and found that there was significant variation in one setup and less variation in the second setup. The less sensitive setup was used for subsequent models. This issue is important to highlight for because the variability in the testing standard could affect future testing setups resulting in misleading conclusions. This is an important finding.

The finite element models were compared with the femoral test specimens, from which they were created, as well as with the specimens from the contralateral side of the same donor. When comparing the models to the experimental testing, the crack mode for the biphasic models was very similar to the mechanical testing crack mode, with a similar shape of the crack, and similar crack path. See Figure 147.

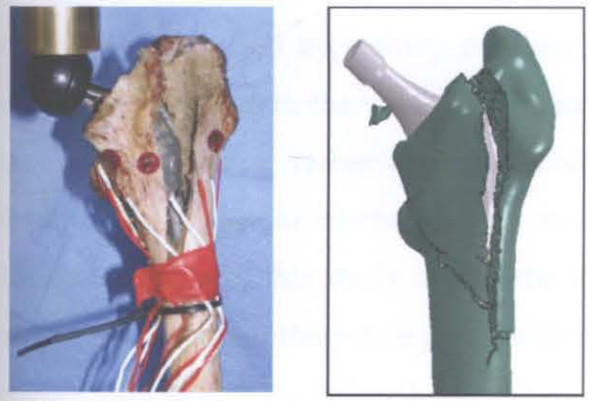

Figure 147 Biphasic models show good agreement with test specimens for crack mode

The results showed that the finite element analysis models over-predicted the femoral strength, especially in the triphasic models. Both the biphasic and the triaphasic models appeared to be stiffer than the test specimens, which may have contributed to the over-prediction. The reason for the additional stiffness is thought to be because of the chosen method of material property assignment.

An explanation for the increased stiffness in the triphasic models would be the presence of middle bone, the layer between cortical and cancellous bone that was included in the finite element model, with a high modulus of elasticity.

Though studies have used complex property mapping strategies to accurately model the heterogeneous nature of bone [354, 356]. The heterogeneous material property mapping was not possible in conjunction with the element deletion failure modeling approach. Instead of heterogeneous properties, we assigned simplified material properties to bone as described by Pastrav et al. [307] for ease of FE modeling.

The process of failure is more complicated than mere identification of a localized failure initiation point; therefore, calculation of a failure risk criteria may be inappropriate, especially in situations with implants being modeled in situ. In the experimental specimen, structural failure was observed due to a brittle crack that occurred in the cortical bone, caused by a sharp decrease in load after reaching a peak value with no noticeable decrease in the slope of the curve immediately before failure. This suggests generalized yielding rather than localized yielding of the cancellous bone supporting the implant. A similar mechanism for structural failure was reported by Schileo [345]. The assumption of this study is that the yielding of the cancellous bone is a precursor and a critical step in the entire process of structural failure but, by itself, may not be the correct indicator of the failure load.

This theory was supported by observations from the experimental testing that prior to failure; the prosthesis was slowly displaced into the femoral canal causing a wedging effect on the cortical bone. Complete structural bone failure is unlikely to result from only yielding of the cancellous bone immediately surrounding the prosthesis. A fracture risk calculation would be inappropriate in a scenario in which hoop stresses generated as a result of the wedging effect contribute significantly to the structural failure of bone

and not localized yielding of cancellous bone. Thus, simulation of bone failure via the "element deactivation" technique seems rather justified.

The strain-based failure criteria used as the threshold value for element deactivation in the finite element model used in this study was as defined by Schileo [345]. This study used the same failure criteria for cortical and cancellous bone. A previous study compared the yield properties of human femoral trabecular and cortical bone tissue and concluded that the yield strain for trabecular bone is 15% lower than that for cortical bone [354]. In the modeled specimen, I believe that the cortical bone appeared to fail due to the tension resulting from hoop strains generated at the surface by the prosthesis wedging further into the prepared canal, while the cancellous bone appeared to fail under compression as the prosthesis crushed and yielded the supporting cancellous bone. My failure criteria did not account for the tensile-compressive yield strength asymmetry of the cancellous bone, which has been reported as 0.62 on average [355].

No previous studies have associated friction coefficients with fracture loads. In this study, the finite element models with lower friction coefficients showed failure loads that were closer to those seen in the experimental specimens. Therefore, I believe that the failure load is sensitive to the friction coefficient. Further studies in this area may help in calibration of the unknown friction coefficient if the failure load is known.

Though studies have used complex property mapping strategies to accurately model the heterogeneous nature of bone [354, 356]. The heterogeneous material property mapping was not possible in conjunction with the element deletion failure modeling approach. Instead of heterogeneous properties, I assigned simplified material properties to bone as described by Pastrav et al. [307] for ease of finite element modeling.

It must be noted that the use of only a single specimen in this chapter is a limitation. However, the presentation of this simplified technique would not have been enhanced by including more specimens.

Chapter 5

Subject-specific Finite Element Model with an Optical Tracking System in Total Hip Replacement Surgery

5.1 Introduction

Intra-operative periprosthetic femoral fractures are a significant concern in total hip arthroplasty [340, 357], and are more commonly observed with cementless implants (5.4%) than in a cemented setting (0.3%) [340]. Revision surgeries have reported considerably higher rates with both cemented (3.6%) and cementless (20.9%) stems [340]. Outcomes of 519 patients in the Danish hip registry suggest that intra-operative peri-prosthetic femoral fracture increases the relative risk of a revision procedure during the first six months after total hip arthroplasty [358].

Intra-operative peri-prosthetic femoral fractures can occur at any time during surgery, with the highest incidence during implant insertion. This is because the surgeon strives to obtain a firm initial press fit to ensure stability to facilitate bony in-growth for long-term fixation [63, 104, 307, 340, 357]. This is usually achieved by preparing a slightly undersized femoral canal and using a mallet for implant insertion [357]. Increased loads exerted to attain a firm fit cause a wedging effect, and fracture occurs when the hoop stresses generated by the implant on the bone are too great for the femur to resist [3, 357]. The frequency of intra-operative fractures varies with implant design, surgical technique, bone quality, and bone deficiency [340]. The femoral stem design is a known risk factor for peri-prosthetic femoral fractures [342], with a significantly high intra-operative fracture rate of 15.2% observed with the cementless Omnifit system [334]. Most of the patients undergoing hip arthroplasty have poor bone quality [342] and consequently, diminished bone strength. During implant insertion, the surgeon needs to balance the force applied to the bone with the load-bearing capacity of the bone. Therefore, load characterization during surgery would be extremely beneficial to the surgeon, thereby reducing the risk of intra-operative peri-prosthetic femoral fracture.

Subject-specific finite element models developed from computed tomography data have been used successfully as a non-destructive tool to investigate bone strength in simulated clinical settings [306, 345]. Most of the parameters, which contribute to bone strength can be modeled using this technique [287]. Additionally, the influence of general and variable external boundaries and loading conditions can also be simulated [345, 359]. Subject-specific finite element bone models can successfully determine the fracture risk in patients [311, 313] if the boundary conditions and the loading scenario are well-defined [345] [360]. However, in order to predict intra-operative peri-prosthetic femoral fracture, it is essential to input accurate force characterization data into the finite element analysis model.

Recently, computer-aided navigation systems, utilizing optical wireless tracking mechanisms in total joint arthroplasty, have gained popularity [2, 47, 361]. During surgery, they can accurately control component placement, leading to improved precision in implant positioning relative to the patient's anatomy [60, 62, 72]. This is important as the mal-positioning of the prosthesis can lead to a peri-prosthetic femoral fracture and lateral insufficiency fractures due to varus positioning of the femoral component of the implant [111]. The optical tracking systems use a tracker to continuously localize the three-dimensional (3D) position of the instruments. It is envisaged that if this position is synchronized with time, the velocity of these tools could be estimated. Using this data, the magnitude of force exerted on the implant and the bone could be measured by inputting the velocity into a dynamic finite element model. [117, 120].

In this chapter, a novel method is presented, which combines subject-specific finite element analysis with an optical tracking system to model patient-specific bone properties as well as procedure-specific loading. This study will demonstrate that this method can account for patient-specific variability in bone strength and aid in characterizing the load application by the surgeon. Further developments to this

method could provide the surgeon with patient-specific feedback that will help reduce the risk of intra-operative peri-prosthetic femoral fracture.

5.2 Methods

5.2.1 Experimental measurement of hammer velocity

A surgical simulation was undertaken to demonstrate quantification of the hammer (mallet) velocity using the Stryker Navigation System (Stryker Navigation, Kalamazoo, MI, USA). This navigation system utilizes active infrared tracking technology to continuously localize battery-powered tracking devices within its field of view with a refresh rate of 100 Hz.

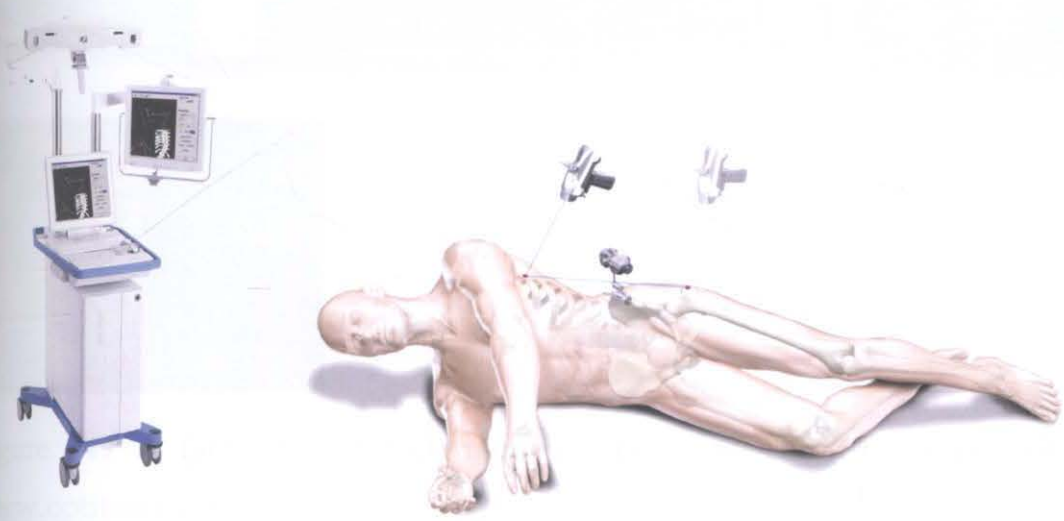

Figure 148-Stryker Navigation System- commercially available optical tracking system

5.2.1.1 Non clinical "Research Version" of software

A nonclinical modified version of the Stryker Knee Navigation Software was provided by Stryker Navigation Advanced Technology, Freiberg, Germany.

5.2.1.1.1 *Purpose of the software*

The research mode add-in software was programmed by the Stryker Advance Technology division, with the purpose of allowing more freeform internal research to be conducted that utilizes the commercial navigation systems hardware. The capabilities of the research version of software are similar to the capabilities of a dedicated motion capture system, such as an Optitrak system, which is familiar to many biomechanical research labs. See Figure 149.

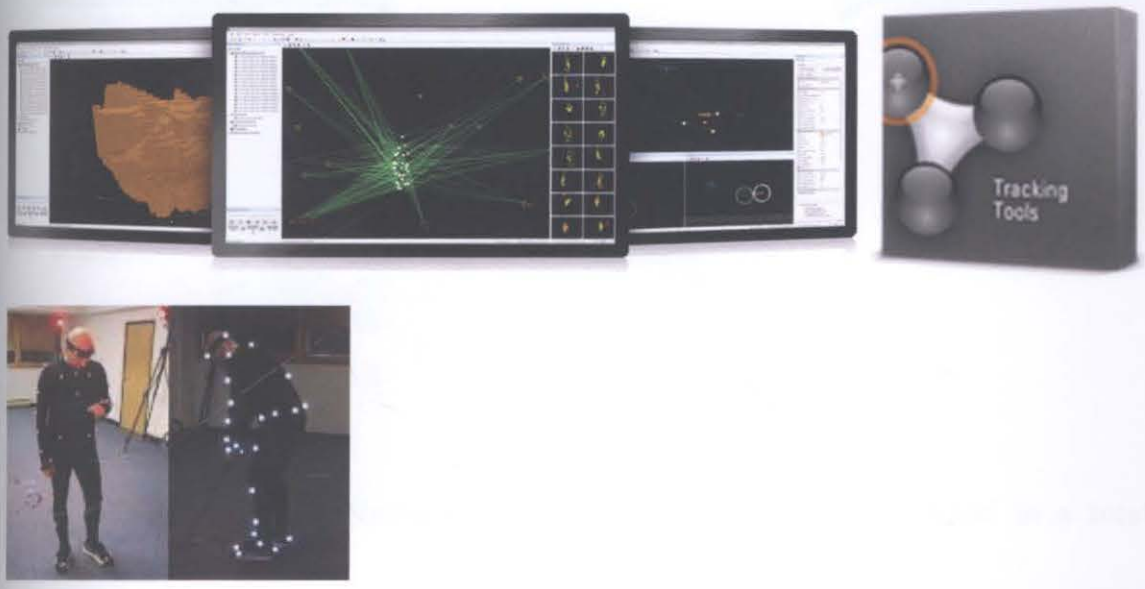

Figure 149 A familiar Optitrack motion capture system (from Optitrack website www.optitrack.com)

The Stryker research add-in software, however, has the distinct advantage that it can utilize the Stryker Hip Navigation instruments, which can be easily incorporated into a surgical simulation. The Stryker Hip navigation instruments already have dedicated attachments to hardware, which interface well with hip replacement surgery. Furthermore, if the work of this chapter progresses further into a real clinical evaluation, the Stryker Navigation hardware has been proven to be clinically safe and approved by

all major healthcare regulators for real hip surgery. Thus rendering it, ethically, a much better choice than another motion capture system.

Figure 150 Stryker Hip Navigation Smart Instruments being utilized in a total hip replacement

The research add-in is available as a graphical user interface that provides additional dialogs to the standard version of the Stryker knee Navigation Software. The additional dialogues allow the user to digitize a different kind of data in a very flexible and customizable way. This is different to the commercial versions of software, which will force the user to digitize only data relevant to the commercial version of software's output. If this were a knee navigation, it would force you to only digitize information related to the knee, whereas the research add-in allows the user flexibility to customize what is digitized and the reference frame in which it is recorded. The recorded data can

be converted into text files in comma-separated format, which can then be imported into Excel or another program for post processing of the data.

Different types of data can be recorded and the reference frame in which this data is recorded can be customized. The available reference frames are:

- The Navigation camera itself;
- Another tracker that is already being localized by the camera;
- An already constructed reference frame constructed by following the standard workflow of the commercial software. For example the femoral axis from the knee software.

The types of data that can be recorded are;

- Points,
- Lines,
- Planes/reference planes
- Point clouds
- Or Movements which is what is recorded for this work

  See Figure 151

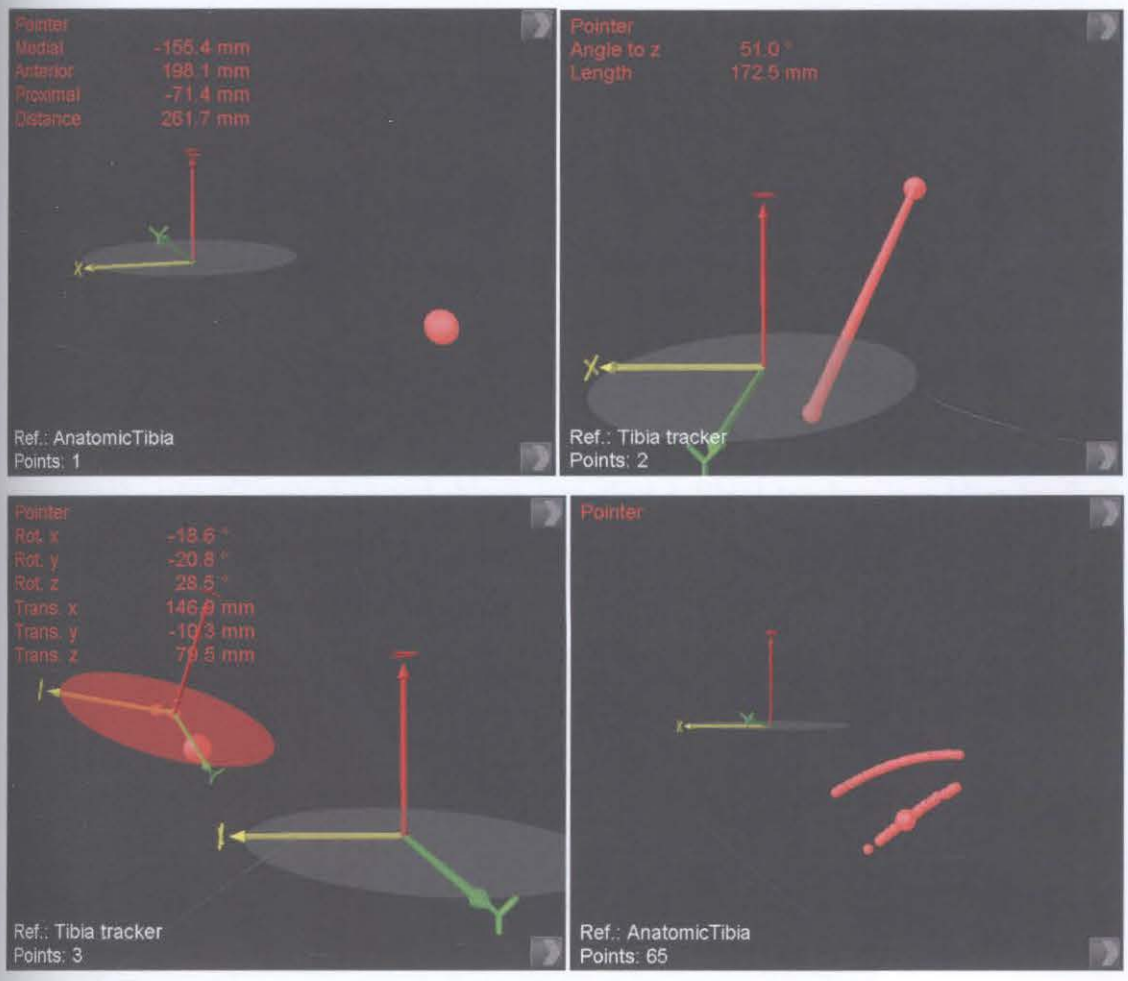

Figure 151 Types of data that can be recorded with the Stryker Navigation research version of software

5.2.1.1.2 *Movements*

A research data item of type movement stores the transformations from the object to the reference systems. An unlimited number of transformations can be stored, thus recording the movements of the object relative to a reference system.

When the record button is pressed, the recording starts and will periodically collect data until the record button is pressed again, stopping the recording. Collecting data will occur 100 times per second, but only when the tracker positions have changed, i.e. when

something has moved. For each transformation the object point relative to the reference and small coordinate axes are displayed.

The Stryker Advanced Technology team in Frieberg, Germany, made a further modification to the research version of software after a special request was made. This was to modify the software to time stamp each of the outputted positions, allowing a velocity calculation to be made. See Figure 152. The software graphical user interface which is displayed in figure 152 was not altered by the change in the software. Only the numerical outputs are changed. Note also that a tibial tracker is a blue tracker in this software. That is the tracker that was attached to the hammer.

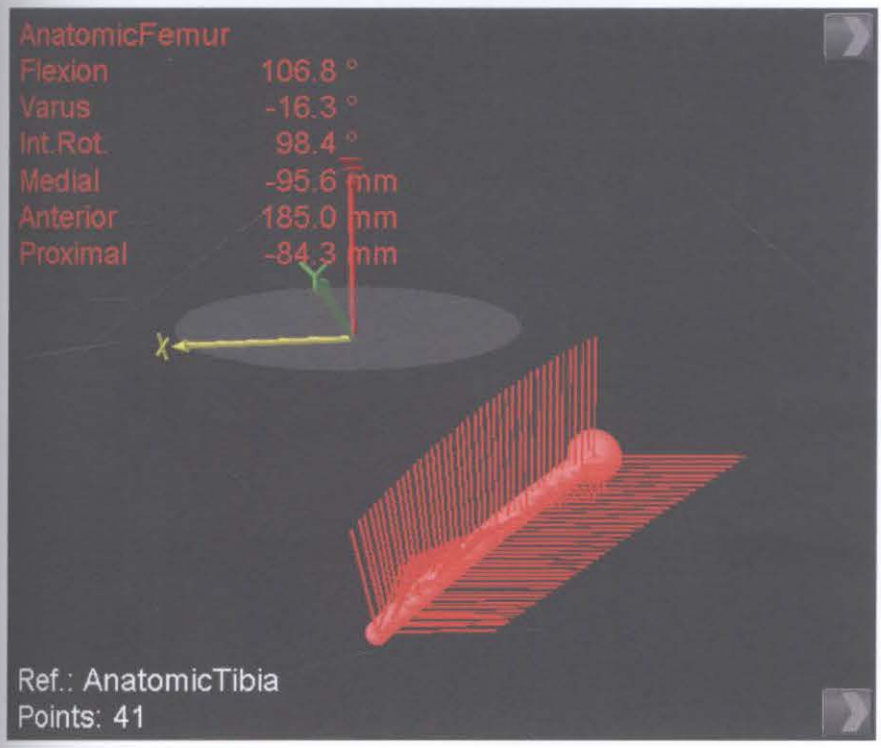

Figure 152 digitizing a movement in the Stryker research version of software

5.2.1.2 Recording the hammer velocity

The software was configured to output information for a tracker that was rigidly attached to the surgical mallet (See Figure 153). The total mass of the mallet and tracker was measured to be 1.6 kg.

Figure 153 Stryker Navigation tibial tracker rigidly attached to the mallet

Using this mallet and the instruments provided by the manufacturer, Stryker, a simulation of the femoral preparation for an ABG II femoral stem (Stryker Orthopaedics, Mahwah, NJ, USA) was undertaken following the company's recommended surgical technique. The simulation was undertaken on a plastic saw bone (Pacific Research Laboratories, Inc, Vashon, Washington, USA). See Figure 154.

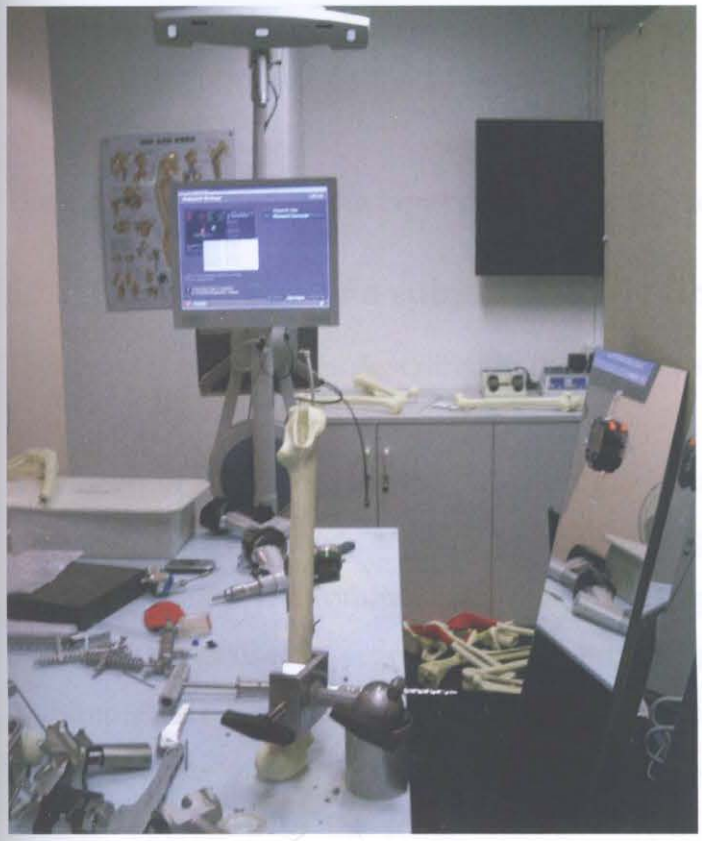

Figure 154 Setup used to record hammer velocity with the Stryker Navigation research version of software

As the risk of intra-operative fracture is highest during stem insertion [357], the output of the 3D co-ordinates relative to the navigation system's reference frame at each time increment during this stage was isolated, exported into Microsoft Excel (Microsoft Corporation, Redmond, WA, USA), and processed. The time immediately before the impact was manually identified for three separate impacts. Using these time points, the x, y, and z co-ordinates for the preceding second in each case were isolated and the velocities were calculated, setting Δ (t) to be 0.1 of a second.

$\Delta d = \sqrt{(x_2 - x_1)^2 + (y_2 - y_1)^2 + (z_2 - z_1)^2}$

Velocity = $\Delta(d)/\Delta(t)$

This value was used as the input data for the explicit finite element model.

5.2.2 Construction of a subject-specific finite element analysis model

This general process was described in the previous chapter.

A CT scan of a cadaveric femur from the previous study, with prior ethics committee approval, was obtained in the digital imaging and communications in medicine (DICOM) format. The commercially available Simpleware ScanIP (Simpleware Limited, Exeter, UK) was used to segment, smoothen, and export the proximal femoral geometry to Simpleware ScanCAD (Simpleware Limited, Exeter, UK). A single-cut neck osteotomy was simulated using a computer-aided design primitive and applying a Boolean operation to the femur model. Stryker Orthopaedics (Mahwah, NJ, USA) provided CAD models of the definitive ABG II prosthesis, with some minor geometrical simplifications (removal of small cut-outs in the proximal region). Within the software, an ABG II size 4 femoral stem was virtually positioned into the bone, with its position verified by a company representative familiar with the surgical technique. Boolean operations were applied to simulate the removal of the cancellous bone by broaches. The distal reaming step, as required by the manufacturer's surgical technique for this stem, was simulated using another computer-aided design primitive positioned around the distal pilot of the stem and another Boolean operation. The femoral shaft was sectioned 30 mm below the distal stem tip to reduce the model size.

5.2.3 Generation of an finite element mesh

The femur from the model described above was exported to the commercially available package Simpleware Scan FE (Simpleware Limited, Exeter, UK), where it was meshed

using the automatic meshing capabilities of the software with 246,653 C3D10 elements. The mesh density was limited by the voxel size of the CT scan, and no further mesh refinements were possible beyond the level obtained. Therefore, no convergence study was performed to check the adequacy of the mesh.

The meshed bone model that was then transferred to ABAQUS CAE (ABAQUS Inc., Providence, RI, USA), the C3D10 elements were changed into C3D10M elements, and some additional geometry was added. The ABG II size 4 stem was reintroduced into the femoral cavity, which had been already prepared as described above, and was meshed using the automatic meshing capabilities of ABAQUS CAE with 48646 C3D10M elements.

Table 13 Finite element mesh information used in this study

Part	Material	Element type	Maximum element size (mm)	Number of elements
Hammer	NA	R3D4	15	68
Plastic guide	Acetyl	C3D8I	15	496
Ring	Acetyl	C3D8I	15	96
Metal guide	Steel	C3D6	5	633
Implant	Titanium	C3D10M	2	48646
Cortical bone	Cortical bone material	C3D10M	2	115548
Cancellous bone	Cancellous bone material	C3D10M	2	131105

5.2.4 Simulation of intra-operative loading scenario

An introducer with a stainless steel shaft and an acetyl handle were modeled (See Figure 155). Thereafter, a 1.6-kg rigid body mass was introduced immediately adjacent and in line with the impactor handle, in order to simulate the mallet of the same weight. A cylindrical guiding jig was then placed to ensure that the punch would transfer the load to the implant stem axially. The finite element mesh information for the hammer and the implant is shown in Table 13.

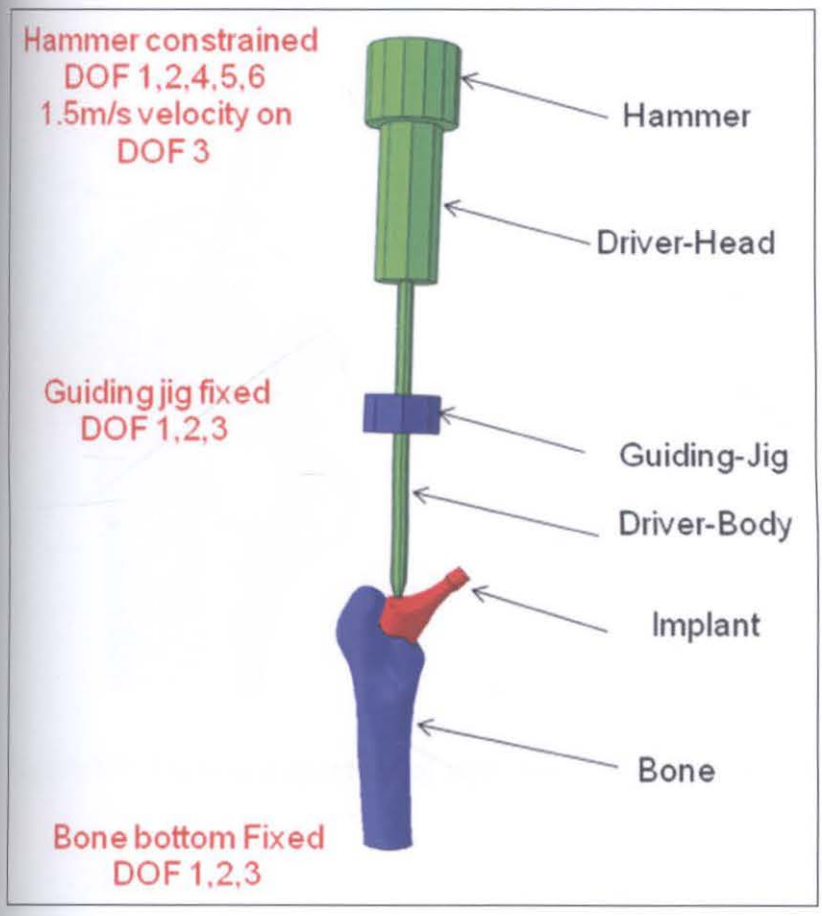

Figure 155 Representation of loading scenario in the Simulation

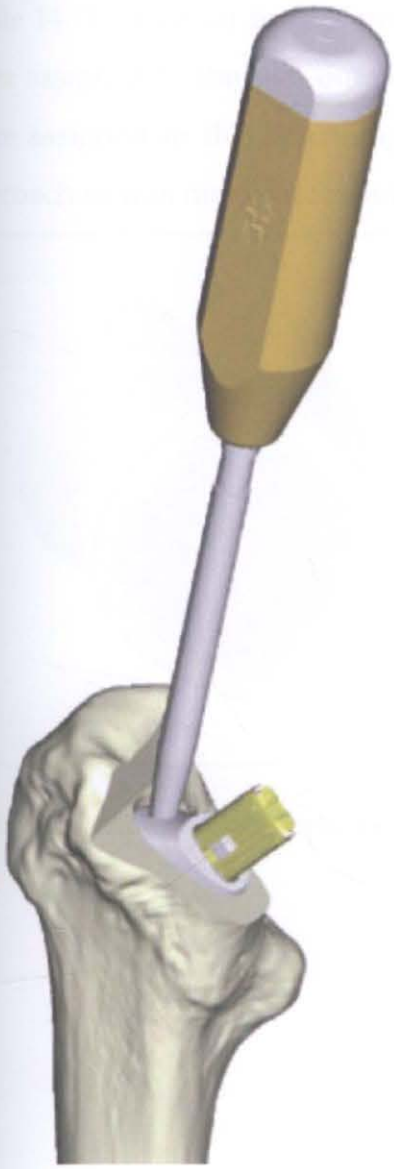

Figure 156 Typical impaction of stem into femur (From ABG II surgical Technique)

5.2.5 Material property assignment

The bone was modeled as an orthotropic, linear-elastic material and the implant material (Ti6A14V) was considered to be isotropic and linear-elastic. The mechanical properties of the materials and the reference orthogonal system are shown in

Table 14. To account for different types of bone in the femur, cortical bone properties were assigned to the two outer layers of the elements and cancellous bone properties were assigned to the remaining inner elements (See Figure 157). This was the same approach as was most successful in the previous chapter of this thesis.

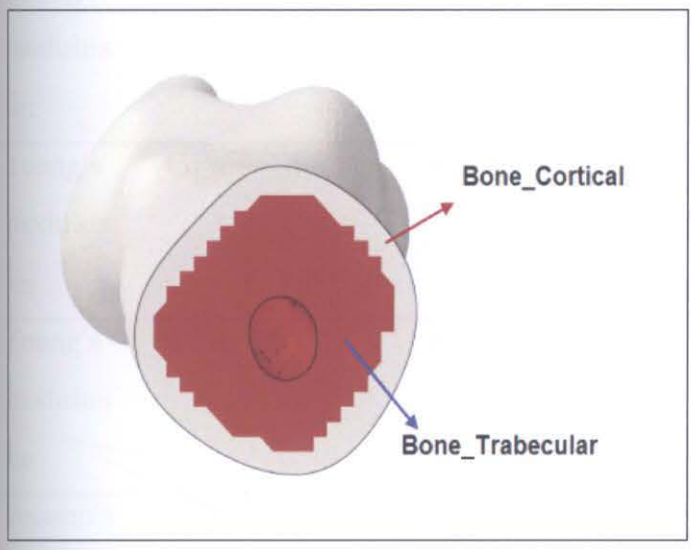

Figure 157 Material property assignment used in this study for byphasic models

Table 14 Material properties assigned to various materials in the finite element model*

Variable	Unit	Cortical bone	Cancellous bone	Titanium	Acetyl	Steel	Orthogonal system
Young's modulus E_{11}	GPa	6	0.375	110	1.73	200	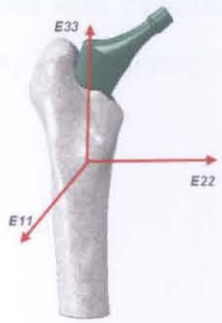
Young's modulus E_{22}	GPa	6	0.375	110	1.73	200	
Young's modulus E_{33}	GPa	13	0.6	110	1.73	200	
Poisson's ratio $v_{12}=v_{23}=v_{31}$		0.3	0.12	0.3	0.3	0.3	
Density	kg/m^3	1800	500	4500	1290	7800	

*adapted from Pastrav [307].

5.2.6 Application of adequate boundary conditions

The boundary conditions were applied as shown in Figure 155. The general contact setting was used for all contact surfaces; all surfaces other than the implant-bone interface were assumed to be frictionless. Two friction states were simulated between the implant and the bone, i.e., friction coefficients of 0.1 and 0.4. All analyses were performed and evaluated using the explicit solver ABAQUS V6.9 (Dassault Systèmes, SIMULIA, Providence, RI, USA).

5.2.7 Modeling approach

An initial quasi-static explicit simulation was performed on both models to seat the implant and stabilize the model. This was attained by an enforced displacement of the implant into the bone until a 200 N reaction force at the punch dimple was achieved. This was followed by a dynamic loading step on both models, simulating the hammer strike by prescribing an initial velocity of 1.5 m/s (the average experimentally measured hammer velocity) to the hammer mass. As the model was only for representative purposes, no further hammer strikes were simulated.

5.2.8 Virtual strain gauge locations

To compare the maximum principal strains between both models, four cortical bone surface strain gauge locations were selected; the posterolateral, posteromedial, anteromedial, and anterolateral (See Figure 158). These locations were based on surface strains observed in the maximum principal strain contour plots of pilot models. Strains were measured in the femur before (quasi-static load) and after impaction for both friction coefficients of 0.1 and 0.4.

Figure 158 Virtual strain gauge locations in the models

1: posterolateral strain gauge

2: posteromedial strain gauge

3: anteromedial strain gauge

4: anterolateral strain gauge

5.3 Results

5.3.1 Outputs measured

The mean velocity of the mallet measured with the navigation system over each second was determined to be 1.5 m/s (range, 1.3–1.8 m/s).

Table 15 Calculated hammer velocity

Hammer Strike	Measured Velocity m/s
1	1.3
2	1.4
3	1.8
Mean	1.5

Observing the animation of the simulation, it was clear to see that during the impact loading step in the finite element analysis simulation, as the hammer hit the driver-head, the pressure wave propagated through the driver to the implant, and then finally to the bone for both models. This was accompanied by a further displacement of the implant into the femur.

The outputs measured from the finite element analysis simulation included implant displacement in the bone, energies in the system, strains, and force measurements for the quasi-static preloading and the impaction steps. The forces at the hammer impact surface, the top of the implant, and at the distal restraint (base of the femur) for both models (friction coefficients of 0.1 and 0.4) were measured.

5.3.2 Displacement and energy measurements

During quasi-static preloading, a larger displacement of the implant into the bone was observed in the model with the lower friction coefficient than in the model with the higher coefficient (See Figure 159). Accordingly, the model with the friction coefficient of 0.1 took longer (0.02 s) to reach the 200 N reaction force threshold (See Figure 160). Higher kinetic,

strain, and total energies were observed in the model with the friction coefficient of 0.1 than in that with the friction coefficient of 0.4. Slightly higher friction energy was observed in the model with the friction coefficient of 0.4. The artificial energies in both models were negligible; with slightly lower energy in the model with the friction coefficient of 0.4 (See Table 16).

Even during the impact step, a slightly greater displacement was observed in the model with the friction coefficient of 0.1. An overall displacement (in both loading steps) of 16.56 mm was seen in the model with the lower friction coefficient as compared to 12.7 mm in the model with the higher friction coefficient (See Table 16). The kinetic energy recorded was equivalent to the total energy in the system as the same hammer mass and velocity measurements were used as input data for both models. Higher strain energy was observed in the model with the friction coefficient of 0.1, while the friction energy was higher in the model with the friction coefficient of 0.4. Similar artificial energies were seen in both models (See Table 16).

Table 16 Displacement and energies in the system during the quasi-static preload and impact loading steps*

Friction coefficient	Loading approach	Displacement (mm)	Energies in the system (J)				
			Total	Kinetic	Strain	Friction	Artificial
Quasi-static preloading							
0.1	Enforce displacement	12.6	0.509	0.029	0.145	0.319	0.0021
0.4	Enforce displacement	9.6	0.457	0.022	0.031	0.345	0.0005
Impact loading							
0.1	Impact	3.96	1.80	1.80	0.573	1.694	0.06
0.4	Impact	3.1	1.80	1.80	0.267	1.759	0.05

*maximum values have been included in the table.

5.3.3 Strain measurements

During quasi-static preloading, the magnitudes of the maximum principal strains in all gauges were higher in the model with the friction coefficient of 0.1 than in that with the friction coefficient of 0.4. In both models, the posteromedial gauge had the highest magnitude of maximum principal strain, followed by the posterolateral gauge, anteromedial gauge, and anterolateral gauge (See Figure 159).

During impact loading, the displacement of the implant into the femur in both models was accompanied by a simultaneous increase in strains in the femur. The highest magnitude of maximum principal strain was observed in the anteromedial and posteromedial gauges in the models with lower and higher friction coefficients, respectively. Lower maximum principal strain was seen in the posteromedial gauge in the model with the lower friction coefficient than in the model with the higher friction coefficient. Higher strains were recorded in the anterior gauges in the model with the lower friction coefficient than in the

model with the higher friction coefficient. The posterolateral gauges recorded similar strains in both models (See Figure 160).

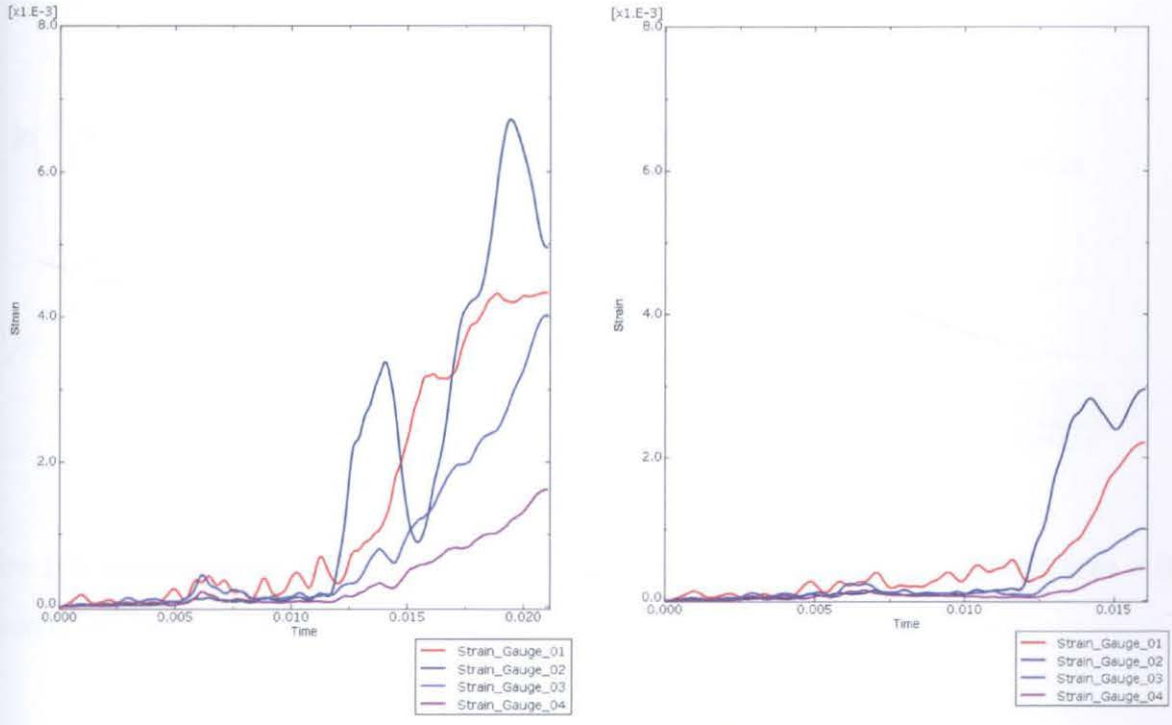

(A) (B)

Figure 159 Strain versus time at the quasi-static preload step in (A) friction coefficient = 0.1(note time is in seconds and strain is dimensionless)

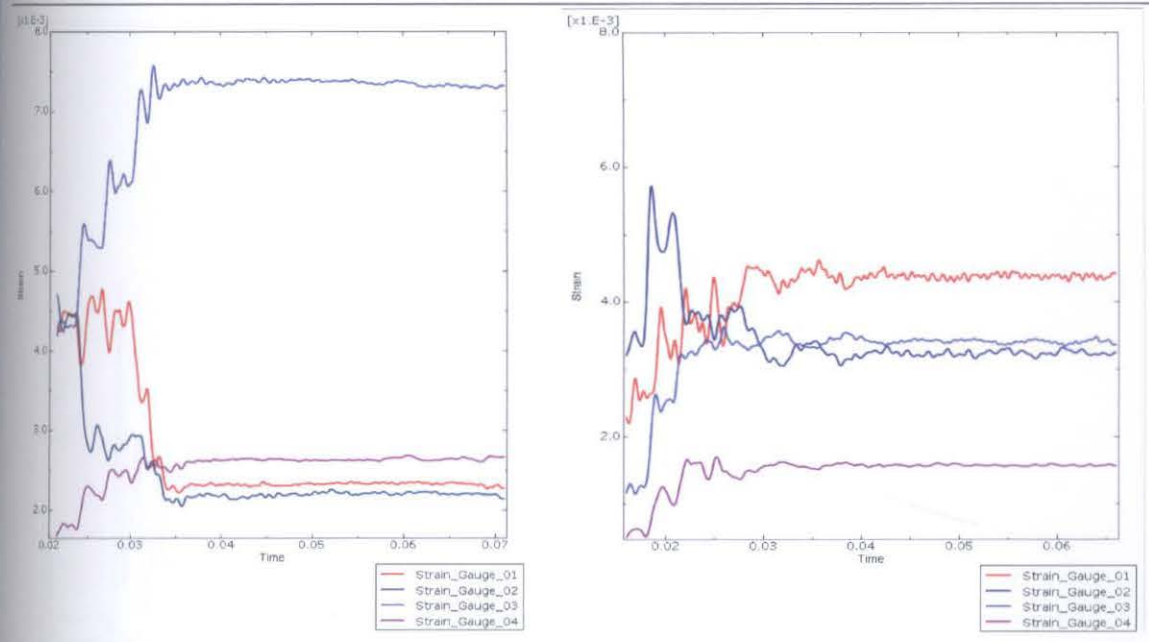

(A) (B)

Figure 160 Strain versus time at the impact loading step in (A) friction coefficient = 0.1 (B) friction coefficient = 0.4 (note time is in seconds and strain is dimensionless)

5.3.4 Force measurements

The peak magnitudes of impulse force were greater in the model with the higher friction coefficient than in the model with the lower friction coefficient, as measured at the hammer impact surface (1.6 kN vs. 1.4 kN, respectively) (See Figure 161), implant top (1 kN vs. 0.7 kN, respectively) (See Figure 162), and at the distal restraint (0.6 kN vs. 0.4 kN, respectively) (See Figure 163).

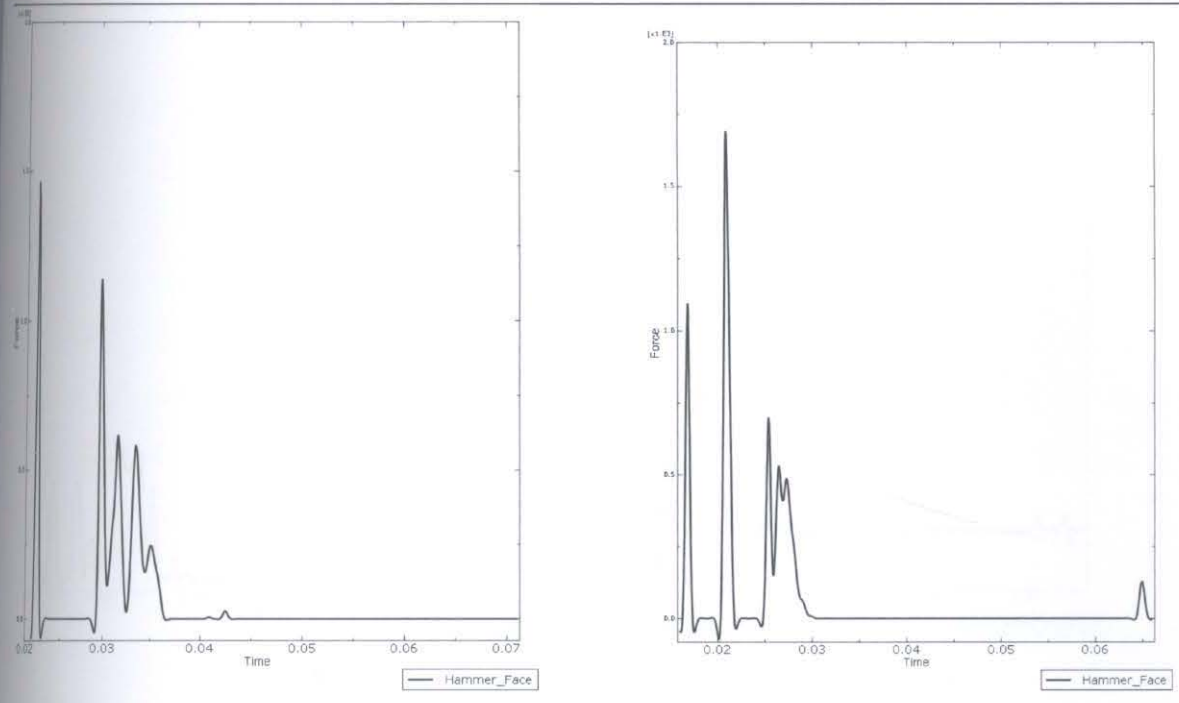

(A) (B)

Figure 161 Force measured at the hammer impact interface in (A) friction coefficient = 0.1 (B) friction coefficient = 0.4 (note time is in seconds and strain is dimensionless)

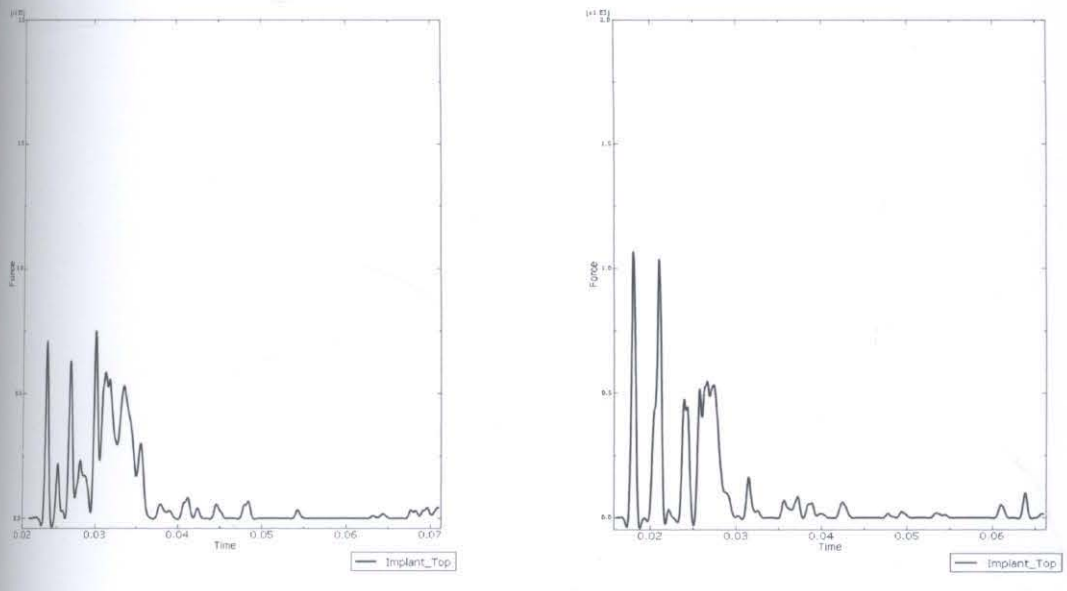

(A) (B)

Figure 162 Force measured at the top of the implant in (A) friction coefficient = 0.1 (B) friction coefficient = 0.4 (note time is in seconds and strain is dimensionless)

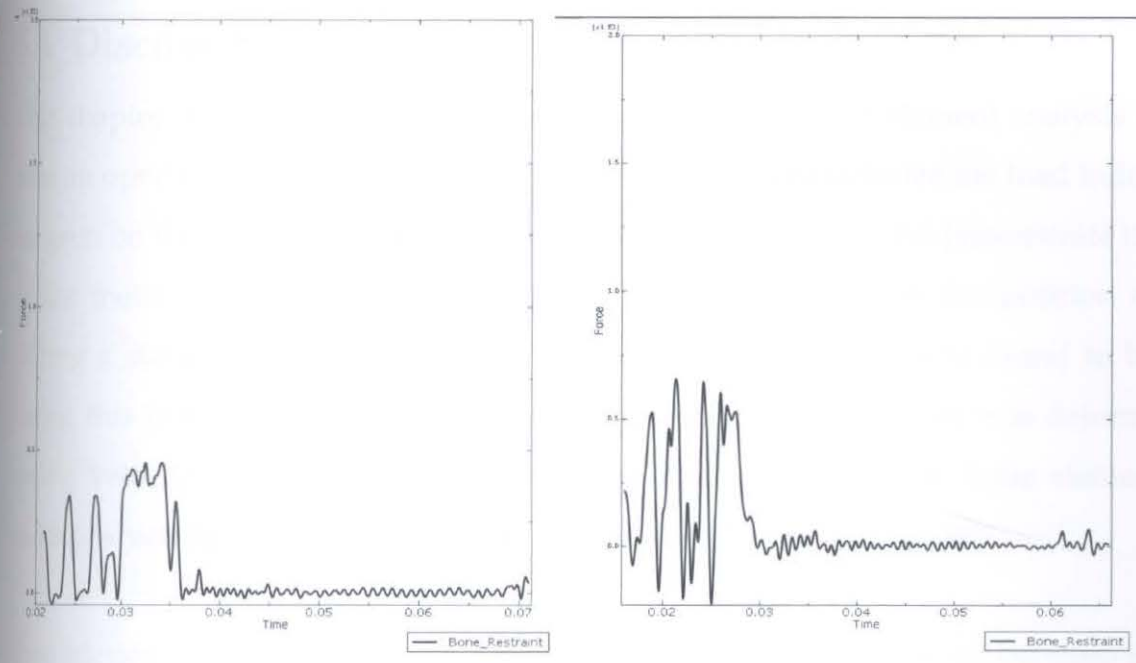

(A) (B)

Figure 163 Resultant force at the base of the femur (distal restraint) in (A) friction coefficient = 0.1 and (B) friction coefficient = 0.4 (note time is in seconds and strain is dimensionless)

5.4 Discussion

This chapter proposes a novel dynamic subject-specific finite element analysis model that uses an optical tracking system (navigation system) to characterize the load induced by the surgeon on the patient during a total hip replacement surgery. To demonstrate the viability of the method, a Stryker navigation system was used to track the position of a mallet during a simulated surgical setting. The mean mallet velocity was found to be 1.5 m/s. Using this positional information, the swing velocity of the mallet was determined. This swing velocity was then input into the dynamic subject specific finite element analysis model, which had first been subjected to a quasi-static preloading step.

Two friction states (friction coefficients of 0.1 and 0.4) were simulated between the implant and the bone. The outputs measured from the finite element analysis simulation included implant displacement in the bone, energies in the system, strains, and force measurements (the forces at the hammer impact surface, the top of the implant, and at the distal restraint) for the quasi-static preloading and the impaction load steps.

Distinct differences between the models were observed, demonstrating that the roughness of the proximal coating has an effect on the mechanics of the stem implantation. Most notably, the highest magnitude of maximum principal strain was observed in the anteromedial and posteromedial gauges in the models with lower and higher friction coefficients, respectively. Lower maximum principal strain was seen in the posteromedial gauge in the model with the lower friction coefficient than in the model with the higher friction coefficient. Higher strains were recorded in the anterior gauges in the model with the lower friction coefficient than in the model with the higher friction coefficient. These differences in strain are thought to be related to the fact that more displacement occurred in the lower friction coefficient model. An overall displacement (in both loading steps) of 16.56 mm was seen in the model with the lower friction coefficient as compared to 12.7 mm in the model with the higher friction coefficient. This caused a wedging effect that was previously described in Chapter 3, causing higher hoop stresses but lower shear stresses in the bone. The results suggest the lowest risk of fracture would be with higher friction coefficient (rougher proximal coating).

In clinical situations, the impact load exerted by the surgeon during implant insertion is variable, and its magnitude depends on factors such as the velocity, weight, and material (density) of the hammer. Furthermore, damping effects in the system determine transmission of the load through the system. An explicit finite element solver accounts for these dynamic parameters if the velocity of the object before it impacts the system is known [117, 120] [360]. Therefore, an explicit finite element solver was used for analysis as the mallet impact load was dynamic and the impulse loads could be easily determined.

With further development, this system (combination of subject specific finite element analysis and a navigation system) could be used to predict a pre-operative swing velocity threshold for the mallet by determining the mallet velocity above which peri-prosthetic femoral fracture could be expected (fracture threshold). Then, during surgery, the navigation system could be used to measure and report to the surgeon in near to real-time, the velocity at which they are swinging the mallet. Further, the system could alert the surgeon if they are approaching the threshold value. This would allow the surgeon to modify their swing velocity to prevent peri-prosthetic femoral fracture.

This novel technique has the potential to be adapted for future clinical use to aid in the prevention of peri-prosthetic femoral fracture. A patient-specific finite element analysis model could be created preoperatively and, if well prepared, could account for the patient-specific parameters of bone strength in this setting. An iterative determination of the maximum mallet velocity, above which excessive surgical loads might lead to intraoperative peri-prosthetic femoral fractures, could be determined and set aside as a threshold value.

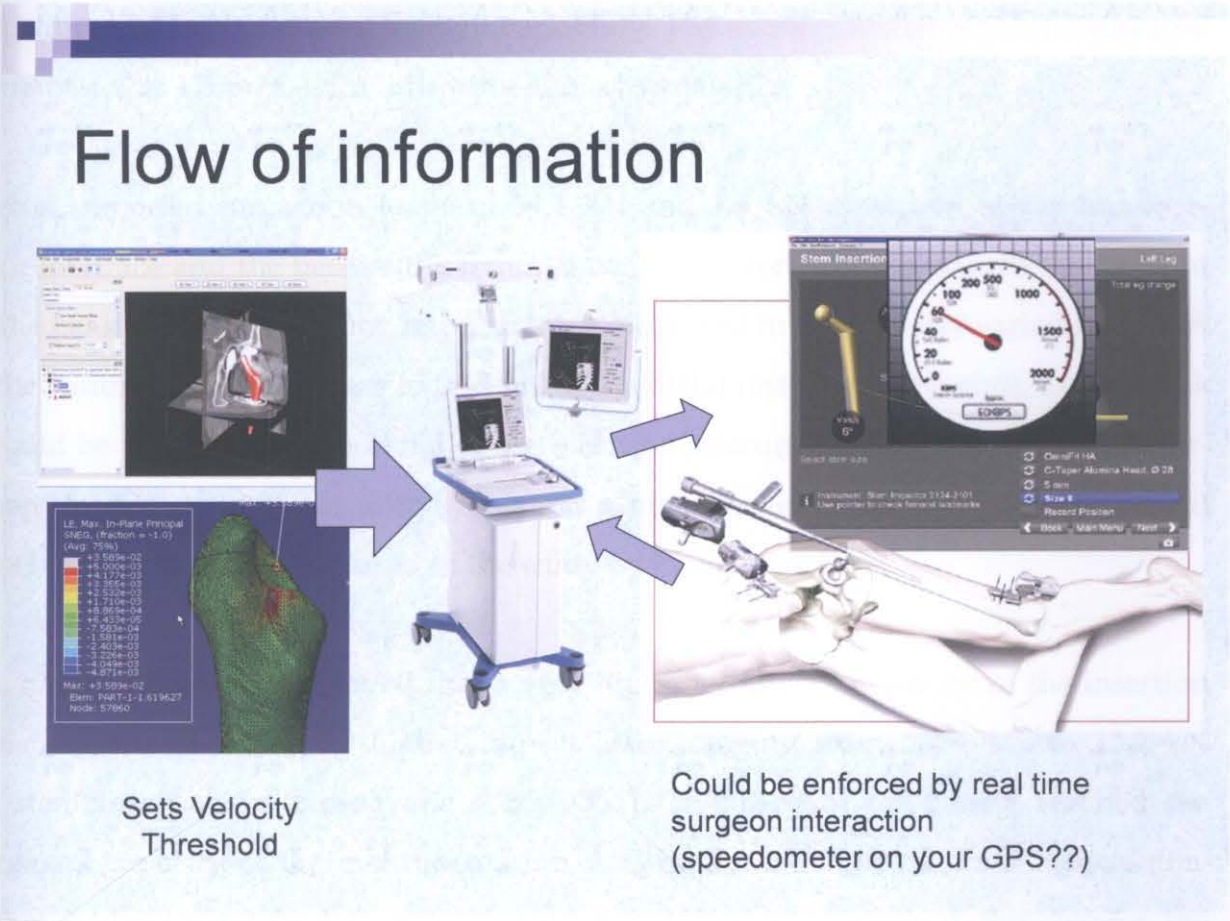

Figure 164 Proposed flow of Information for clinical implementation

Considering previous work, Hogg et al. used dynamic finite element analysis modeling to study the impaction of a cementless acetabular cup. The hammer velocity was found to be 1.826 m/s, which was similar to that observed in the experimental setup of this chapter [120]. In Hogg's study, the velocity was derived from the model in an iterative manner, where a number of analyses were run until the hammer velocity required to seat the cup in four hammer hits was determined. This was different from the approach in this chapter, in which the velocity was determined experimentally.

In a study based on explicit finite element analysis of principal stresses in femoral components in a total knee replacement surgery, Kleuss et al. [362] also measured experimentally the velocity of mallet swing and reported velocities in the range of 1.7–5.5 m/s. They also observed that experienced orthopaedic surgeons hit the impactor with a

significantly lower velocity (1.7–3.0 m/s) than inexperienced surgeons (5–5.5 m/s). Hammer velocities of surgeons with similar experience and comparisons between their own repetitions of impacts showed slight variability. The average mallet velocity measured in this chapter was 1.5 m/s, with little intra-subject variability.

Hogg et al. reported impaction loads of 34.1 kN and 1.4 kN measured at the hammer-impactor interface and the base of the femur during insertion of a hip resurfacing implant [117]. The peak magnitudes of the impulse force measured in this chapter varied from 1.69 kN at the hammer impact surface to 0.45 kN at the distal restraint (bone end). Lower peak loads could be related to the material of the insertion instrument, for example, the driver-head used in this chapter was acetyl. This has a much lower elastic modulus (1.73 GPa) than steel (200 GPa) which was used in the study by Hogg et al. [117]

Although unreported, it is believed that a very high modulus of elasticity of the insertion instrument led to significantly higher impact loads ranging from 5.950 kN to 13.5 kN during stem insertion in a cadaveric study [357]. The 13.5-kN peak force reached the measurement capacity of the instrumentation, and interpolation of the force versus time curve showed the largest peak force to be as high as 16.7 kN. However, in this chapter, the peak force at impulse was reported at the time of contact between the mallet and the stem impactor, and did account for the force being dissipated through the system [357].

In addition to the magnitude, the direction of load application may also be crucial. In the finite element analysis model used in this chapter, it was assumed that the mallet would strike the impactor along its longitudinal axis. However, it can be easily perceived that at some instances, the mallet strike may be off-axis, resulting in different peak loads. A cadaveric study has attributed this variation in peak forces and impulse levels between successive impacts to the difficulty in squarely striking the impactor with the relatively small head of the mallet [357]. It is believed that an off-axis mallet strike would lead to decreased stresses being exerted on the bone in this chapter's scenario. Therefore, a straight impaction would be the worst-case scenario, which is appropriate for this chapter's model.

Another concern may be that the implant itself is not aligned with bone and may be introduced at an angle. A previous dynamic finite element study in a knee replacement setting showed the consequence of implant misalignment relative to the bone by simulating misaligned femoral components tilted at 30° relative to the surgically prepared bone. In this scenario, they reported higher resultant stresses on the implant, which in turn would mean higher loads on the bone [360].

Fracture in human cortical bone is reported to be consistent with strain-controlled failure [363]. Therefore, a subject-specific finite element study advised implementation of strain criteria in finite element bone models and defined the maximum principal strain criterion to determine fracture risk in femurs [345]. In this chapter, the highest maximum principal strain observed was well below the level that would cause cortical bone failure [345]. This is not surprising given that fracture did not occur in the simulated surgery and that the simulated surgery was not done aggressively at all. Infact the measured hammer velocities were low compared to other reports. [362] This may also reflect the inexperience of the hammer holder (the author). As discussed by Kleus et al [362] experiencecd surgeons swing with lower velocities. However, this chapter did not aim to determine strains responsible for bone failure but rather proposes a concept to characterize load application in order to predict fracture risk.

Chapter 6

Subject-specific Implant Positioning for Femoral Head Resurfacing Using Goal Driven Objective Optimization Techniques and Finite Element Analysis

6.1 Introduction

There has been a lot of interest around hip resurfacing arthroplasty as a surgical alternative to total hip arthroplasty. This is due to several advantages including: femoral bone stock conservation, the use of a relatively larger and anatomically sized femoral head that reduces the chance of hip dislocation [228, 229, 364], better stress transfer to proximal femur [365], easier revision surgery for any subsequent revision, and improved technology and surgical technique. Bone conservation and non-violation of the femoral shaft make it a less invasive option. This is a significant advantage for younger and more active patients who are likely to outlive their primary hip replacement [233, 366, 367]. Available registry data suggests that hip resurfacing arthroplasty is a reasonable option for men less than sixty-five years old and women less than fifty-five years old [368].

The most common short-term concern for hip resurfacing arthroplasty is peri-prosthetic femoral neck fracture peri prosthetic femoral neck fracture affecting between 0-4% of patients undergoing the procedure, usually within months of the surgery, and is responsible for approximately 60% of early revisions. [199, 241, 369-371] The Australian National Joint Registry reports the early revision rate (<1 Year) for hip resurfacing arthroplasty in 2004 was 1.9%. This is well above the early revision rate for total hip arthroplasty. Of these revisions, 67% were due to femoral neck fracture. [11]. In a recent study of 3,497 cases of hip resurfacing in Australia, 50 fractures occurred (incidence, 1.46%) [371]. Shimmin and Black [371] also reported that fractures of the femoral neck were twice as likely in women than men and were more prevalent when the femoral implant was placed in the varus. The effect of femoral component positioning on the potential risk of neck fracture was further studied by the finite element analysis or cadaver studies, and the consensus is that valgus placement is recommended to avoid femoral neck fracture [241, 243, 372, 373]. Although Vail and colleagues [242] suggested that small deviations from the anatomic placement of the component result in high localized stresses on the femoral neck.

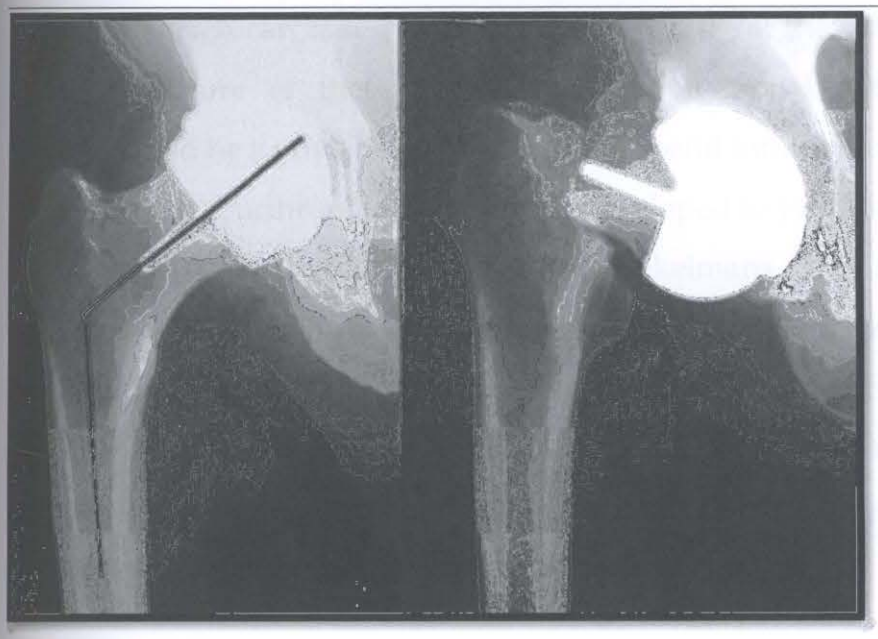

Figure 165 peri-prosthetic femoral neck fracture after femoral head resurfacing

X ray image provided Courtesy of Dr Peter Berton; Orthopaedic Surgeon Newcastle Private Hospital

Figure 165 shows a typical peri-prosthetic femoral neck fracture after femoral head resurfacing. The causes of fracture can be either patient-related or technique-related. Patient-related factors include obesity, decreased bone mass, and inflammatory arthritis. Surgical errors include notching of the femoral neck, tilting of the prosthesis into excess varus (<130° neck-shaft angle), and improper prosthetic seating. Clinical reviews have shown that patient selection [221] and implant positioning are important determinants of peri prosthetic femoral neck fracture in hip resurfacing arthroplasty patients [233, 366, 374]. Fracture rates are lower in younger males. It is assumed that this is because these younger males are more likely to have sufficient bone strength and volume to resist fracture. Also, lower rates of fracture have been observed when the femoral component is in a relatively valgus position [233, 366, 374]. However; too much valgus could lead to superior femoral neck notching, which has also been shown to increase the risk of fracture [367].

One way to enhance the hip resurfacing arthroplasty process is to evaluate the effects of an operation prior to surgery. It is clear that patient specific and technique specific factors are important and should be considered if the rate of fracture is to be minimized. Currently, the only way for surgeons to address these issues is by trial and error and clinical

experience, which can take years to develop [375]. Yet their decisions may determine the success or failure of these operations. Computational patient-specific finite element modeling could be a powerful tool to provide useful information for selection and planning of hip resurfacing arthroplasty if it can be developed to yield results that are rapid, focused and coherent from a clinical perspective. Brekelmans [376] first used an finite element model to investigate the stresses acting in a human bone under the action of physiological loads. Since then, the use of finite element analysis in orthopaedic biomechanics has constantly expanded. However, clinical reviews have relied mostly on 2D coronal plane radiographic assessments of implant position and little is known about the effect of other alignment parameters such as version on fracture.

This study attempts to address the problem of peri prosthetic femoral neck fracture with the development of a novel modelling technique, which optimizes the femoral implant position on a patient specific basis. It can be easily adapted to account for patient specific factors such as bone volume (morphology), bone quality, and load. The modeling technique aims at semi automatically optimizing the position of the femoral resurfacing implant to reduce the peri-prosthetic strain in the femoral neck. This study also investigates the influence of implant version on the peri-prosthetic strain in the femoral neck.

6.2 Methods

Utilizing the CT scan of a cadaveric femur (used for the mechanical testing in Chapter 3) a model was created of the proximal femur using the Simpleware Scan IP software. The femur was randomly selected. There was no experimental data available for comparison as this is a resurfacing rather than THA. Thus the selection of the femur has no meaning. The femoral head and neck geometry was generated by converting segmented 3-D image data from a CT scan directly into meshes suitable for physical-based simulations. The generalised technique for creating an finite element model from a CT scan using Simpleware (previously described in 4.2.2) was used to create the finite element model.

Specifically in this instance the proximal femur was segmented above the lesser trochanter, leaving the proximal femur with the femoral head and neck incorporated into the model. See Figure 166 and Figure 167.

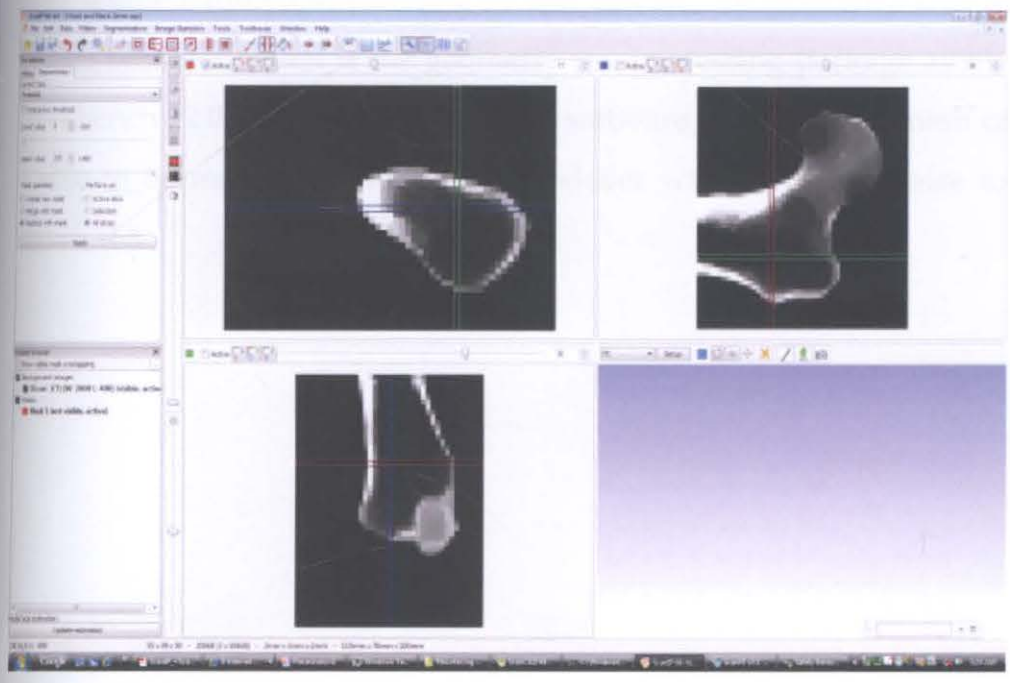

Figure 166 Proximal geometry of femur from CT scan viewed in Simpleware

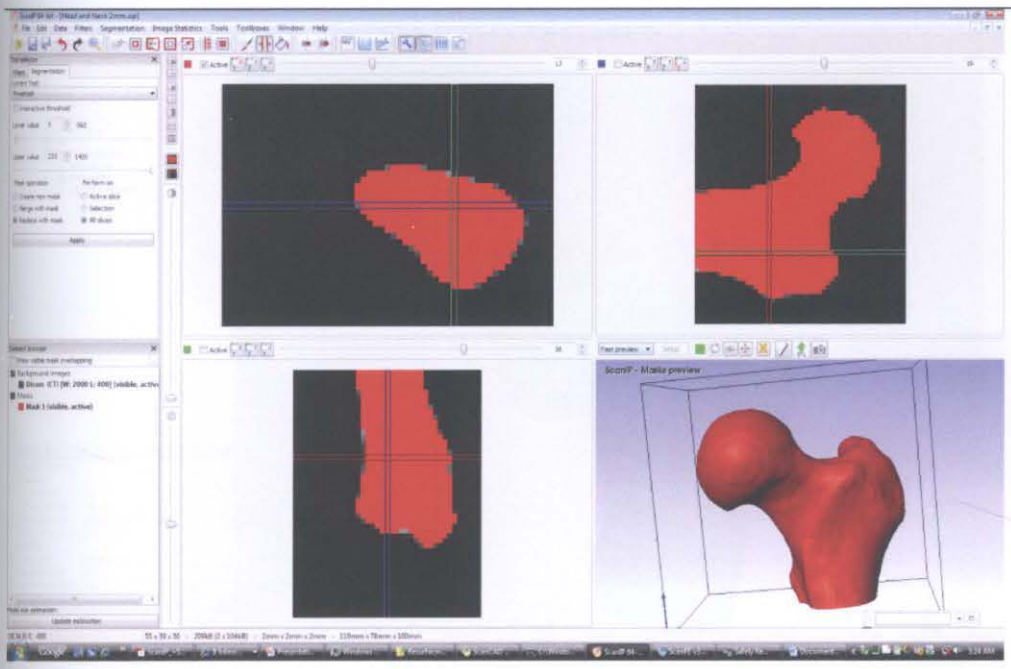

Figure 167 Proximal geometry of femur segmented from CT scan viewed in Simpleware

After segmentation and meshing in Simpleware, the geometry was imported into ANSYS Design Modeler which is the geometry pre-processing package available with the ANSYS Workbench 12.0 finite element analysis software package. The mesh created in Simpleware is able to be maintained in design modeller without compromise to mesh integrity. See Figure 168.

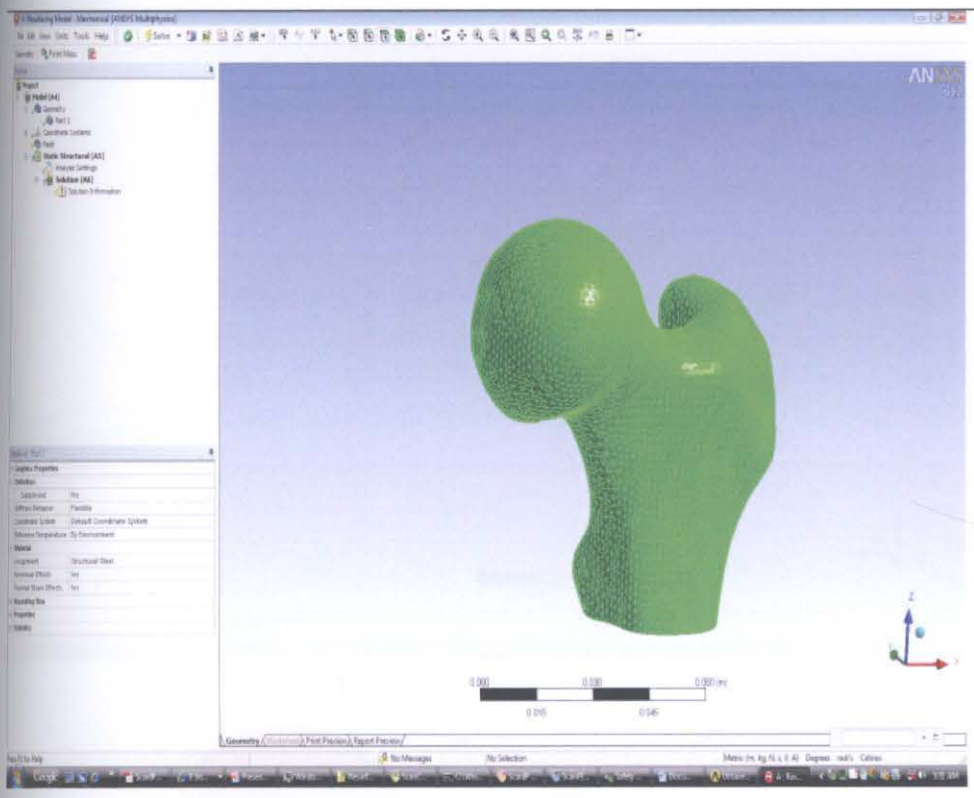

Figure 168 Proximal femoral mesh created in Simpleware is transferred into the ANSYS Design Modeler software for preprocessing

Within the Design Modeler package, some landmarks were manually identified. This was achieved by identifying the coronal plane relative to the bone model. Two points, namely, the centre of the femoral head, and the centre of the femoral neck, lying on the coronal plane, were identified and defined. The two points are depicted in Figure 169. These points were then used to define the native femoral neck axis.

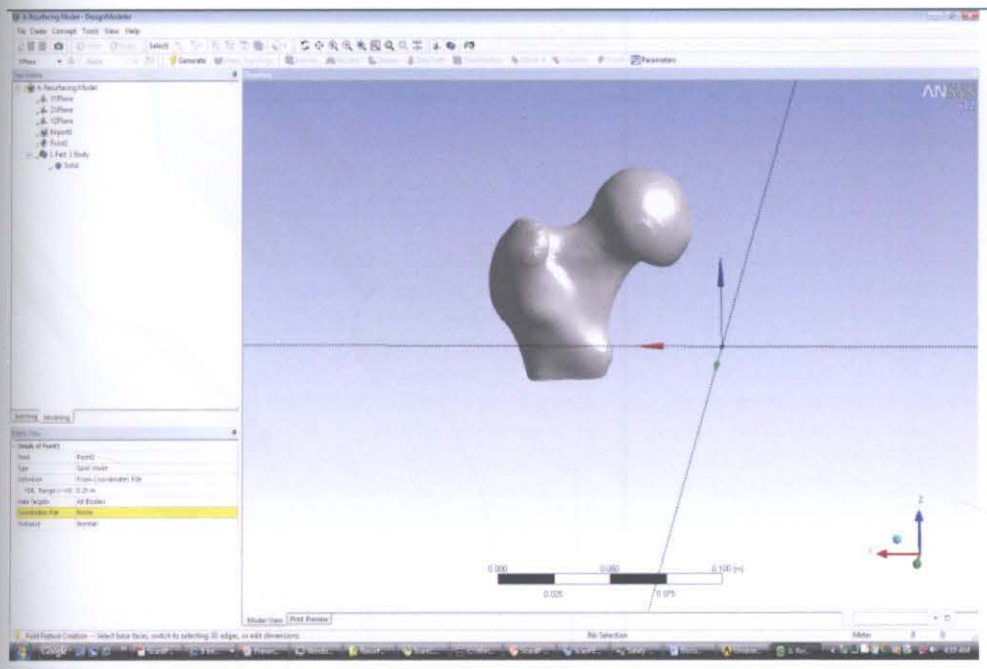

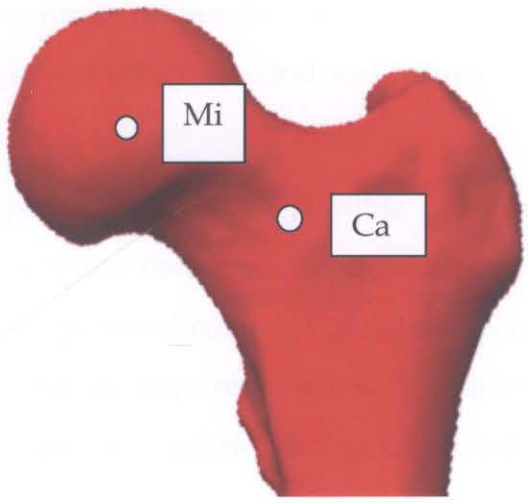

Figure 169 Identify; i) centre of femoral head; ii) centre of femoral neck as applied in this study

Importantly as described in section 2.6.4.2 (Surgical technique for Hip Resurfacing), the varus/valgus and version of the femoral component is defined by the axis of a guide wire pin that is drilled through the femoral head and neck, over which a cylindrical reamer is guided, to prepare the femoral head and neck for the implant. See Figure 170.

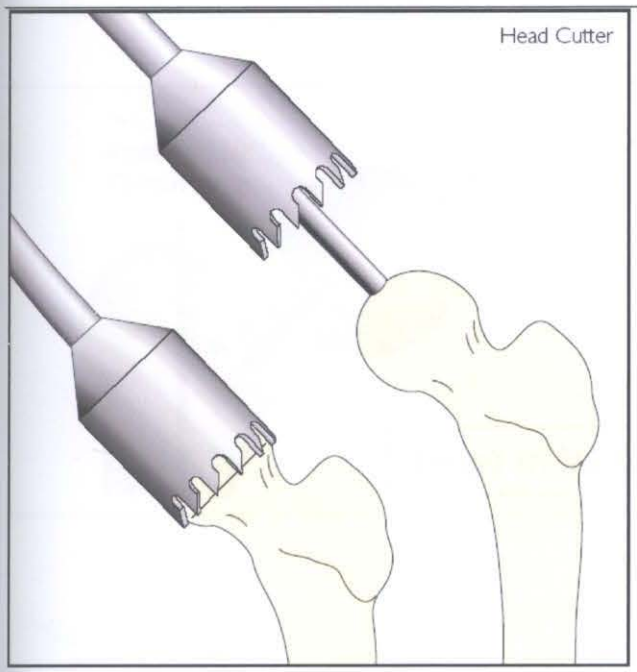

Figure 170 Femoral component position is defined by a guide wire passing through the head and neck over which a cylindrical reamer is passed during a resurfacing procedure

To describe parametrically the possible positions that the femoral component could be placed relative to the native neck axis, a function must be defined. This was achieved by defining a plane perpendicular to the native neck axis just described. To define the function, a floating point is required, whose position can be described by two parametric dimensions: a superior/inferior distance and anterior/posterior distance on the plane.

A second axis (the guide wire axis), was defined by connecting the centre of the femoral head to the floating point. This allows a parametric variation of the implant position relative to the native neck axis. As the floating point is varied in the superior inferior direction, the guide wire changes the varus/valgus position of the femoral component. See Figure 171.

As the floating point is varied in the anterior/posterior directions the guide wire changes the version of the femoral component. See Figure 172. The definition of the floating point and the guide wire axis ensures that the centre of rotation of the implant always coincides with the centre of the native femoral head to maintain femoral leg length and offset.

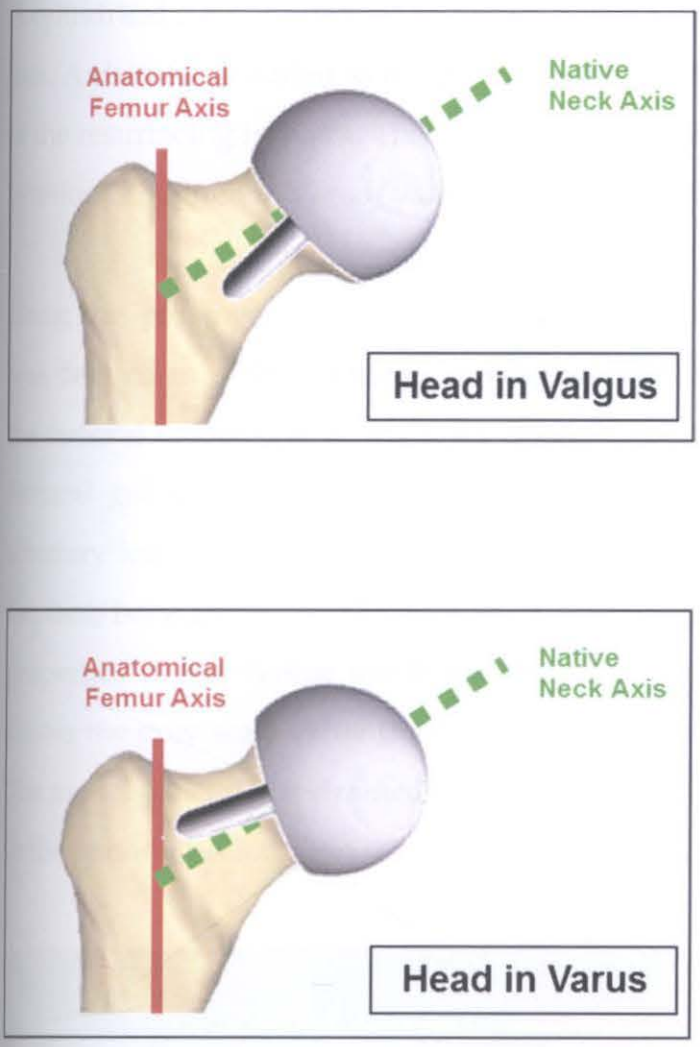

Figure 171 Changing the floating point in the superior inferior direction changes the varus valgus position of the femoral implant

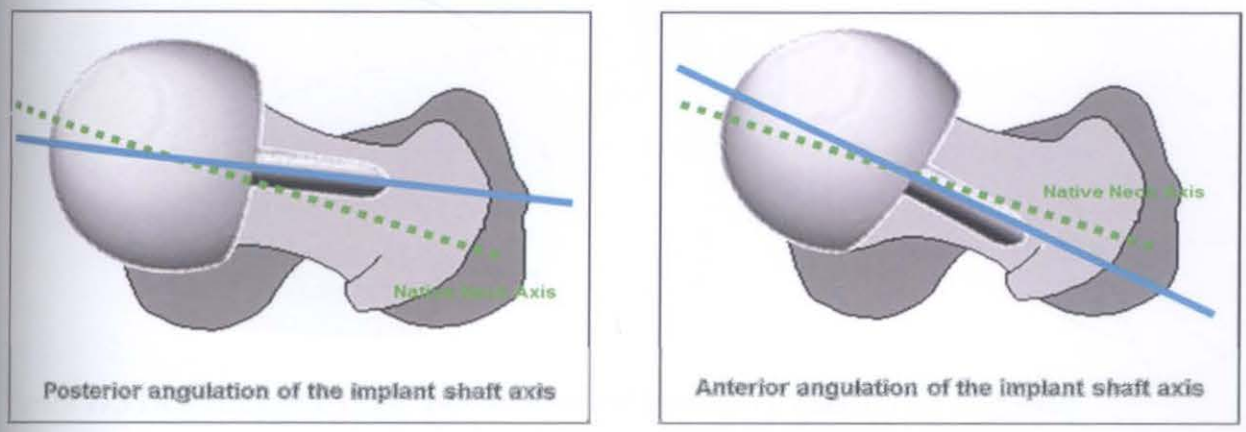

Figure 172 Changing the anterior/posterior position of the floating point changes the version of the femoral implant

A cylindrical cut out representing the surgical reaming operation, is then defined about this axis. A chamfer is added to the profile of the cut that is the same as the internal dimensions of the resurfacing implant. The cylindrical cut position and therefore the simulated femoral position is defined in varus/valgus and version by the floating point.

Using this parametric model, a deterministic finite element model as shown in Figure 173 was defined in ANSYS Design simulation. The arbitrary position (or starting position) of the femoral component is when the floating point lies on the femoral neck axis. That is the femoral guide wire axis is co-incident with the native femoral neck axis. A simplified arbitrary load of 1000N, representing patient specific load, was applied to the bone at the implant/bone interface. To conserve computational resources, I assumed that the material properties of the femur are homogeneous. Although a material mapping strategy that relates the grey scale value from the CT scan to the material properties could also be used. The model was fully restrained at the distal face of the bone. The maximum principal strain in the femoral neck region was designated as the output parameter. See Figure 174.

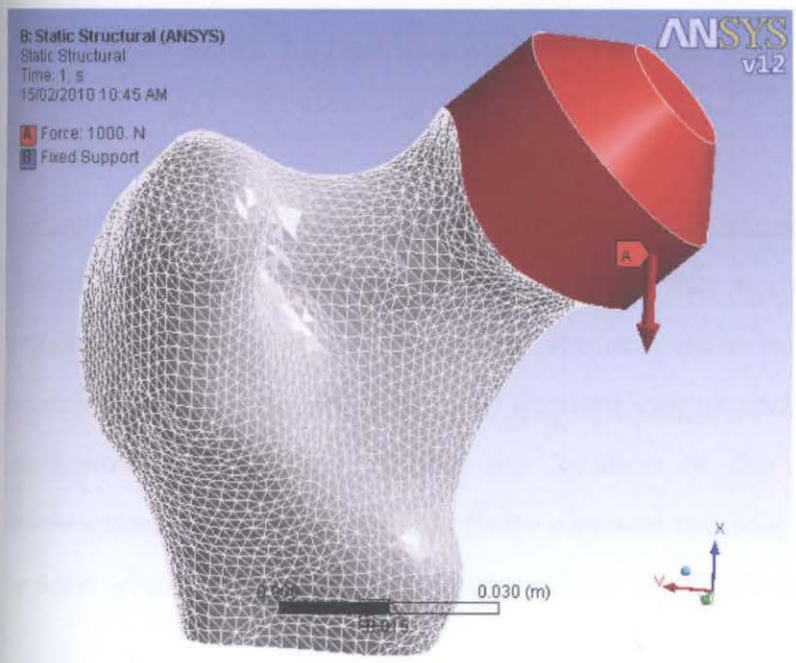

Figure 173 Deterministic finite element model boundary conditions and load

6.2.1 Goal driven optimisation

6.2.1.1 Sample space

Before the automated goal driven optimisation can be undertaken the sample space must be defined. This is achieved by manually varying the floating point to find the extremes at which the cylindrical reaming operation actually cuts into the femoral neck causing a notch.

6.2.1.2 Design of Experiments

A Design of Experiments was then setup within the ANSYS Workbench 12.0 interface. A Kringin type Design of Experiments was used, where the two continuous input parameters defined by anterior/posterior and superior/inferior dimensions of the floating point were varied in the range or sample space determined.

6.2.1.3 Goal driven optimization

The Design of Experiments was solved and a response surface was generated. The Goal Driven Optimization was set as the point where the maximum principal strain gets minimized with the highest importance. The input parameters were not given a goal.

6.3 Results

Figure 174 shows a typical strain contour plot obtained from the optimization. All of the deterministic finite element models that are not on the extremes show the maximum principal strain to be at the superior femoral neck, near to but not at the implant/bone boundary. The extreme positions of implant valgus and version angles have relatively high maximum principal strains but the location of the maximum is at the notch. When investigated using deterministic finite element models, very small notches of the neck can be seen where the high strain concentrations are observed.

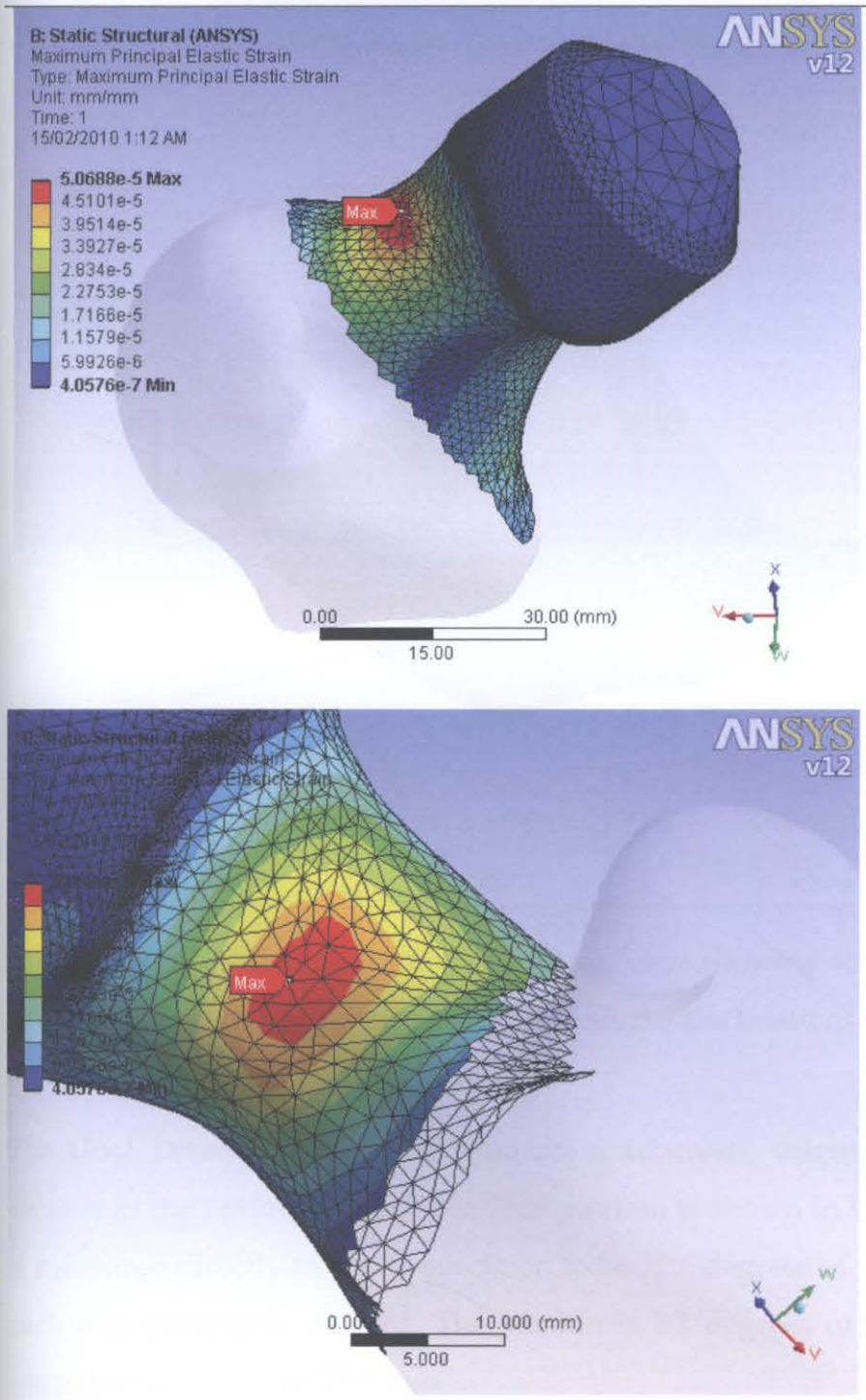

Figure 174 Typical strain contour plot- maximum principal strain location

The response curve from the Design of Experiments, as shown in Figure 175, shows that the model is sensitive to changes in implant varus / valgus and version, with a tendency towards relative valgus and neutral version giving the lowest maximum principal strain in the neck.

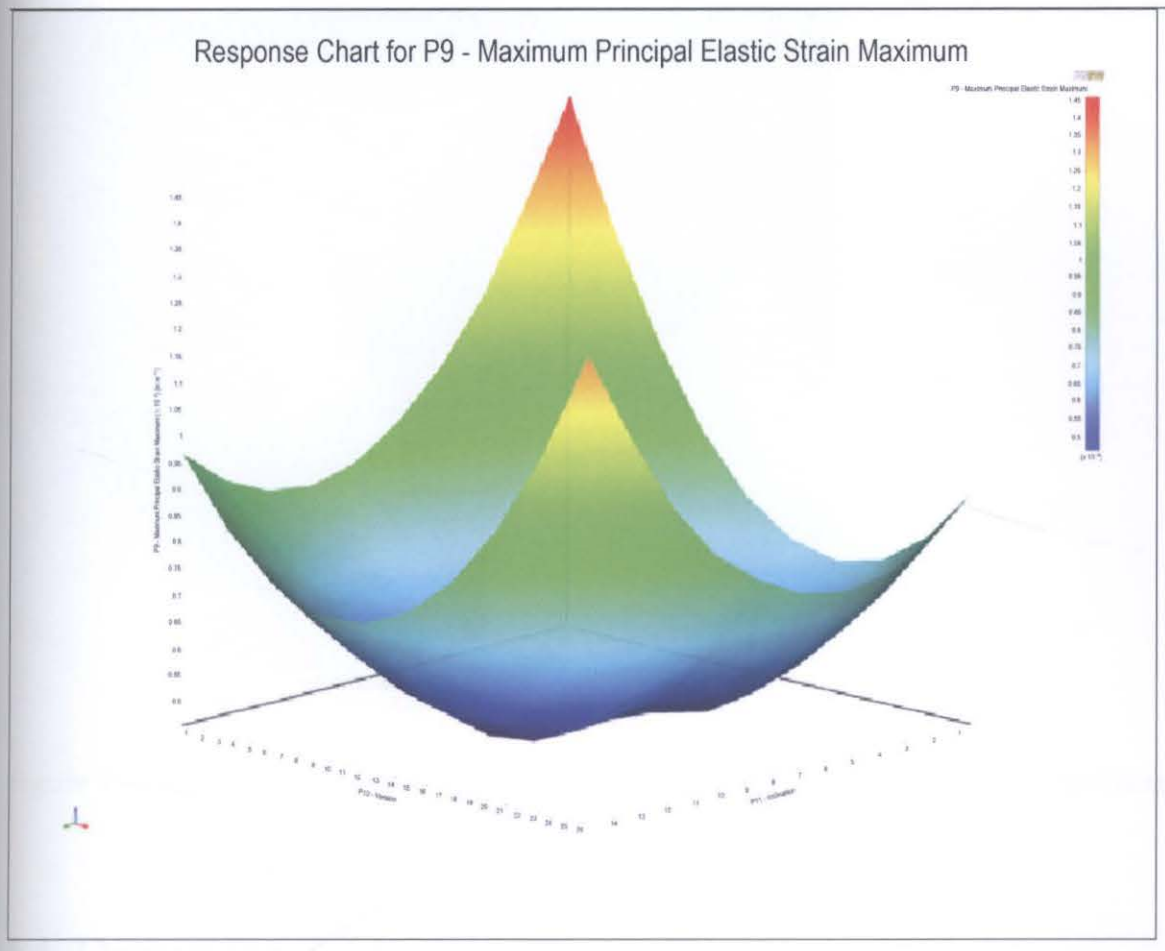

Figure 175 Design of Experiments response curve showing strain level on the vertical axes, version on the left horizontal and varus/valugus (inclination) on the right side horizontal

The Goal Driven Optimization outputs a relatively valgus neck position with neutral version as the optimized position. This position is shown in Figure 176. The exact position is measured directly from the specimen to be 12.6 degrees of valgus relative to the femoral neck axis previously defined. The version is 0.1 degrees of ante version (approximately neutral) relative to the neck axis.

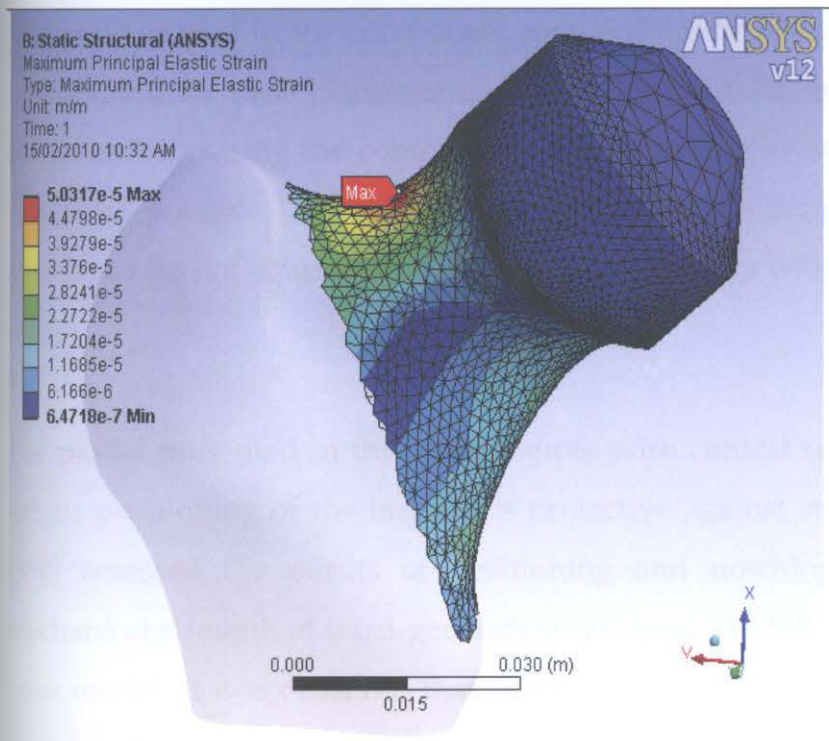

Figure 176 The optimized position and contour plot from the goal driven optimization

6.4 Discussion

This Chapter describes the development of a novel, patient specific finite element analysis modeling technique that utilizes a Design of Experiments approach with a goal driven optimization. It shows a simplified finite element modeling technique that reliably predicts an optimal implant position, which will give minimal strain in the peri-prosthetic bone tissue. This should translate to an implant position that has a reduced risk of peri prosthetic femoral neck fracture.

The study shows that the location of the maximum strain, for all non-notching positions, was on the superior femoral neck, in the peri-prosthetic bone tissue. It showed that varus positioning resulted in higher strain while valgus positioning reduced the strain. This is consistent with other reports from the literature as described below. Further, it showed that neutral version had lower strain.

Concern about the possibility of femoral neck fracture is a major issue currently limiting hip resurfacing arthroplasty. Several authors [233, 234] have suggested the degree of varus-

valgus placement of the component stem within the femoral neck affects the likelihood of fracture, but the ideal placement is yet to be known. Recommendations have been made to surgeons for placing the component range from slight valgus, [228, 377, 378] to as much valgus as possible [227, 374, 379]. These recommendations are generic and not patient specific so do not consider patient specific variability which is known to influence fracture risk.

The model presented in this study agrees with clinical reviews and previous studies that valgus positioning of the implant is protective against strain. For example, Nabavi et al. [380] assessed the effects of positioning and notching of resurfaced femurs on the mechanical strength of third-generation saw bone (TGSB) femurs using an *in vitro* analogue bone model. It was observed that, compared to the intact femurs, the load to failure in all resurfaced femurs was significantly decreased (29% - 57% reduction). Among the resurfaced femurs, valgus and anatomic femurs had the highest load to failure, followed by valgus notched, varus, and anatomically notched femurs. Notching weakened the construct by a further 24% - 30%.

Richards et al. [243] also suggested that a valgus orientation decreases the risk of peri prosthetic femoral neck fracture following hip resurfacing. Furthermore, obtaining the maximum possible valgus angle, while avoiding notching, may in fact provide the optimum protection from peri prosthetic femoral neck fractures. The model in this chapter also predicts that an implant version, relatively neutral to the femoral neck, is optimum.

The actual magnitudes of principle strains were not relevant in this scenario because of the simplification of material properties. Rather there is relevance in the relative values, which are shown.

Chapter 7

Conclusions

7.1 Concluding Points:

7.1.1 Chapter 3: A Plasma-Sprayed Titanium Proximal Coating Reduces the Risk of Peri-Prosthetic Femoral Fracture in Cementless Hip Arthroplasty

- In this study, two experimental cementless femoral designs were compared; the ABG II-plasma and ABG II-NMS, with the commercially available ABG II-standard cementless implant.
- Results show that the modified ABG II-plasma, with a high-friction titanium plasma-sprayed proximal coating, was associated with increased load-bearing capacity and lower surface strains as compared to the ABG II-standard.
- The surface strains with the plasma-sprayed stem were closer to those of the native bone, suggesting a more anatomic load transfer to the proximal femur.
- Less dramatic differences between the ABGII-NMS and the ABG-II standard were observed with only a localized change in the strain sensitivity in the gauges immediately around the modification.
- The most significant finding in this work was that the failure load of the ABG II-plasma-implanted bone was an average 42% (32% median) greater than that of the ABG II-standard-implanted femurs.
- Thus, the load-bearing capacity of the femur in the early post-operative period would be greater when a plasma-sprayed stem is used, rather than a smooth stem. Clinically this would decrease the risk of early peri-prosthetic femoral fracture by creating a factor of safety against fracture.
- The observed differences between the ABGII plasma and the ABGII standard can be explained by an increase in the frictional forces at the bone-implant interface. The increased frictional forces are due to the addition of the roughened plasma-sprayed coating, which increases the friction co-efficient at the interface. The increased frictional force at the interface can better resist the slippage of the implant into the femoral canal when the implant is forced into the femur under simulated anatomic loading.

- The resistance prevents a wedging effect that would expand the proximal femur and result in an increase in hoop strains in the bone.
- This theory is supported by the finding that, when compared to ABG II-standard; the ABG II-plasma implant was on average seated higher in the femur after insertion.
- The higher final seating with the ABGII- Plasma is, however, in itself a concern. The plasma-spray coating of the ABG II-plasma added thickness to the implant and did , therefore, result in an oversize of the implant relative to the broach. The thicker coating might lead the surgeon to inadvertently induce an intra-operative peri-prosthetic femoral fracture by trying to seat the thicker stem further into the canal. Despite the increased friction, the thicker stem would then cause higher hoop stresses in the bone at the same level due to further expansion of the bone canal.
- It can be concluded that the additional thickness of the coating caused the plasma-sprayed stem to be seated higher on average than the other stems.
- Fractures during stem insertion were not observed; however, this may not be the case in a wider clinical setting. It is conceivable that an increased incidence of intra-operative peri-prosthetic femoral fracture could be seen if the addition of a plasma coating to the implant was not accompanied by new broaching instruments and this must be a consideration.
- It is, however, possible that the additional thickness could be advantageous. The addition of thickness will undoubtedly result in a tighter apposition of the implant against the bone. The common design principle for cementless femoral stems is to achieve a close fit of the prosthesis, to restore strains in the proximal femur, and obtain maximum stability of the implant.
- It was also observed that the experimental plasma-sprayed stem appeared to load the femur more anatomically; the surface strains on the specimens implanted with ABG II-plasma were closer to those of the anatomic femur as compared to the other comparative stems. This is advantageous, as anatomic load transfer would cause less pronounced stress shielding, thereby preserving the proximal femoral bone.
- It is important to point out, however, that the differences observed between the ABGII- Plasma and the ABGII-Standard may not persist beyond the early post-operative period.

- The ABG II-NMS version was devoid of medial scales that are intended to promote proximal load transfer. The experimental results show that the removal of the medial scales did not appear to have a dramatic effect on the overall scenario. There was no observed difference in the maximum impaction strains, the seating heights, nor any difference for the residual strains. However, a localized difference was observed for the strain sensitivity measurements at the M and PM gauges. The ABG II-NMS stem was significantly more tensile than ABG II-standard for the M gauge ($P < 0.0001$), and significantly less tensile for the PM gauge ($P < 0.0001$). No strong conclusions could be drawn from this result, other than to say that the removal of the medial scales has a less dramatic effect on the strain state of the proximal femur than the addition of the plasma coating

7.1.2 Chapter 4: Subject-specific Finite Element Modeling of Peri-prosthetic Femoral Fracture using Element Deactivation to Simulate Bone Failure

- In this chapter, the development of a simplified patient-specific finite element modeling methodology to predict peri-prosthetic femoral fracture in the early postoperative period is described. This novel patient-specific modeling methodology, which uses crack propagation (element deletion), can help predict peri-prosthetic femoral fracture in the early postoperative period.
- This study has determined that the element deletion tool may be a good tool to aid the prediction of fracture load in addition to fracture risk characterization.
- The approach taken was a significant advance because it used a novel technique to simulate bone failure and was not derived from an element-specific failure risk calculation. The novel technique utilised a newly available feature in the ABAQUS CAE module to simulate the failure of the bone. That is, the capability to set element deactivation or deletion based upon a threshold field value.
- The threshold field value chosen for this analysis was strain. The use of strain-based criteria was used because it has become clear that strain-based failure criteria are superior to other failure criteria.

- The failure load is sensitive to the friction coefficient at the implant-bone interface, as was also found in Chapter 3.
- No previous studies have associated friction coefficients with fracture loads. In this study, the finite element models with lower friction coefficients showed failure loads that were closer to those seen in the experimental specimens. Therefore, I believe that the failure load is sensitive to the friction coefficient. Further studies in this area may help in calibration of the unknown friction coefficient if the failure load is known.
- Ambiguity in the ISO 7206 - 4 testing standard exists because of broad specification for the experimental setup allowed. The ambiguity exists because friction between the test machine and the implant is not standardised.
- This chapter investigated the allowable setups and proposes a setup that has less sensitivity to friction. This issue is important to highlight for because the variability in the testing standard could affect future testing setups resulting in misleading conclusions. This is a very important finding from this work.
- The finite element models were compared with the femoral test specimens, from which they were created, as well as with the specimens from the contralateral side of the same donor.
- When comparing the models to the experimental testing, the crack mode for the biphasic models was very similar to the mechanical testing crack mode, with a similar shape of the crack, and similar crack path.
- The results showed that the finite element analysis models over-predicted the femoral strength, especially in the triphasic models. Both the biphasic and the triaphasic models appeared to be stiffer than the test specimens, which may have contributed to the over-prediction.
- The reason for the additional stiffness is thought to be because of the chosen method of material property assignment.
- An explanation for the increased stiffness in the triphasic models would be the presence of middle bone, the layer between cortical and cancellous bone that was included in the finite element model, with a high modulus of elasticity.
- As the process of failure is more complicated than mere identification of a localized failure initiation point; calculation of a failure risk criteria may be inappropriate,

especially in situations with implants being modeled in situ. Thus, simulation of bone failure via the "element deactivation" technique seems rather justified.

- In the experimental specimen, structural failure was observed due to a brittle crack that occurred in the cortical bone, caused by a sharp decrease in load after reaching a peak value with no noticeable decrease in the slope of the curve immediately before failure. This suggests generalized yielding rather than localized yielding of the cancellous bone supporting the implant. This theory was supported by observations from the experimental testing that prior to failure; the prosthesis was slowly displaced into the femoral canal causing a wedging effect on the cortical bone.
- When comparing the models to the experimental testing, the crack mode for the biphasic models was very similar to the mechanical testing crack mode, with a similar shape of the crack, and similar crack path. The new modeling technique is promising and could, allow for the characterisation of subject specific peri-prosthetic femoral fracture in the early post-operative period.

7.1.3 Chapter 5: Subject-specific finite element model with an optical tracking system in total hip replacement surgery

- I proposed a novel dynamic subject specific finite element analysis model that can be used in conjunction with a navigation system to characterise the load the surgeon places on the patient's bone tissue during total hip replacement surgery
- I experimentally measured the swing velocity of a mallet in a simulated surgical setting to be 1.5 m/s with little variability (1.3 - 1.8 m/s)
- This value compared reasonably with previous studies
- In the finite element analysis model, I simulated two friction states between the implant and the bone (0.1 and 0.4 friction coefficients) and showed significant differences between the friction states
- This is consistent with the previous work in this thesis, showing that the roughness (friction coefficient) has an effect on the mechanics of the implant / bone construct

- Higher strains were recorded in the anterior gauges of the model with the lower friction coefficient
- Higher displacement of the implant into the femur was observed with the lower friction model
- This caused a wedging effect (described in Chapter 3) which caused higher hoop stresses and lower shear stresses in the model
- The results suggest the lowest risk of fracture would be with higher friction coefficient (rougher proximal coating)
- With further development, this system (combination of subject specific finite element analysis and a navigation system) could be used to predict a pre-operative swing velocity threshold for the mallet by determining the mallet velocity above which peri-prosthetic femoral fracture could be expected (fracture threshold).
- During surgery, the navigation system could be used to measure and report to the surgeon in near to real-time, the velocity at which they are swinging the mallet.
- The system could alert the surgeon if they are approaching the threshold value. This would allow the surgeon to modify their swing velocity to prevent peri-prosthetic femoral fracture.
- This novel technique has the potential to be adapted for future clinical use to aid in the prevention of peri-prosthetic femoral fracture. A patient-specific finite element analysis model could be created preoperatively and, if well prepared, could account for the patient-specific parameters of bone strength in this setting.
- An iterative determination of the maximum mallet velocity, above which excessive surgical loads might lead to intraoperative Peri-Prosthetic Femoral Fracture, could be determined and set aside as a threshold value.

7.1.4 Chapter 6: Patient specific implant positioning for femoral head resurfacing using goal driven objective optimization techniques and Finite Element Analysis

- This Chapter describes the development of a novel, patient specific Finite Element Analysis modeling technique that utilizes a Design of Experiment approach with a goal driven optimization.
- It shows a simplified finite element modeling technique that reliably predicts an optimal implant position, which will give minimal strain in the peri-prosthetic bone tissue. This should translate to an implant position that has a reduced risk of peri-prosthetic femoral fracture.
- The study shows that the location of the maximum strain, for all non-notching positions, was on the superior femoral neck, in the peri-prosthetic bone tissue.
- It showed that varus positioning resulted in higher strain while valgus positioning reduced the strain. This is consistent with other reports from the literature as described below.
- Further, it showed that neutral version had lower strain.
- Concern about the possibility of femoral neck fracture is a major issue currently limiting hip resurfacing arthroplasty.
- Recommendations have been made to surgeons for placing the component range from slight valgus, to as much valgus as possible. These recommendations are generic and not patient specific so do not consider patient specific variability which is known to influence fracture risk.
- The model presented in this study agrees with clinical reviews and previous studies that valgus positioning of the implant is protective against strain.
- The model in this chapter also predicts that an implant version, relatively neutral to the femoral neck, is optimum.
- Further work needs to be directed towards testing the sensitivity of the predictions to these simplifications. Such as:
    (i) investigating the sensitivity of the model to heterogeneous material properties, abnormal and arthritic bone morphologies,
    (ii) automating the parameterization of the geometry,

(iii) including patient specific loading characteristics,

(iv) including combined acetabular and femoral component position parameters in the optimization to include maximum range of motion and/or improved biomechanics, and reduce the edge loading effects on the hard on hard bearing, and

(v) investigating the possibility of including centre of joint rotation changes in the optimization.

7.2 Thesis Summary

This thesis project has looked to reduce the risk of peri-prosthetic femoral fracture for total hip replacement and femoral head resurfacing patients by considering; implant design, patient specific factors and procedure-specific factors. Where possible these factors are considered in a combined sense. Towards this pursuit, special attention has been given to the application of subject specific finite element analysis and computer assisted orthopaedic surgery.

This work begins in Chapter 3 by answering an important question around implant design and the risk of peri-prosthetic femoral fracture in total hip arthroplasty: To reduce the risk of peri-prosthetic femoral fracture, should the proximal femoral coating of a femoral stem be roughened or smooth? Utilizing mechanical testing with matched pairs of cadaveric femoral specimens it has been conclusively shown that the risk of peri-prosthetic femoral fracture in the early post-operative period is significantly diminished if a roughened coating is utilized. Specifically, in this instance, a plasma sprayed titanium proximal coating on the ABGII stem increased the load bearing capacity of the femur-implant construct by an average of 42% when compared to the currently available grit blasted with HA coating implant. This work has initiated a redesign of the current ABGII femoral stem with the manufacturer Stryker planning to discontinue the smooth ABGII stem and release a version in 2012 that has a roughened proximal coating.

Building on this work in Chapter 4, a novel patient-specific Finite Element Analysis modeling technique was developed, which attempts to predict peri-prosthetic femoral fracture around an implanted cementless femoral stem. The technique considers the design

(shape and material properties) of the implant together with patient-specific bone parameters, including patient specific bone geometry and the incorporation of bone material properties.

The technique utilizes the element deletion capability within ABAQUS 6.9 to simulate material failure and crack propagation. This allows for a determination of the load to failure of the entire bone/implant structure; not just a localized failure initiation point. Accounting for the post failure behavior of the localized bone (which may contribute to, but not fully characterize, the full structural failure of the bone/implant structure) is the major advance with this technique. With this approach, there is the potential to preoperatively characterize a specific patient's risk of peri-prosthetic femoral fracture if a particular implant design is chosen.

However, a significant limitation of this approach is evident in the intra-operative setting where many peri-prosthetic femoral fracture do occur. How to account for the surgical variable load that the surgeon applies to the patient during the procedure is the main problem with predicting peri-prosthetic femoral fracture in an intra-operative setting. Firstly, the load is not consistent or regulated; and secondly it is not quasi static, it is a dynamic impulse force. The method proposed and presented in Chapter 5 overcomes both of these issues. Firstly, utilizing a computer assisted orthopaedic surgery system in a novel way to collect velocity information that is derived from positional information creates an input into a dynamic patient-specific finite element analysis model. Secondly, the fact that the Explicit finite element solver allows for the modeling of a dynamic impulse, rather than a quasi-static load, allows for realistic modeling of the surgery-specific loading conditions. This technique could be used to reduce the risk of peri-prosthetic femoral fracture by regulating a surgeons behavior (avoiding overloading) in the operating room whilst also considering that specific patient's bone strength in that specific scenario. The unique combination of all these technologies as a system in the operating room could provide a significant step towards eliminating the risk of peri-prosthetic femoral fracture in conventional total hip arthroplasty

Chapter 6 looks at femoral head resurfacing where peri-prosthetic femoral fracture is a major concern. Efforts to reduce the risk of peri-prosthetic femoral fracture around a femoral head resurfacing should also consider both procedure-specific and patient-specific factors. Much work has been done characterizing procedure-specific and patient-specific factors in isolation from each other, with consensus converging on two different focal points. Firstly, efforts should be made by the surgeon to orientate the femoral component into relative valgus. Secondly, patient selection should be utilized to eliminate patients with a poor bone strength capacity. Looking towards a patient-specific modeling technique used to consider both of these points together would minimize that patient's risk of peri-prosthetic femoral fracture. This was achieved by setting up a Design of Experiments approach and utilizing a goal driven optimization methodology in conjunction with patient specific finite element analysis techniques to isolate the optimum patient-specific femoral component alignment. Combining this patient specific determination of an ideal implant position with a computer assisted orthopaedic surgery system would allow not only for the determination of an ideal position, but also the delivery of that ideal position.

This body of work has made significant progress in addressing the need to reduce the instance of peri-prosthetic femoral fracture for both total hip replacement and femoral head resurfacing by considering the prosthesis, the patient and the procedure.

References

1. Adams, S., *Illustrated Essentials of Musculoskeletal Anatomy, Fifth Edition (2009).* , 2009.
2. Kim SJ, M.M., Hernandez J, Wixson RL, *Computer assisted navigation in total knee arthroplasty: improved coronal alignment.* J Arthroplasty, 2005. **20**(7 Suppl 3): p. 123-131.
3. Giardini S, F.C., Laney D, Rutherford A, *Monitoring Femoral Component Insertion in Cementless total hip arthroplasty.* In Proceedings of the Twenty third International Modal Analysis Conference (IMAC) on Structural Dynamics, 2005. **31**.
4. *(Arthritis - the bottom line. The economic impact of arthritis in Australia.* Access Economics, 2005.
5. *Centers for disease control and prevention; Prevalence of disabilities and associated health conditions among adults-United States, .* MMWR Morb Mortal Wkly Rep, 1999, 2001. **50(7)**: p. 120-125.
6. *(National population projections, 2008-based.* Office for National Statistics, 2009.
7. *(The bone and joint decade 2000-2010 for prevention and treatment of musculo-skeletal disorders* Acta Orthop Scand Suppl, 1998. **281**: p. 1-86.
8. Kurtz, S., et al., *Prevalence of primary and revision total hip and knee arthroplasty in the United States from 1990 through 2002.* J Bone Joint Surg Am, 2005. **87**(7): p. 1487-97.
9. Kurtz, S.M., et al., *Future clinical and economic impact of revision total hip and knee arthroplasty.* J Bone Joint Surg Am, 2007. **89 Suppl 3**: p. 144-51.
10. Kurtz, S., et al., *Projections of primary and revision hip and knee arthroplasty in the United States from 2005 to 2030.* J Bone Joint Surg Am, 2007. **89**(4): p. 780-5.
11. Graves, D., Ingerson, et al. , *The Australian Orthopaedic Association National Joint Replacement Registry.* Med J Aust 2004. **180**: p. S31-4.
12. Herberts, Kärrholm, and Garellick, *The Swedish National Hip Arthroplasty Register, Department of Orthopaedics Sahlgrenska University Hospital.* 2005.
13. Mont, Amstutz, and Boyd, *Modern Generation Metal-on-Metal Total Hip Resurfacings.* Proceedings of 2007 Annual Meeting of the American Academy of Orthopedics Surgeons, 2007: p. Poster NO. P034.
14. Elias, J.J., et al., *Medial cortex strain distribution during noncemented total hip arthroplasty.* Clin Orthop Relat Res, 2000(370): p. 250-8.
15. Young, S.W., C.G. Walker, and R.P. Pitto, *Functional outcome of femoral peri prosthetic fracture and revision hip arthroplasty: a matched-pair study from the New Zealand Registry.* Acta Orthop, 2008. **79**(4): p. 483-8.

16. Franklin, J. and H. Malchau, *Risk factors for periprosthetic femoral fracture.* Injury, 2007. **38**(6): p. 655-60.
17. Amstutz, H.C., et al., *Complications after metal-on-metal hip resurfacing arthroplasty.* Orthop Clin North Am, 2011. **42**(2): p. 207-30, viii.
18. Schileo, E., et al., *Subject-specific finite element models implementing a maximum principal strain criterion are able to estimate failure risk and fracture location on human femurs tested in vitro.* J Biomech, 2008. **41**(2): p. 356-67.
19. Nogler, M., et al., *Reduced variability of acetabular cup positioning with use of an imageless navigation system.* Clin Orthop Relat Res, 2004(426): p. 159-63.
20. Kalteis, T., et al., *Imageless navigation for insertion of the acetabular component in total hip arthroplasty: is it as accurate as CT-based navigation?* J Bone Joint Surg Br, 2006. **88**(2): p. 163-7.
21. Wixson, R.L. and M.A. MacDonald, *Total hip arthroplasty through a minimal posterior approach using imageless computer-assisted hip navigation.* J Arthroplasty, 2005. **20**(7 Suppl 3): p. 51-6.
22. Weiner, S. and H. Wagner, *The material bone: structure-mechanical function relations. .* Ann Rev Mater Sci 1998. **28**: p. 271-98.
23. Elliott, S.R. and R.A. Robinson, *The water content of bone. I. The mass of water, inorganic crystals, organic matrix, and CO2 space components in a unit volume of the dog bone.* J Bone Joint Surg Am, 1957. **39-A**(1): p. 167-88.
24. Martin, R.B., *Porosity and specific surface of bone.* Crit Rev Biomed Eng, 1984. **10**(3): p. 179-222.
25. Lucchinetti, E., *Composite models of bone properties.* In: Bone mechanics handbook, 2nd ed2001, Boca Raton, FL: CRC Press.
26. Zhu, W., P. Robey, and A. Boskey, *The regulatory role of matrix proteins in mineralization of bone.* In: Osteoporosis. 3rd ed, ed. Marcus R and N.D. Feldman D, Rosen CJ, editors. Vol. Chapter 9. 2008, New York, NY: Academic

Press.
27. Boskey, A., *Mineralization of bones and teeth.* Elements Magazine, 2007. **3**: p. 385-391.
28. Grynpas, M.D., et al., *Effect of age and osteoarthritis on bone mineral in rhesus monkey vertebrae.* J Bone Miner Res, 1993. **8**(8): p. 909-17.
29. Grynpas, M., *Age and disease-related changes in the mineral of bone.* Calcif Tissue Int, 1993. **53 Suppl 1**: p. S57-64.
30. Ginebra, M., J. Planell, and M. Onta~n_on, Aparicio, C. , *Structure and mechanical properties of cortical bone.* In: Structural biological

materials.2000, New York: Pergamon Press.
31. Martin, R., D. Burr, and N. Sharkey, *Skeletal tissue mechanics*1998, New York: Springer-Verlarg.
32. Cowin, S.C., *Bone poroelasticity.* J Biomech, 1999. **32**(3): p. 217-38.

33. Currey, J., *Bones.* Structure and mechanics2002, Princeton, NJ: Princeton University Press.
34. Miller, S. and W. Jee, *Bone lining cells.* In: Bone. Vol. vol. 4. 1992, Boca Raton, FL: CRC Press.
35. Cowin, S.C., L. Moss-Salentijn, and M.L. Moss, *Candidates for the mechanosensory system in bone.* J Biomech Eng, 1991. **113**(2): p. 191-7.
36. Lanyon, L.E., *Osteocytes, strain detection, bone modeling and remodeling.* Calcif Tissue Int, 1993. **53 Suppl 1**: p. S102-6; discussion S106-7.
37. Skerry, T.M., et al., *Early strain-related changes in enzyme activity in osteocytes following bone loading in vivo.* J Bone Miner Res, 1989. **4**(5): p. 783-8.
38. Burger, E., *Experiments on cell mechanosensivity: bone cells as mechanical engineers.* In: Bone mechanics handbook. Vol. chapter 28. 2001, Boca Raton, FL: CRC Press.
39. Moore, K.L., *The Lower Limb.* 3rd Edition ed. In: Clinically orientated anatomy1992, Baltimore, MD, USA: Williams & Wilkins.
40. Dean, C. and J. Pegington, *The gluteal region and the hip joint.* In: Core anatomy for students. The limbs and vertebral column2000, London: W.B. Saunders Company Ltd. 106-116.
41. Murray, I.M., *The Lower Limb* In: Human Anatomy Made Simple1971, London: W.H. Allen.
42. Dean, C. and J. Pegington, *The front and sides of the thigh.* Core anatomy for students. The limbs and vertebral column2000, London: W.B. Saunders Company Ltd.
43. Churchill, M.A., M. Brookes, and J.D. Spencer, *The blood supply of the greater trochanter.* J Bone Joint Surg Br, 1992. **74**(2): p. 272-4.
44. Nalla RK, K.J., Ritchie RO, *Mechanistic fracture criteria for the failure of human cortical bone.* Nat Mater 2003. **2**: p. 164-168.
45. Carter DR, H.W., *The compressive behavior of bone as a two phase porous structure.* J Bone Joint Surg Am 1977. **59**: p. 954-962.
46. clinic, M.; Available from: http://www.mayoclinic.com/health/medical/IM03867.
47. Stöckl B, N.M., Rosiek R, Fischer M, Krismer M, Kessler O, *Navigation improves accuracy of rotational alignment in total knee arthroplasty.* Clin Orthop Relat Res, 2004. **426**: p. 180-186.
48. Smith-Petersen, M.N., *The classic: Evolution of mould arthroplasty of the hip joint by M. N. Smith-Petersen, J. Bone Joint Surg. 30B:L:59, 1948.* Clin Orthop Relat Res, 1978(134): p. 5-11.
49. Pramanik, S., A.K. Agarwal, and R. K.N, *Chronology of Total Hip Joint Replacement and Materials Development.* Trends Biomater. Artif. Organs, 2005. **19**(1): p. 15-26.

50. Charnley, J., *Low Friction Arthroplasty of the Hip - Theory and Practice*1979, Berlin Springer-Verlag.
51. Ritter, H., U. Dege, and R. Kubba, *Initial experiences with a total knee prosthesis implanted without bone cement.* Arch Orthop Trauma Surg, 1979. **95**(1-2): p. 89-93.
52. Itami, Y., et al., *A cementless system of total hip prosthesis. Experimental studies on total hip prosthesis in dogs.* Arch Orthop Trauma Surg, 1982. **100**(3): p. 183-9.
53. Saito, S., et al., *The Harris-Galante Cementless THA: A 19- to 25-Year Follow-Up Study.* Orthopedics, 2011. **34**(1): p. doi: 10.3928/01477447-20101123-08.
54. Stastny, E., et al., *[Cementless total hip replacement type S.F.: mid-term results].* Acta Chir Orthop Traumatol Cech, 2009. **76**(6): p. 487-94.
55. Mantelos, G., et al., *Consistent new bone formation in 95 revisions: average 9-year follow-up.* Orthopedics, 2008. **31**(7): p. 654.
56. Mallory, T.H., et al., *Clinical and radiographic outcome of a cementless, titanium, plasma spray-coated total hip arthroplasty femoral component. Justification for continuance of use.* J Arthroplasty, 1996. **11**(6): p. 653-60.
57. Weiss, R.J., et al., *Minimum 5-year follow-up of a cementless, modular, tapered stem in hip revision arthroplasty.* J Arthroplasty, 2011. **26**(1): p. 16-23.
58. Unnanuntana, A., Dimitroulias, A., Bolognesi, M.P., Hwang, K.L., Goodman, S.B., Marcus, R.E.,, *Cementless femoral prostheses cost more to implant than cemented femoral prostheses.* Clin. Orthop. Relat. Res, 2009. **467**: p. 1546-1551.
59. Bourne, R.B., Rorabeck, C.H., Burkart, B.C., Kirk, P.G., *Ingrowth surfaces. Plasma spray coating to titanium alloy hip replacements.* Clin. Orthop. Relat. Res, 1994. **298**: p. 37-46.
60. Bottros J, K.A., Lee HH, Polousky J, Barsoum WK, *The use of navigation in total knee arthroplasty for patients with extra-articular deformity.* J Arthroplasty 2008. **23**: p. 74-78.
61. Fowler, J.L., et al., *Experience with the Exeter total hip replacement since 1970.* Orthop Clin North Am, 1988. **19**(3): p. 477-89.
62. Matziolis G, K.D., Weiss U, Tohtz S, Perka C, *A prospective, randomized study of computer-assisted and conventional total knee arthroplasty Three-dimensional evaluation of implant alignment and rotation.* J Bone Joint Surg Am 2007. **89**: p. 236-243.
63. Aamodt, A., Lund-Larsen, J., Eine, J., Andersen, E., Benum, P., Husby, O.S, *Changes in proximal femoral strain after insertion of uncemented standard and customised femoral stems. An experimental study in human femora.* J. Bone Joint Surg Br, 2001. **83**: p. 921-929.
64. Park, M.S., et al., *Management of periprosthetic femoral fractures.* J Arthroplasty, 2003. **18**(7): p. 903-6.

65. Serekian, P., *Hydroxyapatite: from Plasma Spray to Electrochemical Deposition.* Fifteen Years of Clinical Experience with Hydroxyapatite Coatings in Joint Arthroplasty, 2004: p. 29-33.
66. U. Hansson, S.T., – Larsen;, *A Randomized RSA Study of Peri-ApatiteTM HA Coating of a Knee Prosthesis.* Key Engineering Materials, 2004. **254 – 256 (2004)**: p. 624 – 626.
67. H. Aberman, e.a., *Gap Healing In a Non-weight Bearing Dog Model.* Effectiveness of a Solution Precipitated Apatite Coating (39th Annual Meeting, Orthopaedic Research Society, Feb. 1993), 1993: p. 406.
68. H. Aberman, e.a., *The Effectiveness of Peri-Apatite Coatings in Bridging Implant Gaps* 42nd Annual Meeting, Orthopaedic Research Society, Feb 1996, 1996: p. 522.
69. *Australian Orthopedic Association National Joint Replacement Registry (AOANJRR). Annual Report 2010.* 2010. **34**.
70. Graves, S.E., et al., *The Australian Orthopaedic Association National Joint Replacement Registry.* Med J Aust, 2004. **180**(5 Suppl): p. S31-4.
71. YH Zhu, K.C.a.W.T., *Polyethylene wear and osteolysis in total hip arthroplasty.* Journal of Orthopaedic Surgery`, 2001. **9**(1).
72. Ybinger T, K.W., Hoffart HE, Muschalik B, Bullmann W, Zweymüller K, *Accuracy of navigation-assisted acetabular component positioning studied by computed tomography measurements: methods and results.* J Arthroplasty 2007. **22**: p. 812-817.
73. Wan, A., and Dorr, L. D., *Natural history of femoral focal osteolysis with proximal ingrowth of smooth stem implant.* J Arthroplasty, 1996. **6**: p. 718-725.
74. Vigorita VJ, M.B., Dichiara JF, Higham PA, *A histomorphometric and histologic analysis of the implant interface in five successful, autopsy-retrieved, noncemented porous-coated knee arthroplasties.* Clin Orthop Relat Res, 1993. **293**: p. 211-8.
75. Kwang Woo Nam, M.J.J.Y., MD; Yong Lae Kim, MD; Young-Min Kim, MD; Myung-Hyun Lee, PhD; Hee Joong Kim, MD, *Alumina-Debris-Induced Osteolysis in Contemporary Alumina-on-Alumina total hip arthroplasty: A Case Report.* J Bone Joint Surg Am, November 01, 2007. **89**(11): p. 2499-2503.
76. Hallab NJ, M.K., Vermes C, et al, *Orthopaedic implant related metal toxicity in terms of human lymphocyte reactivity to metal-protein complexes produced from cobalt-base and titanium base implant alloy degradation.* Mol Cell Biochem 2001, 2001. **222(1–2)**: p. 127– 36.
77. Evans E, F.M., Miller A, Vernon-Roberts B., *Metal sensitivity as a cause of bone necrosis and loosening of the prosthesis in total joint replacement.* J Bone Joint Surg Br, 1974. **56**(4).
78. Willert H, B.G., Fayyazi A, et al. , *Metal-on-metal bearings and hypersensitivity in patients with artificial hip joints: A clinical and histomorphological study. .* J Bone Joint Surg Am, 2005. **87(1)**(28).

79. Jacobs J, H.N., *Loosening and osteolysis associated with metal-on-metal bearings: a local effect of metal hypersensitivity?* The Journal of Bone and Joint Surgery, 2006. **88**(6): p. 1171.
80. Watters T, C.D., Menon K, Vinson E, Bolognesi M, Dodd L. . ;. *Aseptic Lymphocyte-Dominated Vasculitis- Associated Lesion.* Am J Clin Pathol, 2010. **134**(6): p. 886.
81. Park Y, M.Y., Lim S, Yang J, Ahn G, Choi Y., *Early osteolysis following second-generation metal-on-metal hip replacement.* J Bone Joint Surg Am, 2005. **87**(7): p. 1515.
82. Kwon Y, O.S., McLardy-Smith P, et al. , *Asymptomatic "pseudotumors" after metal-on-metal hip resurfacing arthroplasty prevalence and metal ion study.* J Arthroplasty. , 2010. **Jun 28; Epub ahead of print.**
83. Kwon Y, G.-J.S., Simpson D, et al. ;. *Analysis of wear of retrieved metal-on-metal hip resurfacing implants revised due to pseudotumours.* J Bone Joint Surg Br., 2010. **92**(3): p. 356.
84. Tyler Steven Watters, W.C.E., MD, Rhett K. Hallows, Leslie G. Dodd, Samuel S. Wellman, Michael P. Bolognesi,, *Pseudotumor with Superimposed Periprosthetic Infection Following Metal-on-Metal total hip arthroplasty: A Case Report.* The Journal of Bone & Joint Surgery., 2010. **92**: p. 1666-1669.
85. Bannister, G., *Mechanical failure in the femoral component in total hip replacement.* Orthop Clin North Am, 1988. **19(3)**: p. 567-573.
86. Bannister, G., *Mechanical failure in the femoral component in total hip replacement.* Orthop Clin North Am, 1988. **19**(3): p. 567-73.
87. Marston, R.A., A.G. Cobb, and G. Bentley, *Stanmore compared with Charnley total hip replacement. A prospective study of 413 arthroplasties.* J Bone Joint Surg Br, 1996. **78**(2): p. 178-84.
88. Garellick, G., H. Malchau, and P. Herberts, *Survival of hip replacements. A comparison of a randomized trial and a registry.* Clin Orthop Relat Res, 2000(375): p. 157-67.
89. Malchau, H., et al., *The Swedish Total Hip Replacement Register.* J Bone Joint Surg Am, 2002. **84-A Suppl 2**: p. 2-20.
90. Krismer, M., et al., *The prediction of failure of the stem in THR by measurement of early migration using EBRA-FCA. Einzel-Bild-Roentgen-Analyse-femoral component analysis.* J Bone Joint Surg Br, 1999. **81**(2): p. 273-80.
91. Lennon, A.B. and P.J. Prendergast, *Evaluation of cement stresses in finite element analyses of cemented orthopaedic implants.* J Biomech Eng, 2001. **123**(6): p. 623-8.
92. Berry, D.J., *Management of periprosthetic fractures: the hip.* J Arthroplasty, 2002. **17**(4 Suppl 1): p. 11-3.
93. HORWITZ IB, L.M., *Artificial hip prosthesis in acute and nonunion fractures of the femoral neck: follow-up study of seventy cases.* J Am Med Assoc., 1954. **Jun 5**(155(6)): p. 564-7.

94. Lewallen, D.G. and D.J. Berry, *Periprosthetic fracture of the femur after total hip arthroplasty: treatment and results to date.* Instr Course Lect, 1998. **47**: p. 243-9.
95. Lindahl, H., et al., *Risk factors for failure after treatment of a periprosthetic fracture of the femur.* J Bone Joint Surg Br, 2006. **88**(1): p. 26-30.
96. Berry, D.J., *Epidemiology: hip and knee.* Orthop Clin North Am, 1999. **30**(2): p. 183-90.
97. Haddad, F.S., et al., *Periprosthetic femoral fractures around well-fixed implants: use of cortical onlay allografts with or without a plate.* J Bone Joint Surg Am, 2002. **84-A**(6): p. 945-50.
98. Beals, R.K. and S.S. Tower, *Periprosthetic fractures of the femur. An analysis of 93 fractures.* Clin Orthop Relat Res, 1996(327): p. 238-46.
99. Brady, O.H., et al., *Classification of the hip.* Orthop Clin North Am, 1999. **30**(2): p. 215-20.
100. Greidanus, N.V., et al., *Principles of management and results of treating the fractured femur during and after total hip arthroplasty.* Instr Course Lect, 2003. **52**: p. 309-22.
101. Mitchell, P.A., et al., *The prevention of periprosthetic fractures of the femur during and after total hip arthroplasty.* Instr Course Lect, 2003. **52**: p. 301-8.
102. Schmidt, A.H. and R.F. Kyle, *Periprosthetic fractures of the femur.* Orthop Clin North Am, 2002. **33**(1): p. 143-52, ix.
103. Tower, S.S. and R.K. Beals, *Fractures of the femur after hip replacement: the Oregon experience.* Orthop Clin North Am, 1999. **30**(2): p. 235-47.
104. Lindahl, H., *Epidemiology of periprosthetic femur fracture around a total hip arthroplasty.* Injury, 2007. **38**(6): p. 651-654.
105. Meek, R.M., et al., *Intraoperative fracture of the femur in revision total hip arthroplasty with a diaphyseal fitting stem.* J Bone Joint Surg Am, 2004. **86-A**(3): p. 480-5.
106. Adolphson, P., U. Jonsson, and R. Kalen, *Fractures of the ipsilateral femur after total hip arthroplasty.* Arch Orthop Trauma Surg, 1987. **106**(6): p. 353-7.
107. Mont, M.A. and D.C. Maar, *Fractures of the ipsilateral femur after hip arthroplasty. A statistical analysis of outcome based on 487 patients.* J Arthroplasty, 1994. **9**(5): p. 511-9.
108. Masri, B.A., R.M. Meek, and C.P. Duncan, *Periprosthetic fractures evaluation and treatment.* Clin Orthop Relat Res, 2004(420): p. 80-95.
109. Learmonth, I.D., *The management of periprosthetic fractures around the femoral stem.* J Bone Joint Surg Br, 2004. **86**(1): p. 13-19.
110. Brady, O.H., et al., *The reliability and validity of the Vancouver classification of femoral fractures after hip replacement.* J Arthroplasty, 2000. **15**(1): p. 59-62.

111. Gill TJ, S.J., Orler R, Ganz R, *Lateral insufficiency fractures of the femur caused by osteopenia and varus angulation: a complication of total hip arthroplasty.* J Arthroplasty 1999. **14**: p. 982-987.
112. Haddad, F.S. and C.P. Duncan, *Cortical onlay allograft struts in the treatment of periprosthetic femoral fractures.* Instr Course Lect, 2003. **52**: p. 291-300.
113. Ritter, M.A., P.M. Faris, and E.M. Keating, *Anterior femoral notching and ipsilateral supracondylar femur fracture in total knee arthroplasty.* J Arthroplasty, 1988. **3**(2): p. 185-7.
114. Short, W.H., D.R. Hootnick, and D.G. Murray, *Ipsilateral supracondylar femur fractures following knee arthroplasty.* Clin Orthop Relat Res, 1981(158): p. 111-6.
115. Kavanagh, B.F., *Femoral fractures associated with total hip arthroplasty.* Orthop Clin North Am, 1992. **23**(2): p. 249-257.
116. Tsiridis, E., F.S. Haddad, and G.A. Gie, *The management of periprosthetic femoral fractures around hip replacements.* Injury, 2003. **34**(2): p. 95-105.
117. Hogg MC, K.L., Appleyard R, Gillies RM, *Impaction loads during insertion of hip resurfacing implant: a finite element study.* In Proceedings of the Fifty fourth Annual Meeting of the Orthopaedic Research Society, 2008.
118. Engh, C.A. and P. Massin, *Cementless total hip arthroplasty using the anatomic medullary locking stem. Results using a survivorship analysis.* Clin Orthop Relat Res, 1989(249): p. 141-58.
119. Pilliar, R.M., et al., *Radiographic and morphologic studies of load-bearing porous-surfaced structured implants.* Clin Orthop Relat Res, 1981(156): p. 249-57.
120. Hogg MC, G.R., *Impaction of a press-fit acetabular cup using a dynamic finite element model.* In Proceedings of Fifty fifth Annual Meeting of the Orthopaedic Research Society, 2009.
121. Fitzgerald, R.H., Jr., G.W. Brindley, and B.F. Kavanagh, *The uncemented total hip arthroplasty. Intraoperative femoral fractures.* Clin Orthop Relat Res, 1988(235): p. 61-6.
122. Duncan, C.P. and B.A. Masri, *Fractures of the femur after hip replacement.* Instr Course Lect, 1995. **44**: p. 293-304.
123. Mallory, T.H., T.J. Kraus, and B.K. Vaughn, *Intraoperative femoral fractures associated with cementless total hip arthroplasty.* Orthopedics, 1989. **12**(2): p. 231-9.
124. Johansson, A., et al., *Improved operations for femoral neck fracture. A radiographic evaluation.* Acta Orthop Scand, 1986. **57**(6): p. 505-9.
125. Stuchin, S.A., *Femoral shaft fracture in porous and press-fit total hip arthroplasty.* Orthop Rev, 1990. **19**(2): p. 153-159.
126. Van Flandern, G.J., *Periprosthetic fractures in total hip arthroplasty.* Orthopedics, 2005. **28**(9): p. 1089-1095.

127. Davidson, D., et al., *Intraoperative periprosthetic fractures during total hip arthroplasty. Evaluation and management.* J Bone Joint Surg Am, 2008. **90**(9): p. 2000-12.
128. Larson, J.E., E.Y. Chao, and R.H. Fitzgerald, *Bypassing femoral cortical defects with cemented intramedullary stems.* J Orthop Res, 1991. **9**(3): p. 414-21.
129. Kuptniratsaikul, S., et al., *Plate-screw-wiring technique for the treatment of periprosthetic fracture around the hip: a biomechanical study.* J Med Assoc Thai, 2001. **84 Suppl 1**: p. S415-22.
130. Schmotzer, H., G.H. Tchejeyan, and D.M. Dall, *Surgical management of intra- and postoperative fractures of the femur about the tip of the stem in total hip arthroplasty.* J Arthroplasty, 1996. **11**(6): p. 709-17.
131. Wilson, A.W., M. Ethunandan, and P.A. Brennan, *Transmasseteric antero-parotid approach for open reduction and internal fixation of condylar fractures.* Br J Oral Maxillofac Surg, 2005. **43**(1): p. 57-60.
132. Wilson, D., et al., *A biomechanical study comparing cortical onlay allograft struts and plates in the treatment of periprosthetic femoral fractures.* Clin Biomech (Bristol, Avon), 2005. **20**(1): p. 70-6.
133. Rupprecht, M., et al., *Biomechanical evaluation for mechanisms of periprosthetic femoral fractures.* J Trauma, 2011. **70**(4): p. E62-6.
134. Sarvilinna, R., et al., *Factors predisposing to periprosthetic fracture after hip arthroplasty: a case (n = 31)-control study.* Acta Orthop Scand, 2004. **75**(1): p. 16-20.
135. Lindahl, H., et al., *Periprosthetic femoral fractures classification and demographics of 1049 periprosthetic femoral fractures from the Swedish National Hip Arthroplasty Register.* J Arthroplasty, 2005. **20**(7): p. 857-65.
136. Berry, D.J., *Periprosthic fractures after major joint replacement.* Orthop Clin North Am, 1999. **30**(2): p. 183-190.
137. Morrey, B.F. and B.F. Kavanagh, *Complications with revision of the femoral component of total hip arthroplasty. Comparison between cemented and uncemented techniques.* J Arthroplasty, 1992. **7**(1): p. 71-9.
138. Whittaker, R.P., L.N. Sotos, and E.L. Ralston, *Fractures of the femur about femoral endoprostheses.* J Trauma, 1974. **14**(8): p. 675-94.
139. Wilson, D., B.A. Masri, and C.P. Duncan, *Periprosthetic fractures: an operative algorithm.* Orthopedics, 2001. **24**(9): p. 869-70.
140. Biggi, F., et al., *Periprosthetic fractures of the femur: the stability of the implant dictates the type of treatment.* J Orthop Traumatol, 2010. **11**(1): p. 1-5.
141. Van Flandern, G.J., *Periprosthetic fractures in total hip arthroplasty.* Orthopedics, 2005. **28**(9 Suppl): p. s1089-95.
142. Charnley, J., *The healing of human fractures in contact with self-curing acrylic cement.* Clin Orthop Relat Res, 1966. **47**: p. 157-63.

143. Macdonald, S.J., et al., *Periprosthetic femoral fractures treated with a long-stem cementless component.* J Arthroplasty, 2001. **16**(3): p. 379-83.
144. Springer, B.D., D.J. Berry, and D.G. Lewallen, *Treatment of periprosthetic femoral fractures following total hip arthroplasty with femoral component revision.* J Bone Joint Surg Am, 2003. **85-A**(11): p. 2156-62.
145. Dennis, M.G., et al., *Fixation of periprosthetic femoral shaft fractures: a biomechanical comparison of two techniques.* J Orthop Trauma, 2001. **15**(3): p. 177-80.
146. Jacobs, R.R., B.A. Rahn, and S.M. Perren, *Effects of plates on cortical bone perfusion.* J Trauma, 1981. **21**(2): p. 91-5.
147. Kregor, P.J., J.L. Hughes, and P.A. Cole, *Fixation of distal femoral fractures above total knee arthroplasty utilizing the Less Invasive Stabilization System (L.I.S.S.).* Injury, 2001. **32 Suppl 3**: p. SC64-75.
148. Perren, S.M., *The concept of biological plating using the limited contact-dynamic compression plate (LC-DCP). Scientific background, design and application.* Injury, 1991. **22 Suppl 1**: p. 1-41.
149. Schutz, M., et al., *Minimally invasive fracture stabilization of distal femoral fractures with the LISS: a prospective multicenter study. Results of a clinical study with special emphasis on difficult cases.* Injury, 2001. **32 Suppl 3**: p. SC48-54.
150. Muller, M., et al., *Periprosthetic femoral fractures: outcome after treatment with LISS internal fixation or stem replacement in 36 patients.* Acta Orthop Belg, 2009. **75**(6): p. 776-83.
151. Shimmin, A.J., J. Bare, and D.L. Back, *Complications associated with hip resurfacing arthroplasty.* Orthop Clin North Am, 2005. **36**(2): p. 187-93, ix.
152. Lesh, M.L., et al., *The consequences of anterior femoral notching in total knee arthroplasty. A biomechanical study.* J Bone Joint Surg Am, 2000. **82-A**(8): p. 1096-101.
153. Pazzaglia, U. and P.D. Byers, *Fractured femoral shaft through an osteolytic lesion resulting from the reaction to a prosthesis. A case report.* J Bone Joint Surg Br, 1984. **66**(3): p. 337-9.
154. Reich, S.M. and W.L. Jaffe, *Femoral fractures associated with loose cemented total hip arthroplasty.* Orthopedics, 1994. **17**(2): p. 185-9.
155. Harris, W.H., et al., *Extensive localized bone resorption in the femur following total hip replacement.* J Bone Joint Surg Am, 1976. **58**(5): p. 612-8.
156. Garbuz, D.S., B.A. Masri, and C.P. Duncan, *Periprosthetic fractures of the femur: principles of prevention and management.* Instr Course Lect, 1998. **47**: p. 237-42.
157. McElfresh, E.C. and M.B. Coventry, *Femoral and pelvic fractures after total hip arthroplasty.* J Bone Joint Surg Am, 1974. **56**(3): p. 483-92.

158. Bethea, J.S., 3rd, et al., *Proximal femoral fractures following total hip arthroplasty.* Clin Orthop Relat Res, 1982(170): p. 95-106.
159. Fredin, H.O., H. Lindberg, and A.S. Carlsson, *Femoral fracture following hip arthroplasty.* Acta Orthop Scand, 1987. **58**(1): p. 20-2.
160. Johansson, J.E., et al., *Fracture of the ipsilateral femur in patients wih total hip replacement.* J Bone Joint Surg Am, 1981. **63**(9): p. 1435-42.
161. Scott, R.D., et al., *Femoral fractures in conjunction with total hip replacement.* J Bone Joint Surg Am, 1975. **57**(4): p. 494-501.
162. Talab, Y.A., J.D. States, and C.M. Evarts, *Femoral shaft perforation: a complication of total hip reconstruction.* Clin Orthop Relat Res, 1979(141): p. 158-65.
163. Lindahl, H., et al., *Three hundred and twenty-one periprosthetic femoral fractures.* J Bone Joint Surg Am, 2006. **88**(6): p. 1215-22.
164. Berry, D.J., *Periprosthetic fractures associated with osteolysis: a problem on the rise.* J Arthroplasty, 2003. **18**(3 Suppl 1): p. 107-11.
165. Gotze, C., et al., *Primary stability in cementless femoral stems: custom-made versus conventional femoral prosthesis.* Clin Biomech (Bristol, Avon), 2002. **17**(4): p. 267-73.
166. Rietbergen Bert van, P., and Huiskes, Rik PhD, *Load Transfer and Stress Shielding of the Hydroxyapatite-ABG Hip: A Study of Stem Length and Proximal Fixation.* J Arthroplasty, 2001. **16**(No. 8 Suppl. 1).
167. Tonino AJ, R.A., *The International ABG Study Group: The hydroxyapatite-ABG hip system: 5- to 7-year results from an international multicenter study.* J Arthroplasty, 2000. **15**(3): p. 274-282.
168. Herrera A, P.J., Ibarz E, Cegoñino J, Puértolas JA, Gracia L., *Comparison between DEXA and finite element studies in the long-term bone remodeling of an anatomical femoral stem.* J Biomech Eng, 2009. **131(4)**: p. 041013.
169. Panisello JJ, C.V., Herrero L, Herrera A, Mateo J, Caballero MJ., *Changes in periprosthetic bone remodelling after redesigning an anatomic cementless stem.* Int Orthop., 2009. **33(2)**: p. 373-9.
170. Gracia, L.I., E. Puértolas, S. Cegoñino, J. López-Prats, F. Panisello, JJ. Herrera, A, *Study of bone remodeling of two models of femoral cementless stems by means of DEXA and finite elements.* BioMedical Engineering OnLine, 2010. **9**: p. 22.
171. Wang K, G.L., Dumbleton J., *The Characterization of Ti-12Mo-6Zr-2Fe – a New Biocompatible Titanium Alloy Developed for Surgical Implants.* Beta Titanium Alloys in the 1990's, 1993: p. 49-60.
172. Tonino, A.J., Thèrin, M., Doyle, C., *Hydroxyapatite-coated femoral stems. Histology and histomorphometry around five components retrieved at post mortem.* J. Bone Joint Surg. Br., 1999. **81**: p. 148-154.
173. van der Wal, B.C., Rahmy, A., Grimm, B., Heyligers, I., Tonino, A.,, *Preoperative bone quality as a factor in dual-energy X-ray*

absorptiometry analysis comparing bone remodelling between two implant types. Int. Orthop. Int. Orthop, 2008. **32**(1): p. 39-45.
174. van Rietbergen, B., Huiskes, R, *Load transfer and stress shielding of the hydroxyapatite-ABG hip: a study of stem length and proximal fixation.* J. Arthroplasty, 2001. **16**: p. 55-63.
175. Nourissat C, A.J., Berteaux D, Goalard C, Walter W., , *The ABG II hip system implantation technique.* Surg Technol Int, 2002. **Sep;10**: p. 205-11.
176. Stryker, *ABGII MIS Posterior lateral Surgical technique*, 2004. p. 61.
177. Sugano, N., *Computer-assisted orthopedic surgery.* J Orthop Sci, 2003. **8**(3): p. 442-448.
178. Hofstetter, R., et al., *Fluoroscopy as an imaging means for computer-assisted surgical navigation.* Comput Aided Surg, 1999. **4**(2): p. 65-76.
179. Krackow, K.A., et al., *A new technique for determining proper mechanical axis alignment during total knee arthroplasty: progress toward computer-assisted TKA.* Orthopedics, 1999. **22**(7): p. 698-702.
180. Nogler, M., *Navigated minimal invasive total hip arthroplasty.* Surg Technol Int, 2004. **12**: p. 259-262.
181. Brown, R.A., *A computerized tomography-computer graphics approach to stereotaxic localization.* J Neurosurg, 1979. **50**(6): p. 715-20.
182. I. Kowal , F.L., , L.-P Nolte, *Navigation and MIS with in Orthopedic Surgery*, in *Basics of Computer-Assisted Orthopedic Surgery,*, Stiehl, Editor 2007.
183. Nogler, M., Kessler, O., Prassl, A., Donnelly, B., Streicher, R., Sledge, J. B., et al., *Reduced variability of acetabular cup positioning with use of an imageless navigation system.* Clin Orthop Relat Res, 2004. **426**: p. 159-163.
184. Langlotz F, N.L., *Technical approaches to computer-assisted orthopedic surgery. Eur J Trauma.* Eur J Trauma, 2004. **30**: p. 1-11.
185. Kowal , F.L., , L.-P Nolte, Stiehl., *Navigation and MIS with in Orthopedic Surgery, in Basics of Computer-Assisted Orthopedic Surgery*. 2007.
186. Maintz JB, V.M., *A survey of medical image registration.* Med Image Anal, 1998. **2**(1): p. 1-36.
187. Germano, I.M., Advanced Techniques in Image Guided Brain and Spine Surgery, Thieme Medical Publisers Inc, NY, USA 10001, 2002.
188. Foley KT, S.D., Rampersaud YR, *Virtual fluoroscopy: computer-assisted fluoroscopic navigation.* Spine (Phila Pa 1976). 2001 Feb 15, 2001. **26(4)**: p. 347-51.
189. Stulberg SD, P.F., Saragaglia D, *Computer-assisted total knee replacement arthroplasty.* Oper Tech Orthop, 2000. **10**(1): p. 25-39.
190. Sati M, S.H., Bourquin Y, Kunz M, Kasermann S, Nolte LP, *Clinical integration of computer-assisted technology for arthroscopic anterior cruciate ligament reconstruction.* Oper Tech Ortho, 2000. **10**(1): p. 40-49.

191. Jakopec, M., et al., *The first clinical application of a "hands-on" robotic knee surgery system.* Comput Aided Surg, 2001. **6**(6): p. 329-39.
192. Bargar, W.L., A. Bauer, and M. Borner, *Primary and revision total hip replacement using the Robodoc system.* Clin Orthop Relat Res, 1998(354): p. 82-91.
193. Siebert, W., et al., *Technique and first clinical results of robot-assisted total knee replacement.* Knee, 2002. **9**(3): p. 173-80.
194. Amstutz HC, T.B., Jinnah R, Kim W, Grogan T, Yale C., *Treatment of primary osteoarthritis of the hip. A comparison of total joint and surface replacement arthroplasty.* J Bone Joint Surg Am. 1984, 1984. **66**: p. 228-41.
195. Gore DR, M.M., Gardner GM, Sepic SB, *Hip function after total vs. surface replacement.* Acta Orthop Scand. 1985, 1985. **56**: p. 386-90.
196. Capello WN, T.T., Misamore G, Eaton R, *Analysis of revision surgery of resurfacing hip arthroplasty.* Clin Orthop Relat Res. 1982, 1982. **170**: p. 50-5.
197. Amstutz HC, G.P., Dorey FJ, *Evolution and future of surface replacement of the hip.* J Orthop Sci. 1998, 1983. **3**: p. 169-86.
198. Amstutz HC, S.E., Le Duff MJ, *Surface arthroplasty in young patients with hip arthritis secondary to childhood disorders.* Orthop Clin North Am. 2005, 2005. **36**: p. 223-30.
199. Treacy RB, M.C., Pynsent PB, *Birmingham hip resurfacing arthroplasty.A minimum follow-up of five years.* J Bone Joint Surg Br. 2005, 2005. **87**: p. 167-70.
200. Smith-Petersen, M.N., *The classic: Evolution of mould arthroplasty of the hip joint.* Clin Orthop Relat Res, 1978: p. 5-11.
201. JC;, C., *Arthroplasty of the hip: a new operation.* Lancet, 1961: p. 1129-32.
202. Charnley J, K.A., Longfield MD, *The optimum size of prosthetic heads in relation to the wear of plastic sockets in total replacement of the hip.* Med Biol Eng 1969, 1969. **7(1)**: p. 31– 9.
203. CO., T., *Hemi and total articular replacement arthroplasty of the hip with the fixed femoral cup.* Orthop Clin N Am 1982, 1982. **13(4):**: p. 869– 94.
204. ME, M., *The benefits of metal-on-metal total hip replacements.* Clin Orthop 1995, 1995. **311**: p. 54– 9.
205. Y, G., *Hip arthroplasty by matching cups.* Clin Orthop, 1978. **134**: p. 25–35.
206. Salzer M, K.K., Locke H, et al, *Cement-free bioceramic double-cup endoprosthesis of the hip joint.* Clin Orthop 1978, 1978. **134**: p. 80– 6.
207. Capello WN, I.P., Trammell TR, Eicher P, *Conservative total hip arthroplasty:a procedure to conserve bone stock. Part I: analysis of sixty-six patients. Part II: analysis of failures.* Clin Orthop Relat Res. 1978, 1978. **134**: p. 59-74.

208. Freeman, S.S., Cameron H, et al, *ICLH cemented double cup total replacement of the hip.* J Bone Joint Surg Br 1978, 1978. **60**: p. 137– 8.
209. Wagner M, W.H., *Preliminary results of uncemented metal-on-metal stemmed and resurfacing hip replacement arthroplasty.* Clin Orthop 1996, 1996. **329**: p. S78– 88.
210. Furuya K, T.M., Kawachi S, *Socket-cup arthroplasty.* Clin Orthop 1978, 1978. **134**: p. 41–4.
211. Nishio A, E.M., Kaibara N, *Socket and cup surface replacement of the hip.* Clin Orthop 1978, 1978. **134**: p. 53–8.
212. Papas, B.a., *Resurfacing total hip replacement for avascular necrosis in young patients: durability, revision options and future technology.* 6th Annual Current Concepts in Joint Replacement Symposium, 1990.
213. Amstutz HC, G.P., *Metal-on-metal bearings in hip arthroplasty.* Clin Orthop 1996, 1996. **329**: p. S11 – 34.
214. McMinn D, T.R., Lin K, et al, *Metal-on-metal surface replacement of the hip.* Clin Orthop 1996, 1996. **329**: p. S89– 98.
215. Clarke IC, D.T., Bowsher JG, Nasser S, Takahashi T., *Current concepts of metal-on-metal hip resurfacing.* Orthop Clin North Am. , 2005. **Apr;36(**(2): p. 143-62.
216. Clarke IC, G.V., Anissian L, et al, *Charnley wear model for validation of hip simulators—ball diameter versus polytetrafluoroethylene and polyethylene wear.* Proc Inst Mech Eng [H] 1997, 1997. **211(1)**: p. 25–36.
217. Charnley J, K.A., Longfield MD. . ;():. *The optimum size of prosthetic heads in relation to the wear of plastic sockets in total replacement of the hip.* Med Biol Eng, 1969. **7**(1): p. 31– 9.
218. Mai MT, S.T., Dorey FJ, et al, *The contribution of frictional torque to loosening at the cement-bone interface in Tharies hip replacements.* J Bone Joint Surg [Am] 1996, 1996. **78(4)**: p. 505–11.
219. IC., C., *Symposium on surface replacement arthroplasty of the hip. Bbiomechanics: mutifactorial design choices—an essential compromise?* Orthop Clin N Am, 1982. **13**(4): p. 681– 707.
220. Grigoris P, R.P., Panousis K, Bosch H, *The Evolution of Hip Resurfacing Arthroplasty.* Orthop Clin N Am 36 (2005) 2005. **36**: p. 125 – 134.
221. Beaule PE, A.J., *Patient Selection and Surgical Technique for Surface Arthroplasty of the Hip.* Orthop Clin N Am 36 (2005) 2005. **36**: p. 177 – 185.
222. Shimmin A.J. Bare J, B.D.L., *Complications Associated with Hip Resurfacing Arthroplasty.* Orthop Clin N Am 36 (2005) 2005. **36**: p. 187 – 193.
223. Garbuz DS, T.M., Greidanus NV, Masri BA, Duncan CP., *The John Charnley Award: Metal-on-metal hip resurfacing versus large-diameter head metal-on-metal total hip arthroplasty: a randomized clinical trial.* Clin Orthop Relat Res, 2010 **Feb;468**(2): p. 318-25.

224. Wales, T.N.J.R.N.o.E.a., *Seventh Annual Report (April 2009 - March 2010).* September 2010.
225. Bolland B, C.D., Langton D, Millington J, Arden N, Latham J. , *High failure rates with a largediameter hybrid metal-on-metal total hip replacement: clinical, adiological and retrieval analysis.* Journal of Bone and Joint Surgery British Volume, 2011. **93**(5): p. 608-615.
226. http://www.azhippain.com/choosewright/bfh.asp. *Better Range of Motion.* 2011.
227. Freeman, *Some anatomical and mechanical considerations relevant to the surface replacement of the femoral head.* Clin Orthop 1978, 1978. **134**: p. 19– 24.
228. Amstutz HC, B.P., Dorey FJ, et al, *Metal-onmetal hybrid surface arthroplasty: two to six year follow-up.* J Bone Joint Surg [Am] 2004, 2004. **86(1)**: p. 28 – 39.
229. Daniel J, P.P., McMinn DJ, *Metal-on-metal resurfacing of the hip in patients under the age of 55 years with osteoarthritis.* J Bone Joint Surg Br. 2004, 2004. **86**: p. 177-84.
230. Campbell P, M.H., Amstutz HC, *Viability of femoral heads treated with surface arthroplasty.* J Arthroplasty 2000, 2000. **15(1)**: p. 120– 2.
231. Steffen RT, S.S., Urban JP, McLardy-Smith P, Beard DJ, Gill HS, Murray DW, *The effect of hip resurfacing on oxygen concentration in the femoral head.* J Bone Joint Surg Br. 2005, 2005. **87**: p. 1468-74.
232. Morlock MM, B.N., Stahmer F, Zustin J, Sauter G, Hahn M, Krause M, Rüther W, Amling M., *Reasons for failure of hip resurfacing implants. A failure analysis based on 250 revision specimens.* Orthopade., 2008 German. **Jul;37**(7): p. 695-703.
233. Shimmin A, B.P.E., Campbell P, *Metal-on-Metal Hip Resurfacing Arthroplasty.* J Bone Joint Surg Am. 2008, 2008. **90**: p. 637-54.
234. Cossey AJ, B.D., Shimmin A, Young D, Spriggins AJ, *The nonoperative management of periprosthetic fractures associated with the Birmingham hip resurfacing procedure.* J Arthroplasty. 2005, 2005. **20**: p. 358-61.
235. Beaulé, P.E., Harvey N, Zaragoza E, Le Duff M. J., Dorey F. J, *femoral head/neck offset and hip resurfacing.* The Journal of Bone and Joint Surgery, 2007. **89-B**.
236. Silva M, L.K.H., Heisel C, *The Biomechanical Results of Total Hip Resurfacing Arthroplasty.* The Journal of Bone and Joint Surgery, 2004. **86**: p. 40-46.
237. Loughead JM, M.W., Holland JP., *Outcome of hip resurfacing in obese patients.* Acta Orthop Belg., 2011. **77**(1): p. 47-52.
238. Chandler DR, G.R., Hull D, McGuire PJ, Kim IS, Clarke IC, Sarmiento A., *Prosthetic hip range of motion and impingement. The effects of head and neck geometry.* Clin Orthop Relat Res., 1982. **Jun;(166)**: p. 284-91.

239. Girard J, K.N., Bocquet D, Wavreille G, Migaud H., *Femoral head to neck offset after hip resurfacing is critical for range of motion.* Clin Biomech. , 2011. **Sep 16.**
240. Dickinson AS, T.A., Jeffers JR, Browne M., *Performance of the resurfaced hip. Part 2: The influence of prosthesis stem design on remodelling and fracture of the femoral neck.* Proc Inst Mech Eng H, 2010. **224**(7): p. 841-51.
241. Anglin C, M.B., Tonetti J, Hodgson A J, Greidanus N V, *Hip Resurfacing Femoral Neck Fracture Influenced by Valgus Placement.* Clin Orthop Relat Res. 2007, 2007. **465**: p. 71-9.
242. Vail T P, G.R.R., Dominguez D E, Kitaoka K, Ottaviano D., *Position of Hip Resurfacing Component Affects Strain and Resistance to Fracture in the Femoral Neck.* J Bone Joint Surg Am. 2008, 2008. **90**: p. 1951-60.
243. Richards C J, G.D., Huk O L, Zukor D J, Steffen T, Antoniou J, *Risk of Periprosthetic Femoral Neck Fracture after Hip Resurfacing Arthroplasty: Valgus Compared with Anatomic Alignment'.* J Bone Joint Surg Am. 2008, 2008. **90, 3**: p. 96-101.
244. Amstutz HC, B.P., Dorey FJ, LeDuff MJ, Campbell PA, Gruen TA, *Metal-on-Metal Hybrid Surface Arthroplasty: Surgical Technique.* The Journal of Bone and Joint Surgery,2006, 2006. **86-A**: p. 28-39.
245. Olsen M, S.E., *Avoiding short-term femoral neck fracture with imageless computer navigation for hip resurfacing.* Clin Orthop Relat Res, 2011. **Jun;469**(6): p. 1621-6.
246. Olsen M, C.M., Gamble P, Boyle RA, Tumia N, Schemitsch EH., *A comparison of conventional guidewire alignment jigs with imageless computer navigation in hip resurfacing arthroplasty.* J Bone Joint Surg Am. , 2010. **Aug 4;92**(9): p. 1834-41.
247. Schnurr C, N.J., Koebke J, Michael JW, Eysel P, König DP., *Imageless computer navigation of hip resurfacing arthroplasty. (German).* Oper Orthop Traumatol. . 2010 **Jul;22**(3): p. 307-16.
248. Gravius S, B.P., de la Fuente M, Radermacher K, Mumme T., *Evaluation of a new fluoroscopy-based navigation system in the placement of the femoral component in hip resurfacing.* Proc Inst Mech Eng H., 2010. **224**(4): p. 565-76.
249. Saithna A, D.A., *The influence of computer navigation on trainee learning in hip resurfacing arthroplasty.* Comput Aided Surg., 2009. **14**(4-6): p. 117-22.
250. Davis E T, G.P., Macgroarty K, Waddell J P, Schemitsch E, *The accuracy of image free computer navigation in the placement of the femoral component of the Birmingham hip resurfacing.* J Bone Joint Surg,2007, 2007. **89-B**: p. 557-60.
251. Schnurr C., M.W.P., Eysel P., König D. P, *Imageless navigation of hip resurfacing arthroplasty increases the implant accuracy.* International Orthopaedics (SICOT) 2007, 2007.

252. Berme N, P.J., *Load actions transmitted by implants.* J Biomed Eng, 1979. **1(4)**: p. 268-72.
253. Lu, T.W., Taylor, S. J., O'Connor, J. J., & Walker, P. S. , *Influence of muscle activity on the forces in the femur: an in vivo study.* J Biomech, 1997. **30**: p. 1101-1106.
254. Lu, T.W., et al., *Influence of muscle activity on the forces in the femur: an in vivo study.* J Biomech, 1997. **30**(11-12): p. 1101-6.
255. Bergmann, G., Deuretzbacher, G., Heller, M., Graichen, F., Rohlmann, A., Strauss, J., et al., *Hip contact forces and gait patterns from routine activities.* J. Biomech. , 2001. **34**: p. 859-871.
256. Hurwitz, D.E., K.C. Foucher, and T.P. Andriacchi, *A new parametric approach for modeling hip forces during gait.* J Biomech, 2003. **36**(1): p. 113-9.
257. Lenaerts, G., De Groote, F., Demeulenaere, B., Mulier, M., Van der Perre, G., Spaepen, A., et al., *Subject-specific hip geometry affects predicted hip joint contact forces during gait.* J Biomech, 2008. **41**(6): p. 1243-1252.
258. Lenaerts, G., Mulier, M., Spaepen, A., Van der Perre, G., & Jonkers, I, *Aberrant pelvis and hip kinematics impair hip loading before and after total hip replacement.* Gait Posture, 2009. **30**(3): p. 296-302.
259. Lenaerts, G., et al., *Subject-specific hip geometry affects predicted hip joint contact forces during gait.* J Biomech, 2008. **41**(6): p. 1243-52.
260. Lenaerts, G., et al., *Aberrant pelvis and hip kinematics impair hip loading before and after total hip replacement.* Gait Posture, 2009. **30**(3): p. 296-302.
261. Jonkers, I., Sauwen, N., Lenaerts, G., Mulier, M., Van der Perre, G., & Jaecques, S., *Relation between subject-specific hip joint loading, stress distribution in the proximal femur and bone mineral density changes after total hip replacement.* J Biomech, 2008. **41**(16): p. 3405-3413.
262. Huiskes, R. and E.Y. Chao, *A survey of finite element analysis in orthopedic biomechanics: the first decade.* J Biomech, 1983. **16**(6): p. 385-409.
263. Rhyu KH, K.Y., Park WM, Kim K, Cho TJ, Choi IH., *Application of finite element analysis in pre-operative planning for deformity correction of abnormal hip joints--a case series.* Proc Inst Mech Eng H. , 2011. **Sep;225**(9): p. 929-36.
264. Amin S, K.D., Melton LJ 3rd, Achenbach SJ, Therneau TM, Riggs BL, Keaveny TM, Khosla S., *Association of hip strength estimates by finite-element analysis with fractures in women and men.* J Bone Miner Res., 2011. **Jul;26**(7): p. 1593-600.
265. Eberle S, G.C., von Oldenburg G, Högel F, Augat P., *A biomechanical evaluation of orthopaedic implants for hip fractures by finite element analysis and in-vitro tests.* Proc Inst Mech Eng H., 2010. **Oct;224**(10): p. 1141-52.

266. Behrens BA, N.I., Wefstaedt P, Stukenborg-Colsman C, Bouguecha A., *Numerical investigations on the strain-adaptive bone remodelling in the periprosthetic femur: influence of the boundary conditions.* Biomed Eng Online. , 2009 **Apr ;16**(8:7).
267. Hopkins AR, N.A., Rodriguez-y-Baena F, Taylor M., *Finite element analysis of unicompartmental knee arthroplasty.* Med Eng Phys., 2010. **Jan;32**(1): p. 14-21.
268. Wawro M, F.-T.M., *A parallel framework for the FE-based simulation of knee joint motion.* IEEE Trans Biomed Eng, 2004. **Aug;51**(8): p. 1490-4.
269. Homyk A, O.A., Wibby S, Yang N, Nayeb-Hashemi H, Canavan PK., *Failure locus of the anterior cruciate ligament: 3D finite element analysis.* Comput Methods Biomech Biomed Engin. , 2011 **May 1:1 [Epub ahead of print]**.
270. Bouguecha A, W.N., Behrens BA, Stukenborg-Colsman C, Waizy H., *Numerical simulation of strain-adaptive bone remodelling in the ankle joint.* Biomed Eng Online. , 2011. **Jul 5;10:58.**
271. Podnos E, B.E., Klawitter J, Strzepa P., *FEA analysis of silicone MCP implant.* J Biomech., 2006. **39**(7): p. 1217-26.
272. Lim D, S.R., Wee JY, Tom J, Nunes L., *The effect of the loading condition corresponding to functional shoulder activities on trabecular architecture of glenoid.* J Biomech Eng. , 2006. **Apr;128**(2): p. 250-8.
273. Hopkins AR, H.U., Amis AA., *Finite element models of total shoulder replacement: application of boundary conditions.* Comput Methods Biomech Biomed Engin. , 2005. **Feb;8**(1): p. 39-44.
274. Ehnes DL, S.J., Cofield RH, An KN., *Analysis of the shoulder implant.* Biomed Sci Instrum, 2000. **36**: p. 129-34.
275. Kamposiora P, P.G., Bayne SC, Felton DA., *Finite element analysis estimates of cement microfracture under complete veneer crowns.* J Prosthet Dent. , 1994. **May;71:**((5)): p. 435-41.
276. Keyak, J.H., et al., *Automated three-dimensional finite element modelling of bone: a new method.* J Biomed Eng, 1990. **12**(5): p. 389-97.
277. Keyak, J.H., et al., *Prediction of femoral fracture load using automated finite element modeling.* J Biomech, 1998. **31**(2): p. 125-33.
278. Cody, D.D., et al., *Femoral strength is better predicted by finite element models than QCT and DXA.* J Biomech, 1999. **32**(10): p. 1013-20.
279. Keyak, J.H., et al., *Prediction of fracture location in the proximal femur using finite element models.* Med Eng Phys, 2001. **23**(9): p. 657-64.
280. Viceconti, M., et al., *Automatic generation of accurate subject-specific bone finite element models to be used in clinical studies.* J Biomech, 2004. **37**(10): p. 1597-605.
281. Testi, D., et al., *Border-tracing algorithm implementation for the femoral geometry reconstruction.* Comput Methods Programs Biomed, 2001. **65**(3): p. 175-82.

282. Keyak, J.H. and S.A. Rossi, *Prediction of femoral fracture load using finite element models: an examination of stress- and strain-based failure theories.* J Biomech, 2000. **33**(2): p. 209-14.
283. Dalstra, M., R. Huiskes, and L. van Erning, *Development and validation of a three-dimensional finite element model of the pelvic bone.* J Biomech Eng, 1995. **117**(3): p. 272-8.
284. Viceconti, M. and F. Taddei, *Automatic generation of finite element meshes from computed tomography data.* Crit Rev Biomed Eng, 2003. **31**(1-2): p. 27-72.
285. CE, C., *Quantitative CT for determination of bone mineral density: a review.* Radiology 1988, 1988. **166(2):**: p. 509–22.
286. named, N.A. http://en.wikipedia.org/wiki/Voxel. Voxel 2011 June 2011].
287. Keyak, J.H., Kaneko, T. S., Tehranzadeh, J., & Skinner, H. B. , *Predicting proximal femoral strength using structural engineering models.* Clin Orthop Relat Res, 2005. **437**: p. 219-228.
288. Fyhrie, D.P., et al., *Direct three-dimensional finite element analysis of human vertebral cancellous bone. .* Trans. Ann. Meeting Orthop Res. Soc. , 1992. **17**: p. 551.
289. Charras, G.T. and R.E. Guldberg, *Improving the local solution accuracy of large-scale digital image-based finite element analyses.* J Biomech, 2000. **33**(2): p. 255-9.
290. Boyd, S.K. and R. Muller, *Smooth surface meshing for automated finite element model generation from 3D image data.* J Biomech, 2006. **39**(7): p. 1287-95.
291. Young PG, B.-W.T., Coward SRL, Notarberardino B, Walker B and Abdul-Aziz A *An efficient approach to converting three-dimensional image data into highly accurate computational models.* Phil. Trans. R. Soc. A, 2008. **366**: p. 3155–3173.
292. Taddei, F., et al., *Subject-specific finite element models of long bones: An in vitro evaluation of the overall accuracy.* J Biomech, 2006. **39**(13): p. 2457-67.
293. Lotz, J.C., E.J. Cheal, and W.C. Hayes, *Fracture prediction for the proximal femur using finite element models: Part II--Nonlinear analysis.* J Biomech Eng, 1991. **113**(4): p. 361-5.
294. Lotz, J.C., E.J. Cheal, and W.C. Hayes, *Fracture prediction for the proximal femur using finite element models: Part I--Linear analysis.* J Biomech Eng, 1991. **113**(4): p. 353-60.
295. Zohar Yosibasha, N.T., Charles Milgromb, *Reliable simulations of the human proximal femur by high-order finite*
element analysis validated by experimental observations. Journal of Biomechanics 2007. **40**(3688–3699).
296. Ramos, A. and J.A. Simoes, *Tetrahedral versus hexahedral finite elements in numerical modelling of the proximal femur.* Med Eng Phys, 2006. **28**(9): p. 916-24.

297. Yosibash, Z., N. Trabelsi, and C. Milgrom, *Reliable simulations of the human proximal femur by high-order finite element analysis validated by experimental observations.* J Biomech, 2007. **40**(16): p. 3688-99.
298. Yosibash, Z., et al., *A CT-based high-order finite element analysis of the human proximal femur compared to in-vitro experiments.* J Biomech Eng, 2007. **129**(3): p. 297-309.
299. Mueller, R., & Ruegseggar, P. , *Three dimensional finite element modeling of non-invasively assessed trabecular bone structures.* J Med. Eng. Phys, 1994. **17**(126-133).
300. Young, P.G., et al., *An efficient approach to converting three-dimensional image data into highly accurate computational models.* Philos Transact A Math Phys Eng Sci, 2008. **366**(1878): p. 3155-73.
301. Vose GP, K.A., *Bone strength—its relationship to X-ray-determined ash content.* Human Biol 1959. **31**: p. 261–70.
302. A, U., *Prediction of Colles' fracture load in human radius using cohesive finite element modeling.* J Biomech. , 2009 **Jan 5;42**(1): p. 22-8.
303. Wirtz DC, P.T., Portheine F, Radermacher K, Schiffers N, Prescher A, Weichert D, Niethard FU., *Concept and development of an orthotropic FE model of the proximal femur.* J Biomech. , 2003 **Feb;36:**(2): p. 289-93.
304. Carter, D.R. and W.C. Hayes, *The compressive behavior of bone as a two-phase porous structure.* J Bone Joint Surg Am, 1977. **59**(7): p. 954-62.
305. Cann, C.E., *Quantitative CT for determination of bone mineral density: a review.* Radiology, 1988. **166**(2): p. 509-22.
306. Bessho M, O.I., Matsuyama J, Matsumoto T, Imai K, Nakamura K, *Prediction of strength and strain of the proximal femur by a CT-based finite element method.* J Biomech, 2007. **40**: p. 1745-1753.
307. Pastrav, L.C., Devos, J., Van der Perre, G., Jaecques, S.V, *A finite element analysis of the vibrational behaviour of the intra-operatively manufactured prosthesis-femur system.* Med. Eng. Phys., 2009. **31**: p. 489-494.
308. Taddei, F., et al., *Mechanical strength of a femoral reconstruction in paediatric oncology: a finite element study.* Proc Inst Mech Eng H, 2003. **217**(2): p. 111-9.
309. Keyak, J.H., Meagher, J. M., Skinner, H. B., & Mote, C. D., Jr., *Automated three-dimensional finite element modelling of bone: a new method.* J Biomed Eng, 1990. **12**(5): p. 389-397.
310. Keyak, J.H.a.S., H.B, *Three dimensional finite element modelling of bone: effects of element size.* J. Biomed. Eng, 1992. **14**: p. 483–489.
311. Keyak JH, R.S., Jones KA, Skinner HB, *Prediction of femoral fracture load using automated finite element modeling.* J Biomech 1998. **31**: p. 125-133.

312. Keyak, J.H., & Rossi, S. A., *Prediction of femoral fracture load using finite element models: an examination of stress- and strain-based failure theories.* J Biomech, 2000. **33**(2): p. 209-214.
313. JH, K., *Improved prediction of proximal femoral fracture load using nonlinear finite element models.* Med Eng Phys 2001. **23**: p. 165-173.
314. Crawford, R.P., C.E. Cann, and T.M. Keaveny, *Finite element models predict in vitro vertebral body compressive strength better than quantitative computed tomography.* Bone, 2003. **33**(4): p. 744-50.
315. Keyak, J.H., et al., *Predicting proximal femoral strength using structural engineering models.* Clin Orthop Relat Res, 2005(437): p. 219-28.
316. Cody, D.D., et al., *Short term in vivo precision of proximal femoral finite element modeling.* Ann Biomed Eng, 2000. **28**(4): p. 408-14.
317. Ford, C.M., T.M. Keaveny, and W.C. Hayes, *The effect of impact direction on the structural capacity of the proximal femur during falls.* J Bone Miner Res, 1996. **11**(3): p. 377-83.
318. Oden, Z.M., D.M. Selvitelli, and M.L. Bouxsein, *Effect of local density changes on the failure load of the proximal femur.* J Orthop Res, 1999. **17**(5): p. 661-7.
319. Pietruszczak, S., D. Inglis, and G.N. Pande, *A fabric-dependent fracture criterion for bone.* J Biomech, 1999. **32**(10): p. 1071-9.
320. Nalla, R.K., J.H. Kinney, and R.O. Ritchie, *Mechanistic fracture criteria for the failure of human cortical bone.* Nat Mater, 2003. **2**(3): p. 164-8.
321. Taylor, D., *Fracture mechanics: How does bone break?* Nat Mater, 2003. **2**(3): p. 133-134.
322. Bayraktar, H.H., et al., *Comparison of the elastic and yield properties of human femoral trabecular and cortical bone tissue.* J Biomech, 2004. **37**(1): p. 27-35.
323. Kopperdahl, D.L. and T.M. Keaveny, *Yield strain behavior of trabecular bone.* J Biomech, 1998. **31**(7): p. 601-8.
324. Chang, W.C., et al., *Uniaxial yield strains for bovine trabecular bone are isotropic and asymmetric.* J Orthop Res, 1999. **17**(4): p. 582-5.
325. Cowin, S.C. and Q.C. He, *Tensile and compressive stress yield criteria for cancellous bone.* J Biomech, 2005. **38**(1): p. 141-4.
326. Currey, J.D., *Tensile yield in compact bone is determined by strain, post-yield behaviour by mineral content.* J Biomech, 2004. **37**(4): p. 549-56.
327. Weinans Harrie, N.S.R.D., Igloria Ruben, Natarajan Raghu N., *Sensitivity of periprosthetic stress-shielding to load and the bone density-modulus relationship in subject-specific finite element models.* Journal of Biomechanics, 33 (2000) 2000. **33**: p. 809-817.
328. Moazen, M., Jones, A.C., Jin, Z., Wilcox, R.K., Tsiridis, E, *Periprosthetic fracture fixation of the femur following total hip arthroplasty: a review of biomechanical testing.* Clin. Biomech. (Bristol, Avon), 2011. **26**: p. 13-22.

329. Franklin J, M.H., *Risk factors for periprosthetic femoral fracture.* Injury 2007. **38**: p. 655-660.
330. Rupprecht, M., Sellenschloh, K., Grossterlinden, L., Puschel, K., Morlock, M., Amling, M., et al., *Biomechanical evaluation for mechanisms of periprosthetic femoral fractures.* J Trauma, 2011. **70**(4): p. E62-66.
331. Elias, J.J., et al., *Medial cortex strain distribution during noncemented total hip arthroplasty.* Clin Orthop Relat Res, 2000. **370**: p. 250-8.
332. Masri, B.A., Meek, R.M., Duncan, C.P, *Periprosthetic fractures evaluation and treatment. .* Clin. Orthop. Relat. Res, 2004: p. 80-95.
333. Mabry, T.M., Cabanela, M.E., Hanssen, A.D, *Intra-operative fractures during primary total hip arthroplasty.* U.S. Musculoskeletal Review, 2006: p. 31-32.
334. Fitzgerald, R.H., Jr., Brindley, G.W., Kavanagh, B.F, *The uncemented total hip arthroplasty. Intraoperative femoral fractures.* Clin. Orthop. Relat. Res, 1988. **235**: p. 61-66.
335. Kim, Y.H., Kim, J.S., Cho, S.H., *Strain distribution in the proximal human femur. An in vitro comparison in the intact femur and after insertion of reference and experimental femoral stems.* J. Bone Joint Surg. Br., 2001. **83**: p. 295-301.
336. Decking, R., Puhl, W., Simon, U., Claes, L.E., *Changes in strain distribution of loaded proximal femora caused by different types of cementless femoral stems.* Clin. Biomech. (Bristol, Avon), 2006. **21**: p. 495-501.
337. Schneider, E., Kinast, C., Eulenberger, J., Wyder, D., Eskilsson, G., Perren, S.M, *A comparative study of the initial stability of cementless hip prostheses.* Clin. Orthop. Relat. Res., 1989. **248**: p. 200-209.
338. Bühler, D.W., Berlemann, U., Lippuner, K., Jaeger, P., Nolte, L.P., *Three-dimensional primary stability of cementless femoral stems.* Clin. Biomech. (Bristol, Avon), 1997. **12**: p. 75-86.
339. Gotze, C., Steens, W., Vieth, V., Poremba, C., Claes, L., Steinbeck, J., *Primary stability in cementless femoral stems: custom-made versus conventional femoral prosthesis.* Clin. Biomech. (Bristol, Avon), 2002. **17**: p. 267-273.
340. Berry, D.J., *Epidemiology: hip and knee.* Orthop. Clin. North Am, 1999. **30**: p. 183-190.
341. Jakubowitz E, S.J., Lee C, Heisel C, Kretzer JP, Thomsen MN, *Do short-stemmed-prostheses induce periprosthetic fractures earlier than standard hip stems? A biomechanical ex-vivo study of two different stem designs.* Arch Orthop Trauma Surg 2009. **129**: p. 849-855.
342. Franklin, J., Malchau, H., *Risk factors for periprosthetic femoral fracture.* Injury, 2007. **38**: p. 655-660.
343. Schileo E, T.F., Malandrino A, Cristofolini L, Viceconti M, *Subject-specific finite element models can accurately predict strain levels in long bones.* J Biomech 2007. **40**: p. 2982-2989.

344. Keyak, J.H., Rossi, S. A., Jones, K. A., & Skinner, H. B., *Prediction of femoral fracture load using automated finite element modeling.* J Biomech, 1998. **31**(2): p. 125-133.
345. Schileo, E., Taddei, F., Cristofolini, L., & Viceconti, M., *Subject-specific finite element models implementing a maximum principal strain criterion are able to estimate failure risk and fracture location on human femurs tested in vitro.* J Biomech, 2008. **41**(2): p. 356-367.
346. Pietruszczak, S., Inglis, D., & Pande, G. N. , *A fabric-dependent fracture criterion for bone.* J Biomech, 1999. **32**(10): p. 1071-1079.
347. A.W.L. Turner a, b., R.M. Gillies a, R. Sekel b, P. Morris a, W. Bruce a, W.R. Walsh a,, *Computational bone remodelling simulations and comparisons*
with DEXA results Journal of Orthopaedic Research 2005. **23**: p. 705–712.
348. a, A.-. *Abaqus/CAE User's Manual*, in *Dassault Systemes Simulia Corp: Providence:*2009.
349. b, A.-. *Abaqus Theory Manual.* , in *Dassault Systemes Simulia Corp: Providence*2009.
350. c, A.-. *Getting Started with Abaqus: Keywords Edition*, in *Dassault Systemes Simulia Corp: Providence.*2009.
351. Carter DR, H.W., *The compressive behavior of bone as a two-phase porous structure.* J Bone Joint Surg Am 1977, 1977. **59(7)**: p. 954– 62.
352. Pastrav LC, D.J., Van der Perre G, Jaecques SV, *A finite element analysis of the vibrational behaviour of the intra-operatively manufactured prosthesis-femur system.* Med. Eng Phys, 2009. **31**: p. 489-494.
353. Keyak, J.H., Rossi, S. A., Jones, K. A., Les, C. M., & Skinner, H. B., *Prediction of fracture location in the proximal femur using finite element models.* Med Eng Phys, 2001. **23**(9): p. 657-664.
354. Budyn E, T.H.T., Jonvaux J, *Fracture strength assessment and aging signs detection in human cortical bone using an X-FEM multiple scale approach.* Computational Mechanics, 2008. **42**: p. 579-591.
355. Bayraktar, H.H., Morgan, E. F., Niebur, G. L., Morris, G. E., Wong, E. K., & Keaveny, T. M., *Comparison of the elastic and yield properties of human femoral trabecular and cortical bone tissue.* J Biomech, , 2004. **37(1)**: p. 27-35.
356. Christen D, W.D., Müller R, *Multiscale modelling and nonlinear finite element analysis as clinical tools for the assessment of fracture risk.* Philos Transact A Math Phys Eng Sci, 2010. **368**: p. 2653-2668.
357. John J. Elias, M.N., Yung-Hua Chu,John J. Carbone,Dennis W. Lennox,Edmund Y.S. Chao., , *Medial Cortex Strain Distribution During Noncemented total hip arthroplasty.* CLINICAL ORTHOPAEDICS AND RELATED RESEARCH, 2000. **370**: p. 250-258.
358. Thillemann TM, P.A., Johnsen SP, Soballe K, *Inferior outcome after intraoperative femoral fracture in total hip arthroplasty: outcome in 519*

patients from the Danish hip arthroplasty registry. Acta Orthop, 2008. **79**: p. 327-334.
359. Taddei, F., Cristofolini, L., Martelli, S., Gill, H. S., & Viceconti, M. , *Subject-specific finite element models of long bones: An in vitro evaluation of the overall accuracy.* J Biomech, 2006. **39**(13): p. 2457-2467.
360. Kluess D, M.W., Bader R, *Intraoperative impaction of total knee replacements: an explicit finite-element-analysis of principal stresses in ceramic vs. cobalt-chromium femoral components.* Clin Biomech (Bristol, Avon) 2010. **25**: p. 1018-1024.
361. Anderson KC, B.K., Markel DC, *Computer assisted navigation in total knee arthroplasty: comparison with conventional methods.* J Arthroplasty 2005. **20**(7 Suppl 3): p. 132-138.
362. Kluess D, M.W., Bader R., *Intraoperative impaction of total knee replacements: an explicit finite-element-analysis of principal stresses in ceramic vs. cobalt-chromium femoral components.* Clin Biomech (Bristol, Avon). , 2010. **25**(10): p. 1018-24.
363. Nalla, R.K., Kinney, J. H., & Ritchie, R. O., *Mechanistic fracture criteria for the failure of human cortical bone.* Nat Mater, 2003. **2**(3): p. 164-168.
364. Mont MA, R.P., Bezwada HP, Thomas CM, Etienne G, *The results of metal-on-metal resurfacing hip arthroplasty: Learning curve stratification of results.* 72nd Annual Meeting Proceedings. American Academy of Orthopaedic Surgeons, 2005: p. 368.
365. Kishida Y, S.N., Nishii T, Miki H, Yamaguchi K, Yoshikawa H *Preservation of the bone mineral density of the femur after surface replacement of the hip.* J Bone Joint Surg Br, 2004. **86**: p. 185-189.
366. Hing CB, B.D., Bailey M, Young DA, Dalziel RE, Shimmin AJ *The results of primary Birmingham hip resurfacings at a mean of five years: an independent prospective review of the first 230 hips.* J Bone Joint Surg Br, 2007. **89**: p. 1431-1438.
367. Beaulé PE, C.P., Hoke R, Dorey F *Notching of the femoral neck during resurfacing arthroplasty of the hip.* Bone Joint Surg Br, 2006. **88**(1): p. 35–39.
368. Association, A.O., *National joint replacement registry annual report. Adelaide: AOA*, 2007.
369. Beaule PE, A.H., Le Duff M, Dorey F *Surface arthroplasty for osteonecrosis of the hip: Hemiresurfacing versus metal-on-metal hybrid resurfacing.* Arthroplasty, 2004. **19**: p. 54-58.
370. Beaule PE, D.F., LeDuff M, Gruen T, Amstutz HC, *Risk factors affecting outcome of metal-on-metal surface arthroplasty of the hip.* Clin Orthop Relat Res, 2004. **418**: p. 87-93.
371. Shimmin AJ, B.D., *Femoral neck fractures following Birmingham hip resurfacing: A national review of 50 cases.* Bone Joint Surg Br, 2005. **87**: p. 463-464.

372. Radcliffe I, T.M., *Investigation into the effect of varus-valgus orientation on load transfer in the resurfaced femoral head: a multi-femur finite element analysis.* Clin Biomech 2007. **22**(7): p. 780–786
373. Davis E, O.M., Zdero R et al, *Femoral neck fracture following hip resurfacing: the effect of alignment of the femoral component.* J Bone Joint Surg Br, 2008. **90**(11): p. 1522–1527
374. Beaulé, P.E., Le Duff M. J., Lee J.L., Amstutz H.C., Ebramzadeh E, *Orientation of the Femoral Component in Surface Arthroplasty of the Hip.* The Journal of Bone and Joint Surgery, 2004. **86**: p. 2015-21.
375. AM, D., *Bringing simulation to surgery: Improving the success rate of Hip replacements.* White paper, Shadyside Hospital, Carnegie Mellon University, 1996.
376. Brekelmans WA, P.H., Slooff TJ *A new method to analyse the mechanical behaviour of skeletal parts.* Acta Orthopaedica Scandinavica, 1972. **43**(5): p. 301–317.
377. De Smet KA, P.C., Verdonk R *Early results of primary Birmingham hip resurfacing using a hybrid metal-on-metal couple.* Hip Int, 2002. **12**: p. 158-162
378. KA, D.S., *Belgium experience with metal-on-metal surface arthroplasty.* Orthop Clin North Am, 2005. **36**: p. 203-213.
379. Hess T, G.T., Köttgen C, Szawlowski B *Intraoperative navigation for hip resurfacing: methods and first results [in German].* Orthopade, 2004. **33**: p. 1183-1193
380. Nabavi A, Y.K., Shidiac L, Appleyard R, Gillies RM, Turnbull A *Effects of positioning and notching of resurfaced femurs on femoral neck strength: a biomechanical test.* Journal of Orthopaedic Surgery, 2009. **17**(1): p. 47-50.